# Post-traumatic syringomyelia:

## Investigations into pathophysiology

Johnny Ho Yin Wong

BSc(Med), MBBS (Hons), MMed (Clin Epi)

A thesis submitted to fulfil the requirements of Doctor of Philosophy at the Australian School of Advanced Medicine, Faculty of Human Sciences, Macquarie University


31st May, 2013

# Table of Contents

**Table of Contents** ..... **2**
**Figures** ..... **12**
**Tables** ..... **15**
**Abbreviations** ..... **17**
**Statement of originality** ..... **18**
**Acknowledgements** ..... **19**
**Summary** ..... **21**
**Chapter 1 Introduction** ..... **23**

*1.1 Syringomyelia* ..... *23*
1.1.1 History ..... 23
1.1.2 Definition & Terminology ..... 24
1.1.3 Classification and pathology ..... 25
1.1.4 Epidemiology ..... 28
1.1.5 Natural history ..... 29
1.1.6 Clinical features ..... 30
1.1.7 Imaging ..... 33
1.1.8 Associated conditions ..... 35
1.1.9 Treatment ..... 42
1.1.10 Conclusion ..... 50
*1.2 Pathophysiology of syringomyelia* ..... *50*
1.2.1 Theories for pathogenesis of canalicular syringomyelia ..... 51
1.2.2 Theories for pathogenesis of extra-canalicular syringomyelia ..... 60
1.2.3 Conclusion ..... 67
*1.3 Animal models of syringomyelia and spinal cord injury* ..... *68*
1.3.1 Introduction ..... 68
1.3.2 Animal models of canalicular syringomyelia ..... 68

1.3.3 Animal models of spinal cord injury ..... 73
1.3.4 Animal models of extra-canalicular syringomyelia ..... 78
1.3.5 Conclusion ..... 82
*1.4 Spinal Cord Anatomy ..... 82*
1.4.1 Introduction ..... 82
1.4.2 Embryology and development ..... 83
1.4.3 Gross anatomy ..... 83
1.4.4 Internal structure and cellular organization ..... 84
1.4.5 Central canal and ventricular system ..... 86
1.4.6 Spinal meninges ..... 87
1.4.7 Vasculature ..... 88
1.4.8 Fluid interfaces ..... 90
*1.5 Cerebrospinal Fluid Physiology ..... 92*
1.5.1 Introduction ..... 92
1.5.2 CSF Pathways ..... 93
1.5.3 CSF Biochemistry ..... 94
1.5.4 CSF pressure pulsations and flow ..... 95
1.5.5 Conclusion ..... 98
*1.6 Aquaporins ..... 98*
1.6.1 Introduction ..... 98
1.6.2 Structure of aquaporins ..... 99
1.6.3 Role of aquaporins outside the central nervous system ..... 100
1.6.4 Role of aquaporins in the central nervous system ..... 101
1.6.5 Aquaporin-4 in clinical settings ..... 103
1.6.6 Regulation of Aquaporin-4 ..... 109
1.6.7 Modulation of Aquaporin-4 ..... 113
1.6.8 Potential clinical implications ..... 117

1.6.9 Conclusion ..... 119

*1.7 Summary ..... 119*

*1.8 Hypotheses and aims ..... 120*

1.8.1 Hypotheses ..... 120

1.8.2 Aims ..... 121

**Chapter 2 General methods ..... 123**

*2.1 Animal care ..... 123*

2.1.1 Ethical approval and number of animals used ..... 123

2.1.2 General care of rodents ..... 123

2.1.3 General care of sheep ..... 124

*2.2 Anaesthesia and peri-operative monitoring ..... 125*

2.2.1 Anaesthesia and monitoring of rodents ..... 125

2.2.2 Anaesthesia and monitoring of sheep ..... 126

*2.3 Experimental procedures ..... 126*

2.3.1 Laminectomy and induction of spinal arachnoiditis in rodents ..... 126

2.3.2 Laminectomy and induction of spinal arachnoiditis in sheep ..... 127

2.3.3 Post-traumatic syringomyelia induction with spinal cord impactor ..... 128

2.3.4 Post-traumatic syringomyelia induction with quisqualic acid injection in rodents 128

2.3.5 Post-traumatic syringomyelia induction with quisqualic acid injection in sheep 129

2.3.6 CSF flow studies in rodents ..... 129

*2.4 Perfusion-fixation ..... 130*

2.4.1 Perfusion-fixation in rodents ..... 130

2.4.2 Perfusion-fixation in sheep ..... 130

*2.5 Solution preparations ..... 131*

2.5.1 Horseradish peroxidase (HRP) ..... 131

2.5.2 Alexa-Fluor 647 Ovalbumin (AFO) ..... 131

2.5.3 Paraformaldehyde ..... 131

2.5.4 Quisqualic acid in Evans' blue solution ..... 132

*2.6 Tissue processing ..... 132*

2.6.1 Tissue removal from rodents ..... 132

2.6.2 Paraffin embedding ..... 132

2.6.3 Vibratome sectioning ..... 133

*2.7 Staining ..... 133*

2.7.1 Haematoxylin and eosin staining ..... 133

2.7.2 HRP staining using TMB ..... 134

2.7.3 AQP4, AQP1 and GFAP immunohistochemical staining ..... 134

*2.8 Measurements ..... 135*

2.8.1 Randomisation ..... 135

2.8.2 Blinding ..... 135

2.8.3 Statistical analyses ..... 135

2.8.4 Optical and immunohistochemical density measurements ..... 136

**Chapter 3 Biochemical analysis of syringomyelia fluid ..... 139**

*3.1 Abstract ..... 139*

*3.2 Introduction ..... 140*

*3.3 Methods ..... 140*

3.3.1 Procedure for aspiration of CSF and syrinx fluid ..... 141

3.3.2 Chemical analysis ..... 142

*3.4 Results ..... 142*

*3.5 Discussion ..... 146*

*3.6 Conclusion ..... 153*

*3.7 Contributions to the study ..... 154*

*3.8 Acknowledgements ..... 154*

**Chapter 4 Direct-trauma model of post-traumatic syringomyelia with a computer controlled motorised spinal cord impactor ..... 155**

*4.1 Abstract ..... 155*

*4.2 Introduction ..... 157*

*4.3 Materials and methods ..... 158*

4.3.1 Experiment 1: Determining the optimal force setting ..... 158

4.3.2 Experiment 2: Temporal progression of cystic cavity ..... 159

4.3.3 Operative procedure ..... 160

4.3.4 Perfusion and fixation ..... 161

4.3.5 Histology ..... 161

4.3.6 Image acquisition and processing ..... 162

4.3.7 Statistical analysis ..... 162

*4.4 Results ..... 163*

4.4.1 Experiment 1: Determining the optimal force setting ..... 163

4.4.2 Experiment 2: Temporal progression of cystic cavity ..... 166

*4.5 Discussion ..... 170*

*4.6 Contributions to the study ..... 177*

*4.7 Acknowledgements ..... 177*

**Chapter 5 Cerebrospinal fluid flow in spinal arachnoiditis using horseradish peroxidase (HRP) ..... 179**

*5.1 Abstract ..... 179*

*5.2 Introduction ..... 181*

*5.3 Materials and methods ..... 181*

5.3.1 Operative procedure ..... 182

5.3.2 CSF tracer injection, perfusion and fixation ..... 183

5.3.3 Tissue processing ..... 184

5.3.4 Microscopic image acquisition ..... 185

5.3.5 Qualitative and semi-quantitative assessments of transverse sections ..... 185

5.3.6 Statistical analysis ..... 186

*5.4 Results* ..... *187*

5.4.1 Qualitative analyses ..... 187

5.4.2 Semi-quantitative analyses ..... 190

*5.5 Discussion* ..... *194*

*5.6 Conclusion* ..... *199*

*5.7 Contributions to the study* ..... *200*

**Chapter 6 Cerebrospinal fluid flow in spinal arachnoiditis using Alexa-Fluor 647 ovalbumin (AFO) ..... 201**

*6.1 Abstract* ..... *201*

*6.2 Introduction* ..... *204*

*6.3 Materials and methods* ..... *204*

6.3.1 Operative procedure ..... 206

6.3.2 *In-vivo* imaging: Alexa-Fluor 647 Ovalbumin injection, macroscopic fluorescent imaging and perfusion-fixation ..... 207

6.3.3 Post-mortem imaging: Alexa-Fluor 647 Ovalbumin injection, perfusion-fixation and macroscopic fluorescent imaging ..... 208

6.3.4 Tissue processing ..... 209

6.3.5 Microscopic image acquisition ..... 210

*6.4 Results* ..... *210*

6.4.1 In-vivo macroscopic fluorescent imaging ..... 210

6.4.2 Post-mortem macroscopic fluorescent imaging ..... 211

6.4.3 Microscopic fluorescent imaging ..... 213

*6.5 Discussion* ..... *214*

*6.6 Conclusion* ..... *218*

*6.7 Contributions to the study* ..... *219*

**Chapter 7 *In-vivo* telemetry of cerebrospinal fluid pulsations in spinal arachnoiditis ..... 221**

*7.1 Abstract ..... 221*

*7.2 Introduction ..... 223*

*7.3 Materials and methods ..... 224*

7.3.1 Induction of arachnoiditis and insertion of telemetry pressure monitors ..224

7.3.2 Telemetry recordings of CSF pulsations ..... 226

7.3.3 Injection of fluid tracer and perfusion/fixation ..... 226

7.3.4 Tissue processing and retrieval of telemetry monitors ..... 227

7.3.5 Statistical analyses ..... 228

*7.4 Results ..... 228*

7.4.1 Telemetry pulsation data ..... 228

7.4.2 CSF flow studies with HRP ..... 235

*7.5 Discussion ..... 236*

*7.6 Conclusions ..... 241*

*7.7 Contributions to the study ..... 241*

**Chapter 8 Fluid outflow in large animal model of post-traumatic syringomyelia 243**

*8.1 Abstract ..... 243*

*8.2 Introduction ..... 245*

*8.3 Materials and methods ..... 246*

8.3.1 Syrinx induction ..... 246

8.3.2 Injection of fluid tracer into syrinx cavity and perfusion/fixation ..... 247

8.3.3 Tissue processing ..... 248

8.3.4 Image acquisition ..... 249

*8.4 Results ..... 249*

*8.5 Discussion ..... 252*

*8.6 Conclusions* ..... *258*

*8.7 Contributions to the study* ..... *258*

**Chapter 9 Aquaporin-4 and Aquaporin-1 expression in spinal cord injury and post-traumatic syringomyelia** ..... **259**

*9.1 Abstract* ..... *259*

*9.2 Introduction* ..... *261*

*9.3 Materials and methods* ..... *262*

9.3.1 Operative procedure ..... 263

9.3.2 Perfusion-fixation and tissue processing ..... 264

9.3.3 Immunohistochemical staining ..... 264

9.3.4 Image acquisition and processing ..... 266

9.3.5 Statistical analysis ..... 268

*9.4 Results* ..... *269*

9.4.1 Triple labelling with AQP4, AQP1 and GFAP ..... 269

9.4.2 Dual labelling with AQP4 and GFAP ..... 270

*9.5 Discussion* ..... *274*

*9.6 Conclusion* ..... *279*

*9.7 Contributions to the study* ..... *279*

**Chapter 10 The effect of Aquaporin-4 modulation in a rodent model of post-traumatic syringomyelia** ..... **281**

*10.1 Abstract* ..... *281*

*10.2 Introduction* ..... *283*

*10.3 Materials and methods* ..... *284*

10.3.1 Post-traumatic syrinx induction ..... 285

10.3.2 Administration of AQP4 Modulation agents ..... 286

10.3.3 Perfusion and fixation ..... 286

10.3.4 Tissue processing, histology and immunohistochemistry ..... 286
10.3.5 Image acquisition and processing ..... 288
10.3.6 Statistical analysis ..... 289
*10.4 Results ..... 289*
10.4.1 Neurological function ..... 289
10.4.2 Histological appearances on H&E ..... 289
10.4.3 Cavity measurements ..... 291
10.4.4 AQP4/GFAP immunohistochemistry ..... 293
*10.5 Discussion ..... 296*
*10.6 Conclusion ..... 301*
*10.7 Contributions to the study ..... 301*

**Chapter 11 General discussion ..... 303**

*11.1 Pathophysiology of post-traumatic syringomyelia ..... 303*
11.1.1 Nature of syrinx fluid ..... 304
11.1.2 Models of syringomyelia ..... 304
11.1.3 Pathophysiological processes ..... 306
11.1.4 Modulation of processes and treatment implications ..... 309
*11.2 Future investigations ..... 309*

**Chapter 12 Conclusions ..... 313**
**Chapter 13 Appendices ..... 315**

*13.1 Publications ..... 315*
*13.2 Manuscripts in preparation or submitted for publication ..... 315*
*13.3 Presentations at scientific meetings ..... 316*
*13.4 Prizes and scholarships ..... 317*
*13.5 Ethics approval documents ..... 318*
*13.6 Operative monitoring and post-operative monitoring sheets ..... 321*

*13.7 Paraffin embedding and staining protocols ..... 323*

13.7.1 Paraffin Embedding Schedule (Leica ASP200S) ..... 323

13.7.2 Haematoxylin and eosin staining (Lillie-Mayer method) ..... 324

13.7.3 TMB staining for HRP ..... 325

**Chapter 14 References ..... 327**

# Figures

Figure 1.1-1 Classification of syringomyelia.....26

Figure 1.1-2 T2-weighted MRI sagittal image of post-traumatic syringomyelia. .....34

Figure 1.1-3 Intraoperative images of syringe-subarachnoid shunt insertion.....48

Figure 3.4-1 Flowchart of patients recruited for syrinx fluid sampling study .....143

Figure 4.3-1 Flowchart of animals allocated for experiment 1.....159

Figure 4.3-2 Flowchart of animals allocated for experiment 2.....160

Figure 4.4-1 Relationships between: (A) programmed force and delivered force; (B) delivered force and displacement.....163

Figure 4.4-2 Neurological outcomes (Tarlov Scale) in Experiment 1.....164

Figure 4.4-3 H&E sections at C8 with increasing programmed forces. .....165

Figure 4.4-4 Actual force and displacement graphs across groups in Experiment 2..167

Figure 4.4-5 Mean C8 cavity lateral dimensions and percentage area of cord.....167

Figure 4.4-6 H&E section at C8 of an animal with kaolin at 6 week timepoint.....168

Figure 4.4-7 H&E sections at C8 level in non-kaolin (left) and kaolin groups (right) at timepoints from 1 – 12 weeks.....169

Figure 5.4-1 HRP tracer flow into the normal spinal cord.....188

Figure 5.4-2 HRP tracer in control animal after 5 minutes perfusion.....188

Figure 5.4-3 Gradual decrease in HRP staining in the ventral median fissure and central canal from rostral-caudal direction in a control animal. ..... 189

Figure 5.4-4 Increased HRP staining in region of arachnoiditis. ..... 190

Figure 5.4-5 Most caudal level at which reaction product staining was greatest. ..... 191

Figure 5.4-6 Central Canal ROD ratios of each animal. ..... 193

Figure 6.3-1 Flowchart of processes used with AFO tracer ..... 206

Figure 6.4-1 Limited AFO penetrance through overlying tissues. ..... 211

Figure 6.4-2 Post-mortem macroscopic fluorescent imaging (3 days – 6 weeks) ..... 213

Figure 6.4-3 Fluorescent microscopic sections from animal with arachnoiditis ..... 214

Figure 7.3-1 Schematic illustration of the arrangement of cranial and caudal CSF pressure transducers implanted into the spinal subarachnoid space. ..... 225

Figure 7.4-1 CSF and ECG telemetry traces at implantation ..... 230

Figure 7.4-2 Mean ECG – cranial CSFpulsation delay in arachnoiditis and control animals 234

Figure 7.4-3 Mean Cranial – caudal CSF pulation delay in arachnoiditis and control animals 235

Figure 8.3-1 Intraoperative longitudinal ultrasound images of the spinal cord. ..... 248

Figure 8.4-1 Histological section of a sheep spinal cord with post-traumatic syrinx . 251

Figure 8.4-2 Histological section of spinal cord with no syrinx. ..... 252

Figure 9.3-1 Steps to quantitative analysis using Image-J software ..... 268

Figure 9.4-1 Immunohistochemical staining for (i) AQP4, (ii) GFAP, (iii) AQP1, and (iv) triple labelling with AQP4, GFAP and AQP1. ..... 270

Figure 9.4-2 AQP4 (in red) and GFAP (in green) expressions at C8 level in PTS model from 1 – 12 weeks ..... 272

Figure 9.4-3 Mean integrated signal intensity for groups stratified according to time point, experimental group and presence of a syrinx. ..... 273

Figure 10.3-1 Flowchart of animals for AQP4 modulation ..... 284

Figure 10.3-2 Measurements for cavity dimensions and areas ..... 288

Figure 10.4-1 Histological images at C8 level for AQP modulation groups. ..... 290

Figure 10.4-2 Percentage area of syrinx cavity to spinal cord at: (A) C7 level; (B) C8 level; (C) T1 level; (D) Average of maximum 2 levels ..... 293

Figure 10.4-3 AQP4 / GFAP expression in control animal from C5 to T2 levels. ..... 294

Figure 10.4-4 AQP4 / GFAP expression at C8 level across AQP modulation groups. 295

Figure 11.1-1 Conceptual approach to syringomyelia research ..... 304

# Tables

Table 1.1-1 Clinical manifestations of syringomyelia....31

Table 1.1-2 Conditions associated with syringomyelia....37

Table 1.5-1 Biochemical profile of CSF and plasma....95

Table 2.1-1 Number of animals used in experiments in this thesis.....124

Table 3.4-1 Clinical synopsis and biochemical profile of syrinx shunt cases....145

Table 3.5-1 Summary of case series with CSF & syrinx fluid sampling....151

Table 4.4-1 Experiment 1 results with programmed forces from 50 to 150 kDyn....164

Table 4.4-2 Experiment 2 results in kaolin and non-kaolin groups.....166

Table 5.3-1 Allocation of animals for the HRP study....182

Table 5.3-2 Semi-quantitative grading system for extent of HRP tracer flow....186

Table 6.3-1 Allocation of animals with AFO tracer....205

Table 7.4-1 Minimum-maximum amplitudes (in mmHg) of cranial and caudal CSF pulsation waves in arachnoiditis animals....231

Table 7.4-2 Minimum-maximum amplitudes (in mmHg) of cranial and caudal CSF pulsation waves in control animals....232

Table 7.4-3 ECG – Cranial CSF pulsation delay over 6 weeks....233

Table 7.4-4 Cranial – Caudal CSF pulsation delay over 6 weeks....233

Table 9.3-1 Allocation of animals in the AQP expression study. .....262

Table 10.4-1 AQP modulation results: No. of levels and area .....291

Table 10.4-2 AQP modulation results: Dimensions. .....291

Table 13.7-1 Paraffin embedding schedule for Leica ASP200S .....323

Table 13.7-2 Haematoxylin and eosin staining (Lillie-Mayer) method .....324

Table 13.7-3 TMB staining method for HRP .....325

# Abbreviations

| | |
|---|---|
| ACEC | Animal Care and Ethics Committee |
| AFO | Alexa-Fluor Ovalbumin |
| AMPA | 2-amino-3-(5-methyl-3-oxo-1,2-oxazol-4-yl)propanoic acid |
| AQP | Aquaporin |
| ARA | Animal research authority |
| ASA | Anterior spinal artery |
| BFFE | Balanced fast field echo |
| cAMP | Cyclic-Adenosine monophosphate |
| CC | Central canal |
| CK | Casein kinase |
| CNS | Central nervous system |
| CSF | Cerebrospinal fluid |
| CT | Computerised tomography |
| D | Dura |
| DMSO | Dimethyl sulfoxide |
| EAA | Excitotoxic amino acid |
| ECG | Electrocardiogram |
| GFAP | Glial fibrillary acidic protein |
| H&E | Haemotoxylin and eosin |
| HiF-a | Hypoxia inducing factor-a |
| HRP | Horseradish peroxidase |
| ICP | Intracranial pressure |
| IH | Infinite-Horizon |
| IMVS | Institute of medical and veterinary sciences |
| Kir | Potassium inwardly rectifying channel |
| MRI | Magnetic resonance imaging |
| mRNA | Messenger ribonucleic acid |
| NHMRC | National Health andMedical Research Council |
| NMO | Neuromyelitis optica |
| NYU | New York University |
| OSU | Ohio State University |
| PKA, PKC | Protein Kinase A, Protein Kinase C |
| PTS | Post-traumatic syringomyelia |
| PVS | Peri-vascular space |
| ROD | Relative optical density |
| S | Syrinx |
| SAS | Subarachnoid space |
| SCI | Spinal cord injury |
| TMB | 3, 3’, 5, 5’ tetramethylbenzidine |

# Statement of originality

I hereby declare that the work presented in this thesis has not been submitted for a higher degree to any other university or institution. To the best of my knowledge this submission contains no material previously published or written by another person, and is my own work unless stated otherwise. Any contribution made to the research by others is explicitly acknowledged.

The work was carried out with ethical approval from the Macquarie University Animal Ethics Committee (ARA 2009/49, 2009/50 and 2010/26), the Macquarie University Human Ethics Committee (HE29MAY2009-D06558), the University of NSW Animal Care and Ethics Committee (ACEC 09/75A) and the Institute of Medical & Veterinary Science Animal Ethics Committee (Veterinary Services Division) (Project No. 81a/10, 48/07, 79/06).

Johnny Ho Yin Wong

31st May, 2013

## Acknowledgements

This thesis is dedicated to my wife, Sarah, to whom I am most grateful for her unconditional support and encouragement during my doctorate research journey into post-traumatic syringomyelia. She has endured the highs and lows, the sacrifices, the joys, trials and tribulations at every stage, without whom this thesis would not have been completed. I would also like to thank my parents and family for their patience and understanding.

My utmost gratitude goes to my supervisor, Marcus Stoodley, for not only his mentorship and intellectual guidance, but also his friendship and persistence in urging me to complete this thesis.

The experimental projects outlined in this thesis received much assistance from many people at different institutions, of whom I would like to particularly thank the following: From ASAM, Xin Song (research assistant) and Angela Hwang (medical student) for their technical expertise and tireless efforts in animal care, tissue processing, antibody staining and image acquisition; Sarah Hemley (post-doctoral fellow) for her advice on experimental plans and animal care. From IMVS Adelaide, the animal theatre staff, Stephen Helps, Adam Wells, Claire Jones and Ryan Quarrington for their assistance in preparing the sheep experiments, the post-operative care, and data acquisition for the telemetry project. I would also like to acknowledge the contributions by Lynne Bilston, Shaokoon Cheng (NeuRA) and Andrea Yool (University of Adelaide), who collaborated on the sheep and AQP projects; and Laverty Pathology for processing the CSF and syrinx fluid samples on the biochemistry study.

Research projects could only be conducted with financial support, and I am indebted to the NHMRC and Column of Hope Foundation for their research grants for the whole syringomyelia project. I would also like to acknowledge the Royal Australian College of

Surgeons and Neurosurgical Society of Australasia for their scholarships for supporting each year of my doctoral research. Last, and not the least, I would like to thank God for granting me the opportunities and privilege of undertaking this doctorate, and moreover a purpose in life.

# Summary

*Background and object*: Post-traumatic syringomyelia is a disabling neurological condition that occurs in approximately 28% of patients following a spinal cord injury, although not all of these cases may be symptomatic. The pathogenesis of syringomyelia is not adequately understood, and treatment is associated with high failure rates. More effective treatment can only be developed when a better understanding of the pathophysiological processes is achieved. The objectives in this thesis were: (i) to determine the biochemical profile of syrinx fluid; (ii) to develop a reproducible and relevant post-traumatic syringomyelia model; (iii) to characterise the nature of syrinx inflow and outflow; (iv) to investigate the possibility of CSF-arterial pulsation delay; and (v) to determine the effect of modulating aquaporin-4 (AQP4) water channel function.

*Methods*: Human and animal studies were performed. Human syrinx and spinal CSF samples were obtained intraoperatively for biochemical analyses. A computer-controlled motorised spinal cord impactor was used to develop a rodent model of post-traumatic syringomyelia. Syrinx fluid inflow and outflow were assessed in sheep and rodent models using kaolin to induce spinal arachoniditis, and horseradish peroxidase and fluorescent-labelled ovalbumin as CSF tracers. Telemetry pressure transmission was performed in a sheep arachnoiditis model. AQP4 expression and modulation were evaluated on rodent impactor and excitotoxic models.

*Results*: Syrinx fluid had a similar biochemical profile to CSF. A reliable direct-impact model was developed with histological resemblance to human syrinxes. In the presence of arachnoiditis, CSF flow into the spinal cord was increased along perivascular spaces with progressive CSF pulsation delay. Fluid outflow occurred in a diffuse manner into the interstitial space in a new large animal model. AQP4 expression was increased in the

impactor model, and AQP4 inhibition produced larger syrinxes with increased AQP4 expression in the surrounding areas.

*Conclusions*: Multiple factors contribute to post-traumatic syringomyelia development beyond the initial spinal cord trauma. Arachnoiditis, CSF pulsations, outflow and aquaporins are likely to play important roles in syrinx expansion. Modulation of AQP4 and other molecular processes may be potential avenues for development of new treatments.

# Chapter 1 Introduction

## *1.1 Syringomyelia*

Syringomyelia is a condition characterised by cystic cavitations in the spinal cord containing fluid identical or similar to cerebrospinal fluid or extracellular fluid [1].

It occurs in association with a number of conditions, but the pathophysiology of syringomyelia in its formation and subsequent development is not well understood.

### 1.1.1 History

"Syringomyelia" is derived from two Greek words: συριγξ ("syrinx") meaning a tube or a pipe, and μυελος ("myelos") meaning marrow [2-4]. In Greek folklore, the god Pan was attracted to a beautiful nymph, called Syrinx. Not wanting his attention, she ran away from Mount Lycaeum. Pan was in pursuit of Syrinx, and at the bank of the River Ladon, he overtook her. At this point, Syrinx prayed to the water nymphs, who changed her into a tuft of reeds. Upon embracing her, Pan grasped only a clump of reeds, which he cut and made into a pipe [4, 5].

The first pathological description of spinal cord cysts was by Charles Estienne in 1546 [1, 3, 4, 6]. This was followed by a description of a canal within the spinal cord by Fernel eight years later. In 1700, Brunner attempted to fenestrate an intramedullary cyst in a neonate with spinal dysraphism and hydrocephalus [4, 7]. Portal in 1804 outlined the clinical manifestations of syringomyelia, reporting a case of man with bilateral lower limb numbness followed by ascending paralysis and he was the first to correlate the clinical findings with the presence of the lesion [1, 8]. Surgical treatment for

syringomyelia was reported in 1892 by Abbe, who he explored and decompressed spinal cord cysts [9, 10].

In 1883, Cleland described a case of spina bifida, spinal cord cysts and hindbrain abnormalities, later termed Arnold-Chiari malformation [10-12]. Chiari classified these posterior fossa abnormalities as Chiari I and II malformation in his two publications in 1891 and 1896 [13, 14]. He recognised the association between descent of the inferior vermis, pons and medulla, with fourth ventricle elongation into the spinal canal and syringomyelia.

The association between spinal cord trauma and development of a syrinx was recognised first in 1864 by Bastian [15], who described a trauma-induced rupture of the spinal cord. Further contribution to the understanding of the post-traumatic syringomyelia was made by Wagner and Stolper in 1898 [16].

However, the diagnosis of syringomyelia remained problematic. Prior to magnetic resonance imaging (MRI), even though the condition may have been suspected, the diagnosis could only be confirmed at autopsy [1]. Since the advent of MRI in the 1980-1990's, the diagnostic capability has significantly improved.

### 1.1.2 Definition & Terminology

The term "syringomyelia" was first introduced by Ollivier d'Angers in 1827 to describe the pathological dilatation of the central canal [1, 4, 17, 18]. Other terms, such as hydromyelia, syringohydromyelia and hydrosyringomyelia have been used in the literature to describe cystic dilations within the spinal cord.

Simon in 1875, and subsequently Virchow and Leyden, proposed that the term "hydromyelia" should be used where the central canal was pathologically dilated, whilst

"syringomyelia" was reserved for cystic cavities without connections to the central canal [19]. Subsequently, Ballantine suggested combining the two entities under the one term, "syringohydromyelia" [20].

In this thesis, syringomyelia will be defined as all abnormal fluid-filled cavities in the spinal cord, except non-enlarging cavities secondary to necrosis or trauma. The various types of syringomyelia will be differentiated by qualifying terms, such as communicating, non-communicating, canalicular and extracanalicular.

### 1.1.3 Classification and pathology

Syringomyelia can be classified according to the associated condition, the presumed pathological processes, or the histological findings. Barnett, in 1973, classified syringomyelia into five groups according to the presumed pathophysiology: 1) Communicating syringomyelia associated with either congenital anomalies at the foramen magnum or acquired abnormalities at the skull base; 2) Syringomyelia as a sequel to spinal canal arachnoiditis; 3) Syringomyelia associated with spinal cord tumours; 4) Syringomyelia as a late sequel to trauma; and 5) Idiopathic syringomyelia [8, 21]. Similarly, DiLorenzo classified syringomyelia according to its causation. The subtypes were : 1) Chiari I malformation; 2) vertebral trauma; 3) basilar invagination; 4) tetraventricular hydrocephalus; 4) arachnoiditis; 5) tethered cord; 6) acquired tonsillar herniation; 7) extramedullary compression [22].

Currently, the most widely accepted classification was proposed by Milhorat et al., which was based on pathological findings from autopsy and findings from MRI [23]. This classification includes the following entities, as illustrated in Figure 1.1-1:

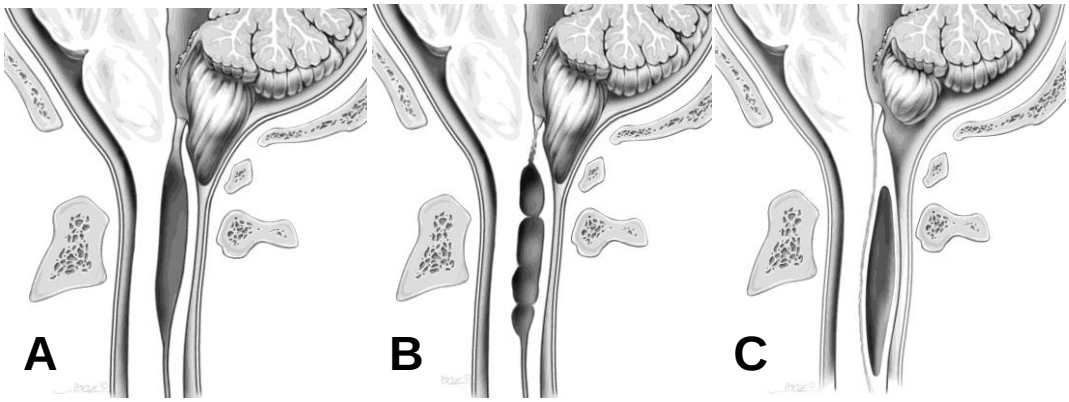


**Figure 1.1-1 Classification of syringomyelia**

**A) Communicating canalicular syringomyelia; B) Non-communicating canalicular syringomyelia; C) Extra-canalicular syringomyelia (Milhorat et al.,)**

## 1. Communicating canalicular syringomyelia

Communicating canalicular syrinxes are dilations of the central canal that are continuous with the fourth ventricle and associated with hydrocephalus, presumably from obstruction of the outlets of the fourth ventricle. Causative factors include postmeningitic and posthaemorrhagic hydrocephalus, complex hindbrain malformations, Chiari II malformation and encephalocoele, or Dandy Walker cysts [23]. Communicating syringomyelia tends to affect children and young adults, who may remain asymptomatic throughout life, or experience only minor neurological symptoms. Rupture of the syrinx into paracentral cord is rare, and treatment usually involves the insertion of a ventricular shunt [23].

Histological examination reveals dilation of the central canal, which is lined wholly or partially by ependyma. The cavity is defined caudally by central canal stenosis in acquired examples.

## Non-communicating canalicular syringomyelia

Non-communicating canalicular syrinxes are dilations of the central canal that do not communicate with the fourth ventricle and are associated with Chiari I malformation, basilar invagination, spinal arachnoiditis, extramedullary compressions, tethered cord, or acquired tonsillar herniation. Typical symptoms include segmental pain and neurological deficits [23].

Histological findings include isolated cavities with both rostral and caudal canal stenosis, extensive denuding of ependymal lining, paracentral dissection and intracanalicular septae. Dissection preferentially occurs into the dorsolateral quadrant of the spinal cord, and may extend into subarachnoid space [23].

## Extracanalicular syringomyelia

Extracanalicular syringomyelia includes cavitations that primarily involve the parenchyma of the spinal cord with no communication with the fourth ventricle. Commonly, they are caused by trauma, ischaemia or infarction, or spontaneous intramedullary haemorrhage. The typical presentation for extracanalicular syrinxes is similar to non-communicating canalicular syringomyelia, which includes segmental deficits and pain [23].

Cavities typically form dorsolateral to the central canal, in the watershed area of the cord. Histological appearance is characterised by varying degrees of necrosis, neuronophagia, and Wallerian degeneration [23]. The cavities appear to be lined by cell processes of astrocytes with flattened ependymal cells, representing the remnants of the central canal. The ultrastructural appearance is similar to communicating syringomyelia and periventricular changes in hydrocephalus. Increased gliosis in the regions surrounding the

syrinx cavity has been reported, which may be related to the duration of syrinx formation and the distensile forces within the syrinx cavity [24-26].

### Atrophic syringomyelia (ex-vacuo syringomyelia)

Spinal cord atrophy can lead to the formation of microcysts, intramedullary clefts and localised dilations of the central canal. These cavitations are caused by loss of parenchymal tissue and they do not propagate. On MRI, they are confined to the area of myelomalacia [23].

### Neoplastic cysts

Syrinx-like cavities can be formed by the cystic degeneration of intramedullary tumour, such as astrocytomas, ependymomas and other less common neoplasms. The walls of the cyst are lined by tumour and glial tissue around a solid nodule [23]. Neoplastic cysts may begin centrally and then propagate from the poles of the tumour. The fluid within neoplastic cysts contains proteinaceous fluid that is different from CSF.[23]

## 1.1.4 Epidemiology

Prior to the widespread use of MRI, the estimated incidence of syringomyelia was 0.44 per 100,000 per year [2, 27]. More recent estimates of the incidence are approximately 8.4 per 100,000 per year [22]. The impact of the improved diagnostic capabilities can be seen in the increased incidence in a syrinx series from New Zealand. The incidence was 0.76 per 100,000 in 1962-1971, compared with 4.7 per 100,000 in 1992 – 2001 [28]. The overall prevalence remained at 8.3 per 100,000, with a higher prevalence amongst the Maori and Pacific Island ethnic groups [28].

In post-traumatic syringomyelia, the incidence of symptomatic cases has been reported as between 0.3 – 8% of patients following a spinal cord injury in most clinical series [29-33]. However, from radiological and autopsy studies, the incidence was from 20 – 30%. In one particular series, the incidence was reported as high as 64% [34-36]. There was a preponderance of males in post-traumatic syringomyelia, representing over 80% of patients with this condition [30, 33]. This is a likely reflection of the gender bias in the incidence of spinal cord injury, which more commonly affects young males.

### 1.1.5 Natural history

The natural history of syringomyelia has not been well defined. There is significant variability among patients, with some having a relatively static course, and others having a rapidly progressive deterioration. Post-traumatic syringomyelia (PTS) may occur from 1 month to 37 years following the initial spinal cord injury [2, 25, 37, 38]. On rare occasions, syrinxes may undergo spontaneous resolution [39].

In Mariani's series of 50 patients with syringomyelia, 14 patients were treated conservatively with a mean follow-up of 13.7 years [40]. 36% patients had a stable clinical course, whilst 43% had slowly progressive disease within 3 years of diagnosis and 21% had a rapid progression of symptoms within a year. Schlesinger reported that 40% of patients with syringomyelia had a stable clinical course over 5 years, 33% had slow progression during a 2 – 5 year period, and 27% had rapidly progressively disease. The mean age of the cohort with rapid progression was significantly younger than those with a slower evolution (24 versus 32 years) [41]. Rossier followed 19 patients with PTS conservatively. 32% had a stable course over 3 years, while the remainder had slowly progressive disease. None had rapid progression [31].

No predictors for clinical progression have been identified [42]. However, Mariani suggested a possible correlation between the size of the spinal cord at diagnosis and the likelihood of subsequent clinical deterioration [40]. The size of the spinal cord at diagnosis may in fact be a surrogate marker of the initial size of the syrinx cavity, and hence the likelihood of progression may be related to the size of the syrinx cavity.

### 1.1.6 Clinical features

The classical description of the clinical presentation in syringomyelia is a suspended sensory disturbance, which progresses from distal to proximal upper extremity, eventually involving a cape-like distribution over the upper torso. The disturbance involving different sensory modalities is dissociated, such that there is greater sensory loss to pain and temperature than light touch or proprioception and vibration sense [43, 44]. There is also associated weakness and trophic changes in the upper extremities and spasticity in the lower extremities [41]. This constellation of symptoms can be explained anatomically by the interference of the decussating spinothalamic fibres in the anterior commissure. However, this is based on the assumption that the syrinx is located in the region of the central canal [44].

In fact, the clinical presentation of syringomyelia is varied and may reflect the different syrinx locations within the spinal cord parenchyma and their underlying associated conditions. In the Chiari-related type of syringomyelia, most patients (66%) become symptomatic in the second to third decade [40, 41]. They may present with symptoms related to the Chiari malformation or symptoms directly related to syringomyelia, such as upper limb sensory or motor changes. In patients with post-traumatic syrinxes, the mean age of presentation is 43 years [31, 41], with the main symptoms being limb weakness, sensory disturbances, radicular pain and neck or back pain [37, 38]. Their incidence is

listed in Table 1.1-1. In recent times, an increasing proportion of asymptomatic cases have been diagnosed incidentally from spinal MRI for other indications.

**Table 1.1-1 Clinical manifestations of syringomyelia**

| Symptom | Incidence | Reference |
|---|---|---|
| **Upper Limb Numbness** | 66% | Nakamura 2009 |
| | 20% | Mariani 1991 |
| | 63% | Carroll 2005 |
| | 90% | Schlesinger 1981 |
| | 20% | Rossier 1985 |
| | 71% | El Masry 1996 |
| **Upper Limb Weakness** | 54% | Mariani 1991 |
| | 20% | Nakamura 2009 |
| | 38% | Carroll 2005 |
| | 60% | Schlesinger 1981 |
| | 20% | Rossier 1985 |
| | 36% | El Masry |
| **Lower Limb Weakness** | 8% | Schlesinger 1981 |
| **Pain** | 70% | Rossier 1985 |
| | 75% | El Masry 1996 |
| **Headache** | 14% | Mariani 1991` |
| **Neck pain** | 40% | Mariani 1991 |
| | 33% | Nakamura 2009 |
| | 8% | Schlesinger 1981 |
| **Dysaesthesia / Radicular pain** | 25% | Carroll 2005 |
| | 20% | Schlesinger 1981 |
| **Hyperhidrosis** | 3% | Rossier 1985 |
| | 36% | El Masry 1996 |
| **Muscle spasm** | 6% | Carroll 2005 |
| **Areflexia** | 39% | El Masry 1996 |

The three most common initial symptoms are pain, numbness, and weakness, occurring in 50 – 90% of adult patients [40, 41, 45, 46]. The pattern of sensory changes is quite variable and the classical suspended pattern occurs in 40 – 70% of cases [31, 41]. In

Williams's series of 210 cases, 49% had dissociated sensory loss, 8% had posterior column loss only, 17% had posterior column and spinothalamic loss and 26% had no sensory loss [44]. Weakness tends to occur in combination with sensory changes, but may be asymmetrical and later in onset [2, 43]. The pain description may vary from a dull aching and constant pain to burning, dysaesthetic and intermittent in nature [43]. Its intensity may vary from being mild to severe, and aggravating factors include coughing, sneezing or straining [2, 31, 43]. Dysaesthetic pain has also been described in patients with intramedullary tumours, multiple sclerosis and traumatic injuries [46]. However, the pathological basis for neuropathic pain has not been completely eludicidated, but may be mediated by Substance-P or the sympathetic nervous system [46]. In patients with Chiari-related syringomyelia and neuropathic pain, Nakamura et al. and Ono et al. reported that the severity of pain and the likelihood of pain improvement from foramen magnum decompression appeared to be correlated with the "deviated" type of syrinx, which had a posterolateral location on MRI [47, 48]. Similarly, Attal et al. demonstrated that neuropathic pain on exertion improved after surgery, but greater improvement was noted in patients with shorter duration of syrmptoms pre-operatively [49].

Syringomyelia generally affects the cervical and thoracic spine, although the exact proportion of the regions affected varies among surgical series [33, 43]. In rare cases, syringomyelia may involve the lower brainstem, termed syringobulbia, or even the centrum semiovale, termed syringoecephalomyelia or syringocephalus [50]. When the brainstem is involved, cranial nerve abnormalities and anhidrosis of the face may be present [2, 31, 41, 51]. Other symptoms include: hyperhydrosis, loss of reflexes, muscle spasms, ataxia and scoliosis, autonomic dysreflexia, Horner's syndrome [31, 37, 38, 41, 43]. In long-standing cases, patients may present with atrophy, trophic changes and rarely

Charcot joints [41]. Bladder and bowel disturbances are rare in syringomyelia, but may be caused by extension of the syrinx to involve the conus [43].

In the paediatric population, syringomyelia may also lead to scoliosis. Resolution of syringomyelia through surgical treatment may result in improvement or stabilisation of scoliosis [52, 53].

### 1.1.7 Imaging

#### Myelography

Prior to the advent of CT and MRI, myelography was in common use. Pneumomyelography and myelography with Pantopaque (or iophendylate) were the available imaging modalities, which would demonstrate a widening of the spinal cord at the affected level and dye reaching the syrinx cavity [41]. Myelography was useful in determining the area of maximum cyst dilation, length of the syrinx and any communication with the 4$^{th}$ ventricle [43].

#### CT and CT myelography

Although the introduction of CT scanning was a significant step forward in the diagnosis of syringomyelia, CT without contrast does not have the soft tissue discrimination of modern MRIs, and images of the spinal cord can be degraded by surrounding bone [2, 18].

Spinal CT and intraspinal metrizamide have been used to evaluate CSF flow and to diagnose syringomyelia and spinal cord tumours [54]. The syrinx cavity would appear hypodense to the cord parenchyma, and, following the injection of intrathecal metrizamide at C1 – 2 level, contrast could be traced into the syrinx cavity, giving a

hyperdense appearance [31]. Contrast enhancement with metrizamide may last up to 8 hours. In patients who are contraindicated for MRI, CT myelography may be a valid alternative, demonstrating areas of subarachnoid adhesions [2].

## Magnetic resonance imaging – sequences

MRI is the diagnostic imaging of choice, as it is noninvasive, multi-planar and has better anatomical definition for neural structures than CT [2]. MRIs are useful for the initial diagnosis and serial monitoring of syringomyelia, in addition to identification of associated causes [2, 37, 43, 55, 56].


**Figure 1.1-2 T2-weighted MRI sagittal image of post-traumatic syringomyelia.**

**This patient had complete T9 paraplegia and a large syrinx expanding the spinal cord with extension to C2.**

The typical radiological features on MRI include: T1-weighted images demonstrating hypointense fluid within the syrinx cavity, and areas of gliosis, demyelination and oedema on the T2-weighted images [55, 57]. Oedema may precede the development or enlargement of a syrinx [57-59].

Though it may be difficult, it is important to differentiate myelomalacia and oedema from syringomyelia on MRI especially if direct shunting of the syrinx is planned [43, 60]. Phase-contrast cine-MRIs and, more recently, balanced fast-field echo (BFFE) sequences permit the evaluation of CSF flow around regions of obstruction, such as the foramen magnum in Chiari-related

syringomyelia and spinal arachnoiditis in post-traumatic syringomyelia [2, 61-63]. This can also be utilised post-operatively for monitoring of efficacy of treatment [61, 62, 64].

### Electrophysiology and ultrasound

Intraoperative ultrasonagraphy is useful for confirming the location of the syrinx cavity prior to the durotomy, identifying arachnoid adhesions, or webs or bands within the subarachnoid space, and once the durotomy is performed, identifying any septations or loculations within the syrinx cavity and selecting the optimal position for the myelotomy and shunt insertion [2, 65].

Electrophysiological studies generally have a limited role in the diagnosis and monitoring of syringomyelia. The findings from electromyogram and nerve conduction studies do not have sufficient specificity [43]. Therefore, preoperative electrophysiological studies have minimal utility, but intraoperative somatosensory evoked potentials may be beneficial for neurological monitoring under anaesthesia [2].

## 1.1.8 Associated conditions

There are many conditions associated with syringomyelia. In a survey of 1243 Japanese patients with syringomyelia, it was found that 51.2% of cases were associated with Chiari malformations, 3.7% with spinal dysraphism, 11% with post-traumatic syringomyelia, 6% with post-arachnoiditis and 10.5% with spinal cord tumour [66]. A complete list of associated conditions is attached in Table 1.1-2, and can be broadly divided into conditions at the craniocervical junction, and spinal conditions.

### Craniocervical junction conditions

#### *1.1.8.1.1 Chiari Malformations*

*Post-traumatic syringomyelia*

Chiari malformations are a group of craniospinal disorders characterised by descent of the cerebellar tonsils below the level of foramen magnum [10].Chiari malformations are commonly associated with a smaller posterior fossa based on volumetric measurements, and reduced retrocerebellar CSF spaces [67]. In particular, they are the most common group of conditions associated with syringomyelia, which is reported in about 30 – 85% of patients with Chiari malformations [11, 40, 66, 67].

The original descriptions of Chiari malformations by Cleland in 1883, Chiari in 1891 and Arnold in 1894, all included features consistent with Chiari Type II malformations, namely spina bifida, hydrocephalus, and descent of the cerebellar tonsils and medulla oblongata [10].

The usual classification of Chiari malformations consists of Chiari Types I, II, III and IV [10]. More recently, however, a new classification has been introduced, which include entitites such as Chiari Type 0 and Type 1.5 [11, 68].

Chiari Type I malformations are characterised by descent of the cerebellar tonsils into the cervical spinal canal, usually without associated hydrocephalus [10]. Based on MRI measurements, cerebellar tonsillar descent of up to 3 mm below the foramen magnum has been observed in normal subjects, while Chiari I patients had descent greater than 5 mm [69]. Relative to the volume of the cerebellum, a small posterior fossa is present and tonsillar descent occurs, which may be congenital or acquired in origin.

**Table 1.1-2 Conditions associated with syringomyelia**

**(From Brodbelt AR, Stoodley, MA, Jones NR. Non-traumatic syringomyelia. In: The Cervical Spine Research Society, eds. The cervical spine. 4th Edition. 2005. [70])**

| Craniocervical junction | Spine |
|---|---|
| **Congenital** | **Congenital** |
| *Chiari malformation Type 1* | *Myelomeningocoele* |
| *Chiari malformation Type 2* | *Tethered spinal cord* |
| *Dandy-Walker malformation* | *Diastematomyelia* |
| *Posterior fossa arachnoid cysts* | *Lipomyelomeningocoele* |
| *Apert's syndrome with tonsillar herniation* | *Spinal Dermoid* |
| *Crouzon's syndrome* | *Neurenteric cysts* |
| *Noonan's syndrome* | *Sacral agenesis* |
| *Achondroplasia* | *Anorectal anomalies* |
| | *Familial spinal arachnoiditis* |
| **Acquired** | **Acquired** |
| *Tonsillar herniation secondary to*: | <u>*Intramedullary*</u> |
| Posterior fossa tumour | *Neoplastic* – Primary ependymoma, haemangioblastoma, astrocytoma, lymphoma, metastases |
| Supratentorial tumours | *Non-neoplastic* – Spinal trauma, demyelination, multiple sclerosis, spinal sarcoidosis, tuberculosis |
| Lumboperitoneal shunts | |
| Chronic subdural haematoma | |
| Lhermitte-Duclos disease | |
| Nocardia brain abscess | |
| *Basilar impression* | <u>*Extramedullary*</u> |
| *Pannus deformity of the odontoid* | *Neoplastic* – Meningioma, schwannoma, lymphoma, myeloma, lipomatosis |
| *Arachnoiditis* | *Non-neoplastic* – Intervertebral disc protrusion, cervical spinal stenosis, arachnoiditis, arachnoid telangiectasia inducing arachnoiditis, intraventricular haemorrhage, subarachnoid haemorrhage, meningitis, arachonid webs, arachnoid ossification, sarcoidosis, spinal lipomas, multiple sclerosis. |
| *Idiopathic* | *Idiopathic* |

In congenital types, a disorder of mesodermal origin has been postulated to produce small posterior fossa volume. Milhorat et al. examined 364 patients with Chiari I malformations with MRI and demonstrated significantly smaller total posterior fossa and CSF volumes, with reduced height of the supraocciput, increased slope of tentorium and clival hypoplasia [67]. Interestingly, controversy exists whether a correlation exists between the extent of tonsillar herniation and the likelihood of syringomyelia [71, 72].

Chiari Type II malformations are characterised by descent of the cerebellar vermis, brainstem and fourth ventricle through the foramen magnum [10, 68]. They are associated with myelomeningocoele, hydrocephalus, and other complex intracranial abnormalities. Similar to Chiari Type I, the extent of cerebellar descent does not correlate with the severity of symptoms [73].

Chiari Types III and IV occur much more rarely. Type III is associated with caudal herniation of the medulla and an occipital or cervical meningocoele, while type IV has features of cerebellar aplasia and agenesis of the tentorium cerebelli. Recently, Chiari 1.5 has been introduced to describe cases with a combination of features of Chiari Types I and II, while in Chiari 0, disturbances in CSF flow are present without hindbrain herniation [10, 11, 74-76].

#### *1.1.8.1.2 Other conditions at craniocervical junction*

A number of other conditions at the craniocervical junction have been associated with syringomyelia, including foramen magnum arachnoiditis or tumours within the posterior fossa causing CSF obstruction at the foramen magnum [77, 78]. These include haemangioblastic meningiomas, synovialoma, medulloblastoma and meningiomas.

Resection of foramen magnum tumours in such cases resulted in resolution of both the obstructive hydrocephalus and cervical syringomyelia.

Although the above case reports are rare, they further illustrate the association between craniospinal pathologies with syringomyelia. Despite the widely accepted concept that syrinxes develop as a result of alterations to CSF flow at the craniocervical junction, the relationship and the precise mechanism between CSF flow and syrinx development remain nebulous.

## Spinal conditions

Spinal conditions associated with syringomyelia include spinal cord injury, arachnoiditis, spinal cord tumours, other extrinsic compressive lesions and spinal dysraphism. This group of conditions has been termed "Primary spinal syringomyelia" by Batzdorf [34].

#### *1.1.8.1.3 Post-traumatic*

Syringomyelia is a well-known cause of subsequent neurological deterioration following a spinal cord injury. It presents clinically in 1 - 9% of spinal cord injury cases, but has a incidence of about 21-28% based on autopsy and radiological findings [2].

Spinal cord injuries are associated with subarachnoid scarring, spinal column deformity and stenosis, which are important postulated aetiological factors for post-traumatic syringomyelia [2]. Post-traumatic syrinxes may develop from 1 month to 37 years following the initial spinal cord injury, with the mean of 9 years post injury [29-31, 37]. Whether there is a correlation between the severity of the spinal cord injury and the time interval to development of post-traumatic syringomyelia is controversial [30, 31, 42, 79]. Both el Masry and Rossier reported an earlier onset of post-traumatic syringomyelia in

complete spinal cord injuries when compared with incomplete injuries (6.9 & 7.5 years *versus* 9.4 & 9.9 years respectively) [31, 42]. This difference was, however, not statistically significant.

A possible predisposing factor to syrinx formation is the severity of the initial spinal cord injury. Rossier et al. reported the incidence of post-traumatic syringmyelia as 2.4% in patients with incomplete spinal cord injuries, as compared with 3.9% in complete injuries [31]. In a systematic review by Bonfield et al., the proportion of post-traumatic syringomyelia patients who had a complete spinal cord injury varied from 69 – 82%, as compared to 42 – 47% of spinal cord injury patients in general [29]. The degree of residual spinal deformity may also predispose to subsequent syrinx formation with a residual kyphosis of greater than 15 degrees or spinal stenosis of greater than 25% having twice the incidence of post-traumatic syringomyelia [29].

#### *1.1.8.1.4 Post-arachnoiditis (non-traumatic)*

The association between arachnoiditis within the spinal subarachnoid space and syringomyelia has been well established [80-83]. Besides trauma, arachnoiditis may arise as a consequence of: infections, including bacterial and tuberculous meningitis; subarachnoid haemorrhage; and iatrogenic causes, such as myelograms, surgery and spinal anaesthetics [18, 83-86].

#### *1.1.8.1.5 Spinal cord tumours*

A wide range of spinal cord tumours has been associated with syringomyelia. In a case series of 100 intramedullary tumours, Samii et al. reported that syringomyelia occurred in 45% of patients [87]. The syrinx cavities were more likely to extend rostrally in 49% of cases, compared with a caudal direction in 11%, and both directions in 40% [87].

Syringomyelia was most commonly found in association with haemangioblastomas and ependymomas, and less commonly with astrocytomas [88, 89]. Regardless of the histology of the intramedullary tumour, Samii et al. stated that disturbances of CSF and extracellular flow were considered the more important causative factors in syrinx formation [87]. However, the exact mechanism by which intramedullary tumours cause CSF disturbances, nor how such disturbances lead to eventual syrinx formation have only been theorised and have not been investigated experimentally.

#### *1.1.8.1.6 Spinal dysraphism*

Occult spinal dysraphism encompasses a number of conditions, including thickened filum terminale, lipoma, lipomeningocoele and diastematomyelia [90-92]. Spinal dysraphism may result in tethering of the spinal cord and is associated with syringomyelia in the region of the tethering in 30 – 50% of cases, often rostral to underlying lesion [90-93]. The extent of syrinx involvement appears to be related to the severity of spinal dysraphism, with the caudal third of the spinal cord affected in spina bifida occulta. In contrast, syringomyelia may affect the cervical spinal cord in myelomeningocoeles [92, 93]. Treatment involves detethering of the spinal cord, which can result in resolution of syrinx cavities.

#### *1.1.8.1.7 Other extrinsic compressive lesions*

Syringomyelia has been uncommonly described in association with extrinsic compression from neoplasms, cervical spondylosis, disc prolapses, lipomas and cysts [94-99]. The syrinx cavity may be either cranial or caudal to the underlying lesion [100]. In the majority of cases, relief from the extrinsic compression results in resolution of the syrinxes [94-96].

## Idiopathic

Despite the available imaging, an underlying cause may not identified in some patients [85]. Nakamura et al. suggested a classification of two types of idiopathic syringomyelia in their series of 15 patients according to the extent of the syrinx and its natural history [45]. The "localised" type was defined as syrinxes extending less than three vertebrae, whilst the "extended" type had syrinxes distributed over four or more vertebral levels. The localised group of 12 patients was clinically stable when treated conservatively, with no further enlargement of syrinxes on MRI at a mean follow-up of 10 years. The extended group of three patients had neurological deterioration and was treated with syringosubarachnoid shunts, as an underlying cause could not be identified. There have been several case reports of spontaneous resolution of idiopathic syringomyelia, while Iskandar et al. reported syrinx resolution in a series of five patients following a posterior fossa decompression [75, 101-103]. The exact mechanism for this is not known.

However, with the advent of more sophisticated imaging, such as cardiac-gated and higher resolution MRI, idiopathic syringomyelia may have an underlying aetiology, such as arachnoid adhesions or webs [56, 104, 105].

### 1.1.9 Treatment

Satisfactory treatment for syringomyelia remains elusive. At present, there is no consensus regarding the indications or methods for treatment. Several surgical techniques have been described, with most series reporting reasonable short term efficacy rates up to 5 years, and significant recurrence or failure rate thereafter. Mariani reported 36 patients who underwent surgical treatment for syringomyelia, 72% of surgical patients showed

short-term improvement at 1 year, but 63% of patients had recurrence of symptoms at 3 years' follow-up [40].

Surgical techniques generally aim to re-establish normal CSF pathways, or to drain the syrinx cavity. If possible, the therapeutic approach should be directed at the underlying cause. In Chiari-related syringomyelia and other disorders at the craniocervical junction, restoration of the subarachnoid space dorsal to the cerebellar tonsils at the foramen magnum with a posterior fossa decompression appears to result in syrinx resolution in the majority of cases. Spinal cord detethering or adhesiolysis with or without duraplasty have been performed for arachnoiditis with similar results [82]. In cases of external compression, such as from a prolapsed disc or extradural tumour or spinal deformity, removal of the underlying lesion may result in collapse of the syrinx [34, 106, 107].

Syrinx drainage procedures include syrinx shunting, cord transections in patients with complete spinal cord injuries, and terminal ventriculostomy [2, 42]. Other procedures, such as omental transposition for post-traumatic syringomyelia, have been less commonly used [42].

## Indications

The optimal timing of treatment is controversial. Whilst some authors have advocated early treatment to prevent clinical deterioration, [22, 108] most authors agree that surgical treatment is indicated for worsening clinical symptoms, deterioration of neurological function and progressive myelopathy [2, 29, 43, 109, 110]. The objective of surgical treatment is to arrest the clinical deterioration and possibly to reverse the neurological deficits [42, 110]. In patients with syrinx enlargement on serial radiological imaging, treatment may be indicated. However, the evidence for this is weak, and, in a systematic

review by Bonfield et al., operative treatment on the basis of radiological progression is not recommended [29].

Conservative treatment with serial MRIs may be suitable in patients with stable disease, minimal functional impairment or poor general medical condition [2, 43, 111].

## Posterior fossa decompression

Generally, posterior fossa decompression is the preferred surgical procedure in patients with syringomyelia in association with Chiari-I malformation or other conditions of the craniocervical junction [112]. However, in cases secondary to hydrocephalus, treatment of the underlying association may be appropriate [22].

#### *1.1.9.1.1 Operative technique*

Posterior fossa decompression involves a midline suboccipital craniectomy, and C1 laminectomy, such that the posterior rim of the foramen magnum is removed and the dura is allowed to expand posteriorly [113-116]. However, many variations exist, particularly in regards to the degree of osseous removal, the necessity for dural and arachnoid opening, resection of the cerebellar tonsils, plugging of the opening of the central canal, the significance of pseudomeningocoele formation, and the use and specific materials for duraplasty [113, 114, 117-121]. In the series by Attenello et al., better outcomes were obtained with an expanded polytetrafluoroethylene graft, as compared with pericranium [114].

As reported in a survey amongst paediatric neurosurgeons in 2006, 85% of respondents would perform a posterior fossa decompression for Chiari-I malformation with syringomyelia [112]. However, amongst the respondents, 7% would perform bony

decompression alone, 36% would open the dura, while 27% would resect the cerebellar tonsils [112]. The wide spectrum of opinions regarding the optimal technique for posterior fossa decompression highlights the controversies in treatment, especially when no significant differences in efficacy have been demonstrated among the various techniques.

## Adhesiolysis and duraplasty

For syringomyelia without a Chiari-malformation, the optimal treatment option remains unclear. In patients with focal areas of arachnoiditis or CSF obstruction, adhesiolysis with or without duraplasty may be the preferred procedure. Pathology involving the subarachnoid space may be apparent on pre-operative imaging, such as the CSF flow studies with cine-MRI or BFFE sequences on MRI [122].

The theoretical benefits of adhesiolysis and duraplasty include: (1) restororation of the spinal subarachnoid space and spinal cord movement by detethering the spinal cord, and expanding the subarachnoid space with a dural patch [18, 22]; (2) avoidance of a myelotomy and introduction of a foreign body, with risks of infection or spinal cord tethering [34]; Surgical series have reported better efficacy rates, albeit with similar or slightly higher complication rates when compared with syrinx shunting [2].

#### *1.1.9.1.2 Operative technique*

After a laminectomy is performed over the region of the syrinx and careful extradural haemostasis is obtained, the dura is opened and hitched up to the wound edges. The dural incision is extended to regions free of arachoniditis, both cranial and caudal to the region of arachnoiditis [34]. Arachnoid adhesions are divided with sharp dissection, such that CSF loculations communicate with the adjacent subarachnoid space. The spinal cord

should be detethered as much as possible, although it may be necessary to leave a thin layer of scarring over the spinal cord to avoid disturbing the blood supply or damaging the spinal cord [2].

In instances where the spinal cord cannot be safely detethered, a subarachnoid-subarachnoid shunt may be inserted from unaffected cranial to caudal subarachnoid space. This allows CSF communication around the region of arachoniditis.

The dura may be closed primarily or with a duraplasty in a watertight fashion. Dural graft options include artificial dural patches and autologous fascia, such as fascia lata and thoracolumbar fascia. Artificial fascia may be preferred as there is less tendency to cause additional scarring [34].

## Shunting procedures

Initial attempts at decompressing the syrinx cavity used simple needle aspiration or myelotomy alone [41]. This is no longer recommended because of poor long-term results due to the inability to maintain continued drainage of the syrinx [2, 34, 123].

Shunting procedures are usually indicated in instances of failed treatments from posterior fossa decompression or arachnolysis and duraplasty, extensive arachnoiditis, or in syrinxes where the region of spinal cord tethering cannot be identified [2, 27, 124]. In some instances, larger syrinxes may be better treated with direct syrinx shunting [124]. Several shunting options are available, including syringosubarachnoid, syringopleural or syringoperitoneal shunts [122]. The technique of choice is more based on the surgeon's preference, rather than any firm evidence, with no demonstrated superiority of one technique over another [32, 42]. Proponents for the syringopleural shunts include Sgouros et al., Batzdorf et al. and diLorenzo et al. [22, 125, 126]. The difficulty with

syringopleural and syringoperitoneal shunts is the possibility of spinal cord tethering. Syringosubarachnoid shunts have been recommended by Tator et al. and Iwasaki et al., but they rely on a subarachnoid space that is free of scarring and able to absorb CSF [34, 127, 128].

Syrinx shunts have the advantages of being technically less challenging and offering immediate drainage and collapse of the cystic cavity. The disadvantages include the neurological deficits associated with the myelotomy for the shunt, and the difficulty of draining multiple or septated cysts [34].

#### *1.1.9.1.3 Operative technique*

Intraoperative images of the operative technique are illustrated in Figure 1.1-3. Following a laminectomy and midline durotomy, the syrinx cavity and an adequate cranial or caudal subarachnoid space is identified with an intraoperative ultrasound. Myelotomy is performed over the thinnest portion of the spinal cord, preferably along the posterior median sulcus or dorsal root entry zone [2, 129, 130]. The shunt is usually placed in the cranial direction at the most caudal aspect of the syrinx cavity, to minimise further neurological damage.

In a syringosubarachnoid shunt, the drainage holes are placed both internal and external to the syrinx cavity to allow for communication to the subarachnoid space [122]. The distal catheter should be positioned in a subarachnoid space free of any arachnoiditis or adhesions. The catheter is secured with a pial suture to prevent shunt migration.

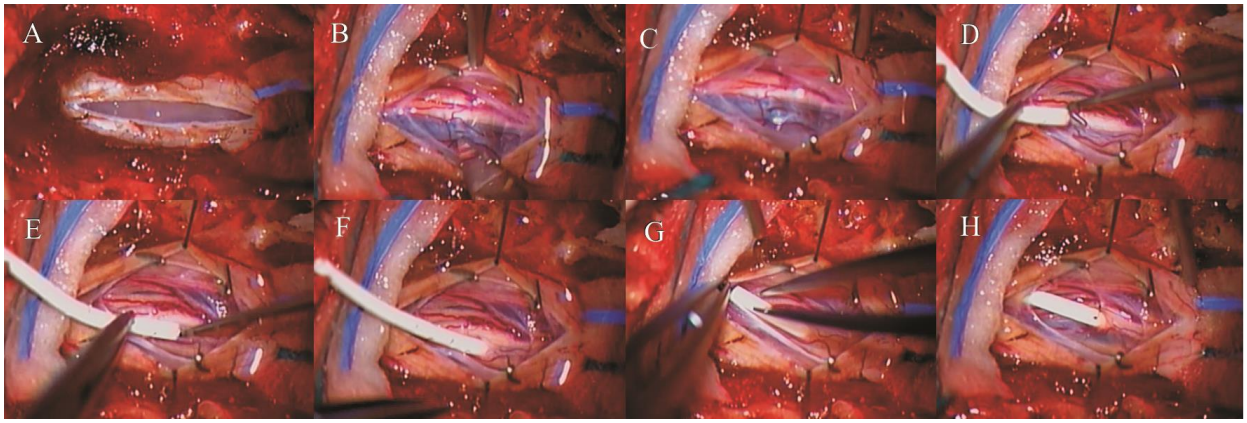


**Figure 1.1-3 Intraoperative images of syringe-subarachnoid shunt insertion**

**A) Durotomy; B) Midline myelotomy; C) Syrinx cavity entered and syrinx fluid drainage under pressure; D) – G) Insertion of spinal end of lumboperitoneal shunt catheter into syrinx cavity with the assistance of a blunt hook; H) Distal end of catheter positioned into subarachnoid space.**

In a syringopleural shunt, drainage holes are placed entirely within the syrinx cavity to avoid overdrainage and resultant low-pressure headaches [2]. The distal catheter is tunnelled to the pleural space and secured with a suture.

Minor variations to syrinx shunts have been reported, such as insertion of a syringosubrachnoid shunt through a “keyhole” hemilaminectomy approach [129-131].

## Other treatments

Besides simple aspiration, other techniques have included terminal ventriculostomy or spinal cord transections. This has been performed in paraplegic patients, in whom a small minority showed symptomatic improvement, but the majority of patients continued to deteriorate [2]. Omental grafting, implantation of foetal tissue and radiotherapy have also been attempted to obliterate syrinx cavities with limited success [41, 132].

Recently, Lam et al. detailed a retrospective series of seven patients with a thecoperitoneal shunt to bypass an obstructed spinal subarachnoid space. Despite complications occurring in three patients, there were symptomatic improvements in six

patients [133]. Similarly, Chang et al reported a case of syrinx resolution after insertion of a subarachnoid-peritoneal shunt with an adjustable valve. They reported an initial expansion of the syrinx after insertion of the shunt, but resolution of the syrinx when the subarachnoid pressure was increased [134].

In patients with hydrocephalus and syringomyelia, treatment of the hydrocephalus with a ventriculoperitoneal shunt or endoscopic third ventriculostomy may result in resolution of the syrinx cavity [97, 135].

## Efficacy and complications

Posterior fossa decompression for Chiari-related syringomyelia is the most effective of the available techniques. Short-term efficacy has been reported as 82%, with a relapse rate of 50% in Mariani's series [40]. In contrast, other surgical series have reported reduction in the size of syrinxes over a median time period of 3.6 – 5 months after posterior fossa decompression, which was maintained at follow-up of up to 8 years with serial MRIs [114, 116, 136]. Symptomatic improvement or clinical stability was achieved in 94% of patients and preceded radiological improvement. However, in several series, including Wetjen et al. and Aghkahani et al., a moderately large proportion of patients had incomplete symptom resolution [116, 136].

The main complications of posterior fossa decompression include pseudomeningocoele formation and CSF leakage, chemical and bacterial meningitis, hydrocephalus and spinal instability [112].

Syringosubarachnoid shunts were effective in relief of pain in approximately 80 – 89% of patients, weakness in 63%, ascending sensory level in 30% and areflexia in 10% [31]. Syringosubarachnoid shunts have good short-term results but are prone to blockage and

recurrence of syringomyelia [43, 86, 109, 127]. In the syrinx shunt series from Sgouros et al, and Batzdorf et al., failure rates were reported at about 50% [34, 125]. Syringopleural shunts have similar results, with 69% of patients reporting 'good' outcomes, and 15% 'fair' [42]. Other shunt series have cited complication rates of 10 – 100 %, which included: (1) shunt obstruction; (2) tethering of spinal cord; (3) low CSF-pressure state; (4) shunt-related infection; (5) shunt dislocation; (6) epidural fibrosis and (7) spinal instability [2, 131].

Schlesinger et al. reported a series of 18 patients who underwent adhesiolysis and duraplasty. This was associated with efficacy and relapse rates of 38% and 44% respectively [41].

### 1.1.10 Conclusion

At present, the long-term clinical outcomes reported in many surgical series reveal that treatment for post-traumatic syringomyelia is suboptimal. The ideal treatment has not yet been established, but it appears that restoration of the spinal subarachnoid space is an important factor to syrinx resolution. Surgery is currently the mainstay of treatment, but the precise mechanism of action is not known. In particular, the effect of treatment on altering CSF flow and pulsations has not been established. A more detailed understanding of the pathophysiology of syringomyelia is required to develop novel treatments.

## *1.2 Pathophysiology of syringomyelia*

The term, "syringomyelia", was first introduced by Ollivier d'Angers in 1827 to describe pathological dilatation of the central canal. Since then, it has been discovered that cystic cavities within the spinal cord may occur outside of the central canal [1, 4]. The pathophysiology of both canalicular and extracanalicular syringomyelia remains

enigmatic. Many theories have been proposed regarding the mechanism for initial cyst formation and subsequent expansion. The following section will be an overview of the theories on the pathogenesis of canalicular and extracanalicular syringomyelia.

### 1.2.1 Theories for pathogenesis of canalicular syringomyelia

According to the autopsy studies by Milhorat et al., communicating syringomyelia was associated with fourth-ventricular outlet obstruction, while non-communicating syringomyelia was associated with Chiari-I malformation, basilar invagination and spinal arachnoiditis [23, 97]. Of these conditions, the most common association is Chiari-I malformation. Indeed, most of the theories for pathogenesis of canalicular syringomyelia have concentrated on the Chiari-related subtype.

#### Developmental anomalies and dysraphism

Early descriptions of syringomyelia were associated with hydrocephalus and myelomeningocoele, which probably were related to the Chiari-II malformation [1, 7, 13, 14]. This led to the conclusion that syringomyelia itself was a developmental anomaly or part of a dysraphic syndrome. Olliver d'Angers in 1827 proposed that syringomyelia resulted from an arrest of spinal cord development [17, 137]. Cleland observed dilatation of the central canal in a patient with spina bifida and hydrocephalus, which was associated with descent of the brainstem [12]. He theorised that primary dysgenesis of the brainstem caused hydrocephalus and dilatation of the central canal, with rupture of the myelocoele into the spinal canal. Hindsdale in 1897 postulated that syringomyelia arose from developmental defects of the glial and ependymal cells [1].

Later, it was discovered that syringomyelia was not necessarily associated with hydrocephalus or Chiari malformations, but could occur in association with acquired conditions, which were unrelated to developmental anomalies [138].

## Familial / genetic factors

Genetic factors have been implicated in the pathogenesis from several reports of familial clustering of syringomyelia [139-143]. The incidence of familial syringomyelia is rare, but appears to be more common in Chiari-related syringomyelia than other aetiologies[144]. It is likely that there is a genetic predisposition to development of Chiari malformations, but not necessarily to syringomyelia [139].

Evidence in support of a genetic basis for Chiari malformations includes familial aggregation and association with other genetic disorders, such as achrondoplasia, Klippel-Feil, phakomatoses and primary basilar impression [139]. However, the mode of inheritance and the gene responsible have yet not been confirmed, with some studies reporting an autosomal dominant transmission, and an autosomal recessive transmission in others [67, 140, 143]. At present, a causal association between genetic factors and syringomyelia still remains tenuous.

## Birth trauma

Although the precise mechanism has not been elucidated, a number of authors have observed a higher incidence of difficult births in syringomyelia patients [145-147]. Williams claimed that difficult birth was the main contributing factor to communicating syringomyelia [147, 148]. He suggested that moulding of the skull bones, compression of the brain downwards into the foramen magnum, transient swelling due to anoxia, haemorrhage into the basal cisterns and resultant hydrocephalus were contributory [147].

Newman et al. also investigated the influence of birth trauma. A history of forceps delivery and difficult birth was more prevalent in Chiari patients with syringomyelia, than Chiari patients without syringomyelia [146]. It was hypothesised that the combination of further impaction of the cerebellar tonsils, rupture of the ependyma of the central canal, and resultant arachnoiditis from traumatic subarachnoid or intraventricular haemorrhage from birth trauma would lead to obstruction of CSF flow and subsequent syrinx development [146]. However, the causal relationship between CSF obstruction and the development of syringomyelia remains a theory without any substantial experimental evidence.

## Inflammatory and immunological factors

An inflammatory process has also been implicated in the initial formation of syringomyelia, as well as its subsequent enlargement. Inflammation involving the central canal may result in occlusion and segmental dilatation of the canal. Hallopeau, in 1869, described syringomyelia as an inflammatory process of ependymal cells which undergo sclerotic change, causing obstruction to the central canal and subsequent syrinx formation [1]. More recently, Milhorat et al. demonstrated that, in suckling hamsters injected with reovirus type I, obstruction of the central canal occurred with disorganisation of the ependyma, subependymal glial scarring and intracanalicular gliosis [149]. These histological findings correlated with human autopsy specimens of the central canal in 232 normal subjects [150]. However, viral infections have not been identified in human syrinx patients.

Alternatively, arachnoiditis may occur following meningitis, subarachnoid haemorrhage or chemical agents, such as from radiopaque myelographic contrast [151]. Arachnoiditis,

particularly at the craniocervical junction, can produce syringomyelia with a similar clinical presentation to Chiari malformations [78, 84, 152].

Immunological mechanisms have been suggested by Blagodatsky et al., who found elevated levels of immunoglobulins (IgG, IgM and IgA) in the syrinx fluid from 16 of 22 Chiari patients with syringomyelia [153]. However, there have been limited further studies in support of the immunological hypothesis.

## Secretory hypothesis

Based on the fact that syrinx fluid had a similar appearance to CSF, it was postulated that CSF was secreted by ependymal cells within the central canal, which caused syrinx cavities to form when obstruction of the central canal occurred [154, 155]. There is limited evidence to support this concept.

## Hydrodynamic theories

The hydrodynamic theories have focused on different mechanisms by which alterations in pressure and pulsations within the subarachnoid space promote CSF flow into the spinal cord.

#### *1.2.1.1.1 Water-hammer*

The original hydrodynamic theory was described by Gull in 1862, who noted accumulation of CSF within the central canal, which he termed, "hydromyelus" [1, 156]. Subsequently, Cleland and Lichtenstein separately proposed that a cavity of the spinal cord could develop due to hydrocephalus and fourth ventricular outlet obstruction [1, 12, 157]. Gardner and Angel refined this concept, which became popularised and is commonly known as the "water-hammer effect" [158, 159]. Gardner postulated that, in

the setting of fourth ventricular outlet obstruction, systolic arterial pulsations would cause an increase in intracranial pressure that would direct CSF pulsation downwards into the spinal central canal [22, 160]. This would cause expansion of the central canal to form a syrinx.

Gardner's theory is potentially applicable for communicating syringomyelia, where the connection between the fourth ventricle and the spinal central canal remains patent. However, strong evidence against this theory is that the central canal is commonly not patent in adults, and, in the majority of cases, syringomyelia is not associated with hydrocephalus and fourth ventricular outlet obstruction [63, 97, 150, 160].

#### *1.2.1.1.2 Craniospinal dissociation*

Williams formulated the "craniospinal dissociation" theory", which stated that CSF would be driven into the central canal due to the pressure differential between the intracranial and spinal compartments after exertion [147]. He postulated that, during exertion from coughing or straining, increased pressure in the spinal subarachnoid space would drive CSF into the cranial cavity, but CSF was prevented from returning into the spinal subarachnoid space once the pressure had normalised due to the descent of the cerebellar tonsils at the foramen magnum. CSF would then preferentially travel into the fourth ventricle and then into central canal, causing enlargement of central canal and eventually formation of syringomyelia [22, 160]. Plugging of the obex during foramen magnum decompression was therefore advocated to prevent CSF from draining into the syrinx cavity.

The objection to this theory is similar to Gardner's water-hammer theory. The craniospinal dissociation theory relies on a patent communication between the fourth

ventricle and central canal. Also, there is no evidence that, in syringomyelia associated with Chiari malformations and other posterior fossa abnormalities, such as arachnoiditis or tumours, any valve effect exists [63, 160]. In a review by Ball and Dayan, there was no benefit demonstrated in plugging of the obex [161]. This surgical technique is no longer recommended due to significant mortality associated.

#### *1.2.1.1.3 Respiratory transmedullary*

In contrast to William's craniospinal theory, Ball and Dayan proposed that tonsillar hermiation in Chiari malformation prevented rostral CSF flow at the foramen magnum. They observed from myelograms that radiographic dye ascended from the lumbar cisterns to the cervical subarachnoid space and subsequently into the syrinx cavity in patients with Chiari-I malformations [161]. Based on these studies, they proposed that during periods of exertion, such as coughing or straining, upward CSF flow would be obstructed by the cerebellar tonsillar herniation and then diverted into the spinal cord parenchyma via perivascular spaces [161]. According to this theory, fluid will accumulate in the extracellular spaces within the spinal cord, and eventually coalesce to form a syrinx cavity. The central canal will only be involved if the syrinx cavity ruptures into it.

#### *1.2.1.1.4 Obstructed CSF drainage*

Aboulker postulated that CSF flowed rostrally into the fourth ventricle from the central canal. Obstruction to either venous drainage or CSF flow at the foramen magnum would result in increased oedema within the spinal cord. The increased oedema would subsequently lead to syrinx formation if alternative CSF drainage pathways could not be established [162].

#### *1.2.1.1.5 Arterial transmedullary*

Similar to Ball and Dayan's theory, Heiss et al. and Oldfield et al. suggested that the route of CSF flow was transmedullary via the perivascular spaces [163, 164]. Based on observations made from MRI CSF flow studies, they emphasised the downward movement of cerebellar tonsils in Chiari I patients, which acted as pistons in response to systolic arterial pulsations [163, 164]. This piston action would propel CSF caudally in the spinal subarachnoid space and then into the spinal cord via the perivascular spaces [22].

However, pressure recordings of the syrinx cavity and spinal subarachnoid space have shown that the pressure within the syrinx is at least as high as the surrounding subarachnoid pressure [165, 166]. Therefore, the objections to this theory are: (1) the pressure generated by the cerebellar tonsils is unlikely to be sufficient to promote fluid flow into the syrinx cavity against a pressure gradient; (2) in other conditions associated with syringomyelia, cerebellar tonsillar movement is limited.

#### *1.2.1.1.6 Arterial pulsation driven perivascular space flow*

Experimental evidence for perivascular CSF flow is based on animal and computational experimental studies. Stoodley et al. demonstrated that CSF flow into the spinal cord occurred via perivascular spaces when CSF tracers were injected into the cisterna magna in sheep and rat models [167]. This flow was dependent on arterial pulsations [168]. Furthermore, in a model of canalicular syringomyelia, CSF tracers were seen along perivascular spaces and into the syrinx cavity within the central canal [169].

Bilston et al. have examined the wave properties of flow in the perivascular spaces and subarachnoid space in computational models. They demonstrated that mismatch in timing

between the arterial and CSF pressure wave pulsations at the interface between the perivascular space and the subarachnoid space could result in increased flow during systole [170, 171]. This could act as a partial one-way valve and may drive fluid along the perivascular space against a mean positive pressure gradient between the syrinx and subarachnoid space. In a recent study, Clarke et al. (unpublished data) demonstrated that the timing mismatch was present in patients with Chiari malformation, but not in normal subjects based on measurements from cine-MRI CSF flow studies.

#### *1.2.1.1.7 Elastic-jump hypothesis*

Using fluid-filled coaxial elastic tubes as an experimental model, Carpenter et al. proposed the “elastic-jump” hypothesis [172]. They suggested that coughing or straining could produce a pressure wave that would result in a focal increase in pressure within the spinal cord at a region of stenosis in the subarachnoid space. In the instance of Chiari malformations, the stenosis could be caused by tonsillar herniation [172]. However, Elliot et al. evaluated the assumptions of the elastic jump theory from a mechanical stand-point and concluded that the magnitude of the effect was too small to be significant [160, 173].

## Other sources of syrinx fluid

The major problem with the hydrodynamic theories is that the pressure within a syrinx cavity must at some time be higher than the spinal subarachnoid space in order for the syrinx to enlarge [165, 166]. Other sources of syrinx fluid, such as extracellular fluid, disruptions in blood-spinal cord barrier or other cellular transport mechanisms, have been proposed to contribute to syrinx expansion [160].

#### *1.2.1.1.8 Accumulation of extracellular fluid*

Klekamp proposed that extracellular fluid accumulation could contribute to both canalicular and extracanalicular syringomyelia, either from an obstruction to extracellular fluid flow into the spinal subarachnoid space, or extracellular fluid exceeding the interstitial space volume in the spinal cord. This may be caused of blockage of perivascular spaces, cord tethering, or changes in arterial or venous circulation [1].

Levine et al. and Koyanagi et al. both suggested that impairment of venous drainage was the cause of increased extracellular fluid in the spinal cord [138, 174]. Levine et al. hypothesised that compression of the venous circulation was due to the difference in subarachnoid pressures across the CSF obstruction and would encourage increased leakage of fluid from the microcirculation [138]. In contrast, Koyanagi explained that the accumulation of interstitial fluid was due to impaired ECF drainage into the venous system [174].

#### *1.2.1.1.9 Intramedullary pulse pressure theory*

Josephson et al. proposed that obstructions to CSF by the cerebellar tonsils in Chiari malformation would result in lower subarachnoid pressure distal to the CSF block, but the pulse wave continues in the spinal cord, thus causing expansion of the spinal cord and accumulation of extracellular fluid, leading to syrinx formation [175]. Greitz et al. and Rusbridge et al. had a similar hypothesis but suggested that the expansion of the spinal cord was due to the Venturi effect from decreased subarachnoid space pressure [176, 177].

Objections to these theories are based on the following intra-operative observations: (1) The spinal cord may remain swollen when the Venturi effect has been eliminated after

durotomy and CSF in the spinal subarachnoid space has been drained. (2) The pressure within the syrinx cavity appears much higher than the surrounding spinal cord or subarachnoid space and the passive filling implied by these theories cannot overcome this pressure gradient [160].

#### *1.2.1.1.10 Disruptions in blood-spinal cord barrier*

Ravaglia et al. postulated that CSF obstruction, for example, in Chiari malformation may lead to pressure-induced breakdown of the microcirculation, resulting in intra-spinal leakage and fluid accumulation [178]. The evidence for this hypothesis, however, is limited.

### 1.2.2 Theories for pathogenesis of extra-canalicular syringomyelia

A number of factors have been studied regarding the pathogenesis of extra-canalicular syringomyelia. Multiple factors and different mechanisms may be involved both in the initial formation and subsequent expansion of the syrinx cavity [2].

#### Neoplasms

The association between syringomyelia and intramedullary tumours has been known since its first description in 1875 by Simon [1, 19, 179, 180]. The mechanism for this association is still unknown, but several possible explanations have been proposed: (1) the syrinx cavity is part of the neoplasm itself; (2) both the neoplasm and the syrinx cavity are the results of the one basic developmental abnormality; (3) syringomyelia is a secondary effect of the neoplasm, such as disturbed blood supply, stasis of tissue fluid from occlusion to drainage pathways, spread of oedema or tumour autolysis and haemorrhage [89, 179].

Initially, the gliosis surrounding the syrinx cavity was assumed to be due to degeneration of a low grade glioma, and indeed, radiotherapy and chemotherapy were administered as treatment [1]. However, the efficacy from radiotherapy was low, raising doubts about the neoplastic hypothesis as a basis for syrinx formation.

Lonser et al. observed increased peri-tumoural oedema associated with intramedullary haemangioblastomas, suggesting increased vascular leakage and impaired fluid drainage as the underlying cause of cyst formation [181, 182]. Similarly, Lohle et al. reported increased protein content in syrinx fluid from an intramedullary ependymoma, and exudation from a disruption of the blood-spinal barrier was the cause of oedema [179]. However, Batzdorf made the distinction between a tumour cyst, and true syringomyelia. He stated that fluid from tumour cysts had higher protein content, as compared with true syringomyelic fluid, which was more consistent with the composition of CSF [27]. Based on their series of 100 intramedullary tumours, Samii et al. concluded that the mechanism for syrinx formation in association with spinal cord tumours was more likely to be due to disturbances of CSF flow instead [87]. However, exactly how spinal cord tumours contribute to disturbances in CSF flow and how such disturbances would lead to syrinx development and enlargement have remained only a theory, and have not been substantiated by clinical or experimental evidence.

## Ischaemia

Several case reports have demonstrated that obstruction of the anterior spinal artery following severe meningitis produced intramedullary cavitations [84, 97, 183, 184]. Similar histological findings were reported in experimental studies, which induced ischaemia by ligating the anterior spinal artery in a cat model [1, 185]. Apart from arterial obstruction, venous infarction also produced cavitations in rats [1]. Moreover, the

dorsolateral grey area within the spinal cord is a common area for extracanalicular syrinxes and has been thought to be a watershed area [2, 23, 186]. Therefore, the ischaemic theory has been proposed as a mechanism of syrinx initiation [2, 33, 84, 97].

Both Milhorat et al. and Young et al. monitored the somatosensory evoked potentials and regional spinal cord blood flow before and after syrinx shunting [187, 188]. They demonstrated intra-operative improvements post-shunting, suggesting that local ischaemia may have a contributory role in syringomyelia pathogenesis [187, 188]. However, other authors have stated that ischaemia may only contribute to the initial spinal cord injury, and does not constitute the main expansion mechanism [1, 138, 189]. Whether ischaemia produces myelomalacia alone, or contributes to progressive enlarging syrinx cavities remains contentious.

## Inflammation, including arachnoiditis

Both clinical and experimental studies have established the association between arachnoiditis and syringomyelia. As previously mentioned, arachnoiditis commonly occurs after both pyogenic and tuberculous meningitis, subarachnoid haemorrhage, previous intradural surgery and chemical irritants, such as oil-based radiopaque contrast substances (Pantopaque) [27, 84]. In patients with focal arachnoiditis, treatment with arachnolysis and restoration of spinal subarachnoid space resulted in a reduction in the size of the syrinx cavities [27, 125, 190].

Experimental data include animal models of arachnoiditis, in which either blood, Pantopaque or kaolin was injected into the subarachnoid space [191-196]. Hoffman et al. induced severe spinal arachnoiditis with Pantopaque in dogs, which produced intramedullary cavities, predominantly from spinal cord ischemia [192]. Tatara used

kaolin in rabbit and rat models, in which about 31% and 22% of animals produced syrinxes [196]. Cho et al. and Yang et al., however, demonstrated a higher incidence of syrinx cavities when subarachnoid kaolin was added, but did not produce any cavities in the spinal cord when kaolin alone was injected [191, 195]. Klekamp induced focal arachnoiditis in a cat model and reported increased interstitial oedema and higher intramedullary pressure at the corresponding region. Increased interstitial oedema within the cord may predispose to subsequent syrinx formation by coalescing into a cyst [193]. Recently, Austin et al. examined the levels of cytokine production, blood-spinal cord permeability and degree of intraparenchymal inflammation in rodents following spinal cord injury from aneurysm clip compression with subarachnoid kaolin injection over a 7 day period [197]. Cytokine levels and blood-spinal cord permeability were increased in the post-traumatic syringomyelia model, when compared with the spinal cord injury only and arachnoiditis only groups. Furthermore, biomarker levels of intraparenchymal inflammation were higher in the post-traumatic syringomyelia group than the combined biomarker levels produced by the spinal cord injury only and arachnoiditis only groups. This suggests that intraparenchymal inflammation may be potentiated by arachnoiditis in the setting of acute spinal cord injury, which may contribute to syrinx development [197].

## Haematomyelia

The initial cyst formation may result from an intraparenchymal haematoma, sustained from spinal cord trauma, or haemorrhagic infarction [33, 198]. As the haematoma liquefies, an area of degeneration occurs and the cavity becomes filled with CSF or extracellular fluid [1, 79, 199, 200]. This cavity may form the basis of subsequent syrinx formation [201, 202].

## Hydrodynamic theories

### *1.2.2.1.1 Pressure dissociation – "Sloshing" and "sucking"*

Williams identified different initiating factors according to the underlying aetiology, but similar factors were involved in the progression of the cysts. For tumour-related syringomyelia, it was thought that cyst fluid was the result of fluid secretion from the tumour cells, particularly haemangioblastomas and juvenile astrocytomas. For syringomyelia associated with arachnoiditis, the initial cyst formation was attributed to ischaemia and tethering of the spinal cord. In spinal cord injury, the initial haematoma was the underlying cause [198].

To explain progressive enlargement in non-communicating syringomeylia, Williams et al. proposed the "slosh" theory, which asserted that increases in arterial and respiratory pulse pressure were transmitted onto the syrinx fluid, which would dissect the cord [2, 198]. The dissection was likely to occur in a rostral direction due to increased epidural venous pressure from Valsalva manouevres producing an ascending pressure wave in the subarachnoid space. To explain caudal extension of the syrinx cavity, he stated the spinal cord would be "sucked" out from the Venturi effect due to low pressure below constrictions in the subarachnoid space [198]. This "slosh" and "suck" fluid movement was thought to be the mechanism for syrinx expansion by causing dissection into tissue planes, in particular, the grey matter [22].

The evidence for this theory is lacking. Williams conceded that this theory had no experimental basis, but relied on "thought experiments" to justify the concept [198]. Indeed, according to observations made from MRI, the forces within the syrinx would not be large enough to cause hydrodissection. Recently, Bertram used a numerical model to

evaluate the effects of the "suck" phenomenon under the influence of arterial pulsations and respiratory exertions [203]. It was demonstrated that pressure dissociation between the syrinx cavity and subarachnoid space ("suck") did not increase the longitudinal movement of the syrinx fluid. Thus the "suck" effect was unlikely to contribute to lengthening of the syrinx cavity [203].

#### *1.2.2.1.2 Arterial pulsation driven perivascular space flow*

Similar to the experiment assessing CSF flow in canalicular syringomyelia by Stoodley et al., CSF tracers were injected into the cisterna magna of rats in an excitotoxic extra-canalicular model of syringomyelia [204]. Brodbelt et al. demonstrated that there was tracer detected along perivascular spaces and towards the syrinx cavity. Also, there was increased CSF flow at the level of the syrinx and arachnoiditis, as compared with more rostral levels.

Bilston et al. suggested that a similar mechanism for pulsation mismatch as Chiari malformations may apply to syringomyelia with arachnoiditis. Arachnoiditis may cause a pulsation delay between the arterial and CSF pulse, such that the disruption in the synchrony of the pulsations may result in increased perivascular flow [171]. This theory has been assessed in a lumped-parameter model by Elliot et al. [205]. It confirmed the existence of a lag-phase difference, which was partially alleviated by the presence of a syrinx and treatment with a syringosubarachnoid shunt [205].

#### *1.2.2.1.3 Elastic-jump hypothesis*

The elastic-jump hypothesis has also been applied in the setting of extra-canalicular syringomeylia. It was postulated that stenosis within the subarachnoid space from

arachnoiditis could produce “elastic-jumps”. However, identical concerns as addressed in the canalicular syringomyelia section would apply to extracanalicular syrinxes [173].

## Other sources of syrinx fluid

#### *1.2.2.1.4 Accumulation of extracellular fluid*

Chang and Nakagawa devised an electrical circuit of CSF dynamics, reducing the spinal cord and the surrounding structures to a series of capacitative-resistive segments [206, 207]. They reported that at the region of adhesive arachnoiditis, there was an increase in pressure within spinal cord, with a pressure gradient down towards the corresponding subarachnoid space [206]. In this model, fluid within the central canal would be forced into the interstitial space, leading to an accumulation of extracellular fluid [160].

Interestingly, Bertram et al. studied the tensile radial forces secondary to arachnoiditis in a numerical model and reported a transient decrease in intramedullary pressure [208]. It was postulated that this decrease in pressure may draw in extracellular fluid in a normal spinal cord, and may initiate syrinx formation [208].

#### *1.2.2.1.5 Intramedullary pulse pressure theory*

The theories proposed by Josephson et al. and Greitz et al. have been also applied in extracanalicular syringomyelia, where arachnoiditis is the cause of spinal cord tethering and CSF stenosis in the subarachnoid space [175, 176].

#### *1.2.2.1.6 Disruptions in blood-spinal cord barrier*

Disruptions in the blood-spinal cord barrier following spinal cord injury and its associated interstitial oedema have been well established [209-212]. Ravalgia et al. and Hemley et

al. have postulated that disturbances in the integrity of the blood-spinal cord barrier may contribute to extra-canalicular syrinx formation [178, 213]. Ravalgia et al. presented a case series of patients who developed syringomyelia after myelitis. Contrast enhancement was noted around the cavitations, suggesting that breakdown of the blood-spinal cord barrier was present [178]. Hemley et al. demonstrated in a rodent extra-canalicular model of syringomyelia that the blood spinal cord barrier was deficient beyond the acute period when the syrinx cavity has been established [213]. Thus, disruptions in blood-spinal cord barrier may be involved both in the initial cyst formation and subsequent expansion.

### 1.2.3 Conclusion

Despite the plethora of theories on the pathogenesis of syringomyelia, there is not one satisfactory theory that completely explains the various aspects of the condition. Each of the theories has its inherent flaws: Some hypotheses are based on limited clinical and experimental evidence, while others only explain a particular type of syringomyelia. Rather than clarifying the mechanisms involved, all the theories have impeded rational progress based on clinical and experimental observation.

Basic fundamental questions still remain answered, such as the source and composition of syrinx fluid, the relationship between syrinx and subarachnoid space pressure, CSF and extracellular fluid flow, and the contribution of cellular and molecular mechanisms. Further clinical and experimental data are required to clarify such issues.

## *1.3 Animal models of syringomyelia and spinal cord injury*

### 1.3.1 Introduction

The need for validation of pathogenetic theories has been mentioned in the previous section. It would be impractical and unfeasible to test these theories on human subjects. Therefore, models of syringomyelia are required and, in particular, a reproducible animal model that replicates the human situation would be ideal.

Current animal models can be broadly divided into canalicular and extracanalicular models. Extracanalicular syringomyelia commonly results from an initial spinal cord injury, of which several models are available. This section will provide an overview of the existing animal models of syringomyelia and spinal cord injury.

### 1.3.2 Animal models of canalicular syringomyelia

#### Spontaneous models of syringomyelia

The first report of an animal model of "spinal gliosis with cavitation" was produced by Ostertag in inbred rabbits in the 1930's [8, 214]. Subsequently, Kawamura et al. reported dilated central canals in congenitally hydrocephalic mice [215]. When intrathecal ferritin was injected, histological examination of the spinal cord revealed an increased extracellular space, which the authors thought was the first step to developing syringomyelia [8, 215]. McGrath noted spinal cavities in Weimeraner dogs associated with spinal dysraphism. However, multiple intraparenchymal abnormalities were recorded independent of the syrinx cavity itself, and did not prove to be an adequate model [8, 214].

Syringomyelia has been found commonly in toy breed dogs, such as cavalier King Charles spaniels and Griffon Bruxellois [177, 216-218]. This is thought to be due to occipital bone hypoplasia, resulting in a small caudal cranial fossa and crowding of the cerebellum at the foramen magnum, which is analogous to Chiari type I malformation [219]. Compared to other breeds, the cavalier King Charles spaniels are associated with larger cerebellar volume relative to the caudal cranial fossa [220]. Furthermore, morphometric measurements have confirmed that cavalier King Charles spaniels with syringomyelia had a greater cerebellar to caudal cranial fossa volume than animals without syringomyelia [219]. In these animals, syringomyelia frequently occurs at the cranial to cervical region, but syrinxes may involve the entire cord [221]. Presentations include neuropathic pain and scratching over the neck and shoulder region. The degree of symptoms was associated with the size of the syrinxes and whether the dorsal columns were involved [218]. However, treatment with craniocervical decompression and durotomy did not result in collapse or resultion of syrinxes and may only provide symptom relief for several years [222]. Histologically, the syrinxes had anomalies of the central canal, with disruption in the ependyma, neuronal necrosis and Wallerian degeneration in the surrounding grey matter, with increased angiogenesis and fibrous tissure proliferation [223]. A database of the pedigrees and DNA in cavalier King Charles spaniels is being established, from which preliminary reports have identified a likely autosomal recessive inheritance for occipital bone hypoplasia [224, 225].

## Communicating model of syringomyelia

McLaurin et al. have been attributed as developing the first acquired model of syringomyelia, in which they modified the technique of Camus and Roussy by injecting a combination of kaolin and ethyl iodophenylundecylate (Pantopaque) into the cisterna

magna of dogs [194]. A dense arachnoiditis developed around the brainstem and posterior fossa, causing fourth ventricular outlet obstruction [60, 226-228]. Dilation of the central canal and a separate cystic cavitation involving the posterior horns of the spinal cord were reported, occurring within 4 – 5 weeks. Rather than attributing the changes to hydrocephalus and pressure transmitted to the central canal, the authors concluded that these changes were secondary to ischaemia, similar to the findings reported by Tauber and Langworthy [8, 185, 194].

The role of ischaemia in this model, however, has been disputed. Barnett noted that the majority of the cavitary lesions produced by ischaemia in this model were microscopic [80]. Hall et al. compared the histological appearance of spinal cords obtained from the kaolin-hydrocephalus model to an ischaemia model [229]. In the kaolin group, the central canal was dilated, with extension of fluid spaces into the surrounding grey matter and the neuronal and glial tissue in "perfect preservation" [229]. In contrast, the ischemic group was associated with necrosis of the grey matter with neuronal loss and the central canal remained unchanged.

Much information has been obtained from McLaurin's kaolin communicating syringomyelia model, which has since been widely used and applied to different animal models [198, 226, 230-234]. Using a dog model, Hall et al. injected radioisotope injections into the lateral ventricle and demonstrated tracer flow from the dilated central canal into the surrounding grey matter, and correlated the findings with clinical isotope scans [235, 236]. Similarly, Nakamura et al. reported preferential flow into the dorsal columns in hydrocephalic cats and concluded that the central canal dilated to allow CSF flow into the subarachnoid space [226].

Becker et al. conducted an experiment to validate Williams' craniospinal dissociation theory, by plugging the central canal at the level of the obex in a cat model of hydrocephalus and syringomyelia [237]. This study revealed no syrinx development in cats with "central canal isolation", which therefore supported Williams' theory.

In a separate experiment, Hall et al. took simultaneous measurements of the ventricular, syrinx and cervical subarachnoid space pressure using this model. Intra-syrinx pressure was shown to be higher than ventricular or subarachnoid space pressure, and was increased when the ventricular pressure was elevated [238] .Similar findings were reported by Williams et al., but some animals were found to have hydrocephalus and not syringomyelia, or vice-versa [198, 239].

Chakrabortty et al. analysed the ultrastructural changes in a rabbit cisternal kaolin model, which included: stretching and flattening of ependymal cells, disruption of the ependymal lining and dilated perivascular spaces [231]. These changes were maintained over tim .[230].

Concerns regarding this model have been raised. James et al. used a cisternal injection of silicone rubber instead of kaolin, but failed to produce a syrinx despite achieving hydrocephalus and a patent communication between the fourth ventricle and central canal [240]. Williams et al. questioned the applicability of this model to the human condition, in that: (1) the canine CSF volume was relatively small compared to humans; (2) the dog model was associated with extensive arachnoiditis and hydrocephalus, which were not common features of human syringomyelia; (3) A patent communication between the fourth ventricle and central canal was demonstrated on the canine model, which was not usually present in humans [8, 239, 241].

In contrast to the kaolin-hydrocephalus model, Yamazaki and colleagues developed a "chronic tonsillar herniation" model by implanting mammary cancer cells into the supraoccipital bone [242]. Over a period of 8 – 14 weeks, the transplanted cancer destroyed the supraoccipital bone and caused an extradural compression of the cerebellum, thus producing tonsillar herniation. In six of the ten rats used, a thoracic syrinx developed between the C5 to T8 spinal segments, with central canal dilatation [242]. Histologically, stretching and thinning of the ependymal cells, swelling of the astrocytic processes and extracellular oedema were reported [243]. When CSF tracers were injected into the lateral ventricle, tracers were detected in the spinal cord parenchyma around the central canal.[243]. This would indicate that a communicating type of syrinx was modelled.

## Non-communicating model of syringomyelia

Williams and Weller described the development of syrinx cavities which involved the central canal without hydrocephalus in a dog model, using repeated injections of saline or CSF into the spinal cord [244]  The cervical region was most prone to syrinx development, despite the injections being performed at the thoracic level. A spongy appearance was noted within the tissues, and cystic cavity was presumed to have opened into the central canal. The authors did not regard the arachnoiditis at the catheter insertion site as an important contributer to syrinx development.

In developing a non-communicating syringomyelia model, Milhorat et al. developed a rodent haematomyelia model, in which 2 μL of blood were injected into the dorsal columns of the thoracic spinal cord [245]. Blood was seen in the central canal, up to the fourth ventricle within six hours of the injection. It was also noted on histological sectioning that fibrin, proteinaceous material and cellular debris were found within the

rostral central canal for up to 15 days. The authors concluded that blood was removed by phagocytosis and drainage of blood products in a rostral direction through the central canal. This phenomenon was termed the "sink action" [245].

Subsequent to this study, Milhorat et al. injected 1.2 – 1.6 μL kaolin suspension into the dorsal columns of 30 Sprague-Dawley rats [246]. Transient neurological deficits were noted in four animals, but within 24 hours, kaolin and polymorphonuclear cells were observed in the rostral central canal. In all animals that survived 48 hours, the central canal became dilated and formed an ependymal-lined syrinx that continued to enlarge up to 6 weeks. Histological findings were characterised by stretching and thinning of the ependyma, elongation of the intracanalicular septae, and the formation of periependymal oedema. No hydrocephalus was noted in these animals. This model has been used in a number of experimental studies [169, 247, 248]. Using this model, Stoodley et al. showed CSF flow into the syrinx cavity when CSF tracers were injected into the cisterna magna [169, 248]. Although this model does not precisely replicate the human condition as seen in Chiari-related syringomyelia, the histological resemblances and paucity of neurological deficits make this a suibtable model that can be used for extended periods of time.

### 1.3.3 Animal models of spinal cord injury

The following section will provide a brief overview of the models of spinal cord injury as a precursor to post-traumatic syringomyelia. The pathogenesis of acute spinal cord injury consists of mulitple mechanisms. It involves contusion, compression, axonal transection, ischaemia, excitotoxic acid release and secondary insults [249-251]. No single model will be able to replicate each component of spinal cord injury, but the advantages and disadvantages of each model are discussed below.

## Contusional model of spinal cord injury

The first experimental spinal cord injury model was described by Allen et al. [252-254]. Using a canine model, the thoracic spinal cord was exposed with a laminectomy and a standardized weight was dropped on to the spinal cord through a vented tube. As the weight struck the spinal cord, either directly or though an impounder plate, the underlying tissue was subjected to a dynamic compression [251]. Unfortunately, the technique was associated with inconsistent impacts, which were affected by the shape and diameter of the impounder plate, or the resistance during the "free fall" [255-258]. The same technique was applied to other species, including feline, primate and rodent models [259-262]. An impactor tip was adapted to the weight drop model by Wrathall et al., but this technique was considered too inaccurate by Khan and Griebel except for severe spinal cord injuries [261, 263-265]. Later models were scaled down and offered greater reproducibility, but limited information could be obtained about the biomechanical properties of the impact [251, 266]. Despite its problems, much research has been conducted using this model, such as histological and molecular responses, vascular changes and benefits from administration of therapeutic agents in acute spinal cord injury [259, 267-272].

The New York Univeristy (NYU) / MASCIS impactor was initially developed by Kwo et al. and was first reported by Gruner in 1992 [273, 274]. The NYU impactor used electrical circuits to determine the cord surface before the impact to eliminate preload injury. It consisted of dropping a 10 g steel rod from heights of 6.25, 12.5, 25 and 50 mm directly onto exposed dorsal spinal cord, replicating mild, moderate and severe spinal cord injury [251, 259, 273, 274]. The advantages of this model are the ability to monitor the impact parameters, such as the impact velocity and tissue displacement, and reduced

riskof multiple injuries from drop-weight “bounce” [251, 259]. Similar histological, vascular and secondary injury experiments were performed with this impactor. In addition, functional recovery, gene expression and therapeutic studies were conducted [259, 275-277]. A correllation study by Metz et al. was performed between the weight drop model and human spinal cord injury, which showed histological and radiological resemblances.

A number of controlled pneumatic compression models were developed to control the injury severity by separating the impact velocity from the degree of cord compression [278, 279]. The Ohio State University (OSU) impactor used a solenoid-controlled air cylinder mounted on a rigid frame with an impactor tip [251, 280]. This impactor permitted graded spinal cord injury and demonstrated immediate functional deficits with recovery within 2 – 3 weeks [281-283]. However, the lack of commercial availability of this model has limited the use of this device [251].

More recently, a commercially available computer-controlled motorised impactor, the Infinite-Horizon (IH) spinal cord impactor, was developed [284]. Similar to the OSU device, exposure of the spinal cord and rigid stabilisation of the spinal column are required. In contrast, it uses force, rather than tissue displacement to injure the spinal cord, and the delivered force and displacement are recorded by sensors within the impactor tip.[251] Rabchevsky et al. undertook a comparsion study between the NYU and IH devices and reported very similar functional profiles [285]. The reported benefits of this impactor model, as compared with the weight-drop models, are the more precise and accurate delivery of a designated impact force to the spinal cord without prior contact, and the ability to monitor biomechanical parameters [251]. The disadvantages of computerised contusional models are the the high cost, variable completeness of the

lesion and suboptimal tracing methods to distinguish spared and regenerated neural tissue [286].

## Compression model of spinal cord injury

In 1953, Tarlov developed acute and gradual compression model of spinal cord injury in dogs. A 1 mL capacity balloon was passed into the T5 – 9 spinal cord levels following a T12 laminectomy, and varying degrees of extradural compression were applied to the spinal cord [254, 287]. It was reported that the degree and length of compression correlated with the functional deficits and recovery interval [287-289].

Sustained compression models on small animals were subsequently developed for a few reasons: human spinal cord injuries often involved ventral compression, which was not replicated in previous models and the original weight drop and compression models were restricted by size considerations in rodents. Initially, specially modified Kerr-Lougheed aneurysm clips were used by Rivlin and Tator in 1978, who applied one blade of the aneurysm clip under the ventral surface, and the other over the dorsal surface of the spinal cord [254, 290, 291]. The clip was rapidly released to deliver 180 g of compression force for a pre-determined amount of time [291]. The degree of neurological deficits and functional recovery correlated well with the amount of compression force applied [251, 290, 291].

Modified calibrated forceps were subsequently used to replicate a less focal spinal cord injury, as was commonly produced by aneurysm clips. Calibrated forceps provided a larger volume of compression and displacement than aneurysm clips, and could offer gradations of spinal cord injury severity [292]. This model has been used on mice, rats and guinea pigs, with suggestions of species differences in functional recovery [292-294].

Compression models were used to assess the benefits of methylprednisolone in spinal cord injury. It was found that cats receiving steroids had a benefit in functional recovery and greater tissue preservation [295].

The benefit of balloon or clip compression techniques is the ability to control precisely the degree of compression, and in the case of balloon compression, a laminectomy is not necessary. However, it does not mimic human spinal cord injury, in regards to delivering an acute impact to the cord [254, 286].

## Transection model of spinal cord injury

Many methods of spinal cord transection have been described, ranging from complete transection, focal myelotomy, and dorsal or lateral hemisections [251, 296, 297]. These models are useful in examining the ascending and descending axonal pathways, and their regeneration and potential recovery [297-303]. Interestingly, Kao et al. observed microcysts formation at the cord transection, which was thought to be a precursor to subsequent cyst enlargement [300]. The advantage of complete transection is the reproducibility of the technique, but transection injuries rarely occur in human spinal cord injury and the deficits cannot be graded [286].

## Excitotoxic model of spinal cord injury

The role of excitotoxic amino acids (EAA) following spinal cord injury has not been completely elucidated. EAA are known to be released following trauma and ischaemia, causing increased pathology in white and grey matter [304-309]. Microinjections of kainate or quisqualic acid, agonists of the AMPA-metabotropic receptor, into the grey matter resulted in degeneration of the grey matter, with neuronal loss, inflammation and development of an extracanalicular cavity [310-314]. From these studies, selective grey

matter loss with paralysis could be achieved, without significant disruptions to the descending white matter tracts [313, 314].

### Ischaemic model of spinal cord injury

Tauber and Langworthy's model of ischaemia has been mentioned previously, which involved ligation of the anterior spinal artery [185]. Subsequent authors were able to produce an ischaemic cystic cavity by occluding the artery of Adamkiewicz and the adjacent caudal anterior spinal artery, which produced paraparesis [315, 316]. More recent techniques included the use of laser and photochemical coagulation to induce vascular thrombosis [251, 309, 317, 318]. However, significant cystic cavities have not been observed with these techniques.

## 1.3.4 Animal models of extra-canalicular syringomyelia

Arachnoiditis appears to be an important factor in post-traumatic syrinx pathogenesis. The contribution of arachnoiditis was assessed by Faulhauer et al., who demonstrated that a syrinx cavity did not form from an intradural injection of kaolin alone in a cat model [234]. Interestingly, Klekamp et al. used kaolin soaked gauzes, which were placed extradurally at the C2 level, to induce focal arachnoiditis [193]. Although a syrinx did not develop, there were increased perivascular spaces and interstitial oedema, which pointed to a possible pre-syrinx state [193].

Animal models of post-traumatic syringomyelia have used various mechanisms of spinal cord injury with or without induction of arachnoiditis. These models have been divided according to the underlying mechanism of spinal cord injury.

## Contusional model of syringomyelia

Early experimental work with Allen's weight drop spinal cord injury model reported the formation of extracanalicular syrinx cavities without additional arachnoiditis [191, 261, 266, 319-324]. However, only a small proportion of animals developed cavities and some of these cavities resorbed over time, making the distinction between myelomalacia and true syringomyelia difficult [320].

Cho et al. combined a weight drop spinal cord injury model at the mid-thoracic level (T7 – 8) with subarachnoid kaolin injection to produce extracanalicular syrinxes [191]. There were 38 female Japanese White rabbits used and the rates of syrinx formation were assessed accordingly across 4 groups: weight drop alone (Group 1), weight drop with a subarachnoid injection of 100mg kaolin (Group 2) or 200mg (Group 3), and subarachnoid kaolin at 200mg alone (Group 4). Syrinx cavities developed in 42% and 56% of animals in Groups 2 and 3 respectively, compared with 13% in Group 1 and 0% in Group 4. The variable rate of syrinx formation and the lack of reproducibility have made this model unsuitable for further physiological investigations. The results, however, confirm the important contribution of arachnoiditis to syrinx extension, even though the mechanism by which this occurs is unknown.

Radojicic et al. reported an ascending dilatation of the central canal following a contusional spinal cord injury with the Infinite-Horizon spinal cord impactor [325]. The impactor delivered a 250 kDyn impact at the T10 level on fifteen rodents without additional arachnoiditis. The animals were studied at five time points, from 1 to 540 days. Histological assessments were made in 1mm increments away from the epicenter of impact to 6mm. Dilatations of the central canal were noted cranial to the epicenter, associated with disruptions of the ependyma, peri-ependymal oedema and gliosis. The

criticism of this model was that dilatations of the central canal were more characteristic of the previously mentioned haematomyelic and the non-communicating syringomeylia models than that of extra-canalicular syrinxes [245, 246].

## Compression models of syringomyelia

The combination of clip compression with subarachnoid kaolin was developed independently by Mizuno et al. and Seki et al. [326, 327]. Mizuno et al. assessed the syrinx occurrence rates of 22 Wistar male rats, which received spinal cord injuries at the T8 level from an epidurally applied aneurysm clip for 30 seconds [327]. The aneurysm clip (Sugita #53) was calibrated to deliver 70g of force. Overall syrinx cavity rate was approximately 83%, with no difference detected in animals receiving additional lumbar subarachnoid kaolin injections. Similarly, Seki et al. used a compression spinal cord injury model with a modified aneurysm clip applied extradurally in 64 female Wistar rats [326]. The authors reported that all animals developed syrinx cavities at 6 weeks post-operatively. Larger cavities were detected in animals with arachnoiditis from subarachnoid kaolin injection. The animals in both studies developed severe paralysis post-operatively, with no significant improvement in the arachnoiditis group.

Josephson et al. developed a thecal sac constriction model, in which a silk ligature was applied at the mid-thoracic level to obliterate the spinal subarachnoid space in 20 Sprague-Dawley rats [175]. The ligature was tightened to occlude the dorsal vein of the spinal cord. All animals developed permanent hindlimb paralysis and cystic cavities detected on MRI and histologically. An objection to both the compression and constriction methods is the severity of the neurological deficit. In addition, it is difficult to differentiate whether the cystic cavities resulted from ischaemia, myelomalacia or post-

traumatic syringomyelia from a restricted subarachnoid space in the thecal sac constriction model.

## Excitotoxic models

An alternative post-traumatic syrinx model was developed by Yang et al. and refined by Brodbelt et al., using intraparenchymal injections of quisqualic acid, in addition to subarachnoid kaolin injection [195, 321]. This model was based on previous studies by Yezierski et al., who had demonstrated that excitotoxic amino acids, such as glutamate, were released immediately following a spinal cord injury [310, 311]. Excitotoxic amino acids may be responsible for the formation of an initial cyst. Brodbelt et al. reported that the syrinx formation rate was 100% in animals with multiple doses of quisqualic acid (24 mg/mL) at 6 weeks, when given in combination with kaolin [321]. The syrinx cavities were also larger and involved more spinal levels than quisqualic acid alone. Transient forelimb weakness and overgrooming were the only adverse neurological outcomes observed. The advantages of this model are the reliability of syrinx production, the histological similarities to microscopic findings on human post-mortem specimens, and the absence of significant neurological deficits. A major criticism of this technique is that the quisqualic acid model may only represent the secondary injury cascade from excitotoxic amino acid release, and does not replicate the compressive and contusional trauma sustained during human spinal cord injury [326].

Based on this model, several studies have been performed in relation to CSF flow into the syrinx cavity, the effect of altered subarachnoid space compliance, the role of the blood-spinal cord barrier and the fate of neural progenitor cells [204, 213, 328, 329].

### 1.3.5 Conclusion

All the animal models mentioned in this section have their deficiencies. Besides the obvious translation that needs to be considered when applying findings from animal studies, each of the models replicates only specific aspects of the condition.

In the case of canalicular syringomyelia, the ideal model would be a large animal model with congenital Chiari malformation, which is readily accessible, and anatomically feasible to conduct CSF flow studies and pressure monitoring.

With regards to post-traumatic syringomyelia, a reproducible spinal cord injury model that has the same mechanism of injury and consistently produces extra-canalicular cavities would be ideal. At present, such an ideal model does not exist.

## *1.4 Spinal Cord Anatomy*

### 1.4.1 Introduction

The human spinal cord is a continuation of the medulla oblongata and extends from the foramen magnum to the level of the L1 – L2 intervertebral disc. It is approximately 42 – 45 cm in length and lies within the vertebral canal. The spinal cord consists of two enlargements in the cervical and lumbosacral regions, corresponding to the C4 – T1 and L2 – S3 spinal segments respectively in humans [330, 331]. These enlargements are thought to represent the increased numbers of motor neurones in the ventral horns for innervations of the upper and lower limbs.

The gross and histological anatomy of the spinal cord has been well described in many textbooks. This section will focus on the features of spinal cord anatomy that are relevant

to the experimental sections presented in this thesis and the theories regarding the pathophysiology of syringomyelia.

### 1.4.2 Embryology and development

The brain and spinal cord are derived from neurectoderm. By day 22, neurulation occurs where the lips of the neural crest unite to convert the neural plate into the neural tube, with cranial and caudal openings, known as the neuropores [332]. The lumen, or the neural canal, would later develop into the ventricles and the central canal. The cranial and caudal neuropores close by day 24 and 26 respectively [332]. The spinal cord caudal to the caudal neuropore develops by secondary neurulation, which is derived from the pluripotent cells within the caudal eminence, known as the neural cord [332]. The neural cord cavitates and unites with the caudal end of the neural tube by the sixth week.

Differentiation of the neuroblasts occurs within the neural tube on day 24, with the development of the ventricular and mantle layers. The mantle layer contains neuroblasts that later form the grey matter. At the end of the fourth week, the mantle layer of the spinal cord is organized into the dorsal and ventral columns, which become the somatic motor and sensory neurons respectively [330].

During development, the end of the spinal cord "ascends" due to differential growth of the spinal cord and the vertebral column. In the fetus, the spinal cord extends to the level of S2 vertebra. At birth, the conus medullaris lies opposite to the level of L3 vertebra at birth and at the L1 – L2 intervertebral disc space in adulthood [330, 333].

### 1.4.3 Gross anatomy

The spinal cord is flattened in the anteroposterior direction, such that it is elliptical in shape in cross-section. It has a tapered caudal end, known as the conus medullaris. Caudal

to this are the lumbar and sacral nerve roots, which constitute the cauda equine [330, 333].

The macroscopic features of the spinal cord include a deep ventral groove called the anterior or ventral median fissure, and a shallower dorsal groove, known as the posterior or dorsal median sulcus [333]. In many textbooks, it is described that a posterior median septum exists that extends from the dorsal median sulcus to the arachnoid, as well as internally into the spinal cord parenchyma [333, 334]. However, there has been some contention over whether the posterior median septum actually exists [330].

In humans, there are 31 pairs of spinal nerves, consisting of eight cervical, 12 thoracic, five lumbar, five sacral and one coccygeal nerves [330, 333]. Each spinal nerve is composed of ventral and dorsal rami, which unite within the intervertebral foramen. Each ventral ramus is formed by approximately three rootlets, leaving the anterolateral aspect of the spinal cord [330]. At the intervertebral foramen, the dorsal ramus contains a dorsal root ganglion and comprises several rootlets entering the spinal cord at the posterolateral surface, which has also been termed the dorsal root entry zone.

### 1.4.4 Internal structure and cellular organization

The spinal cord in transverse section is organised into central grey matter and surrounding white matter, with the deep anterior median fissure containing the anterior spinal artery and the posterior median septum demarcating the midline. The grey matter is arranged in an H-shape, consisting of the ventral and dorsal horns, and an intermediate zone, which contains the central canal [334]. The ventral horns are composed of alpha and gamma motor neurons, while the dorsal horns contain cell bodies of tract cells that ascend in the white matter [333, 334].

The main cell types present within the grey matter include neurons, interneurons and neuroglial cells. The prinicipal neurolglial cells include oligodendrocytes, astrocytes, microglia and ependymal cells [335]. Oligodendrocytes are responsible for the myelin sheath within the central nervous system, equivalent to the Schwann cells of the peripheral nervous system. The astrocytes provide mechanical support, mediate exchange of metabolites between neurons and the vascular system, participate in tissue repair within the CNS, and also form the blood-brain barrier [335]. Microglial cells are representatives of the monocyte-macrophage system that participate in the defense system and are activated following spinal cord injury [247, 336, 337].

Rexed, in 1952, described the laminar organisation of neurons and neuronal supporting cells within the grey matter of the cat spinal cord [338]. He identified ten laminations, which served different functions. For example, lamina VII, VIII contained the interneurons that regulated motor activity, while the cells of lamina IX were the alpha and gamma motor neurons [333]. Similarly, laminae I – VI contained sensory neurons, with lamina V being the main source of the anterolateral tract that gave rise to the spinothalamic tract for pain sensation [339]. In addition, the relative sizes of each lamina varied according to the spinal cord level, which were consistent with the cervical and lumbar enlargements [340]. Rexed's laminations have been confirmed on rodent and primate spinal cords [341, 342]. Similarly, it is assumed that the same cytoarchitectural organisation can be applied to spinal cords in humnas.

The white matter is divided into the posterior (or dorsal) columns, lateral columns and anterior (or ventral) columns, by the dorsal and ventral rootlets [330]. The dorsal rootlets continue into the spinal cord as the dorsolateral tract of Lissauer. Details regarding the nomenclature and function of individual ascending and descending tracts along the white

matter can be obtained in many anatomy textbooks, and will not be covered in this review.

### 1.4.5 Central canal and ventricular system

The central canal is present in all vertebrates. During embryological development, the ventricular system is continuous with the central canal [186]. However, it is generally accepted that the lumen of the central canal does not remain patent in humans at adulthood [150, 186]. In a study by Hashizume et al., the central canal was examined in 158 autopsy cases from infancy to 116 years [343]. The central canal remained patent in infancy, but by the second decade, the canal was occluded at many levels [343]. In rats, the central canal remains patent and is thought to allow flow of CSF in a rostral direction [246].

The ventricular system consists of the lateral ventricles, third ventricle and the fourth ventricle. Both the ventricular system and the central canal are lined by ependymal cells. Histologically, the ependymal cells form a single layer of ciliated cuboidal to columnar cells, which are bound together at the apical surface by junctional complexes [335, 344]. The function of the cilia on the apical surface of the cells is not known, but may regulate the direction of CSF flow in the ventricles [345]. Specialised ependymal cells, called tanycytes, are also located in the spinal canal. They are characterised by numerous microvilli and radial basal processes that have contact with the neurons and wrap around blood vessels [344, 345]. The tanycytes are postulated to have a neuroendocrine function or regulate transport of molecules between the CSF and blood [344, 346].

### 1.4.6 Spinal meninges

The meninges surround the spinal cord and the spinal nerves, comprising three layers: Dura, arachnoid and pia mater.

The spinal dura mater is an extension of the inner dural layer from the posterior cranial fossa and in humans extends from the edge of the foramen magnum to the S2 vertebra [347]. It is adherent to the tectorial membrane and the posterior body of the axis, but is otherwise free within the vertebral canal, surrounded by epidural adipose tissue and venous plexuses [333]. The main thecal sac has dural sheath extensions that contain the anterior and posterior spinal nerve roots, which unite at the intervertebral foramen [331]. The dural layer consists of dense fibroelastic tissue, which is lined internally by flat cells [335].

The arachnoid mater is closely applied to the inner layer of the dura mater, such that only a small amount of lymph-like fluid separates the two layers and the subdural space is virtually a potential space [335, 348, 349]. The outer layer of the parietal arachnoid layer is impermeable to CSF due to tight intercellular junctions, and contains flattened arachnoidal cells [335, 347]. Within the subarachnoid space, trabeculae are present that connect the arachnoid and pia layers forming septations that are in contact with blood vessels and nerves on the surface of the spinal cord [347]. These trabeculae are most prevalent posteriorly below C5, but become sparser with occasional strands in the anterior compartment rostral to C5 [350].

Covering the surface of the spinal cord, pia mater separates the spinal cord parenchyma from the subarachnoid space. The pial layer consists of a single layer of flattened fibroblasts, separated from the processes of underlying astrocytes by a basement

membrane and containing collagen and fine elastin fibres [335, 344]. The basement membrane from the astrocytic processes forms the glia limitans, which regulates the movement of fluids and solutes across into the spinal cord parenchyma [335, 344]. At the lateral margins of the spinal cord, extensions of the pia form the denticulate ligaments, which attach onto the dura after piercing the arachnoid mater [333, 350].

### 1.4.7 Vasculature

## Arterial supply

The arterial supply of the human cervical spinal cord is derived from the vertebral arteries, ascending cervical, deep cervical and superior intercostals arteries. The anterior and posterior spinal arteries descend longitudinally from the vertebral arteries at the level of the foramen magnum, and participate in the superficial arterial system of the spinal cord [333].

At the cervicothoracic, mid-thoracic and lumbar regions, the arterial supply is supplemented by segmental arteries. The segmental arteries leave as pairs of arteries from the descending aorta or internal iliac arteries to supply the spinal column and paraspinal muscles [351]. The radicular branches of these arteries then traverse the intervertebral foramen to supply the nerve roots, but only a few eventually supply the spinal cord. On average, there are six anterior radiculomedullary arteries, as compared to 11 – 16 posterior radiculomedullary arteries that anastomose with the anterior and posterior spinal arteries [351, 352]. The great radicular artery of Adamkiewicz commonly enters on the left side between the levels of T8 – L2 to supply the lumbar enlargement [351, 352].

The superficial arterial system of the spinal cord consists of the longitudinal and pial plexus. As mentioned previously, the main longitudinal arteries are the anterior and

posterior spinal arteries. The anterior spinal artery (ASA) forms from the confluence of the descending branches from the vertebral artery and travels in the ventral median fissure down to the conus medullaris [333]. It receives collaterals from the segmental arteries mentioned above, but minimal collateralization occurs below the junction of the artery of Adamkiewicz and the ASA, leading to possible vulnerability to ischaemia [351, 352]. The posterior spinal arteries are derived from the ipsilateral vertebral or posterior inferior cerebellar arteries, and form a discontinuous arterial network that travels along the posterolateral part of the spinal cord medial to the dorsal root entry zone [351]. These arteries often cross the midline and supply the posterior one-third of the spinal cord.

A pial plexus exists that connects the anterior and posterior spinal arterial networks [333]. These interconnecting vessels are known as the "vasocorona" and provide arterial supply to the peripheral regions of the spinal cord in a centripetal direction [351].

The intrinsic arterial system of the spinal cord consists of the sulcal arteries, which are the central branches of the ASA, and the perforating branches from the pial plexus. Within the ventral median fissure, the ASA sends sulcal branches that penetrate the grey matter, alternating between the left and right sides [351]. These branches supply the anterior two-thirds of the spinal cord in a centrifugal direction.

## Venous drainage

Similar to the arterial system, there is significant variation in the pattern of venous drainage. This can also be broadly divided into the intrinsic and superficial venous systems. The sulcal (central) and radial (peripheral) veins drain into the superficial venous system, which consists of multiple longitudinal veins. The sulcal veins drain the

ventral horns and grey commissure, while the radial veins drain the white matter up to the grey matter of the dorsal horn [351].

The longitudinal veins include: the anterior median spinal vein, and up to three posterior spinal veins, of which the posterior median septal vein is most consistent and the largest [333]. These vessels drain into the radiculomedullary veins, which eventually, empty into the inferior vena cava via the epidural venous plexus and the azygous-hemiazygous systems [351].

## Lymphatic drainage

Although a lymphatic system does not exist within the CNS, there is experimental evidence to demonstrate that reabsorption of CSF occurs via extracranial lymphatic routes into cervical lymph nodes [353, 354]. In animal studies involving mice, rats, rabbits, cats, guinea pigs, pigs, sheep, dogs and monkeys, CSF tracers were detected in the cervical lymphatics, passing via the nasal mucosa across the cribiform plate. This route has been estimated to account for about 50% of CSF absorption [355]. In addition, greater quantities of intraventricular CSF tracers were reabsorbed into the circulation when the cervical lymphatics were not ligated [356, 357]. Further evidence to support this is suggested by the absence of arachnoid granulations in neonates, prompting the notion that an alternative CSF absorptive pathway exists.

### 1.4.8 Fluid interfaces

The homeostatic environment within the CNS is protected by tightly regulated interfaces, which have barrier, transport and metabolic functions [358]. The interface between CSF, the vasculature and the spinal cord parenchyma occurs at three main regions: The blood-spinal cord barrier, the blood-CSF interface, such as the choroid plexus in the brain and

the perivascular spaces, and the arachnoidal interface between CSF and brain, as demarcated by the glia limitans [358]. The perivascular spaces and blood-spinal cord barrier will be examined in the next section.

## Perivascular spaces

As blood vessels from the subarachnoid space enter the spinal cord, they are surrounded by an investing sleath of pia mater. Eventually, the pial coat becomes fragmented and lost in the spinal cord parenchyma [335, 344]. The space between the pia and the penetrating vessels is called the perivascular space, or Virchow-Robin space. It has generally been assumed that the perivascular space is continuous with the subarachnoid space, based on previous tracer studies in animals [167-169, 359, 360]. However, on light and electron microscopy studies on human autopsy specimens, it has been demonstrated that a continuous layer of cells from the pia mater reflects from the brain surface to the meningeal vessels.[361] Effectively, the pia mater forms a barrier to particulate matter from the subarachnoid space, and the perivascular space is actually continuous with the subpial space, rather than the subarachnoid space. However, the fact that CSF tracer and inflammatory cells have been found in the perivascular spaces indicates that the pia mater is permeable to certain cells and substances [361].

## Blood-spinal cord barrier

The blood-spinal cord barrier is part of the blood-CNS barrier that isolates the CNS from the vasculature. The blood-CNS barrier is characterised by a single layer of endothelial cells connected by tight junctions through cell adhesion molecules and cytoplasmic proteins, such as zona occludens [362]. The endothelial cells are surrounded by astrocytic foot processes and pericytes, which are attached onto a basement membrane. The blood-

spinal cord barrier has several functions: (1) to maintain the chemical composition of interstitial fluid within the CNS; (2) to provide a defense mechanism against systemic toxins; (3) to allow specific transport of certain macromolecules; and (4) to regulate the immunological response in limiting inflammation within the CNS as an immune-privileged organ [358, 362]. Disruption of the blood-spinal cord barrier in the pathobiology of spinal cord injury and syringomyelia is important because breakdown of the barrier leads to increased permeability of fluid into extracellular space and potentiation of the inflammatory response. Disruption of the blood-spinal cord barrier is more prominent during the acute phase of spinal cord injury and syrinx initiation than at the chronic stages of spinal cord injury and in established syringomyelia [197, 213, 363].

## *1.5 Cerebrospinal Fluid Physiology*

### 1.5.1 Introduction

CSF is a clear, colourless fluid that surrounds the central nervous system and circulates through the ventricles, cisterns and subarachnoid space. Traditionally, its main function has been considered to be a protective cushion for the brain and spinal cord to float in [344]. Besides being a mechanical buffer, CSF reduces the weight of the brain from 1500 g to only 50 g, thus reducing the tension on nerve roots [364, 365]. In addition, it has a lymphatic-like function, to transport chemicals, nutrients, solutes and other products, such as hormones and toxins [364, 366, 367].

### 1.5.2 CSF Pathways

## CSF Production

The total volume of the ventricular system and CSF spaces is approximately 140 – 150 mL and CSF is produced at a rate of 500 – 550 mL per day, which equates to approximately 20 mL / h. This suggests that CSF is replenished at least three times daily [365].

CSF production in the choroid plexus has been well- known, as observed in patients with choroid plexus papillomas where an oversecretion of CSF occurs [368]. Previously, it was thought that the choroid plexus was the only site of CSF production, but, in case reports and primate experiments in which the choroid plexus had been removed, CSF continued to be produced [369-371]. Extra-choroidal production from interstitial fluid has been estimated to be approximately 10 – 30 % of total CSF production [344, 365, 371].

CSF production in the choroid plexus is an active metabolic process. Ultrafiltration from the plasma occurs across the basolateral membrane of ependymal cells. Active transport of solutes occurs at the apical layer, creating an osmotic gradient to promote water movement [344, 371].

## CSF Circulation

CSF circulates from the lateral ventricle to the third and fourth ventricles, and then into the cisterna magna via the foramina of Lushka and Magendie. From the cisterna magna, CSF travels into the basal and spinal subarachnoid space. CSF circulates from the cranial subarachnoid space to the arachnoid granulations in the superior sagittal sinus where CSF absorption is thought to occur.

CSF circulation through the ventricles and spinal subarachnoid space occurs due to continuous CSF production and the influences of cardiac pulsations [372, 373]. Based on MRI flow studies, cardiac systole initiates an anterior and caudal spinal cord movement, followed by caudal CSF flow, then a diastolic cranial return [344, 372, 373].

## CSF Absorption

Traditionally, arachnoid granulations have been considered to be the site of CSF absorption. Arachnoid granulations are invaginations of the arachnoid into veins, which are present in the cranial venous sinuses and at the arachnoid angles in spinal nerve roots [344]. CSF flow into the sinuses appears to be passive along a pressure gradient, without a one-way valve mechanism [371, 374]. This supports an energy-independent transcellular route of fluid transport [371, 374].

Apart from the arachnoid granulations, CSF absorption occurs via lymphatics across the cribiform plate and nerve root subarachnoid angles [374]. In sheep experiments, CSF absorption has also been identified via the spinal lymphatics [375, 376].

### 1.5.3 CSF Biochemistry

The chemical composition of CSF and plasma is shown in Table 1.5-1.

CSF has a lower protein, glucose, potassium, and higher chloride level than plasma [365]. However, CSF protein levels tend to differ in different aregions of the subarachnoid space. Protein content tends to be higher in regions of sluggish CSF flow, such as the lumbar cisterns [31].

**Table 1.5-1 Biochemical profile of CSF and plasma**

| Substance | | CSF | Plasma | CSF: Plasma |
|---|---|---|---|---|
| $Na^+$ | meq/kg $H_2O$ | 147.0 | 150.0 | 0.98 |
| $K^+$ | meq/kg $H_2O$ | 2.9 | 4.6 | 0.62 |
| $Mg^{2+}$ | meq/kg $H_2O$ | 2.2 | 1.6 | 1.39 |
| $Ca^{2+}$ | meq/kg $H_2O$ | 2.3 | 4.7 | 0.49 |
| $Cl^-$ | meq/kg $H_2O$ | 113.0 | 99.0 | 1.14 |
| $HCO_3^-$ | meq/L | 25.1 | 24.8 | 1.01 |
| $PCO_2$ | mmHg | 50.2 | 39.5 | 1.28 |
| pH | | 7.33 | 7.40 | |
| Osmolality | mosm/kg $H_2O$ | 289.0 | 289.0 | 1.00 |
| Protein | mg/dL | 20.0 | 6000 | 0.003 |
| Glucose | mg/dL | 64.0 | 100 | 0.64 |
| Inorganic P | mg/dL | 3.4 | 4.7 | 0.73 |
| Urea | mg/dL | 12.0 | 15.0 | 0.80 |
| Creatinine | mg/dL | 1.5 | 1.2 | 1.25 |
| Uric acid | mg/dL | 1.5 | 5.0 | 0.30 |
| Cholesterol | mg/dL | 0.2 | 175.0 | 0.001 |

### 1.5.4 CSF pressure pulsations and flow

## Intracranial CSF pulsations and flow

Information regarding intracranial CSF pulsations has been mainly obtained from invasive ntracranial pressure monitoring and cine-MRI flow and associated computational modeling studies of CSF pressures. Invasive ICP monitoring is often used in the clinical setting for management of severe head injury, high grade subarachnoid haemorrhage, hydrocephalus and benign intracranial hypertension [377]. Methods of invasive ICP monitoring include: ventricular catheter with an external pressure transducer, subdural or intraparenchymal microsensor, or lumbar puncture measurements over extended periods

of time [377]. The ICP waveform consists of several harmonic components, namely the heart rate, the respiratory rate and "slow waves".[377]

Many cardiac-gated phase-contrast MRI and computational flow studies have been performed. During systole, net inflow of blood increases intracranial volume and induces systolic craniocaudal CSF flow and caudal movement of the brainstem [373, 378, 379]. The reverse occurs in diastole. The influence of arterial and venous pulsations on CSF pulsation amplitude and flow has been assessed in normal patients. Bhadelia et al. showed a positive correlation between arterial waveform amplitude and a negative venous waveform with CSF waveform amplitude [379].

## Spinal CSF and syrinx pulsations and flow

The origin of spinal CSF pulsations has been investigated intraoperatively by Nakamura et al. in a series of patients with myelopathy undergoing spinal cord decompression [380]. Patients were assessed with an intradural microsensor pressure monitor to compare the lumbar CSF pulsation pre- and post-operatively. In patients with a complete CSF block on myelogram, the lumbar CSF pulsations were still present, but reduced compared with those with incomplete block. This suggests that lumbar CSF pulse wave pulsations are derived from arteries supplying the spinal cord and transmitted pulsations from the brain to the spinal subarachnoid space [380]. The authors stated that the CSF pulsation wave may be a surrogate marker of spinal cord blood flow. In a follow-up experiment on a dog model, Nakamura et al. demonstrated that CSF pulsations can provide information regarding the spinal cord blood flow in localised regions [381].

A similar question was addressed by Henry-Feugeas et al., who used cine-MRI to analyse the components of the spinal CSF pulsation in normal human subjects [373]. It was

reported that three dynamic channels could be differentiated along the spinal axis: lateral, medioventral and mediodorsal channels. The lateral spinal channel displayed significant craniocaudal propagation from intracranial pulsations, while the medial channels showed a cephalad progression from local vascular pulsations [373].

To complement *in-vivo* studies on the effect of spinal subarachnoid stenosis on CSF pulsation, Martin et al. developed an *in-vitro* model simulating post-traumatic and Chiari-related syringomyelia [382, 383]. In all situations, CSF blockage caused an increase and dissociation of subarachnoid space pressure, while axial pressure in the syrinx remained uniform [383]. Most recently, Martin et al. developed a coupled cardiovascular and cerebrospinal fluid model using computational methods [384]. In this study, the relationship between spinal cord blood flow and CSF pulsations was evaluated along the spinal subarachnoid space. A one-dimensional model of the vascular tree and spinal subarachnoid space was constructed, with CSF and cerebral blood flow derived from previous *in-vivo* measurements. It was found that the cerebral blood flow to CSF transfer function produced a CSF pulsation wave similar to *in-vivo* measurements [384]. In agreement with Bilston et al. and Elliot et al., the spinal cord blood flow to CSF pulse delay was present, but varied according to the craniospinal compliance and vascular anatomy [171, 205]. However, further *in-vivo* measurements are necessary to validate this model.

With regards to syringomyelia, syrinx pressure manometry was performed in a dog communicating model of syringomyelia by Williams and Bentley in 1980 [198, 239]. The cranial and spinal subarachnoid space pressures were monitored before and after the induction of hydrocephalus with kaolin. It was noted that the mean cranial and spinal CSF pressures were elevated after kaolin injection. Craniospinal dissociation was noted during

provocative manoeuvres, such that a differential increase in pressure was observed between the cranial and spinal compartments [239]. A limitation of this study was the influence of general anaesthesia, which altered the cardiac and respiratory patterns with abdominal relaxation [239].

Milhorat et al. performed intramedullary syrinx pressure manometry in patients undergoing syrinx shunt operations [385]. The syrinx pressure was recorded as being between 0.5 – 22 cm $H_2O$ above atmospheric pressure, with elevated arterial and respiratory pulsations indicative of raised CSF pressures. The intramedullary pressure decreased to subatmospheric with improvement in local spinal cord blood flow following syrinx decompression.

### 1.5.5 Conclusion

The effects of arterial and respiratory pulsations on CSF pulsations and flow have been well documented. Current methods of CSF pressure monitoring have relied on measurements in patients for intracranial pressure monitoring and in experimental anaesthetised animals. In contrast, CSF flow studies have only been performed on patients via cine-MRI or experimental animal studies on post-mortem specimens. Novel methods to evaluate in-vivo CSF pressure and flow without the influence of general anaesthetic would be ideal.

## *1.6 Aquaporins*

### 1.6.1 Introduction

Since the 1920's, it has been known that cellular membranes consist of a lipid bilayer that regulates the intracellular environment, even though cells are constantly bathed in

extracellular fluid with solutes and other toxic substances at different pH and concentration gradients. Although specific ion channels, exchangers and co-transporters were discovered in 1950's, water transport was assumed to be due a process of simple diffusion. However, observations from certain cells, such as amphibian bladder and mammalian erythrocytes, demonstrated higher water permeability, suggesting the possibility of water-specific transport across the lipid bilayer [386].

Aquaporins are a family of dedicated water-channel proteins found in prokaryotes and eukaryotes with 10- to 100- fold higher capacity for water permeation than simple diffusion [386, 387]. The first aquaporin was discovered in 1992 by Preston and Agre from erythrocytes and renal tubule cells [386-388]. At least 13 aquaporins have now been identified in mammalian tissues, including in humans [387, 389, 390]. Aquaporins are mainly involved in selective water transport, but an atypical subgroup, the aquaglyceroporins, serve to transport glycerol and various small polar molecules [386, 388-391].

### 1.6.2 Structure of aquaporins

Aquaporins have a common structure consisting of 300 amino acids, with six membrane-spanning alpha-helical domains of approximately 30 kDa [392, 393]. They contain the highly conserved motif of asparagine-proline-alanine, which form a central pore to allow water transport in both directions [394]. The monomeric aquaporins are assembled in the cell membranes typically as homotetramers [386, 388, 392].

In some instances, the central pore can act as a gated ion channel. For example, the transmembrane domains around the central core in AQP1 may permit $Na^+$ permeation when activated. There are multiple regulatory pathways for AQP1, which may give rise to

the tissue-specific differences in permeabilities to water and various ions [387]. Similarly, AQP6 in oocytes was found to mediate ionic conductance sensitive to pH and mercury [387].

### 1.6.3 Role of aquaporins outside the central nervous system

Aquaporins have been identified in many organs, such as kidney, eye, skin, exocrine glands, lungs and gastrointestinal tract [387].

In the kidneys, the selectivity for water over $H^+$ ions allows for large volumes of water to be reabsorbed while excreting acid in urine. AQP1 and AQP2 are involved in the regulation of osmolality through their location on the collecting ducts of nephrons, which promote water reabsorption. When stimulated by vasopressin, AQP2 is translocated to the plasma membrane and becomes active. Vasopressin itself is released by the hypothalamus in response to changes in osmolality, as detected by osmoregulatory cells located in the supraoptic nucleus and subforniceal organs [387]. Therefore, AQP2 may be implicated in some types of nephrogenic diabetes insipidus [386]. Despite their location also in the collecting ducts of nephrons, inhibition of AQP6 demonstrated minimal difference to water permeability. In contrast, AQP6 was activated at low pH, suggesting a role in acid-base balance [386].

AQP0 and AQP5 have been located in the eyes [386]. A deficiency of AQP0 has been implicated in cataracts. In addition, aquaporins in the cornea, lens, ciliary epithelium and retina are involved in ocular surface hydration, corneal and lens transparency, intraocular pressure regulation and visual signal transduction [395].

In the skin, AQP3 is involved in skin hydration and epidermal proliferation, while in exocrine glands, aquaporins may be involved in transepithelial secretions [395].

However, although aquaporins have been identified in the lungs and gastrointestinal tract, the precise functions in these organs have not been established [395].

### 1.6.4 Role of aquaporins in the central nervous system

Although seven aquaporins have been identified in the rodent brain (AQP1, AQP3, AQP4, AQP5, AQP8, AQP9, and AQP12), the main aquaporins that have been found in the central nervous system are AQP1, AQP9, and the most commonly studied, AQP4 [386, 387, 392].

#### Aquaporin-1

AQP1 is expressed most abundantly in the choroid plexus epithelium and a smaller amount is identified in the hippocampal region [388, 391, 392, 396]. Given its location at the choroid plexus, AQP1 has been suggested to play a role in cerebrospinal fluid production [397]. In an experiment by Oshio on AQP1 null mice, there was a 25% decrease in CSF production compared to normal mice [398]. Interestingly, AQP1 expression has been identified in choroid plexus tumours when CSF production is increased, as well as in human malignant glial tumours in association with cerebral oedema [399, 400],

#### Aquaporin-9

AQP9 has been weakly detected by some groups in astrocytic foot processes at the glia limitans and ependymal cells, colocalised with AQP4 [391, 401]. The exact role of AQP9 in the brain has not been established. AQP9 is an aquaglyceroporin that is capable of transporting energy substrates (glycerol, lactate). Due to its location predominantly in hepatocytes, it has been postulated that AQP9 is involved in transportation of glucose into

the liver for gluconeogenesis [386]. Similarly, it has been suggested that AQP9 may have a possible role in brain energy metabolism [388, 392, 393].

## Aquaporin-4

Although AQP4 is also expressed in the lungs and kidneys, it is most abundantly expressed in the supporting cells of the central nervous system [402, 403]. Using immunohistochemistry and immunoelectron microscopy, it has been identified in the foot processes of astrocytes around capillaries, sulcus limitans, central canal, subependyma, and osmosensory areas, such as the supraoptic nucleus and subforniceal organ [386-388, 391, 396, 402, 404].

AQP4 exists in three isoforms: AQP4.M23, AQP4.M1 and AQP.Mz [393]. AQP4.M23 is the shortest isoform, known to form large regular aggregates on plasma membranes. It is the predominant isoform in brain tissue, and may be a potential target for transcriptional regulation [393, 396, 405]. AQP4.M1 is longer in length, has the highest single channel water permeability amongst the three isoforms, and its expression is significantly induced by ischaemia [393].

The physiological function of the AQP4 protein is not yet clear. The fact that AQP4 is located at the borders between the brain parenchyma and major fluid compartments suggests that it has a role in regulating water flow into and out of the brain, and across the blood-brain barrier [386, 388, 391]. In specialised glial cells, AQP4 channels are colocalised with an inwardly rectifying K+ channel (Kir4), which may function to maintain potassium homeostasis in the extracellular space in the nervous system [387, 406]. Kir channels are important in setting the membrane potential, stabilising the resting state and serving as targets for modulation of neuronal excitability [386, 406].

More recently, AQP1 and AQP4 have been studied with regards to astrocytic cell migration [388, 407, 408]. Aquaporin deficiency causes a two- to three-fold decrease in the rate of astrocyte migration, independent of which aquaporins or cell types are involved [408]. This has been confirmed in *in vitro* studies with knock-out astrocytic cultures and *in vivo* with AQP4 deficient astrocytes implanted in mice migrating at a slower rate towards a stab wound, as compared with implantation of wild-type cells [407, 408].

### 1.6.5 Aquaporin-4 in clinical settings

## Aquaporin-4 and cerebral oedema

In the normal central nervous system, water homeostasis is tightly regulated. This is maintained by the blood-brain or blood-spinal cord barrier, in part consisting of tight junctions between endothelial cells and astrocytic endfeet. In pathological conditions, such as cerebral ischaemia, tumours, abscesses and trauma, cerebral oedema occurs due to neuronal cell death and increased permeability of the blood-brain barrier [401].

Cerebral oedema is commonly divided into cytotoxic and vasogenic, as originally proposed by Klatzo et al. [401, 404]. In addition, cerebral oedema can occur from hydrocephalus. Cytotoxic oedema occurs when there is an intracellular accumulation of water due to failure of energy dependent osmotic pumps or their regulation [404]. Hence there is an influx of interstitial water into the cells. This may occur in the setting of ischemia, bacterial meningitis or hyponatraemia [388]. Vasogenic oedema commonly occurs in the setting of brain tumours and abscesses. A breakdown in the blood-brain barrier produces an increase in the amount of isoosmotic fluid in the interstitium [388, 404]. Hydrocephalic oedema arises when the CSF pressure is high, causing extravasion of

fluid from the ventricle through the ependyma. It occurs in association with meningitis and subarachnoid haemorrhage.

Fluid efflux from the interstitium has not been well understood. There are 3 possible mechanisms by which excess brain fluid may be removed from the interstitium: 1. across the blood-brain barrier into the bloodstream; 2. across the ependyma into the ventricle; and 3. across the glia limitans into the CSF in the subarachnoid space [391].

The association between aquaporins and cerebral oedema has been investigated for both cytotoxic and vasogenic oedema in cell cultures and animal models. Although AQP1 and AQP9 have been shown to be upregulated following traumatic brain injury, the main focus has been on AQP4 [409-412]. In AQP4 deficient knock-out mice, there was lower water content in the brain parenchyma and lower mortality in hyponatraemic and ischaemic models of cytotoxic oedema [388, 391, 413]. However, in vasogenic oedema induced by cortical freeze injury or brain tumour implantation, there was increased brain swelling in AQP4-null mice when compared with wild-types [413]. This suggested that AQP4 might have a role in brain water elimination, which may be impaired with AQP4 deficiency [388, 391].

Therefore, AQP4 may have different roles in cytotoxic and vasogenic oedema. In the early stages, it facilitates the formation of cytotoxic oedema, but may be involved in the elimination of interstitial fluid in vasogenic oedema in later stages.

Recently, Badaut et al. proposed three subtypes of cerebral oedema to reflect the timeline of observed changes in AQP4 in the setting of ischaemia: anoxic, ionic and vasogenic oedema [392]. Anoxic oedema occurs during the initial 10 minutes following cessation of cerebral blood flow. This causes cellular swelling of astrocytes and neuronal dendrites due to deprivation of oxygen and glucose, resulting in disruption of ionic gradients and

entry of extracellular potassium and water. The Kir channel associated with astrocytic endplates may be involved during anoxic oedema. During the ionic phase, disruption of endothelial cells occurs, leading to transcapillary flux of $Na^+$ and early transient leakage through the blood-brain barrier. The final step in the oedema cascade is the vasogenic phase, when disruptions of the endothelial tight junctions and leakage of albumin and other plasma proteins occur. AQP4 expression is again increased, which functions to remove excess water from the tissues [392].

## Aquaporin-4 and hydrocephalus

Much focus has been placed on AQP1 in the setting of hydrocephalus due to its location on the choroid plexus epithelium, and, presumably, its involvement in CSF production. The function of AQP4 in hydrocephalus, however, is unknown, but AQP4 may be involved in eliminating excess interstitial fluid as a compensatory mechanism [405]. There have been conflicting reports in AQP4-null phenotype mice in relation to ventricular size and CSF dynamics [405]. In a mouse model of obstructive hydrocephalus using a cisternal kaolin injection by Bloch et al., AQP4-deficient mice developed more severe hydrocephalus and had significantly increased brain parenchymal water content and intracranial pressure compared to wild-types [414]. However, Manley et al. reported no difference in ventricular size or intracranial pressure [415]. A different mouse model was used by Paul et al., who investigated the expressions of AQP1 and AQP4 in congenital hydrocephalus [416]. It was demonstrated that AQP1 expression was decreased at the choroid plexus, but increased on the endothelium of capillaries. Similarly, AQP4 expression was increased on the astrocytic endfeet at the glia limitans [416].

The route of removal of excess fluid in hydrocephalus still remains to be clarified. It may occur from the interstitium via aquaporins into the subarachnoid space, or via a transcapillary process through aquaporin channels, rather than bulk flow into the CSF and through arachnoid granulations for absorption [388, 416].

## Aquaporin-4 and neuromyelitis optica

Neuromyelitis optica (NMO or Devic's syndrome) is a demyelinating condition affecting the optic nerves and spinal cord, resulting in loss of vision and paralysis [417, 418]. The association between AQP4 and NMO is based on several factors, including clinical and experimental evidence: (1) loss of AQP4 expression is noted in early NMO lesions; (2) in mice that have AQP4 deficiency, NMO does not develop; (3) serum AQP4 levels correlate with the extent of disease; and (4) IgG deposition in NMO lesions corresponds to regions of high AQP4 expression [388, 395, 417].

Recently, autoantibodies against AQP4 channels have been detected in human serum and CSF. Serum antibodies have been used as an objective diagnostic test for NMO [388, 418]. Interestingly, when human CSF autoantibodies against AQP4 were injected into rodents, NMO was induced [417].

Therefore the development of antibodies against AQP4 has been postulated as a pathogenetic mechanism for NMO, as well as a possible therapeutic target [395, 418].

## Aquaporin-4 and spinal cord injury

AQP4 and spinal cord oedema have been well studied in the context of spinal cord injuries. Nesic et al. demonstrated a biphasic response in AQP4 response, with an initial downregulation during the acute stages of a contusional spinal cord injury in rats,

followed by an upregulation in the chronic stages [419]. The appearance of early spinal cord oedema was attributed to increased vasogenic oedema from the breakdown of the blood-spinal cord barrier and downregulation of AQP4, thus impairing the removal of excess fluid. In the chronically injured cord, the blood-spinal barrier was restored and upregulation of AQP4 occurred. Chronic spinal cord oedema was thought to be secondary to cytotoxic oedema due to astrocyte swelling [419].

Saadoun et al. and Kimura et al. both examined the role of AQP4 in spinal cord injury models with AQP4 knockout mice [420, 421]. AQP4 knockout mice were compared to wild-type mice in their locomotor function, degree of neuronal loss and demyelination, and the water content within the spinal cord and intraparenchymal pressure in both studies. Saadoun et al. used a compressive model and reported improved neurological outcomes with less spinal cord swelling and myelin vacuolation in the AQP4 deficient animals, suggesting that AQP inhibition was beneficial as an early neuroprotective manoeuvre in spinal cord injury [420]. In contrast, Kimura et al. used a contusional spinal cord injury with the Infinite-Horizon impactor and demonstrated that AQP4 deficiency produced more significant neurological deficits, formation of larger cysts and higher water content at days 14 and 28 post injury [421].

The conflicting results of AQP4 deficiency in response to spinal cord injury in the animal models mentioned above remain a mystery. This may be explained by the fact that different spinal cord injury models may produce varying degrees of cytotoxic and vasogenic spinal cord oedema, and thus different responses to AQP4 deficiency. A compressive spinal cord injury model may produce ischaemia, leading to cytotoxic oedema, while a contusive spinal cord injury model may produce more vasogenic oedema[421]. Saadoun et al. proposed that formation of vasogenic oedema occurred

through the disruption of the blood-spinal cord barrier, independent of AQP4, but cytotoxic oedema formed through an AQP4 dependent route [422]. Thus, AQP4 deletion would reduce the production of cytotoxic oedema and may be beneficial in spinal cord injury [422].

Interestingly, AQP1 expression has also been shown to be increased following a spinal cord injury in the long-term. It may be involved in water homeostasis, neuronal regeneration and plasticity, and possibly development of chronic neuropathic pain [392, 423]. In a rodent model by Nesic et al., AQP1 expression was increased up to 11 months following a spinal cord injury. It has been postulated that this increase might be due to hypoxia, mediated through hypoxia-inducing factors (HiF-1a) [423].

## Aquaporin-4 and syringomyelia

Based on the studies on AQP4 and spinal cord injury, the possibility of AQP4 playing a role in syringomyelia has been highlighted by a number of authors [405, 424, 425]. Since syrinx fluid is likely to be derived from CSF or extracellular fluid, changes in AQP4 expression may alter the flow of fluid from the perivascular spaces or spinal cord parenchyma to the central canal.

Recently, Aghayev et al. used a rodent model of syringomyelia, in which kaolin was injected into the cisterna magna to induce communicating syringomyelia [232]. A slight decrease in AQP4 expression was reported in the syrinx animals, suggesting AQP4 may not play a major role in syrinx pathophysiology [232]. However, the syrinx model used was not representative of the more common types of syringomyelia, such as Chiari-related and post-traumatic syringomyelia. Hemley et al. recently investigated AQP4 expression in the excitotoxic extracanalicular models, and demonstrated an upregulation

of expression at all time points, but particularly beyond 6 weeks from syrinx induction [426]. However, this was not observed in the canalicular model [427]. Further research into the association between AQP4 and syringomyelia is therefore needed.

### Aquaporin-4 and other clinical conditions

AQP4 has been studied in association with a number of other neurological conditions. Given its role in $K^+$ regulation, AQP4 has been implicated in the aetiology of seizures. In AQP4-null mice, the seizure threshold and duration were increased [406, 428, 429]. In cerebral tumours, AQP4 expression has been correlated with increasing grade of astrocytic tumours, metastatic adenocarcinomas and increasing blood-brain barrier permeability [430]. AQP4 has also been identified in meningioma samples, in association with peri-tumoural oedema [393].

The role of AQP4 in astrocytic migration has not been completely elucidated. However, the findings of impaired migration of reactive astrocytes at the site of cortical stab injury in AQP4-null mice may suggest an important function in glial scar formation and maintenance of blood-brain barrier in the setting of cerebral trauma [408].

## 1.6.6 Regulation of Aquaporin-4

Regulation of aquaporins generally occurs via two major mechanisms: short-term and long-term regulation [393].

### Short-term regulation

Short-term regulation can be mediated by conformational changes or gating of the channel. This can occur through: (1) phosphorylation-dephosphorylation events induced by activation of intracellular pathways; (2) internalisation of proteins from the plasma

membrane; (3) protein-protein interactions; (4) binding with metal ions; and (5) binding of an inhibitor [393].

### *Phosphorylation of intracellular pathways*

The water permeability of AQP4 can be regulated by reversible protein phosphorylation, including protein kinase A (PKA), protein kinase C (PKC), casein kinase (CK) and calcium-calmodulin-dependent protein kinases (CaMK) [393, 396]. In renal cell lines, activating PKA increases the water permeability of AQP4 channels, whilst activation of PKC causes a downregulation of water permeability [396].

In brain cells, the activity of AQP4 is stimulated by vasopressin. In primary cultures of astrocytes, vasopressin was reported to increase the rate of cell swelling in hypotonic medium, and may regulate AQP4 via its 2 receptors: V1 and V2 [396]. The V1 receptor is coupled to phospholipid lipase C (PLC), which increases intracellular calcium concentrations to activate PKC and CaMK. The V2 receptor is coupled to adenyl cyclase, which produces cyclic-AMP (cAMP) and activates PKA. Both PKA and CaMK are thought to increase water permeability in AQP4 channels [396].

A number of agents stimulate cAMP, resulting in increased water permeability. These agents include: vasopressin, β-adrenoreceptor agonists and V2 receptor agonists [396]. Similarly, glutamate may exert its effect to upregulate AQP4 through the CaMK phosphorylation pathways [393]. In contrast, dopamine has been shown to downregulate AQP4 water permeability through the PKC-sensitive phosphorylation site [393].

### *Internalisation of proteins*

Another method of aquaporin regulation is “trafficking”, whereby AQP4 channels may be turned over between the plasma membrane and intracellular vesicles. Vasopressin has

been shown to internalise AQP2 in the collecting ducts of kidneys, but with AQP4, it is thought that PKC activation by phosphorylation produces internalisation of AQP4 channels from the plasma membrane [393].

### *Protein-protein interaction*

Interacting proteins have an important influence on AQP4 expression. AQP4 is associated with the dystrophin-glycoprotein complex, which includes dystrophin and α-syntrophin. Syntrophin may serve to as an anchoring protein in the membrane, and in mice lacking α-syntrophin, AQP4 was mislocalised away from the astrocytic endfeet adjacent to blood vessels. A similar finding was observed in mice lacking dystrophin [393, 396, 422].

A number of other proteins have been identified, including α-dystroglycan, actin and connexin that influence AQP4 expression [393, 408].

### *Metal ions, including mercury and lead*

There is some controversy over the effect of mercury on AQP4. The target residue for mercury ($Hg^{2+}$) in AQP4 is intracellular, unlike AQP1. Therefore, in previous studies using *Xenopus* oocytes or astrocytic cell cultures, $Hg^{2+}$ did not inhibit AQP4 because it was not internalised.[403] Recent studies by Yukutake et al. demonstrated that AQP4 was inhibited by both mercury ($Hg^{2+}$) and lead ($Pb^{2+}$), and possibly other metals, such as zinc ($Zn^{2+}$) and copper ($Cu^{2+}$) [393, 431].

## Long-term regulation

Long-term regulation is mediated by changes in aquaporin mRNA and / or protein synthesis or degradation rate [393]. Long-term regulation of AQP4 has been investigated

using developmental modulation, hormonal modulation, hypoxia, osmolality, and ammonia.

### *Developmental regulation*

AQP4 expression is regulated during development, with low AQP4 abundance in rat cerebellum during the first postnatal week, compared with a dramatic increase during the second week and weaning period [432]. In sheep, AQP4 mRNA was detectable during early gestation but increased substantially by 80% of gestation and remained at adult levels by 90% of gestation [433].

### *Hormonal regulation*

Hormonal modulation has been investigated, including corticosteroids, testosterone and progesterone. To date, treatment with steroids has shown conflicting results on AQP4 expression. In neonate lambs, the expected developmental increase in AQP4 expression was decreased by dexamethasone, indicating a post-transcriptional effect.[433]. However, in both astrocyte primary cell cultures and human samples in patients with brain tumours, there was limited effect on AQP4 expression [396].

Testosterone increased AQP4 mRNA expression and protein abundance [393]. In pregnancy, the AQP4 expression was increased in the rat cerebrum and cerebellum.

### *Hypoxia*

In astrocyte cell culture, hypoxia appears to cause a down-regulation of AQP4 expression at the mRNA and protein levels, with rapid recovery upon reoxygenation [396]. In a rodent contusional head injury model, increased cerebral oedema was observed following secondary insults of hypotension and hypoxia, in association with decreased expression of

AQP4 [409]. In a cellular model of traumatic brain injury, Rao et al. recently demonstrated that inhibition of oxidative / nitrative stress, activation of mitogen-activated protein kinases and transcriptional factor nuclear factor-kappa B (NF-κB) reduced the amount of cellular oedema and -reduced the extent of trauma-induced AQP4 upregulation in astrocyte cultures undergoing fluid percussion injury [410].

### *Hyperosmolality and hyponatraemia*

Hyperosmolality causes increased levels of AQP4 and AQP9 expression in astrocytic cell cultures and in rats when intraperitoneal mannitol is administered [396].

Vajda et al. demonstrated in rat brains that AQP4 expression was increased in response to exposure to systemic hyponatraemia for 4 to 48 hours. However, the mRNA was not increased, suggesting increased immunoreactivity, possibly from a conformational change to the structure of the AQP4 protein [434].

### *Ammonia*

Elevated ammonia in acute hepatic encephalopathy and post-nephrectomy causes cerebral oedema, possibly through the up-regulation of AQP4. The mechanism for this is uncertain [396, 435].

## 1.6.7 Modulation of Aquaporin-4

Much attention has been paid to identifying new therapeutic agents to modulate the function of aquaporins. There is tremendous potential for clinical applications in the setting of cerebral and spinal cord oedema, and possibly post-traumatic syringomyelia [392, 395, 404]. Several agents have been trialled on AQP1 and AQP4, including mercurials, phorbol esters, vasopressin antagonists, hypoxia and anti-oxidants, melatonin

and edaravone, hyperosmolar therapy, acetazolamide and anti-epileptics, and diuretics, including their derivatives, AqB013, AqB050 and AqF026. However, until recently, inhibitors of aquaporins have been associated with toxicity, low efficacy, and lack of specificity [436].

## Mercurials

Mercurials have been used to inhibit many aquaporins, including AQP1, and they have previously been found to be ineffective against AQP4 in *Xenopus* oocyte studies [393, 403, 437]. More recently, mercurials have been effective at inhibiting AQP4 in proteoliposomes, but *in vivo* animal studies have not shown any effect [431, 438]. Interestingly, in a rodent study on AQP1 in traumatic cerebral oedema, mercurials selectively blocked the function of AQP1, attenuating the influence of corticosteroids and acidosis [411]. However, the main limitation to the use of mercurials is its toxicity, particularly in humans.

## Protein Kinase C activators / Phorbol esters

Phorbol esters has been demonstrated to activate protein kinase C (PKC) and thereby downregulate the water permeability of AQP4 in *Xenopus* oocyte expression and cultured renal epithelial cells [396].

Phorbol esters have been used to investigate the effects of AQP4 downregulation in cerebral oedema from contusion and MCA ischaemia models [439-442]. In both models, there was a statistically significant decrease in the water content of brain parenchyma. However, phorbol esters are associated with toxicity, including increased respiratory rate, decreased mean blood pressure, decreased granulocyte count, haemorrhagic and interstitial pneumonitis, interstitial pulmonary fibrosis and carcinogenesis [439, 441].

## Vasopressin antagonists (including SR49059)

Vasopressin has been known to regulate AQP4 expression and translocation in renal collecting ducts and brain cells. Vasopressin V1a receptor antagonists have been shown to reduce cerebral oedema in rodent models [443]. Recently, a potent selective V1a receptor antagonist (SR49059) was developed, which demonstrated significant reduction in cerebral oedema in a middle cerebral artery occlusion rodent model of ischaemia [443, 444].

## Hypoxia and anti-oxidants

It has been shown that hypoxia increases the expression of AQP1 via the hypoxia-inducing factor A (HIFa) and reduces AQP4 expression [409, 423]. Taya et al. demonstrated in a rodent head injury model that hypotension and hypoxia resulted in increased vasogenic oedema, and reduced AQP4 expression [409]. Rao et al. showed that antioxidants in a cellular model of traumatic brain injury produced AQP4 downregulation [410].

## Melatonin and Edaravone

Melatonin has been used to suppress the increase in AQP1 expression, which has been typically observed following spinal cord injuries in animal models [423]. Rodents receiving melatonin were noted to have decreased immunolabelling and lower degree of neuropathic pain post spinal cord injury [423].

Edaravone is a free radical scavenger that has been used in the setting of acute ischaemia to reduce the extent of infarction. In animal models, the use of edaravone was associated

with a reduction in AQP4 expression, cerebral oedema and improved neurological outcomes [445].

The mechanisms of action for both melatonin and edaravone are unknown, but these may be mediated through their anti-oxidant effects [445].

## Hyperosmolar therapy

Hypertonic saline has been used in various stroke models to modulate the function of AQP4. However, the effect of hypertonic saline on AQP4 varies depending on the specific stroke model, making development of therapeutic agents difficult [392].

## Acetazolamide and anti-epileptics

Acetazolamide and other sulphonamide carbonic anhydrase inhibitors, such as methazolamide, valproic acid and topiramate, have been investigated as inhibitors of AQP4 by using a combination of *in silico* and *in vitro* methods [392, 405, 436, 438, 446-448]. Several potential agents have been identified, but no effect of acetazolamide on AQP4 function was found in other *in vitro* studies by Yang et al. and Sogaard et al. [435, 449].

## Diuretics (including bumetanide)

Bumetanide, along with furosemide and torsemide, is a loop diuretic drug that blocks the $Na^+$-$K^+$-$2Cl^-$ cotransport in the kidney. It has been shown to be moderately effective in attenuating AQP-mediated osmotic swelling in *Xenopus laevis* oocytes by Migliati et al. [436, 438]. O'Donnell et al. showed that bumetanide demonstrated a protective effect in the rodent brain oedema by a mechanism independent of its renal diuretic activity [450]. Furthermore, bumetanide reduced AQP4 water flux in oocytes, which was not present

when furosemide was applied [436]. Similarly in astrocyte cultures undergoing fluid percussion injury to simulate brain trauma, bumetanide reduced cell swelling and expression of AQP4 [410]. An advantage of bumetanide is that it is relatively well-tolerated without overt toxicity [436]. However, the effect of this cannot be validated due to its concurrent partial inhibition of the endothelial cell Na-Cl-K cotransporter [392].

### AqB013, AqB050 and AqF026

AqB013 is a compound structurally similar to bumetanide that has been demonstrated to be effective at inhibiting mammalian AQP1 and AQP4 in the *X. laevis* oocyte [436, 438]. It blocks the action of AQP4 by occluding the water pore at an intracellular level. AqB013 had no action on the $Na^+$-$K^+$-$2Cl^-$ cotransporter, and has been shown to be specific for the AQP4 channel [436, 438]. Since the development of AqB013, further refinements in the formulation have been made. AqB050 is a more specific antagonist of the AQP1 and AQP4 water pore, while AqF026 was isolated as an agonist of the AQP4 water channel. [Personal communication, Yool et al.] These agents have been trialled *in-vitro* on oocytes, and preliminary pharmacokinetic tests have been performed on animal studies.

## 1.6.8 Potential clinical implications

### Aquaporins and cerebral oedema

Significant morbidity is associated with cerebral oedema secondary from trauma, ischaemia and other causes. Reduction of cerebral oedema through molecular methods, such as modulation of aquaporins offers tremendous therapeutic potential. Since aquaporins have different functions in the various types of cerebral oedema, the ability to both promote and inhibit aquaporin function would be beneficial.

In cytotoxic oedema, an aquaporin inhibitor may limit the amount of initial brain swelling, such as post traumatic brain njury or infarct. For vasogenic oedema, such as in the setting of a cerebral infection, tumour or later stages of trauma, upregulation of aquaporin function may improve the removal of interstitial brain water [387, 409].

## Aquaporins and hydrocephalus

Given the putative role of AQP1 in CSF production, inhibitors of AQP1 may be useful adjuncts to treatments for hydrocephalus and benign intracranial hypertension [388]. Oshio also demonstrated that AQP1-null mice had reduced osmotic permeability of the choroid plexus epithelium and decreased intracranial pressure [398, 405].

## Aquaporins and glial scarring or tumour growth inhibition

The involvement of aquaporins in cell migration shows promise for therapeutic intervention in the setting of neuronal injury and tumour growth. As glial scarring may be an important component inhibiting neuronal regeneration, inhibition of aquaporins may delay glial scarring and promote synaptogenesis [388].

Aquaporins are also upregulated in aggressive, infiltrative tumours, such as lung carcinoma, and glial tumours. Inhibition of aquaporins may slow tumour growth [388].

## Aquaporins and spinal cord trauma / post-traumatic syringomyelia

Given the role of AQP4 in water regulation, there may be a potential role for modulation of AQP4 function as a therapeutic target in the setting of spinal cord injury. In the acute stages of spinal cord injury, inhibition of AQP4 and AQP1 may reduce the extent of spinal cord oedema, and, at later stages, the development of neuropathic pain, myelomalacia and, possibly, post-traumatic syringomyelia [421].

### Aquaporins and other neurological disorders

Associations between aquaporins and neurodegenerative disorders, such as Alzheimer's disease and Parkinson's disease, have been suggested in several studies. Potential therapeutic options are being investigated for AQP1 in Alzheimer's disease and AQP9 in Parkinson's disease [387].

### 1.6.9 Conclusion

Aquaporins are a family of transmembrane water channels that are present throughout the body. In the central nervous system, there are a number of conditions, in which aquaporins may play an important role in regulation of water homeostasis. Given the relationship between spinal cord trauma, CSF circulation and post-traumatic syringomyelia, it is possible that aquaporins, in particular AQP4, may make a substantial contribution to the pathophysiology of post-traumatic syringomyelia. In addition, modulation of AQP4 has the potential to offer novel therapeutic options in many pathological conditions, including spinal cord oedema and post-traumatic syringomyelia.

## *1.7 Summary*

Development of novel treatments for post-traumatic syringomyelia is unlikely to advance until a more complete understanding of the complex pathophysiological processes is acquired [2]. Many theories have been proposed regarding the influences of fluid flow, blood spinal cord barrier, and cellular responses. However, theories on these processes need to be validated first in models of post-traumatic syringomyelia. Improvements in treatment may come from modulation of such pathophysiological processes.

## *1.8 Hypotheses and aims*

### 1.8.1 Hypotheses

The overall hypothesis for this thesis on the pathophysiology of post-traumatic syringomyelia is: syrinx fluid is derived from cerebrospinal fluid, which flows into and out of syrinx cavities via specific pathways. This fluid movement is promoted by spinal arachnoiditis, and is related to pressure pulsations and molecular processes. Specifically, the following hypotheses are proposed:

1. The biochemical composition of fluid within a syrinx cavity reflects the processes involved in fluid movement into a syrinx. An identical composition to cerebrospinal fluid would suggest that syrinx fluid orignates from CSF.

2. A reproducible animal model of post-traumatic syringomyelia can be developed using direct trauma with a spinal cord impactor.

3. Arachnoiditis produces increased cerebrospinal fluid flow from the spinal subarachnoid space into the spinal cord parenchyma via perivascular spaces. This may be caused by mismatch in timing between arterial and CSF pulsations, such that the pulsations are “decoupled”.

4. Fluid outflow from syrinx cavities occurs via specific pathways.

5. Aquaporins are involved in the regulation of fluid movement in post-traumatic syringomylia. The expression of AQP4 and AQP1 is increased in post-traumatic syringomyelia, and may function to remove excess fluid in the spinal cord.

6. Modulation of aquaporin function will alter syrinx size.

### 1.8.2 Aims

The aims of this project were:

1. To compare the biochemistry of fluid aspirated from syrinx cavities with that of CSF and serum in human patients undergoing syrinx shunt operations for syringomyelia.

2. To develop an animal model of post-traumatic syringomyelia using a computer-controlled motorised spinal cord impactor in combination with arachnoiditis, that is reproducible and replicates the human condition.

3. To investigate the characteristics of CSF flow from the subarachnoid space into the spinal cord in animal models of spinal arachnoiditis by assessing:

    a. The pattern and quantity of CSF flow into the spinal cord in a rodent model of spinal arachnoiditis:

        i. using horseradish peroxidase (HRP) as the CSF tracer

        ii. using Alexa-Fluor 647 ovalbumin (AFO) as the CSF tracer

    b. The pattern of CSF pulsations in the spinal subarachnoid space in a sheep model of spinal arachnoiditis via an in-vivo telemetry system and whether CSF pulsation delays occur across the region of arachnoiditis.

4. To investigate whether specific outflow pathways exist in a sheep model of post-traumatic syringomyelia.

5. To investigate the association between AQP4, AQP1 and post-traumatic syringomyelia by assessing:

a. The expression of AQP4 and AQP1 in a contusional spinal cord injury model and an impactor model of post-traumatic syringomyelia in rats.

b. The effect of AQP4 modulation on existing syrinxes using the excitotoxic extracanalicular model of post-traumatic syringomyelia in rats.

# Chapter 2 General methods

## *2.1 Animal care*

All animals were handled in accordance with the Australian Code of Practice for the Care and Use of Animals for Scientific Purposes, NHMRC 7th Edition 2004 and the NSW Animal Research Act 1985 and Regulation 1995.

### 2.1.1 Ethical approval and number of animals used

Ethical approval was obtained from the Macquarie University Animal Ethics Committee (ARA 2009/49, 2009/50 and 2010/26), the University of NSW Animal Care and Ethics Committee (ACEC 09/75A) and the Institute of Medical & Veterinary Science (IMVS) Animal Ethics Committee (Veterinary Services Division) (Project No. 81a/10, 48/07, 79/06).

Sprague-Dawley male rats were used for the rodent experiments and were supplied by the Animal Resource Centre in Perth, Western Australia. Merino male wethers were supplied by the IMVS, Adelaide for the sheep experiments. The number of animals used and the ethical approval references for each project is listed in Table 2.1-1.

### 2.1.2 General care of rodents

Animals were housed in standard cages of no more than four animals to a cage at the animal holding facilities at Macquarie University and University of NSW. Post-operatively, the animals were housed individually for 1 week, and were then housed with previous cage mates. Food and water were provided ad libitum, and bedding was changed weekly. Attempts were made to allow for acclimatisation to new surroundings before any procedures were performed.

**Table 2.1-1 Number of animals used in experiments in this thesis.**

| Experiments | Ethical Approval References | No. of animals used | Average weight |
|---|---|---|---|
| Direct trauma model of post-traumatic syringomyelia using a computer-controlled motorised spinal cord impactor* | ARA 2009/50 | 75 rats | 481 g |
| Cerebrospinal fluid flow in spinal arachnoiditis using horseradish peroxidase | ACEC 09/75a, ARA 2009/49 | 63 rats | 403 g |
| Cerebrospinal fluid flow in spinal arachnoiditis using Alexa-fluor 647 Ovalbumin | ARA 2009/49 | 14 rats | 323 g |
| The effect of aquaporin-4 modulation in a rodent model of post-traumatic syringomyelia | ARA 2010/26 | 32 rats | 416 g |
| Fluid outflow in large animal model of post-traumatic syringomyelia | 81a/10, 48/07, 79/06 | 12 sheep | 45 kg |
| In-vivo telemetry of cerebrospinal fluid pulsations in spinal arachnoiditis | 81a/10 | 8 sheep | 50 kg |

*** Specimens used for additional projects: (1) Aquaporin-4 and Aquaporin-1 expression in spinal cord injury and post-traumatic syringomyelia; (2) Micoglia response in spinal cord injury and post-traumatic syringomyelia.**

### 2.1.3 General care of sheep

Animals were operated upon and monitored in separate pens at the IMVS facility in central Adelaide for 5 days post-operatively. For the outflow study, the sheep were transferred to the Gilles Plains facility following the immediate post-operative period, where they were housed in group pens of three sheep. At the conclusion of the experiment, the animals were transferred back to the central Adelaide facility for

perfusion. For the in-vivo telemetry study, the animals were housed individually for the duration of the study. Food and water were provided ad libitum at all times.

## *2.2 Anaesthesia and peri-operative monitoring*

### 2.2.1 Anaesthesia and monitoring of rodents

Prior to the administration of general anaesthetic, the animals were weighed. Anaesthesia was induced with 4% isoflurane in 2L $O_2$ in an induction chamber, and was maintained via a nose cone at 2 – 2.5% isoflurane in 2L $O_2$ during the operation. The animals were placed prone with thoracic supports, and the hindlimbs were flexed to ensure that the abdominal respiratory movements were free. The depth of anaesthesia was assessed by the respiratory rate, the response to painful stimulation (hindlimb web pinch) and the core temperature at 0, 5, 10, 15, and every 15 minutes thereafter during the anaesthetic (See Appendix 13.6 for anaesthetic monitoring sheet). At the conclusion of the operation, the animals received 0.1 – 0.15 mL of buprenorphine (Temgesic©, Reckitt Benckiser Healthcare, Hull, UK) prior to cessation of anaesthetic, and 100% $O_2$ was administered for 1 – 2 minutes prior to positioning the animal in a left lateral position for recovery. Post-anaesthetic monitoring was performed for 5, 10, 15 minutes and every 15 minutes for an hour under a heat lamp.

Post-operative monitoring was performed on a daily basis for 2 weeks, and then weekly until the conclusion of the experiment. The animals were assessed for levels of distress, weight and neurological function. A modified Tarlov scale was used for neurological monitoring.[289, 451] (See Appendix 13.6 for post-monitoring sheet)

### 2.2.2 Anaesthesia and monitoring of sheep

The administration of general anaesthetic and post-operative monitoring were performed with the assistance of the laboratory support staff at IMVS Adelaide. Anaesthesia was induced with an intravenous dose of 1g thiopentone and was subsequently maintained with 2.5% isoflurane via an endotracheal tube. The animals were allowed to breathe spontaneously, but mechanically assisted ventilation was used if spontaneous respiration was inadequate. In survival experiments, the animals were given 100% $O_2$ prior to the conclusion of the procedure, until they were spontaneously breathing. In non-survival experiments, the anaesthetic and $O_2$ were ceased when the fixative was being administered.

## *2.3 Experimental procedures*

### 2.3.1 Laminectomy and induction of spinal arachnoiditis in rodents

All animals in the rodent experiments received a C7-T1 laminectomy, including the control animals. The animals were positioned prone and the skin was prepared with shaving and application of topical povidone-iodine. The T2 spinous process was used to localise the level of the laminectomies. Following a midline incision, the spinous processes of C6 – T2 were exposed by separating the overlying muscles from the laminae to the medial margin of the lateral masses with blunt and sharp dissection, using microscissors under magnification with the operating microscope. The laminae of T1 and C7 were removed with bone rongeurs, taking care not to traumatise the spinal cord.

Subarachnoid kaolin was injected at the conclusion of the operations for post-traumatic syringomyelia or spinal arachnoiditis induction. The kaolin suspension was prepared pre-operatively by mixing anhydrous kaolin powder (aluminium silicate, Sigma-Aldrich, St

Louis, MO, USA) with 0.9% Saline solution at a concentration of 250 mg / mL. A volume of 5 or 10 μL was measured out with a micropipette and transferred to a 0.5mL 30G insulin syringe (Ultra-Fine II, Beckton Dickinson and Co, NE ,US). The needle was bent to 70 - $80^0$ to allow for easier penetration of the dura and access to the subarachnoid space. The injection was performed slowly over 5 seconds to ensure that the kaolin suspension spread across the midline and remained localised to the C7 – T1 region.

### 2.3.2 Laminectomy and induction of spinal arachnoiditis in sheep

The skin was prepared by shaving and application of povidone-iodine and intravenous antibiotics at induction. After bilateral stripping of paraspinal muscles, a T2 – T3 laminectomy was performed in all animals with bone rongeurs and kerrison punches. The dura and spinal cord were exposed for a length of approximately 5 cm. Two longitudinal incisions of approximately 5mm in length were made in the dura for syrinx induction or implantation of the pressure transducers for telemetry monitoring. To produce arachnoiditis, 0.5 mL of 250 mg/mL kaolin solution was mixed with the thrombin component of a two-component fibrin sealant (Tisseel Duo 500, Baxter Healthcare Pty Ltd, NSW, Australia) and drawn up into the double-barrelled applicator. The blunt needle attached to the applicator was bent to $85^0$ at the tip and care was taken not to traumatise the spinal cord during the kaolin injection. The kaolin and fibrin mixture was slowly injected into the subarachnoid space on both sides of the dural incisions to a total of 0.2 mL. Tisseel was added to prevent kaolin solution from leaking out of the spinal subarachnoid space.

### 2.3.3 Post-traumatic syringomyelia induction with spinal cord impactor

The Infinite-Horizon spinal cord impactor (Precision Systems and Instrumentation, LLC, US) was used for the impactor study (Chapter 4) and the Aquaporin 4 and Aquaporin 1 expression study (Chapter 9). In addition to the operative methods described under the "Laminectomy and induction of spinal arachnoiditis" section, the lateral masses were exposed to the lateral margins from C6 to T2 to permit the application of the stabilising clamps. The clamps were fixed into position such that spinal cord pulsations were still visible through the dura and the subarachnoid space was still present. The clamps were tightened to the extent of preventing any movement during the impact, but without fracturing the C6 lamina. The T2 spinous process was sufficiently strong to withstand the forces applied by the stabilising clamps.

### 2.3.4 Post-traumatic syringomyelia induction with quisqualic acid injection in rodents

The excitotoxic post-traumatic syrinx model was previously described by Yang et al. and Brodbelt et al.[195, 321] This model was used in the effect of aquaporin modulation study (Chapter 10). In addition to the operative methods described under the "Laminectomy and induction of spinal arachnoiditis" section, four injections of 0.5 μL quisqualic acid (24 mg/mL, Tocris Cookson, Bristol, UK), mixed with 1% Evans blue (Sigma-Aldrich, St Louis, MO, USA) were performed along the right dorsal rootlets between C7 and T1. For each injection, the dura and arachnoid were opened with a 0.5mL 30G insulin syringe needle (Ultra-Fine II, Beckton Dickinson and Co, NE ,US), and the pia was punctured. A glass needle-tipped (outer diameter 50 μm) 10-μL syringe (SGE International Pty Ltd, VIC, Australia), held in a stereotaxic micromanipulator, was then introduced through the

dural and pial openings to deliver the quisqualic acid injection into the spinal cord parenchyma at a depth of 1mm. The injection was performed over 30 seconds under microscopic vision to detect any leakage of quisqualic acid, as indicated by the leakage of the Evans' blue solution.

### 2.3.5 Post-traumatic syringomyelia induction with quisqualic acid injection in sheep

The excitotoxic post-traumatic syrinx model in a sheep model was used for the fluid outflow study (Chapter 8). Following the laminectomy, a 10 μL microsyringe (SGE International Pty Ltd, VIC, Australia) with a beveled needle (0.19 mm outer diameter) was used to deliver four 5 μL intraparenchymal injections of 24 mg/mL quisqualic acid (Tocris Cookson, Bristol UK) and 1% Evans Blue solution (Sigma-Aldrich, NSW, Australia) along the right dorsal root entry zones at a depth of 3 mm from the pial surface. Each injection was performed over 30 seconds with the needle held in situ for another 30 seconds to minimize leakage.

### 2.3.6 CSF flow studies in rodents

The CSF flow studies (Chapters 5 & 6) were followed by immediate perfusion-fixation on a downdraft bench. Under general anaesthetic, the animal was positioned prone with the head flexed on a ventral cushion such that the atlantoaxial membrane was taut. A midline incision was made from the external occipital protuberance to the mid-cervical spine. Under the operating microscope, the occiput, C1 lamina and the atlantoccipital membrane were exposed. A sharpened needle on a 10 μL microsyringe held in a stereotaxic manipulator was inserted into the cisterna magna at a depth of 3mm from the bevel tip. The membrane was withdrawn slightly such that the atlantoccipital membrane

was tented up. Care was taken to ensure that there was no leakage of CSF during the injection of CSF tracer. Horseradish peroxidase (Invitrogen, Carlsbad, CA, USA) and Alexa-Fluor 647 Ovalbumin (Invitrogen, Carlsbad, CA, US) were used as CSF tracers and were injected slowly at 2 μL / min over 5 minutes. After the designated time interval, the animal was positioned supine for intracardiac perfusion-fixation.

## *2.4 Perfusion-fixation*

### 2.4.1 Perfusion-fixation in rodents

At the conclusion of the experiment, the animals were positioned supine for transcardiac perfusion. Under general anaesthetic with 2% isoflurane, a subcostal incision through the anterior abdominal musculature was made to access the peritoneal cavity. The diaphragm was divided and longitudinal incisions along the lateral margins of the anterior chest wall were made to expose the heart and aorta. A blunt 18G needle was introduced through the left ventricle to the aorta. The right atrium was transected to allow outflow. Sodium heparin (1000 IU in 1 mL, Hospira, VIC, Australia) was injected, followed by perfusion with at least 200 mL of 4% paraformaldehyde in 0.1 M phosphate buffer (pH = 7.46) at 50 mL / min.

### 2.4.2 Perfusion-fixation in sheep

At the completion of the study, the animals were turned supine under general anaesthetic for perfusion-fixation. The technique for perfusion-fixation in sheep was previously described by Santorenos et al. [452]. Longitudinal cervical incisions were made and the common carotid artery and internal jugular vein were dissected out bilaterally. Following an intravenous injection of 10000 IU of heparin (Hospira, VIC, Australia) into the internal jugular vein, the common carotid arteries were cannulated to allow fixative

inflow directed proximally in the left carotid and distally in the right carotid. The internal jugular veins were divided to permit outflow. Each animal was perfused with 10L of 4% paraformaldehyde in 0.1 M of phosphate buffer (pH = 7.4) at a pressure of 120 mmHg. Perfusion pressures were generated with compressed air in a closed system and monitored with a sphygmomanometer. The drainage from the jugular veins was removed in a collection container.

## *2.5 Solution preparations*

### 2.5.1 Horseradish peroxidase (HRP)

HRP powder (Invitrogen, Carlsbad, CA, US) was stored in a -30$^0$C freezer until use. Solutions were made fresh on the day of the experiment. Various concentrations were trialled for the CSF flow studies, ranging from 3 – 10% solutions (i.e. 3 – 10 g / 100 mL) in sterile 0.9% saline solution. The enzymatic activity varied between batches of HRP depending on the duration of storage prior to use.

### 2.5.2 Alexa-Fluor 647 Ovalbumin (AFO)

AFO powder (Invitrogen, US) was stored within a sealed bag in a -30$^0$C freezer until use. As much as possible, solutions were prepared fresh on the day of the experiment. However, any unused solution was kept in a -30$^0$C freezer in a sealed container, covered with aluminium foil to prevent light exposure. A 10% solution was prepared, mixed in 0.1 M phosphate buffered saline (pH = 7.4) containing 0.01% sodium azide.

### 2.5.3 Paraformaldehyde

Paraformaldehyde 4% solution in phosphate buffer (pH= 7.4) was prepared fresh prior to the perfusion of animals. A volume of approximately 400 mL was prepared for each

animal. Paraformaldehyde powder was weighed and dissolved in distilled water over gentle heating at $60^0$C. Once dissolved, 0.1 M phosphate buffer solution consisting of four-fifths $Na_2HPO_4$ (Sigma-Aldrich, St Louis, MO, USA) and one-fifth $NaH_2PO_4$ (Sigma-Aldrich, St Louis, MO, USA) were added to the paraformaldehyde solution. Finally, the solution was corrected to pH of 7.4, filtered and cooled to room temperature.

### 2.5.4 Quisqualic acid in Evans' blue solution

Quisqualic acid (Tocris Cookson Ltd, Bristol, UK) solution was prepared as a supersaturated suspension at 24 mg / mL. The quisqualic acid powder was mixed with one-fifth 1% Evans' blue solution (Sigma-Aldrich, St Louis, MO, USA), and four-fifths 0.9% sterile saline solution. The preparation was then aliquoted into smaller quantities and stored in a $-30^0$C freezer until use.

## *2.6 Tissue processing*

### 2.6.1 Tissue removal from rodents

The spinal column and skull were removed from each animal immediately after perfusion-fixation. The brain and spinal cord were dissected out and were post-fixed in 4% paraformaldehyde in 0.1 M phosphate buffer solution overnight. The brain was sectioned into 3 mm blocks at the cerebrum, cerebellum and medulla, while the spinal cord was sectioned according to the spinal level as demarcated by the nerve roots from C2 to T4. A lumbar section was also included.

### 2.6.2 Paraffin embedding

Paraffin embedding was performed by an automated tissue processor (Leica ASP200S, Leica Biosystems, Nussloch, Germany) using a 4-hour cycle protocol as devised by

Douglas-Hanly Moir Laboratory, NSW, Australia. The schedule consisted of gradient ethanol baths, followed by xylene and paraffin baths. (See Appendix 13.7.1 for details of schedule). Samples were embedded in paraffin blocks and serial sections were cut at 5 μm thickness. The sections were floated on to Superfrost slides (Menzel-Glaser, Braunschweig, Germany), which were allowed to dry in an oven at $37^0$C for 24 hours.

### 2.6.3 Vibratome sectioning

Specimens were glued onto a block and serial transverse sections were produced at 50 μm thicknesses using a semi-automated vibratome (Leica VT1200S, Leica Biosystems, Nussloch, Germany). The sections were floated in Tris Buffer (pH = 7.6), mounted onto SuperFrost Plus slides (Menzel-Glaser, Braunschweig, Germany) and allowed to air dry at room temperature for at least 4 hours.

## *2.7 Staining*

### 2.7.1 Haematoxylin and eosin staining

Haematoxylin and eosin staining was performed using the Lillie-Meyer method. (See Appendix 0) This consisted of rehydrating the slides with xylene (2 baths at 2 minutes each), and gradient ethanol baths at 100% and 90% concentration at 1 minute each. After rinsing with distilled $H_2O$ for 1 minute, the slides were placed in haematoxylin solution for 5 minutes, followed by a second water rinse and a quick dip in the differentiator (2% acid alcohol). The slides were placed into a blueing agent, dilute Lithium carbonate, for 10 – 15 seconds, and then washed in running tap water for 5 minutes. Following a 2-minute wash in alcoholic Eosin, the slides were dehydrated with gradient ethanol washes (90% for 15 seconds, 2 x 100% for 15 seconds each) before xylene baths (2 minutes

each). Coverslipping was performed with Gurr's Depex mountant (DPX) and the slides were allowed to dry in an oven at $37^0$C for 2 days.

### 2.7.2 HRP staining using TMB

The slides were rinsed in distilled H2O for 15 seconds, and then incubated in 0.01 M sodium acetate buffer containing 0.05% tetramethylbenzidine (TMB) and 0.01% sodium nitroferricyanide (III) dehydrate for 20 minutes with gentle heating and slow magnetic stirrer. Thirty microlitres of hydrogen peroxide was added, and incubation for another 20 minutes was performed. The sections were washed in 0.01 M sodium acetate, followed by 5% ammonium molybdate (IV) tetrahydrate to stablise the reaction product for 15 minutes. After another wash in sodium acetate, the slides were dehydrated using gradient ethanol and xylene baths, and coverslipped with DPX mountant. For details of the staining process, see Appendix 13.7.3

### 2.7.3 AQP4, AQP1 and GFAP immunohistochemical staining

Deparaffinization and rehydration with xylene and gradient ethanol washes were performed prior to antigen retrieval with 0.1M citrate buffer (pH 6.0) at $95^0$C for 20 minutes. The slides were blocked with 10% normal donkey serum and incubated with first with primary anti-AQP4 (1:50 dilution, SC-20812, Rabbit Polyclonal IgG, 0.2mg/ml, Santa Cruz, CA, US) overnight and then with secondary donkey anti-rabbit Alex Fluor 594 (1:400 dilution, A21207, Invitrogen Life Technologies, NY, US). Anti-AQP1 (1:10, SC-34009, goat polyclonal, Santa Cruz, CA, US) and anti-GFAP (1:800, MAB360, Mouse IgG1 mAb, 1mg/ml, Chemicon Millipore, CA, US) were applied for 2 hours, and secondary antibodies were subsequently applied with Donkey anti-goat Dylight 488(1:400, ab96875, Abcam, MA, US) and Donkey anti-mouse Dylight 649 (1:400, 715-

495-140, Jackson Immunoresearch Laboratories, PA, US). The sections were finally incubated in DAPI (1 μg/mL) for 1 minute, coverslipped with fluorescent mounting medium (DAKO, S3023, Carpinteria, CA, US).

## *2.8 Measurements*

### 2.8.1 Randomisation

Allocation of animals to various treatment and time point groups was performed in a random manner without any pre-determined pattern. Randomisation techniques, such as computer-generated or block randomisation, were not used. Allocation concealment was not possible for the primary researchers who performed the operations.

### 2.8.2 Blinding

Although blinding of the group allocations was not possible at the initial operations, tissue processing and measurements were performed with the researchers blinded to the group allocations. The animals were de-identified prior to measurements being undertaken. In some studies, two independent observers were used to reduce measurement bias.

### 2.8.3 Statistical analyses

Qualitative assessments were performed in the majority of experiments and statistical analyses were not applied. Quantitative assessments included measurements of syrinx cavity size (Chapters 4 and 10), relative optical density (Chapter 5) and immunofluorescent signal intensity (Chapter 9). In these studies, univariate analysis of variance (ANOVA) was used to determine the statistical difference between the various treatment groups over all time points. In chapter 5, post-hoc Bonferroni tests were

performed for significance results to adjust for multiple comparisons. A value of $p<0.05$ was considered statistically significant. Software used included Microsoft Excel 2007 (Microsoft Corp, Redmond, WA, US) and IBM SPSS v.19 (IBM Corp, Armonk, NY, US)

### 2.8.4 Optical and immunohistochemical density measurements

Quantification of the intensity of the reaction product of HRP (in Chapter 5) and the expression of AQP4 and GFAP (in Chapter 9) was performed using Image J, a Java-based application (Version 1.4.5, National Institute of Health, Maryland, USA).

For the HRP reaction product in Chapter 5, a method of relative optical density (ROD) was used, in which a 30 pixel diameter region around the central canal was selected and the ROD was calculated for the central canal and the background at each spinal level. The ROD of the background was normalised across the various spinal levels, and the ROD central canal : ROD background ratios were used for comparisons between the experimental groups (arachnoiditis or control), spinal levels, timepoints (3 days, 1, 3, 6 or 12 weeks).

For AQP4 and GFAP expression in Chapter 9, measures were used to reduce inaccuracies associated with immunodensity asessments. Dual-labelled fluorescent images were obtained with the identical exposure times for all spinal levels and animals of 300 ms for AlexaFluor 594, reflecting AQP4 expression and 1500 ms for DyLight 649, reflecting GFAP expression. As mentioned above, the signal density was quantified using the Image-J software. Unfortunately, the integrated density could not be applied to the whole spinal cord section, due to limitations of the Image-J software. Measurements of the integrated density of the perimeter around the cavity were obtained by first outlining a 400 pixel margin by using the “selection brush” function to obtain an overall average. In

addition, separate circular areas of 400 pixel diameter in size representing normal grey and white matter were compared with the adjacent areas of the cavity perimeter within the same section. The representative regions were the dorsal and ventral horns, dorsal columns and ventral tracts. The integrated density of AQP4 and GFAP were determined by using the "Analyze – Set measurements" and "Analyze – Measure" functions on Image J. Finally, the integrated signal intensity of AQP4 was compared to the GFAP expression by converting the intensity as an AQP4:GFAP signal intensity ratio.

Certain limitations exist with this method of assessing AQP4 and GFAP expression by using integrated density. Immunodensity measurements are notorious for inaccuracies due to variations during tissue processing and image acquisition. Changes to exposure times and threshold values can significantly alter the results of immunodensity. In addition, the regions selected for assessment of AQP4 and GFAP expression were arbitrarily chosen, and the results may be influenced by sampling bias. Future experiments could use immunoblotting techniques for quantification of AQP4 and GFAP expression.

# Chapter 3 Biochemical analysis of syringomyelia fluid

## *3.1 Abstract*

**Background**: Syringomyelia remains a difficult condition to treat. The current understanding of syrinx pathophysiology is incomplete and relies on the assumption that syrinx fluid generally originates from CSF and is identical in composition. However, the exact composition and origin of syrinx fluid has not yet been established.

**Object**: The objective of the study was to compare the biochemical composition of syrinx fluid with the composition of spinal CSF and serum.

**Methods**: Symptomatic patients undergoing syrinx shunting surgery were recruited for the study. CSF and syrinx fluid samples were taken intra-operatively prior to syrinx shunt insertion. The fluid samples and serum were examined for electrolytes, protein, glucose and osmolality.

**Results**: Five patients underwent CSF and syrinx fluid sampling. In the biochemistry profile, the results of the electrolytes in CSF and syrinx fluid were very similar. Larger differences between CSF and syrinx fluid protein and glucose content were present. This did not correlate with the underlying etiology.

**Conclusion**: The similarity in biochemical profile between CSF and syrinx fluid suggests that the origin of syrinx fluid in these cases is likely to be CSF, although other sources of syrinx fluid cannot be excluded. However, the underlying molecular processes of fluid and solute movement into a syrinx cavity are yet to be determined.

**Keywords**: Biochemistry, Cerebrospinal fluid, Cerebrospinal fluid shunts, Clinical laboratory techniques, Syringomyelia

## 3.2 Introduction

Syringomyelia affects approximately 8.4 people per 100,000 per year.[22, 28] It commonly occurs in association with conditions such as Chiari malformations, spinal cord injury, arachnoiditis, and neoplasms affecting the spinal cord [23]. While the associations with these conditions are well-known, the pathogenesis of syringomyelia remains enigmatic. Unlike Chiari-related syringomyelia, which has a treatment success rate of 80-90% after posterior fossa decompression, treatment for other types of syringomyelia remains unsatisfactory, with long term recurrence rates of up to 50% [2, 40]. It is unlikely that treatment will improve until the factors contributing to syrinx development and expansion are better understood [2].

Although there has been a multitude of theories proposed, there is still no satisfactory concept that completely explains the mechanisms for syrinx development and expansion [160]. Many fundamental questions have yet to be answered, including the biochemical composition of the syrinx fluid itself. It has generally been assumed that the origin of fluid within the syrinx cavity is cerebrospinal fluid (CSF), but this has not been proven through chemical analysis. The objective of this study was to compare the biochemistry of fluid aspirated from syrinx cavities with that of CSF and serum in patients receiving shunt operations for syringomyelia.

## 3.3 Methods

This study was conducted at Dalcross Private and Macquarie University Hospitals between January 2010 and January 2012 with the approval of the Human Research Ethics Committee at Macquarie University. Participants were invited to the study only if a syrinx shunt was being considered. Written informed consent was obtained from the participants

prior to their operation. It was the preference of the senior author to avoid the use of a syrinx shunt as much as possible, and fluid sampling would only be performed when the insertion of a syrinx shunt was absolutely necessary. It was not considered appropriate to sample syrinx fluid in cases where the cord was not being opened, such as operations for posterior fossa decompression, or arachnolysis and duroplasty without shunt.

### 3.3.1 Procedure for aspiration of CSF and syrinx fluid

A serum sample was taken for biochemistry testing prior to the induction of general anesthetic. With the patient in the prone position, laminectomies were performed to ensure that an adequate spinal subarachnoid space could be accessed to position the distal end of a syrinx-subarachnoid catheter. Prior to dural opening, intra-operative ultrasound was used to confirm the location of the syrinx cavity and the presence of an adequate caudal or rostral spinal subarachnoid space for a CSF sample to be taken. Under microscopic vision, a midline durotomy was performed, without opening the arachnoid layer. The dural edges were then hitched up to the wound edges.

A 30 G ophthalmic needle attached to a 3 mL syringe was introduced into the subarachnoid space under direct vision. The needle was held by the surgeon while the assistant aspirated CSF to the volume of 1 mL. The arachnoid layer was then incised longitudinally and any adhesions were divided.

Prior to myelotomy, the intra-operative ultrasound was again used to confirm the location of the syrinx and the best point of entry for shunt insertion. A second 30 G ophthalmic needle attached to a 3 mL syringe was then introduced into the syrinx cavity by the surgeon, and 1 mL of fluid was aspirated by the assistant under direct microscopic vision.

Care was taken not to contaminate the syrinx fluid sample with CSF or blood in the operative field.

The myelotomy was then extended to 2 – 3 mm in length with a No.11 scalpel blade, straight bayonet microscissors and microdissectors. The shunt was then inserted into the syrinx cavity and the distal end was positioned into the adjacent subarachnoid space. The preferred shunt procedure was a syrinx-subarachnoid shunt with a Spetzler-peritoneal catheter. Meticulous haemostasis and watertight duroplasty were achieved prior to closure of the wound in the usual fashion.

### 3.3.2 Chemical analysis

Biochemical analysis was performed by Laverty Laboratories, North Ryde, NSW, Australia. The biochemical panel consisted of sodium, potassium, chloride, calcium, magnesium, osmolality, albumin, protein and glucose. All analyses were performed within 24 hours of the CSF and syrinx fluid samples being taken.

## *3.4 Results*

The recruitment process is summarised in Figure 3.4-1. Between January 2010 and January 2012, 22 patients underwent operations for syringomyelia by the senior author. Of these, ten patients with enlarging syrinxes were considered for a syrinx shunt operation and were identified as suitable for the study. One patient who had a syrinx-subarachnoid shunt inserted did not consent to the study prior to the operation and aspiration of CSF and syrinx fluid was not performed. The remaining nine patients consented to the study, but syrinx fluid sampling was not carried out in four patients because decompression of the syrinx cavity by needle aspiration or shunt insertion was not required intra-operatively. Five patients underwent syrinx fluid sampling, and of

these, two patients received a syrinx-subarachnoid shunt. The remaining three patients had an expansile duroplasty and arachnolysis only.

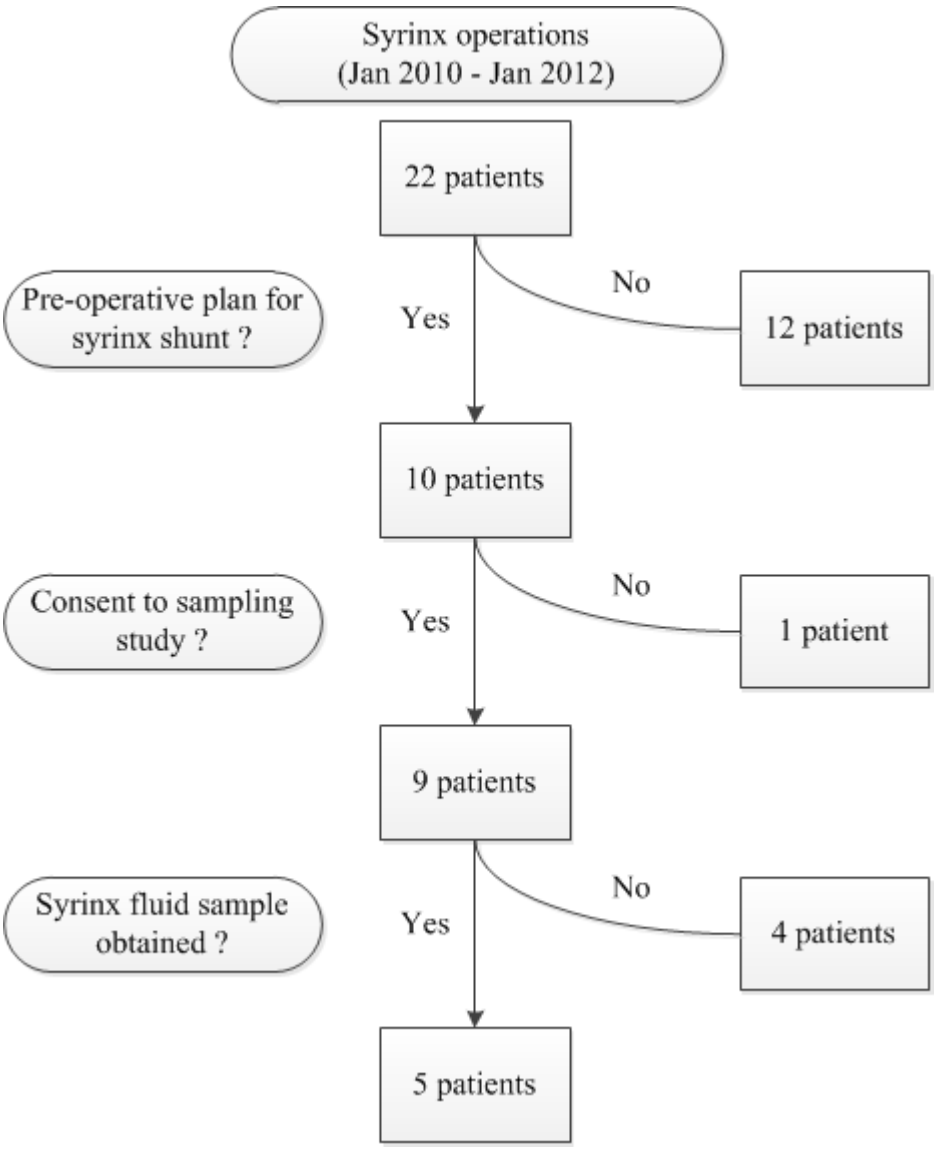


**Figure 3.4-1 Flowchart of patients recruited for syrinx fluid sampling study**

The aetiology of syringomyelia was different in each of the five cases, as shown in Table 3.4-1. Two patients had presented with recurrences following treatments for syringomyelia (Case 4 and 5). Indications for treatment were pain, new neurological deficits, such as upper extremity motor or sensory loss, and radiological evidence of progressive enlargement of the syrinx cavity. The majority of the syrinxes were located in

the upper to mid-thoracic region, but in Cases 1 and 5, the syrinx extended from C2 to the conus. Syrinx shunts were placed into the syrinx at the region where the spinal cord parenchyma was thinnest, or in non-functioning spinal cord to reduce the risk of causing further deficits. All patients had improved clinical and radiological outcomes following their operations at the latest follow-up of up to 18 months.

The results of the biochemistry of serum, CSF and syrinx fluid are shown in Table 3.4-1. Sufficient samples of CSF and syrinx fluid were obtained for the biochemistry panel in all participants except in Case 1. Small differences between CSF and syrinx fluid for the electrolytes and osmolality were noted. More variation was observed between the protein and glucose levels between CSF and syrinx fluid, however, no consistent trend was demonstrated across the cohort of participants. Microscopy cell count of CSF and syrinx fluid demonstrated < 10 $x10^6$/L erythrocytes and leucocytes per high power field.

**Table 3.4-1 Clinical synopsis and biochemical profile of syrinx shunt cases**

| **CLINICAL SYNOPSIS** | | **BIOCHEMISTRY** | | | | | | | |
|---|---|---|---|---|---|---|---|---|---|
| **Aetiology / Levels** | **Fluid type** | **Na (mmol/L)** | **K (mmol/L)** | **Cl (mmol/L)** | **Ca (mmol/L)** | **Mg (mmol/L)** | **Osmo (mmol/kg)** | **Prot (g/L)** | **Gluc (mmol/L)** |
| **Case 1** | CSF | 113 | 2.3 | 107 | 1.14 | 1.12 | 300 | 0.21 | 3.3 |
| Spinal dysraphism | Syrinx fluid | * | * | * | 1.05 | 1.29 | * | 0.72 | 3.9 |
| C2 - Conus | Serum | 144 | 4.0 | 106 | 2.41 | 0.87 | | 73 | |
| **Case 2** | CSF | 147 | 2.8 | 125 | 1.34 | 1.09 | 294 | 0.54 | 4.7 |
| Arachnoiditis | Syrinx fluid | 146 | 2.6 | 123 | 1.17 | 1.09 | 293 | 0.43 | 4.5 |
| T10 - Conus | Serum | 142 | 4.2 | 98 | 2.54 | 0.83 | | 71 | |
| **Case 3** | CSF | 145 | 2.8 | 122 | 1.3 | 1.17 | 299 | 2.00 | 3.1 |
| Post-traumatic | Syrinx fluid | 146 | 2.9 | 123 | 1.33 | 1.15 | * | 0.42 | 4.5 |
| C3 – T10 | Serum | 142 | 3.7 | 103 | 2.44 | 0.78 | | | |
| **Case 4** | CSF | 144 | 2.7 | 122 | 1.09 | 1.12 | 292 | 0.18 | 4.0 |
| Idiopathic | Syrinx fluid | 146 | 2.7 | 123 | 1.16 | 1.11 | 289 | 0.33 | 3.6 |
| T1 – T7 | Serum | 138 | 4.4 | 106 | 2.25 | 0.76 | | 58 | |
| **Case 5** | CSF | 145 | 2.7 | 123 | 1.17 | 1.20 | 292 | 0.85 | 3.4 |
| Chiari – malformation | Syrinx fluid | 150 | 2.8 | 122 | 1.27 | 1.24 | * | 0.85 | 2.9 |
| C2 – Conus | Serum | | | | | | | | |
| **Average** | **CSF** | **145** | **2.8** | **123** | **1.23** | **1.15** | **294** | **0.89** | **3.8** |
| **(Case 2 - 5)** | **Syrinx fluid** | **147** | **2.8** | **123** | **1.23** | **1.15** | ***** | **0.51** | **3.9** |
| | **Serum** | | | | | | | | |

* Indicates insufficient sample

## *3.5 Discussion*

Even though the initial description of syringomyelia by Estienne was in 1546, much is still unknown about the pathogenesis of syringomyelia [1, 453]. Basic information about the origin of syrinx fluid, the nature of fluid flow and the biochemistry and pressure measurements of the fluid within the syrinx cavity have not yet been established.

Early autopsy and intra-operative observations of syringomyelia described cystic cavities within the spinal cord containing a clear and colorless fluid, similar in appearance to cerebrospinal fluid or extracellular fluid [1, 109]. Until recently, it has therefore been generally assumed that fluid within the syrinx cavity originates from CSF [58, 164, 454]. Based on this assumption, a number of pathogenetic theories have arisen, describing how CSF would enter the syrinx cavity, whether from the fourth ventricle via the central canal or from the spinal subarachnoid space via perivascular spaces.

Gardner proposed the water hammer theory, whereby each systolic pulsation would propel CSF down the central canal from the fourth ventricle into the syrinx cavity [158, 159]. Williams postulated that cranio-spinal pressure dissociation during times of relaxation after straining would promote the movement of CSF into the syrinx cavity via the fourth ventricle and central canal due to obstruction of the subarachnoid space at the craniocervical junction [147]. Ball and Dayan proposed that, during exertion, CSF would be diverted from the spinal subarachnoid space into the spinal cord parenchyma via perivascular spaces due to obstruction by the cerebellar tonsils at the foramen magnum in Chiari malformation [161]. Oldfield theorized that the driving force for CSF in the spinal subarachnoid space was the cerebellar tonsils acting as pistons [58, 164]. Another possible explanation was that obstruction to normal CSF flow within the central canal by inflammatory debris might lead to an accumulation of CSF. This would result in

dilatation of the central canal caudal to the obstruction, producing a non-communicating type of syringomyelia [150, 246].

The evidence in support of CSF being the origin of syrinx fluid includes radiological and experimental studies. It has been demonstrated on CT myelograms that contrast agents enter the syrinx cavity via perivascular spaces [58, 455]. This is consistent with subsequent experimental work by Brodbelt et al. and Stoodley et al., who demonstrated in animal models of syringomyelia that there was movement of CSF tracer from the subarachnoid space into the syrinx cavity via the perivascular space, when the tracer was injected into the cisterna magna [167-169, 204].

However, it has recently been proposed that syrinx fluid is derived not necessarily from CSF, but rather, from extracellular fluid (ECF). Greitz et al. suggested that disturbances of the microcirculation in the spinal cord, such as venous constriction, would promote increased transcapillary filtration and thus increase the amount of extracellular fluid [176]. This would be promoted by a Venturi effect caused by constriction of the spinal subarachnoid space by either the cerebellar tonsils or arachnoiditis. Koyanagi postulated that impairment of ECF drainage from the spinal cord parenchyma may be a contributing factor to the accumulation of fluid within the spinal cord and syrinx formation [174]. Other sources of syrinx fluid remain possible, such as disruptions in the blood-spinal cord barrier, which may lead to increased leakiness of the vasculature within the spinal cord and intraparenchymal edema [213].

Despite the plethora of theories, the origin of syrinx fluid has actually not been established. In fact, the direct evidence to support the concept that the composition of syrinx fluid is identical to CSF is limited. Furthermore, the evidence for an origin from CSF in the subarachnoid space is even more scant [456].

Biochemistry of syrinx fluid may provide more information on the origin of fluid in this perplexing condition. A biochemical composition similar to that of CSF would provide evidence for an origin from CSF, and may clarify the metabolic processes for fluid moving into a syrinx [456]. It is well known that samples obtained from different locations along the CSF pathway contain varying amounts of protein. Lumbar CSF has a higher protein concentration than cisternal or ventricular CSF [457-459]. Therefore, an accurate comparison of CSF to syrinx fluid would require a sample of spinal CSF to be taken in the region of the syrinx.

An origin from ECF, however, cannot be disregarded. ECF associated with the central nervous system is thought to be composed of CSF and interstitial fluid (ISF) [460]. The ISF of the nervous system cannot be assumed to be identical to the other body systems because of the tight junctions within the blood – brain (or spinal cord) barrier, which regulate ionic homeostasis and water movement into the CNS [457, 461]. ISF in the CNS itself is thought to be derived from the microcirculation, from metabolism of glucose to $CO_2$ by neurons or infiltration of ventricular CSF [462]. The precise contribution of CSF and ISF to ECF in the nervous system is not known, and their compositions may be difficult to distinguish from each other.

The results from the present study have demonstrated a very similar biochemical profile of the electrolytes within syrinx fluid and CSF (Table 3.4-1). In each of the electrolyte parameters, there were minor differences in the case-matched values between syrinx fluid and CSF, with each of the average values differing by less than 2%. The importance of such small differences is uncertain, but the similarity in biochemical profiles would suggest that the origin of syrinx fluid would largely be cerebrospinal fluid or ECF. In this study, we were unable to determine the composition of ECF within the spinal cord.

Larger differences were reported in the glucose and protein values. Due to the small number of patients in this study, it was not possible to draw any conclusions about the differences in protein content of CSF and syrinx fluid. In the two patients with elevated CSF protein relative to syrinx fluid, the underlying etiologies were post-traumatic and post-Myodil myelogram. This might be due to stagnation of CSF flow in the spinal subarachnoid space from surrounding arachnoiditis. When compared with the CSF and syrinx fluid samples, the serum protein levels were much higher due to the presence of the blood-brain or blood-spinal cord barriers. Microscopic cell counts revealed minimal contamination with erythrocytes and leucocytes, either through extradural run in, or introduced by trauma from the insertion of the aspiration needle.

To the best of our knowledge, this was the first study to provide a comparison of the biochemical composition of serum, CSF and syrinx fluid. Only a small number of case reports have compared the actual composition of syrinx fluid with CSF (Table 3.5-1). In a study of nine post-traumatic syrinx patients, Rossier et al. reported higher protein content, 0.35 – 3.9 g/L (mean 1.15) in syrinx fluid compared with cisternal CSF protein content, 0.1 – 0.44 g/L (mean 0.24) [31]. This finding was consistent with those of other authors, who reported syrinx fluid protein levels ranging from 0.28 to 2.24 g/1 (mean 0.88), and cisternal CSF protein ranging from 0.14 to 0.28 g/1 (mean 0.18) [31, 79, 463-466]. Similarly, the syrinx fluid in cases associated with intramedullary tumours and spinal cord tethering from lipomyelomeningocoeles has been reported to have higher protein content than CSF [179, 456]. In contrast, Shannon et al. reported identical levels of protein in syrinx fluid and CSF in ten of 13 post-traumatic syrinx patients treated with a syringostomy [109]. In 17 of 48 syringomyelia patients with dilated central canals, Schlesinger et al. obtained percutaneous aspirates of spinal fluid from the central canal and subarachnoid space [41]. The protein content of the central canal sample was below

0.5 g/L, which was the same or less than the simultaneous sample obtained from the subarachnoid space. In some series, the CSF protein was not examined, and hence could not be directly compared [31, 467].

The majority of the studies mentioned in Table 3.5-1 only examined the protein content of syrinx fluid and there has been minimal information published on other biochemical parameters. Barnett et al. examined the calcium and magnesium content of intracavitary fluid in one patient with a post-traumatic syrinx. Compared to CSF calcium (1.7 mEq/L) and magnesium (1.7 mEq/L), syrinx fluid had calcium and magnesium values of 1.25 mEq/L and 2.1 mEq/L respectively [79]. Laha et al. reported in 2 patients treated with a syrinx-subarachnoid shunt that the chloride and glucose levels in fluid aspirated from a syrinx were "normal" [464]. However, the absolute values of the measurements were not included in his article.

Another concern from previous studies was the method of fluid sampling. In the majority of the studies, the corresponding CSF sample was obtained either by a lumbar puncture or cisternal aspiration, rather than from the adjacent subarachnoid space. Rossier et al. combined the results of the CSF protein content from different studies despite the variation in the site of CSF sampling [31]. To the best of the authors' knowledge to date, there has been no other study directly comparing the composition of fluid aspirated from the syrinx cavity and CSF from the adjacent spinal subarachnoid space. In addition, some studies had obtained syrinx fluid via a percutaneous aspiration, which might have been inaccurate due to the lack of image guidance to ensure that the needle was completely within the syrinx cavity [41, 79]. This might have resulted in possible contamination with blood or CSF.

**Table 3.5-1 Summary of case series with CSF & syrinx fluid sampling**

| Case series (Year of publication) | No. of patient / samples | Method of syrinx fluid sampling | Site of CSF sampling | Mean Syrinx fluid protein (g/L) | Mean CSF protein (g/L) | Aetiology |
|---|---|---|---|---|---|---|
| Freeman et al. (1959) | 1 | Intradural aspiration | NA | 1.30 | NA | Post-traumatic |
| Werner et al. (1969) | 2 | NA | Cisternal | 0.53 | 0.28 | Post-traumatic |
| | 1 | NA | Lumbar | 0.37 | 0.29 | |
| Nurick et al. (1970) | 1 | Intradural aspiration | Cisternal | 0.55 | 0.20 | Post-traumatic |
| Barnett et al. (1973) | 3 | Intradural aspiration | Cisternal | 1.52 | 0.60 | Post-traumatic |
| | 1 | Intradural aspiration | Lumbar | 0.38 | 15.0 | |
| Laha et al. (1975) | 3 | Shunt | NA | 0.85 | NA | Post-traumatic |
| Shannon et al. (1981) | 10 | Shunt | NA | NA | NA | Post-traumatic |
| Schlesinger et al. (1981) | 17 | Percutaneous aspiration | NA | <0.5 | 0.6 | Chiari – malformation |
| Rossier et al. (1985) | 8 | Shunt | Cisternal | 1.14 | 0.24 | Post-traumatic |
| | 1 | Shunt | Lumbar | 0.66 | 0.46 | |
| | 1 | Shunt | NA | 1.67 | NA | |
| Castillo et al. (1987) | 3 | Shunt | NA | 0.88 | NA | Extramedullary compression |
| Lohle et al. (1994) | 1 | Intradural aspiration | NA | 37 | 0.5 | Intramedullary ependymoma |
| Chapman et al. (1995) | 1 | Shunt | NA | 1.55 | 0.2 | Lipomeningo-coele |

There were several limitations to the present study. In particular, the number of participants was small. However, in current clinical practice, syrinx aspiration and shunt insertions are performed only in a select cohort of syringomyelia patients, which makes recruitment difficult. Laboratory analysis of CSF and syrinx fluid has therefore become less popular in recent years. Other limitations included the small volume of syrinx fluid

and CSF obtained. This restricted the number of biochemical tests that could be performed. Further analysis of syrinx fluid proteins may elucidate more information about the underlying molecular mechanisms involved in fluid and solute transport in syringomyelia.

On a molecular level, it is not known what underlying processes account for fluid movement into the syrinx cavity. Whether this occurs via passive diffusion due to solute concentration gradients, osmotic gradients, active coupled transport or specific protein channels remains conjecture. Recently, there has been much interest in the role of aquaporins in the context of syringomyelia [419, 424]. Aquaporins have been shown to play an important role in water transport in numerous organ systems [386]. In the central nervous system, aquaporin-4 is the predominant aquaporin and has been investigated in the setting of cerebral edema, spinal cord injury, hydrocephalus and communicating syringomyelia [232]. Aquaporin-4 has also been linked to the selective potassium channel, inwardly rectifying $K^+$ channel subunit 4.1 (Kir4.1)**,** which may generate concentration gradients to promote fluid movement into and out of syrinxes [468, 469]. Ion channels, such as Kir4.1 are thought to perform an important role in maintaining cell volume in the brain and spinal cord. Changes in these channels can result in intracellular water accumulation (ie. cytotoxic oedema). In glial cells, Kir channels play a role in the maintenance of extracellular $K^+$, by facilitating the movement of $K^+$ from the extracellular space into glial cells and removal via microvessels [470]. There is a relationship between water clearance and $K^+$ clearance [468]. A decrease in $K^+$ transport disrupts the clearance of intracellular $K^+$, and this in turn causes an influx of water from the vasculature into astrocytes via aquaporin-4 water channels [471]. Kir4.1 is found to be down-regulated in a number of pathological conditions including spinal cord injury, and in the presence of glial scarring [472, 473]. Whatever the underlying molecular mechanisms are, it is likely

that equilibrium exists between fluid and solutes moving into and out of the syrinx cavity and any disturbances to this equilibrium would result in a rapid correction to achieve homeostasis.

Recently, biomarkers in CSF and serum have been investigated in the setting of acute spinal cord injury. Kwon et al. demonstrated that cytokines (IL-6, IL-8, MCP-1, tau, S100β and GFAP) were elevated with increasing severity of spinal cord injury. In particular, there was correlation between the levels of IL-8, S100β and GFAP and the ASIA score on presentation and the degree of neurological recovery. The increase in cytokine levels was most evident in the first 3 – 4 days post spinal cord injury. Although the inflammatory response is of interest in acute spinal cord injury, the role of inflammation may be less important in syringomyelia. Nonetheless, future biochemical studies on CSF and syrinx fluid may benefit from studies on the role of cytokines and other inflammatory proteins [197, 474, 475].

Further research is required on the fundamental concepts in syringomyelia. Basic information such as the origin and nature of syrinx fluid need further clarification before treatment can be improved. It is likely that there are multiple factors involved in the pathophysiology, such as the flow and pressures of CSF within the subarachnoid space, disruptions in blood-spinal cord barriers, nature of molecular processes and glial scar properties. A greater understanding of all these processes is therefore required.

## *3.6 Conclusion*

The pathogenesis of syringomyelia remains a mystery. On a simplistic level, the volume of a syrinx is dependent on the balance between fluid inflow and fluid outflow. The present study of 5 patients has demonstrated a very similar biochemistry electrolyte

profile between syrinx fluid and CSF, though an origin from ECF cannot be disregarded. Further studies will be required to ascertain the molecular mechanisms for fluid movement between the spinal subarachnoid space, extracellular space and syrinx cavity.

## *3.7 Contributions to the study*

Patients were recruited by Prof. Marcus Stoodley, and informed consent was obtained by Dr Johnny Wong. Syrinx fluid samples were obtained during syringosubarachnoid shunt operations performed by Prof Marcus Stoodley and Dr Johnny Wong. The biochemical assays were performed by Symbion Laverty Laboratories (North Ryde, NSW, Australia). Data analysis and preparation of manuscript was done by Dr Johnny Wong.

## *3.8 Acknowledgements*

The authors acknowledge the laboratory staff at Laverty Laboratories, North Ryde, NSW, Australia for their assistance in handling and processing the fluid specimens.

# Chapter 4 Direct-trauma model of post-traumatic syringomyelia with a computer controlled motorised spinal cord impactor

## *4.1 Abstract*

**Objective**: The pathogenesis of post-traumatic syringomyelia remains enigmatic and is not adequately explained by current theories. Experimental investigations require a reproducible animal model that closely replicates the human condition. Current animal models are imperfect due to their low reliability, severe neurological deficits, or dissimilar mechanism of injury. The objective of this study was to develop a reproducible rodent post-traumatic syringomyelia model using a spinal cord impactor that would represent the human condition more closely.

**Method**: The study consisted of two parts. Experiment 1 aimed to determine the optimal force setting to induce a cystic cavity at C8 with a computer-controlled motorised spinal cord impactor. Twenty animals were allocated to five groups receiving impacts from 50 – 150 kDyn. Using the optimal force for production of an initial cyst determined from Experiment 1, Experiment 2 aimed to compare the progression of cavities in animals without and with arachnoiditis induced by kaolin. Forty-eight animals were allocated to 1, 3, 6 or 12 week timepoints after syrinx induction.

**Results**: In Experiment 1, the delivered force was within 10 kDyn of the programmed force and cavities were present in 95% of animals. Impactor displacement, duration of weakness, and spinal cord cavity size correlated with the delivered force. The optimal force chosen for Experiment 2 was 75 kDyn, and cavities occurred in 92% of animals

with histological resemblance to human syrinxes. The kaolin groups developed larger cavities, more vacuolations and enlarged perivascular spaces than the non-kaolin groups.

**Conclusion**: This impact model reliably produces cavities that resembles human post-traumatic syringomyelia and is suitable for further study of post-traumatic syringomyelia pathophysiology.

**Keywords:** Animal disease model, spinal cord injury, post-traumatic myelopathy, syringomyelia

## 4.2 Introduction

Post-traumatic syringomyelia is a disabling neurological condition involving a progressively expanding cystic cavity that occurs from a few months to many years following a spinal cord injury [31, 201]. The symptoms of syringomyelia are variable, consisting of pain, weakness, sensory deficits, and in severe cases, respiratory compromise and death from brainstem involvement [2, 40, 41]. Despite favourable short term results, treatment for this condition remains suboptimal with long-term failure rates as high as 80% [190]. Better treatments are unlikely to be developed until the mechanisms for the formation and expansion of post-traumatic syringomyelia are more clearly understood [2].

A plethora of theories has been proposed regarding the pathogenesis of post-traumatic syringomyelia, but a satisfactory theory remains elusive [160]. Most of these theories have been based on clinical and radiological observations without experimental validation. Experimental validation can generally only be performed on models, including computational, mechanical and animal models.

Existing animal models of post-traumatic syringomyelia include: direct trauma and arachnoiditis models; and an excitotoxic amino acid and arachnoiditis model. Direct trauma and arachnoiditis models consist of a mechanical spinal cord injury, induced by either weight drop or compression [191, 326]. An alternative method is the excitotoxic model, which is highly reproducible and histologically resembles human post-traumatic syringomyelia [195, 321]. Although these models have been useful, they all have inherent flaws, raising doubts about their applicability to the human condition.

Recently, computer-controlled motorised spinal cord impactors have been developed that are capable of delivering more consistent impacts than the weight drop method or clip compression [251]. Spinal cord impactors have been demonstrated to yield more reproducible contusional spinal cord injuries than the traditional weight drop method [251, 285]. The objective of this study was to develop an animal model of post-traumatic syringomyelia by using a spinal cord impactor and subarachnoid kaolin that would reliably produce an initial mild spinal cord injury and enlarging cystic cavities that resemble human post-traumatic syringomyelia histologically.

## *4.3 Materials and methods*

Following ethical approval from Macquarie University Animal Ethics Committee, seventy male Sprague-Dawley rats, weighing 300 – 600g, were used. Two animals were euthanised early due to severe neurological deficits suffered from complications during the application of the stabilising clamps, and were excluded from the remainder of the study.

The study consisted of two experimental parts. The first experiment was to determine the optimal force required to induce an initial cavity without causing significant neurological deficits. Using the optimal force from the first experiment, the second experiment was to observe the temporal progression of the cystic cavities with and without concurrent arachnoiditis.

### 4.3.1 Experiment 1: Determining the optimal force setting

The Infinite-Horizon spinal cord impactor (Precision Systems and Instrumentation, LLC, US) was used for this study. Previous studies using this impactor produced paraplegia with forces greater than 150 kDyn at mid-thoracic levels. In order to determine the force

required to induce an initial cavity in the cervical cord without permanent neurological deficits, twenty animals were allocated to five groups with force settings of 50, 75, 100, 125 and 150 kDyn (Figure 4.3-1). The dwell time for each impact was set at 0 sec. The delivered force and displacement of the impacts were recorded. Neurological outcome was assessed using the Tarlov scale, and the histology was examined at 3 weeks after the initial operation.

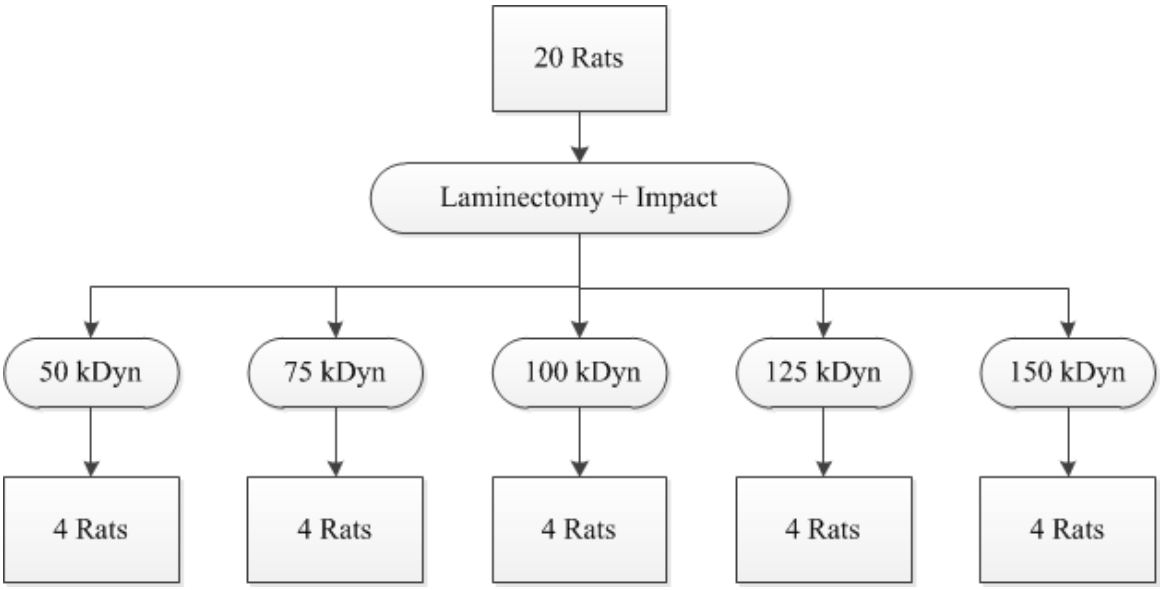


**Figure 4.3-1 Flowchart of animals allocated for experiment 1**

### 4.3.2 Experiment 2: Temporal progression of cystic cavity

The second experiment compared the progression of the cystic cavities following spinal cord impact in animals with and without arachnoiditis over four time points (1, 3, 6 and 12 weeks). Forty-eight animals were used for this part of the study and were separated into either kaolin or non-kaolin groups at each time point, with 6 animals allocated to each group (Figure 4.3-2). All animals received a spinal cord impact at the optimal force from Experiment 1. The outcome measures were the delivered force, impact displacement, impact velocities, neurological function, and cavity dimensions.

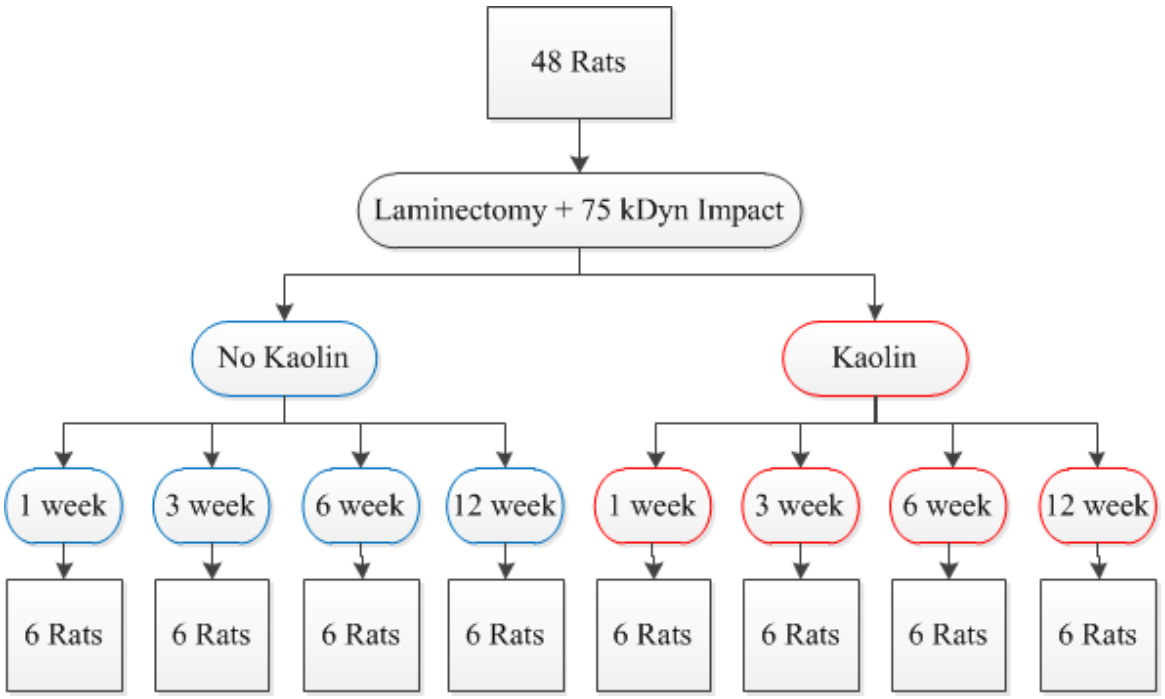


**Figure 4.3-2 Flowchart of animals allocated for experiment 2**

### 4.3.3 Operative procedure

All procedures were performed in a sterile field under general anaesthetic. Anaesthesia was induced with 4% isoflurane and subsequently maintained with 2 – 2.5% isoflurane via a nose cone. The rats were positioned prone on the operating stage, and the skin was shaved and prepared with povidone-iodine. Under magnification with an operating microscope, the C6 – T2 spinous processes, laminae and lateral masses were exposed via a midline incision. A C7 – T1 laminectomy was performed with rongeurs. Stabilising clamps were attached to the lateral masses of C6 and transverse process of T2. The operating stage was then positioned such that the impactor tip was aligned over the midline of the spinal cord at the C8 level. The desired force was programmed and delivered according to the computer software provided (IH Spinal Cord Impactor v.5.0.4, Precision Systems and Instrumentation, Kentucky, USA).

To induce arachnoiditis in the kaolin groups, a 10 μL injection of 250 mg/mL kaolin (Sigma-Aldrich) in 0.9% saline solution was slowly administered into the subarachnoid space with a 0.5 mL 30G insulin syringe (Ultra-Fine II, Beckton Dickinson and Co, NE, USA) following the spinal cord impact.

A layered closure was performed with resorbable sutures to fascia and skin. The animals were allowed to recover with analgesia and antibiotic coverage as required and access to food *ad libitum*. They were monitored for neurological deficits, excessive weight loss and signs of distress.

### 4.3.4 Perfusion and fixation

At the completion of the experiment, the animals were anaesthetised with 4% Isoflurane. Heparin 5000 IU was injected via an intracardiac injection and the left ventricle was cannulated to allow influx of fixative. The right atrium was incised to permit efflux of blood and fixative. Each animal was perfused with 400 mL of 4% paraformaldehyde (Lancaster Synthesis Ltd, UK) in 0.1 M phosphate buffered saline (pH 7.4).

### 4.3.5 Histology

The brain and spinal cord were dissected out and post-fixed in 4% paraformaldehyde solution overnight. The spinal cord was divided into individual segments according to the spinal cord level from C2 to T4. The specimens were processed in paraffin over a 4-hour cycle in an automated tissue processor (Leica ASP200S, Leica Biosystems, Nussloch, Germany) and then embedded in paraffin wax blocks. Transverse sections of 5 μm thickness were cut with a microtome and mounted on glass slides. The slides were allowed to air dry for at least 4 hours prior to staining.

Haemotoxylin and Eosin (H&E) staining was carried out using the Lillie-Mayer protocol. After gradient ethanol baths and xylene washes, the slides were coverslipped with DPX mounting medium (Scharlau Chemie SA, Spain) and allowed to dry in a 37 $^{0}$C oven for 3 days.

### 4.3.6 Image acquisition and processing

The sections were studied using light microscopy with a Zeiss Axio Imager Z1 microscope (Carl Zeiss Microimaging GmbH, Berlin, Germany). Photographs of the H&E sections were taken using the Axiovision program (Release 4.8.1, Carl Zeiss Microimaging GmbH) at x25 and x50 magnification. The dimensions and areas of the cavity and spinal cord were calculated using the "measure - length" and "measure - outline" functions respectively on the Axiovision program (Release 4.8.1, Carl Zeiss Microimaging GmbH). The dimensions measured were the maximum anteroposterior and lateral diameters of the cavities, and the area of the cavity was measured and expressed as a ratio to the total area of the spinal cord section.

### 4.3.7 Statistical analysis

Data were expressed as the mean ± SE for the delivered force, displacement, neurological outcome, dimensions and area of the cavity size. In Experiment 2, the statistical difference between the two groups over all time points was determined by univariate analysis of variance. A value of $p<0.05$ was considered statistically significant. Software used included Microsoft Excel 2007 (Microsoft Corp, Redmond, WA, US) and IBM SPSS v.19 (IBM Corp, Armonk, NY, US)

## *4.4 Results*

### 4.4.1 Experiment 1: Determining the optimal force setting

The delivered force and displacement at the different programmed force settings are summarised in Table 4.4-1. Overall, all rats received impact forces within 10 kDyn of the programmed force (Figure 4.4-1 A). The mean delivered displacement increased in a linear fashion with the programmed force, with a correlation coefficient of 0.851 (Figure 4.4-1 B).

Higher programmed forces were also associated with a greater degree of neurological deficit and a longer duration of recovery to normal power. The mean Tarlov scores for hindlimb function over the first 5 post-operative days are depicted in Figure 4.4-2. In the 150 kDyn group, one animal was euthanised according to the animal ethics protocol at 24 hours following the operation due to complete paraplegia. All other rats recovered to normal neurological function within 3 days of the operation.

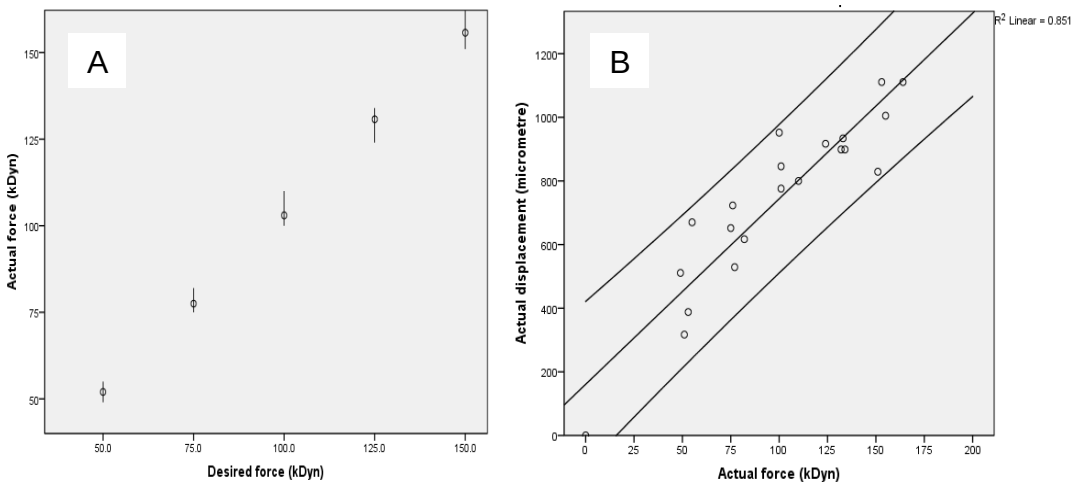


**Figure 4.4-1 Relationships between: (A) programmed force and delivered force; (B) delivered force and displacement.**

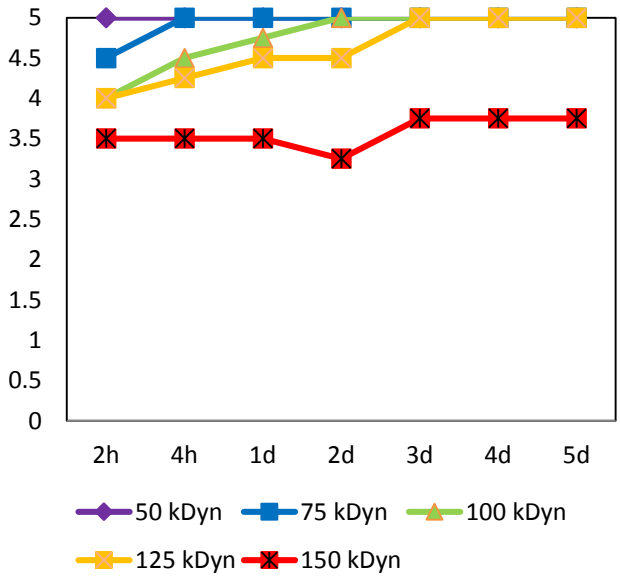


**Figure 4.4-2** **Neurological outcomes (Tarlov Scale) in Experiment 1**

The overall cavity rate, mean cavity dimensions, mean transverse cavity area and number of levels involved were measured from the histological sections obtained with H&E staining (Table 4.4-1). Cavities were present in all animals, except one animal in the 50 kDyn group. The mean cavity dimensions and transverse area increased as the programmed force increased from 50 to 100 kDyn, and then reached a plateau in the 125 and 150 kDyn groups.

**Table 4.4-1** **Experiment 1 results with programmed forces from 50 to 150 kDyn**

| Program-med force (kDyn) | Mean Delivered force (kDyn) | Mean Displace-ment (µm) | Overall cavity rate | Mean max AP cavity dimensions (µm) | Mean max lateral cavity dimensions (µm) | Mean % area of spinal cord (%) |
|---|---|---|---|---|---|---|
| 50 | 52 | 470 | 75% | 1100 | 900 | 12 |
| 75 | 78 | 630 | 100% | 1000 | 1200 | 14 |
| 100 | 100 | 840 | 100% | 1600 | 1600 | 28 |
| 125 | 130 | 910 | 100% | 1300 | 1700 | 21 |
| 150 | 160 | 1010 | 100% | 1300 | 1100 | 24 |

Histological sections revealed a midline cystic cavity involving the dorsal columns only in the 50 kDyn group (Figure 4.4-3 A). At 75 kDyn, the cavity was adjacent to the central canal without disruption of the ependymal lining (Figure 4.4-3 B). At higher forces, the cavity involved the central canal, dorsal horns and medial portions of the ventral gray matter (Figure 4.4-3 C – E). Based on the results of the overall cavity rate, the neurological status and the absence of central canal involvement, it was determined that 75 kDyn would be used as the optimal force setting for Experiment 2.

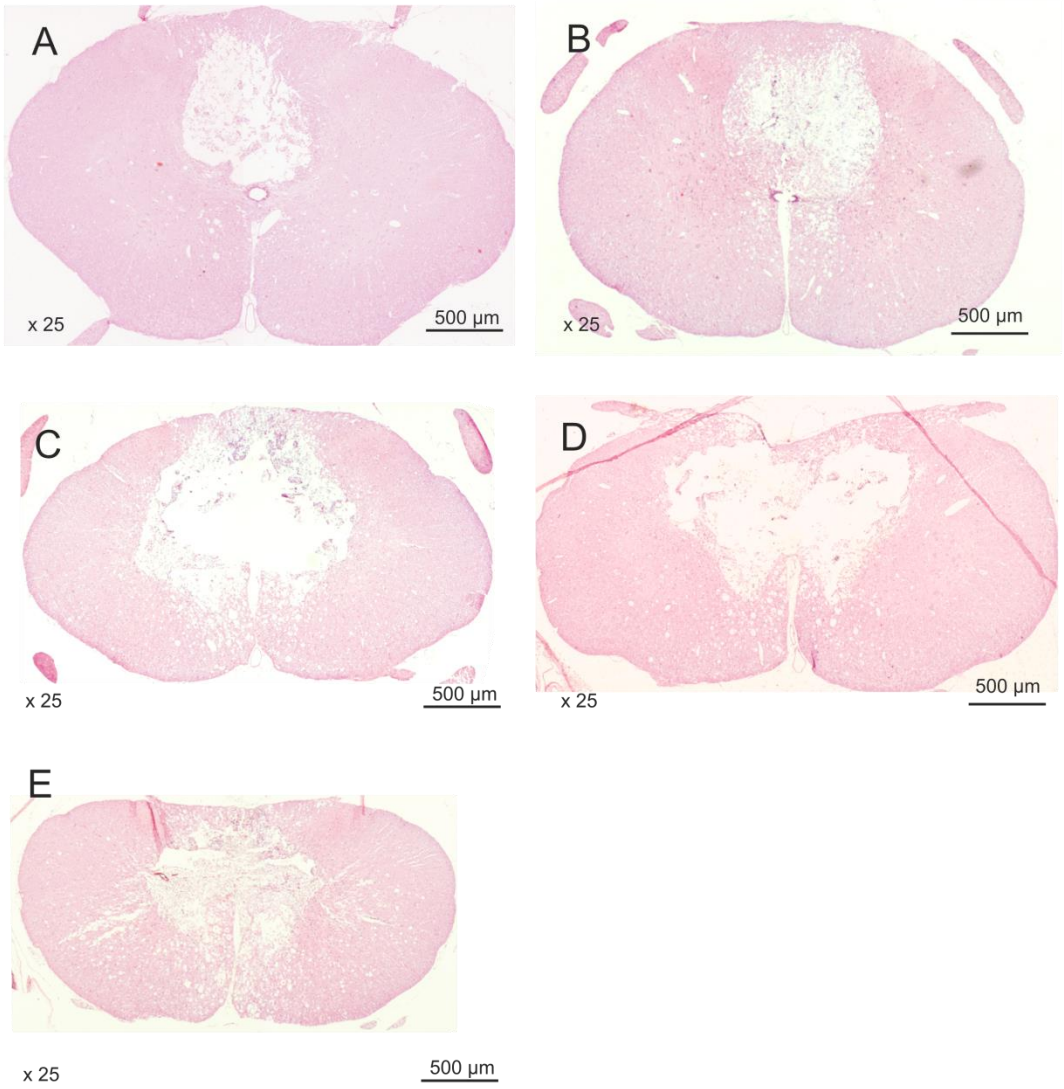


**Figure 4.4-3 H&E sections at C8 with increasing programmed forces.**

**A.) 50 kDyn; B.) 75 kDyn; C.) 100 kDyn; D.) 125 kDyn; E.) 150 kDyn**

### 4.4.2 Experiment 2: Temporal progression of cystic cavity

The results for experiment 2 are summarised in Table 4.4-2. There were no significant differences in the delivered force between the groups. However, there was more variability in the displacement measurement, as demonstrated in Figure 4.4-4. This was most notable in both 12 week kaolin and non-kaolin groups of animals, in which two animals had significantly reduced displacement. The overall cavity rate was 92% in all animals. In the 3 week kaolin and 12 week non-kaolin groups, the cavity rate was 83%, and, in the 12 week kaolin group, the cavity rate was 67%. The remainder of the animals all had cavities.

**Table 4.4-2 Experiment 2 results in kaolin and non-kaolin groups.**

| Time point (Kaolin group) | Mean Delivered force (kDyn) | Mean Displace-ment (µm) | Overall cavity rate | Mean C8 AP dimensions (µm) | Mean C8 lateral dimensions (µm) | Mean % area of spinal cord |
|---|---|---|---|---|---|---|
| 1 Week (No Kaolin) | 79 | 680 | 100 | 1200 | 1400 | 19 |
| 1 Week (Kaolin) | 78 | 660 | 100 | 1200 | 1700 | 21 |
| 3 Weeks (No Kaolin) | 79 | 630 | 100 | 820 | 790 | 11 |
| 3 Weeks (Kaolin) | 83 | 670 | 83 | 840 | 1200 | 16 |
| 6 Weeks (No Kaolin) | 80 | 640 | 100 | 820 | 1400 | 11 |
| 6 Weeks (Kaolin) | 77 | 770 | 100 | 1100 | 1400 | 18 |
| 12 Weeks (No Kaolin) | 80 | 840 | 83 | 460 | 410 | 4.9 |
| 12 Weeks (Kaolin) | 79 | 550 | 66 | 470 | 630 | 6.2 |
| **Overall** | **79** | **680** | **92** | | | |

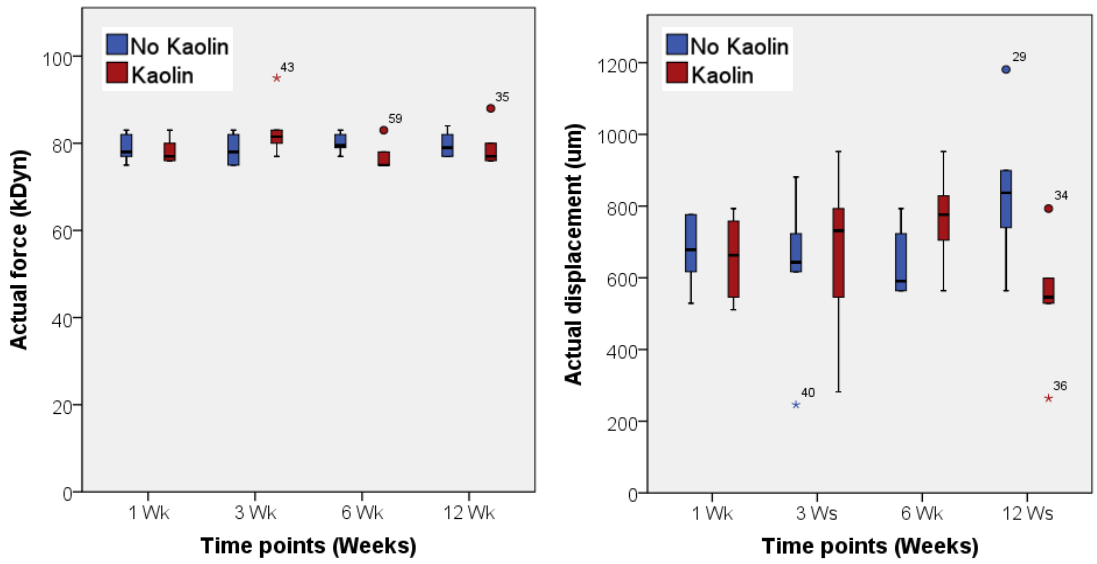


**Figure 4.4-4 Actual force and displacement graphs across groups in Experiment 2.**

Neurological function was similar across the groups, with all animals suffering transient weakness and recovering to normal function within 2 days post-operatively.

At each respective time point, the kaolin groups had larger cavities in dimensions and area when compared with the non-kaolin cohort at each corresponding time point (Figure 4.4-5).

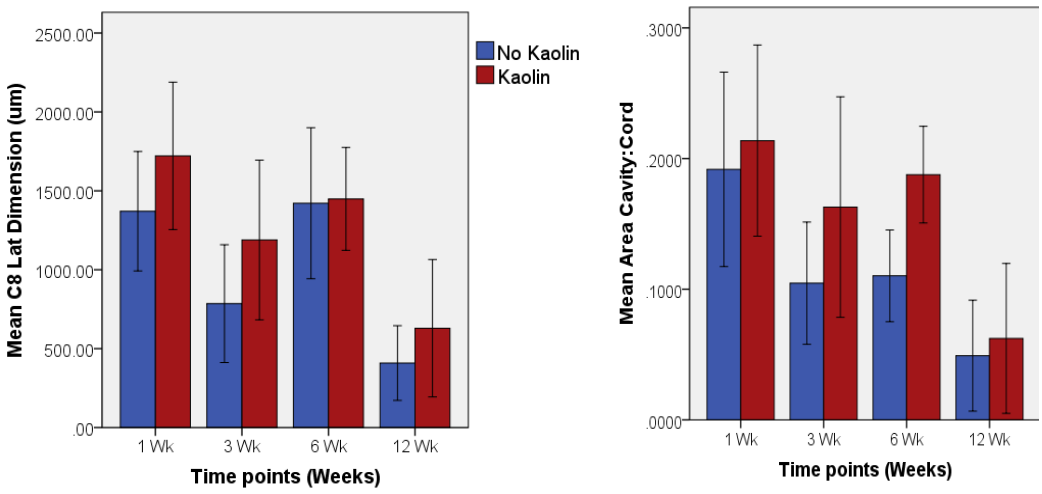


**Figure 4.4-5 Mean C8 cavity lateral dimensions and percentage area of cord**

On histological sections, there were larger, multi-loculated cystic cavities and more dilated perivascular spaces and microcysts in the kaolin group, particularly at the 6- and

12-week timepoints. There was also evidence of an ongoing chronic inflammatory response within the cystic cavities in the kaolin group at these time points (Figure 4.4-6 & Figure 4.4-7).

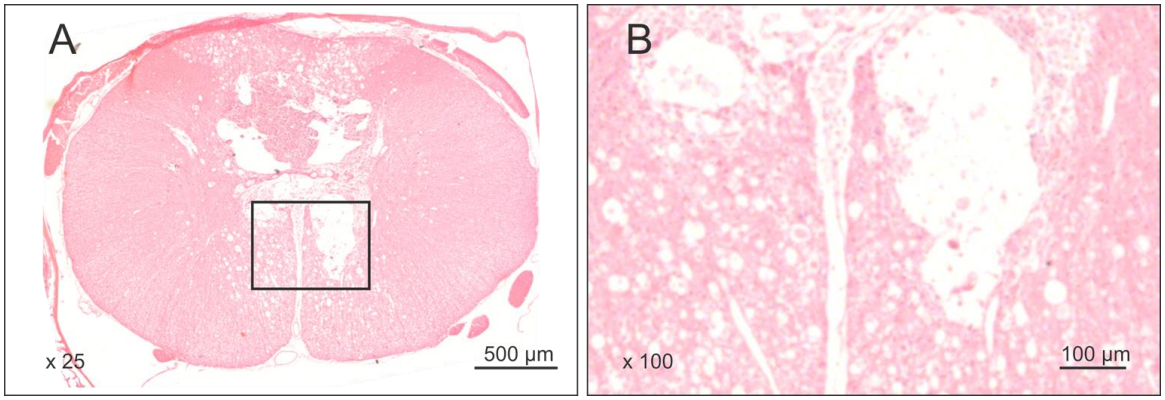


**Figure 4.4-6 H&E section at C8 of an animal with kaolin at 6 week timepoint.**

**A.) Low-power magnification, demonstrating a multi-loculated cystic cavity; B.) Higher-power image of the edge of the cystic cavity with dilated perivascular spaces and vacuolations, which were absent in non-kaolin animals.**

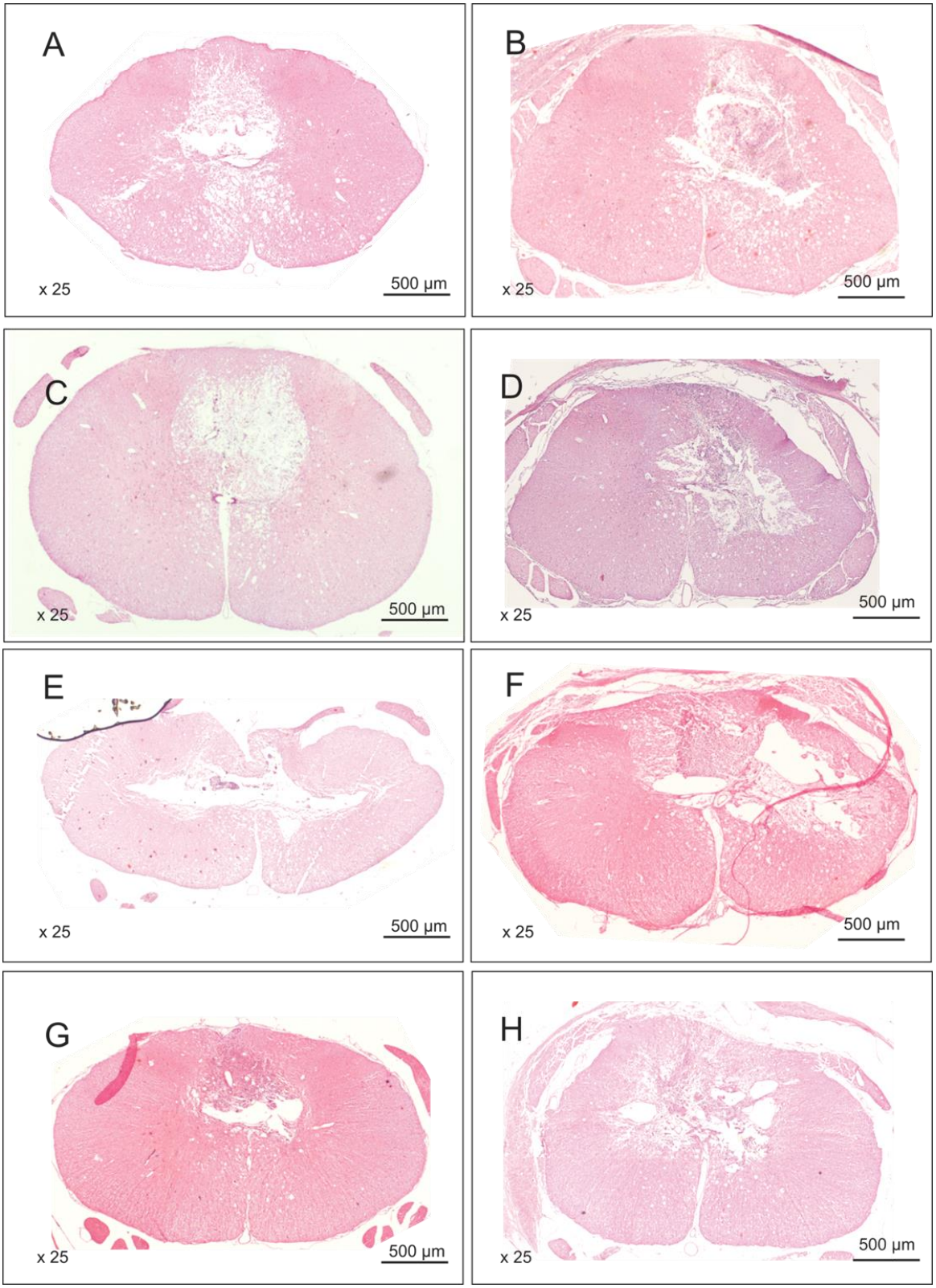


**Figure 4.4-7 H&E sections at C8 level in non-kaolin (left) and kaolin groups (right) at timepoints from 1 – 12 weeks.**

**(A, B) 1 week timepoint; (C, D) 3 week timepoint; (E, F) 6 week timepoint; and (G, H) 12 week timepoint.**

## 4.5 Discussion

Post-traumatic syringomyelia as a clinical entity was first recognised by Holmes in 1915, when he described intramedullary cysts ascending 4 - 5 levels from the site of initial spinal cord injury sustained from gunshot wounds [465]. It has also been known as: "cystic degeneration of the spinal cord", "ascending paralysis" and "progressive cystic myelopathy" [79, 463, 465, 476]. Until the introduction of magnetic resonance imaging, post-traumatic syringomyelia was perceived as a rare complication of spinal cord injury and was diagnosed by clinical symptoms and myelograms. Post-traumatic syringomyelia at present affects approximately 25% of patients following a spinal cord injury, of whom a third become symptomatic [2].

Treatment for this condition has remained limited and unsatisfactory. The mainstay of treatment is surgical, with spinal cord untethering and syrinx shunting being the most common operative methods [42]. Despite successful short term outcomes, the recurrence rate of syringomyelia following surgery remains high, with up to 50% of patients requiring further treatment [38, 126, 190, 204]. More effective therapy is needed, but is unlikely to be developed until a more complete understanding of the pathophysiology of post-traumatic syringomyelia is acquired.

A multitude of theories has been proposed to explain the pathogenesis of syringomyelia, but an adequate explanation is still lacking [42]. Many of these are based on intraoperative observations or radiological investigations and have not been validated by experimental studies [138, 147, 158, 161, 164, 176]. Assumptions and hypotheses arising from these theories can only be examined on models of syringomyelia. At present, the methods available include computational, mechanical and animal modelling.

Computational modelling is often based on data obtained from human MRI studies, and has mainly focused on CSF dynamics within the spinal subarachnoid space, spinal cord and syrinx cavity. In recent years, more complex two- and three- dimensional computational models have been developed, which account for the elastic properties of the spinal cord, syrinx cavity and the porosity of scarring within the subarachnoid space [170, 171, 205, 207, 477, 478]. Mechanical models have also been developed, which replicate flexible spinal cord, syrinx cavity and stenosis within the subarachnoid space and permit actual pressure measurements of CSF waveforms [382, 383]. The advantage of computational and mechanical models is that they reduce the need for animals and can evaluate whether hypotheses are biomechanically feasible. Despite the usefulness of these models, histological and molecular aspects of syrinx pathophysiology cannot be investigated without animal studies. Furthermore, data obtained from animal models can be used to refine current in-vitro models.

Animal syrinx models have been developed for both canalicular and extracanalicular types of syringomyelia [169, 195, 246, 321]. Important data based on these models have been obtained, such as the nature of fluid flow into and out of syrinx cavities, the integrity of the blood-spinal cord barrier, the presence of neural progenitor cells, and aquaporin-4 expression around syrinx cavities [169, 204, 213, 329]. Despite these findings, all existing animal models have their short-comings, and concerns regarding the applicability to the human condition still remain. The ideal post-traumatic syrinx model is yet to be developed, but its characteristics should include: (i) easy reproducibility and reliability of expanding syrinx production; (ii) mechanism of initial injury similar to human spinal cord injuries; (iii) histological resemblance; (iv) extracanalicular location of syrinx cavities; (v) progressive enlargement and neurological deficits similar to the natural history of human syrinxes. A model producing a small initial cavity with mild neurological deficits would

be preferable to separate the effects of myelomalacia due to spinal cord injury from subsequent syrinx enlargement.

Previous animal models of post-traumatic syringomyelia have used various mechanisms of spinal cord injury with or without induction of arachnoiditis. Early experimental work on spinal cord injury models reported the formation of extracanalicular syrinx cavities from a weight drop model of spinal cord injury alone [191, 261, 266, 319-321]. However, only a small proportion of animals developed cavities and some of these cavities resorbed over time [320]. A combined weight drop and arachnoiditis model was developed by Cho et al. to produce extracanalicular syrinxes in rabbits [191]. Syrinx cavities developed in 55% of animals, and the lack of reproducibility made this model unsuitable for further physiological investigations. Compression with aneurysm clips in combination with subarachnoid kaolin was used in post-traumatic syrinx models developed independently by Mizuno et al. and Seki et al. [326, 327]. Josephson et al. developed a rodent thecal sac constriction model, in which a silk ligature was applied to obliterate the spinal subarachnoid space [175]. Significant paralysis in all animals was noted in the 3 studies and the overall syrinx cavity rate was between 83 – 100 %. An objection to both the compression and constriction methods is the severity of the neurological deficit and the difficulty in differentiating whether the resultant cystic cavities represented myelomalacia or post-traumatic syringomyelia.

An alternative post-traumatic syrinx model was developed by Yezierski et al., Yang et al. and Brodbelt et al., using intraparenchymal injections of quisqualic acid combined with a subarachnoid kaolin injection [195, 311, 321]. Quisqualic acid produces selective neuronal cell death, inflammation and extracanalicular cavities [305, 311, 479]. Brodbelt et al. reported syrinx formation in all animals receiving multiple doses of quisqualic acid

at 6 weeks, with larger cavities and involvement of more spinal levels when arachnoiditis was induced. The advantages of this model are the reliability in syrinx production, histological similarities to human specimens, and the absence of significant neurological deficits. A major criticism of this technique is that the mechanism of injury is not the compressive and contusional trauma sustained during human spinal cord injury [326].

Radojicic et al. observed ascending dilatations of the central canal following a contusional spinal cord injury with the Infinite Horizon impactor at 250 kDyn without additional arachnoiditis [325]. The criticisms of this model are the severity of neurological deficits and the dilatations of the central canal being uncharacteristic of extracanalicular syrinxes, as identified by Milhorat et al. from human autopsy specimens [23, 97]. Dilatations of the central canal may be a result of cellular debris draining into and obstructing the central canal in a manner similar to the canalicular syrinx model with parenchymal kaolin injections [246].

The current study utilised the Infinite Horizon impactor to deliver a contusional spinal cord injury at the C7/T1 level, which was the same location as the quisqualic acid model. Lesions at the cervicothoracic region are preferable because human post-traumatic syringomyelia commonly affects the cervical cord. The benefits of the impact model are the more precise and accurate delivery of a designated force without prior contact with the spinal cord, and the ability to measure the force and displacement of the impact using sensors within the impactor tip [251]. In Experiment 1, there were correlations between the amount of impact force with the displacement of the impact, the duration of neurological deficits, and the size of cavities.

Previous studies using the Infinite-Horizon spinal cord impactor on rodents produced paraplegia with forces from 150 – 250 kDyn [325]. The results of Experiment 1

demonstrated that, in rodents receiving spinal cord impacts from 50 to 125 kDyn of force, transient neurological deficits developed and recovery to a normal neurological state occurred within 3 days. The duration of neurological recovery correlated with the size of the cavities on the histological sections at the C8 level. In the 50 and 75 kDyn groups, the cavities involved the dorsal columns without affecting the central canal, while in the 100, 125 and 150 kDyn groups, the cavities involved the dorsal columns, central canal and anterior horn of the spinal cord. To the best of the authors' knowledge, this is the first study on a rodent spinal cord injury model with a spinal cord impactor that investigated the neurological and histological outcomes of mild to moderate spinal cord injuries.

Based on the results from Experiment 1, 50 kDyn was not selected as the optimal force because a cavity was not present in 1 of 4 animals, while in the groups with 100 kDyn or more of force, the central canal was involved. Thus, the optimal impact force selected was 75 kDyn, because: (1) the overall initial cavity rate was 100%; (2) the central canal was not involved, which is a hallmark of post-traumatic syringomyelia based on human autopsy studies; (3) the neurological deficits were mild and transient.

In Experiment 2, the overall cavity rate was 92%. The cavity rate was 100% at all time points except for the 12 week time point, which had cavity rates of 67% and 83% in animals with and without kaolin respectively. This is comparable to the cavity rates in other post-traumatic syrinx models mentioned previously [321, 326, 327]. At each corresponding time point, animals with arachnoiditis had larger cavities, including the AP and lateral dimensions, and the percentage of cavity area to spinal cord area. The results support observations made in previous studies, in which syrinx cavities were larger and involved more spinal levels when combined with arachnoiditis [191, 321, 326, 327]. On histological sections, the cavities were irregular in shape without an ependymal lining and

surrounded by a chronic inflammatory infiltrate containing macrophages and microglia. These findings are consistent with microscopic appearances from human post-traumatic syrinx specimens [2, 97, 321]. In addition, the arachnoiditis animals displayed more multi-loculated cysts, increased vacuolations within the spinal cord parenchyma and enlarged perivascular spaces when compared with animals without arachnoiditis. In a feline model of cervical arachnoiditis, Klekamp et al. also demonstrated enlarged perivascular spaces and proposed that this might lead to increased parenchymal oedema. Coalescence of vacuolations into multi-loculated cysts was postulated to eventually form syrinx cavities [193].

The findings of the current study indicate the importance of arachnoiditis in the pathogenesis of post-traumatic syringomeylia. In fact, the association between syringomyelia, arachnoiditis and spinal cord trauma had already been described by Hallopeau in 1871 and Joffroy in 1887 based on necropsy studies [109]. More recently, Bilston et al. demonstrated that arachnoiditis might cause increased perivascular flow through CSF-arterial pulsation decoupling [171]. Similarly, Cheng et al. used a computational model to show that CSF flow dynamics could be altered with varying degrees of obstruction within the spinal subarachnoid space due to arachnoiditis [478]. However, the exact role of arachnoiditis in the pathophysiology of post-traumatic syringmomyelia is still unknown.

There were several limitations to the current study. While the spinal cord impactor provides a reproducible and reliable model of contusional spinal cord injury, it still does not replicate the entire spectrum of changes following a human spinal cord injury. The mechanism of human spinal cord injuries consists of a combination of contusion, compression, transection, and secondary chemical changes from excitotoxic amino acid

release or ischemia [251]. In addition, the development of arachnoiditis in humans is most likely a result of subarachnoid haemorrhage during the initial injury spinal cord injury, which is not exactly represented by a subarachnoid kaolin injection. In this model, kaolin was used because it is more reliable than autologous blood in producing arachnoiditis.

Another limitation was the absence of progressive enlargement of the syrinx cavities between the 6- and 12-week time points. Most animals in experiment 2 had cavities involving the C8 level only. This might be explained by a greater variation in the impact displacements in the 12-week group of animals. Despite the demonstrated reproducibility in displacements in Experiment 1, the 12-week group of animals showed a wider range of displacements, which could explain the lower cavity rate within this group, and smaller cavity size when compared with 6 weeks. The other explanation for this limitation might be related to tissue processing and sectioning. In humans, syrinx cavities have been observed intraoperatively to be tense and expansile. However, in post-mortem animal specimens, cavities tend to collapse after paraffin embedding and tissue processing, and might give an appearance of a smaller cyst within an atrophic spinal cord. Another concern was the difficulty in differentiating cavities from myelomalacia and syringomyelia. Cho et al. defined a post-traumatic syrinx in a rabbit model as a cavity that extends at least 2cm away from the site of the initial injury [191]. In contrast, Seki et al., Brodbelt et al. and Radojicic et al. did not define the criteria for a syrinx cavity [321, 325, 326]. Finally, axial sections were used to measure the transverse diameters of the syrinx cavities. The limitation with axial sections is that it is difficult to measure the longitudinal dimensions. Conversely, it is impossible to measure the transverse diameter if longitudinal sections were produced.

The pathogenesis of post-traumatic syringomyelia remains largely a mystery. Further investigations on the mechanisms of syrinx formation and expansion will require reproducible and reliable models that replicate the human condition. Despite the availability of computational and mechanical modeling, physiological and molecular studies can only be performed on animal models. An ideal animal model for post-traumatic syringomyelia that completely replicates the human condition remains to be developed. All animal models have their shortcomings, including the impactor model as described in the current study. However, there are several advantages to this model, including reproducible, direct trauma to the spinal cord, transient initial neurological deficits and cavities with histological resemblance to human post-traumatic syringomyelia. The difference in histological appearance and cavity sizes between the kaolin and non-kaolin groups has emphasised the role of arachnoiditis in the pathogenesis of post-traumatic syringomyelia. This model would be suitable for further studies, such as syrinx fluid flow, aquaporin expression, inflammatory responses around syrinx cavities and other investigations into the pathogenesis of post-traumatic syringomyelia.

## 4.6 Contributions to the study

The experiments, animal care, tissue processing, data analysis and preparation of the manuscript and figures were performed by Dr Johnny Wong. Ms Xin Song was involved in tissue processing and image acquisition. The manuscript was edited by the other authors on the paper.

## 4.7 Acknowledgements

The authors acknowledge Prof Peter Putocz at Macquarie University for his assistance with statistical analysis. This project was funded by the Column of Hope Chiari &

Syringomyelia Research Foundation and the National Health and Medical Research Council of Australia Project Grant No. 604008.

# Chapter 5 Cerebrospinal fluid flow in spinal arachnoiditis using horseradish peroxidase (HRP)

## *5.1 Abstract*

**Background**: Post-traumatic syringomyelia affects over a quarter of patients following spinal cord injury. It remains a difficult condition to treat with high rates of recurrence. The pathophysiology of post-traumatic syringomyelia is still poorly understood, but is commonly associated with spinal arachnoiditis. Previous CSF flow studies suggested that perivascular flow was increased at the level of an extracanalicular syrinx [2]. Recent computational studies have demonstrated that CSF flow into the spinal cord was increased at regions of arachnoiditis due to the scarring alone, but this has not been validated on animal models [171].

**Objective**: The objective of the study was to investigate the pattern of CSF flow in an animal model of spinal arachnoiditis in the absence of a syrinx using horseradish peroxidase (HRP) as a CSF tracer.

**Methods**: A total of 63 Sprague-Dawley rats were used for this study. However, technical failures and anaesthetic complications were experienced with 23 animals, which were excluded from the analysis. In the remaining 40 animals, CSF flow was compared between animals that had received spinal arachnoiditis with animals that had laminectomy only. Arachnoiditis was induced by an injection of subarachnoid kaolin. At 3 days, 1, 3, 6 or 12 weeks, CSF tracer studies were performed with an injection of HRP into the cisterna magna. Following perfusion at either 5 or 20 minutes, the spinal cord

was harvested for localisation of the tracers using light microscopy. Qualitative and semi-quantitative methods were used to analyse the extent of tracer flow into the spinal cord.

**Results**: HRP reaction product was observed predominantly in the perivascular spaces of the branches of the anterior spinal artery and the ventral median fissure. In the control animals, there was a gradual decrease in tracer staining towards the caudal levels. In the arachnoiditis animals, there was an abrupt decrease caudal to the level of arachnoiditis. An increased amount of tracer reaction product was observed at the region of arachnoiditis, when compared with more rostral levels in the arachnoiditis animals with qualitative assessment.

**Conclusion**: The current study suggests that CSF flow from the spinal subarachnoid space is potentiated by spinal arachnoiditis via the perivascular spaces. However, a large proportion of animals were excluded from the study due to technical failures. An alternative CSF tracer is required that may be more suitable for future CSF flow studies.

**Keywords / Running title:** Running title: Cerebrospinal fluid flow in spinal arachnoiditis; Keywords: Cerebrospinal fluid, arachnoiditis, horse-radish peroxidase, syringomyelia

## 5.2 Introduction

Post-traumatic syringomyelia develops in over 25% of patients following a spinal cord injury [2, 29, 30, 34, 201]. It remains a perplexing and frustrating condition to treat, with surgery being the main modality of treatment. Many surgical series have reported high rates of recurrences despite early symptomatic improvement, and it is not likely that more effective treatments will be developed until the factors contributing to syrinx formation and enlargement are better understood [37, 38, 115, 126, 190, 480].

An important aetiological factor that has been identified in post-traumatic syringomyelia is spinal arachnoiditis and its effects on CSF flow in the spinal subarachnoid space. Previous animal studies have demonstrated increased perivascular CSF flow from the spinal subarachnoid space at the region of the syrinx [2]. However, it was not determined whether this phenomenon was the result of spinal arachnoiditis alone.

Using computational modeling, it has been demonstrated that increased perivascular flow of CSF from the subarachnoid space into the spinal cord could be achieved in regions of arachnoiditis [170, 171, 477]. The exact mechanism for this increased flow has not yet been elucidated. The objective of the study was to characterise the patterns of CSF flow into the spinal cord in an animal model of spinal arachnoiditis and to develop a method of quantification for perivascular CSF flow.

## 5.3 Materials and methods

Following ethical approvals from the Macquarie University Animal Ethics Committee, 63 male Sprague-Dawley rats weighing 403 ± 115 g were obtained for the study. The animals were divided into an experimental group, which received a laminectomy and induction of arachnoiditis, and a control group, which received a laminectomy only.

Three animals died from anaesthetic-related complications in the peri-operative period and were excluded from the remainder of the study. The allocation of animals is summarised in Table 5.3-1.

However, in the remaining 60 animals, technical failures with tissue processing and staining were encountered in 20 animals. The results from these animals were excluded from further analysis. Forty animals were studied at 3 days, 1, 3, 6 and 12 weeks after the initial operation, and were perfused at either 5 or 20 minute intervals following HRP injection into the cisterna magna. At each time point and perfusion interval, three animals were allocated to the arachnoiditis group, and one animal to the control group.

**Table 5.3-1 Allocation of animals for the HRP study**

| **Groups** | **Perfusion interval (mins)** | **Time points** | | | | |
|---|---|---|---|---|---|---|
| | | 3 days | 1 week | 3 weeks | 6 weeks | 12 weeks |
| Experimental (Laminectomy + kaolin) | 5 | 6 | 3 | 4 | 5 | 4 |
| | | *3* | *3* | *3* | *3* | *3* |
| | 20 | 6 | 5 | 3 | 6 | 4 |
| | | *3* | *3* | *3* | *3* | *3* |
| Control (Laminectomy alone) | 5 | 1 | 1 | 2 | 3 | 1 |
| | | *1* | *1* | *1* | *1* | *1* |
| | 20 | 1 | 1 | 1 | 2 | 2 |
| | | *1* | *1* | *1* | *1* | *1* |

**Number of animals allocated is indicated in black; *Number for final analysis is indicated in italics*.**

## 5.3.1 Operative procedure

All surgical procedures were performed with strict aseptic technique under general anaesthesia. Isoflurane at 5% in 2 L/min oxygen was used for induction of anaesthetic and was subsequently reduced to 2.5% for maintenance of anaesthesia via a nose cone. The rats were positioned prone and the skin was shaved and prepared with povidone-

iodine. A dorsal midline incision was made and a C7 – T1 laminectomy was performed with bony rongeurs in all animals under microscopic magnification.

In the arachnoiditis group, 5 μL of 250 mg/mL kaolin (Sigma-Aldrich) in 0.9% saline solution was measured out with a micropipette and slowly injected into the dorsal subarachnoid space at the C8 level via 0.5 mL 30 G insulin syringe (Ultra-Fine II, Beckton Dickinson and Co, NE, US).

At the completion of the operation, a layered closure was performed with resorbable sutures to fascia and skin. The animals were allowed to recover with analgesia and antibiotic coverage as required and access to food ad libitum. They were monitored daily for 2 weeks post-operatively and then weekly until the experimental endpoint. Neurological deficits, excessive weight loss and signs of distress were recorded.

### 5.3.2 CSF tracer injection, perfusion and fixation

At the required time point for the HRP injection, the animals were re-anaesthetised with isoflurane via a nose cone. The animals were positioned prone and the atlanto-occipital membrane was exposed via a midline incision under the operating microscope. The neck was flexed to ensure that the atlanto-occipital membrane was taut. Using a stereotactic micromanipulator frame, a 10 μL microsyringe with a sharpened, bevelled needle (SGE International Pty Ltd, VIC, Australia) was introduced into the cisterna magna and withdrawn slightly to tent up the atlanto-occipital membrane. A 10 μL injection of CSF tracer was administered at a rate of 2 μL / min over 5 minutes. The CSF tracer, horseradish peroxidase (EIA grade, 012001, Invitrogen Corporation, NY, US), was mixed as a 10% solution in 0.9% saline. Care was taken to minimise CSF leakage.

At 5 or 20 minutes post HRP injection, the needle was removed and the animal was positioned supine for perfusion. Heparin 5000 IU was injected via an intracardiac injection and the left ventricle was cannulated to allow influx of fixative. The right atrium was incised to permit efflux of blood and fixative. Each animal was rapidly perfused with 200 mL of 4% paraformaldehyde (Lancaster Synthesis Ltd, UK) in 0.1 M phosphate buffered saline (pH 7.4).

### 5.3.3 Tissue processing

A solution of 4% paraformaldehyde was used to post-fix the specimens overnight. The dura and arachnoid adhesions were dissected off the spinal cord to aid sectioning. The extent of arachnoiditis was assessed macroscopically and recorded. Transverse sections of 50 μm thickness were produced with a vibratome from the cerebellum, medulla, C2 to T4 and L1 levels. The sections were floated in a bath containing 0.1M Tris buffer (pH 7.6) and were mounted on pre-coated glass slides (SuperFrost Plus, Menzel-Gläser, Braunschweig, Germany). The sections were allowed to air dry for at least 4 hours prior to staining.

Histological localisation was performed with tetramethylbenzidine (TMB) as the chromogen. The sections were incubated in 0.01 M sodium acetate buffer (pH 3.3) containing 0.005% 3,3',4,4' TMB (Lancaster Synthesis Ltd, UK) and 0.1% sodium nitroferricyanide (III) dehydrate (Lancaster Synthesis Ltd, UK). After the addition of 30 μL hydrogen peroxide, the slides were further incubated for 20 minutes and then washed in 0.01 M sodium acetate buffer (pH 3.3). The reaction product was stabilised in 5% ammonium molybdate (IV) solution (Sigma-Aldrich, MO, US) in 0.01M sodium acetate buffer (pH 3.3). After further washing in 0.01 M sodium acetate buffer, the slides were

dehydrated with gradient ethanol baths, immersed in xylene and coverslipped using DPX mounting medium (Scharlau Chemie, SA, Spain).

Immunohistochemical localisation of HRP with anti-HRP antibody was performed on the tissues of ten animals. Ethanol permeabilisation was performed with 50% ethanol solution in phosphate buffered saline (PBS, pH 7.45). Following, PBS washes and blocking with normal horse serum, primary antibody was applied with monoclonal mouse anti-HRP (1:2000 dilution, Santa Cruz) and incubated in a humidifier at $4^0$C overnight. This was followed by application of secondary antibody, donkey anti-mouse IgG-Dylight 649 (1:500, 715-495-140, Jackson Immunoresearch Laboratories, PA, US) for 2 hours at room temperature. The sections were coverslipped with fluorescent mounting medium (DAKO, S3023, Carpinteria, CA, US) and allowed to cure for 24 hours at $4^0$C until microscopy.

### 5.3.4 Microscopic image acquisition

The HRP sections were studied using light microscopy with a Zeiss Axio Imager Z1 microscopes (Carl Zeiss Microimaging GmbH, Germany) respectively. Images of the HRP reaction product were acquired serially from C2 – T4 for qualitative image analysis using the Axiovision program (Release 4.8.1, Carl Zeiss Microimaging GmbH, Germany) at x100 magnification. For semi-quantitative assessment, the images containing the central canal were acquired at x200 magnification.

### 5.3.5 Qualitative and semi-quantitative assessments of transverse sections

Two independent observers, blinded to the group allocations, qualitatively assessed the HRP staining at each spinal level after agreement on a qualitative threshold for HRP reaction product. The patterns of staining at the ventral median fissure, central canal and

the perivascular space at the peripheral white matter were recorded and graded as per Table 5.3-2. The most caudal spinal cord level with the highest staining grade was also recorded. Further quantification of the intensity of the reaction product at each level was performed by a method of relative optical density (ROD). A similar method was used by Rennels et al. in 1985.[359] The ROD of a 30 pixel diameter region around the central canal was calculated using Image J, a Java-based application (Version 1.4.5, National Institute of Health, Maryland, USA) at C2 & C5, C8 and T3, representing levels above, at and below the region of arachnoiditis respectively. The ROD values of the central canal were normalised to the ROD of the background as a ratio and comparisons were made between the experimental groups (arachnoiditis or control), spinal levels (C2, C5, C8 or T3), time interval for perfusion (5 or 20 minutes), timepoints (3 days, 1, 3, 6 or 12 weeks).

**Table 5.3-2 Semi-quantitative grading system for extent of HRP tracer flow**

| Grade | Ventral Median Fissure | Anterior Spinal Artery branches | Peripheral perivascular Space | Transpial staining |
|---|---|---|---|---|
| **0** | $< \frac{1}{3}$ | 0 | Absent | Absent |
| **1** | $\frac{1}{3}$ - $\frac{2}{3}$ | 0 | Present | Minimal |
| **2** | $> \frac{2}{3}$ | 1-3 | Present | Moderate |
| **3** | $> \frac{2}{3}$ | > 3 | Present | Diffuse |

## 5.3.6 Statistical analysis

Comparison of the central canal ROD ratios was performed using an analysis of covariance. Post-hoc Bonferroni tests were performed for significance results to adjust for

multiple comparisons. A value of $p<0.05$ was considered statistically significant. Software used included IBM SPSS v.19 (IBM Corp, NY, US)

## *5.4 Results*

All animals in the study recovered from the initial operation without neurologic deficits. In the twenty animals that were excluded, two were associated with HRP injections into the brainstem and the remaining eighteen did not show any reaction product due to the lack of HRP enzymatic activity. In the arachnoiditis groups, dense arachnoid adhesions were evident macroscopically and histologically at all timepoints except 3 days. At 3 days, an acute inflammatory infiltrate was present in the subarachnoid space and kaolin deposits. In the control animals, arachnoid adhesions were not present. In all animals, there was no morphological evidence of spinal cord trauma or syrinx cavities.

### 5.4.1 Qualitative analyses

HRP reaction product was evident in all animals, located in the spinal subarachnoid space, perivascular spaces along the anterior spinal artery branches in the ventral median fissure and subpial arteries (Figure 5.4-1).

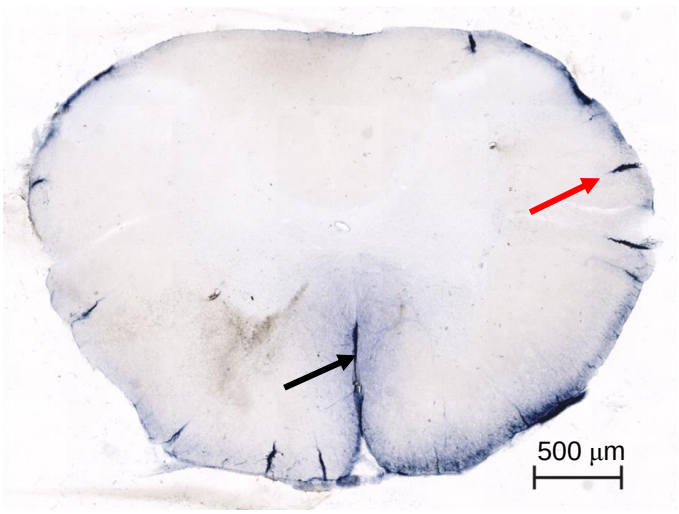

**Figure 5.4-1 HRP tracer flow into the normal spinal cord. Tetramethylbenzidine (TMB) was used to visualise HRP. HRP can be located in the ventral median fissure (black arrow) and along the peripheral perivascular spaces (red arrow). A small amount of transpial staining is also observed.**

Staining in the central canal and adjacent grey matter was seen in some sections. In the control animals, there was rapid distribution of HRP reaction product from the upper cervical to the lumbar levels at both 5 minute and 20 minute intervals. Staining reached the lumbar levels in 70% of animals. Reaction product was extensively found in the perivascular spaces of intraspinal arteries, ventral median fissure and central canal at most spinal cord levels. The relative density of reaction product staining demonstrated a consistent gradual decrease in the rostal-caudal direction (Figure 5.4-2 and Figure 5.4-3). This pattern of CSF tracer distribution was observed at all timepoints.

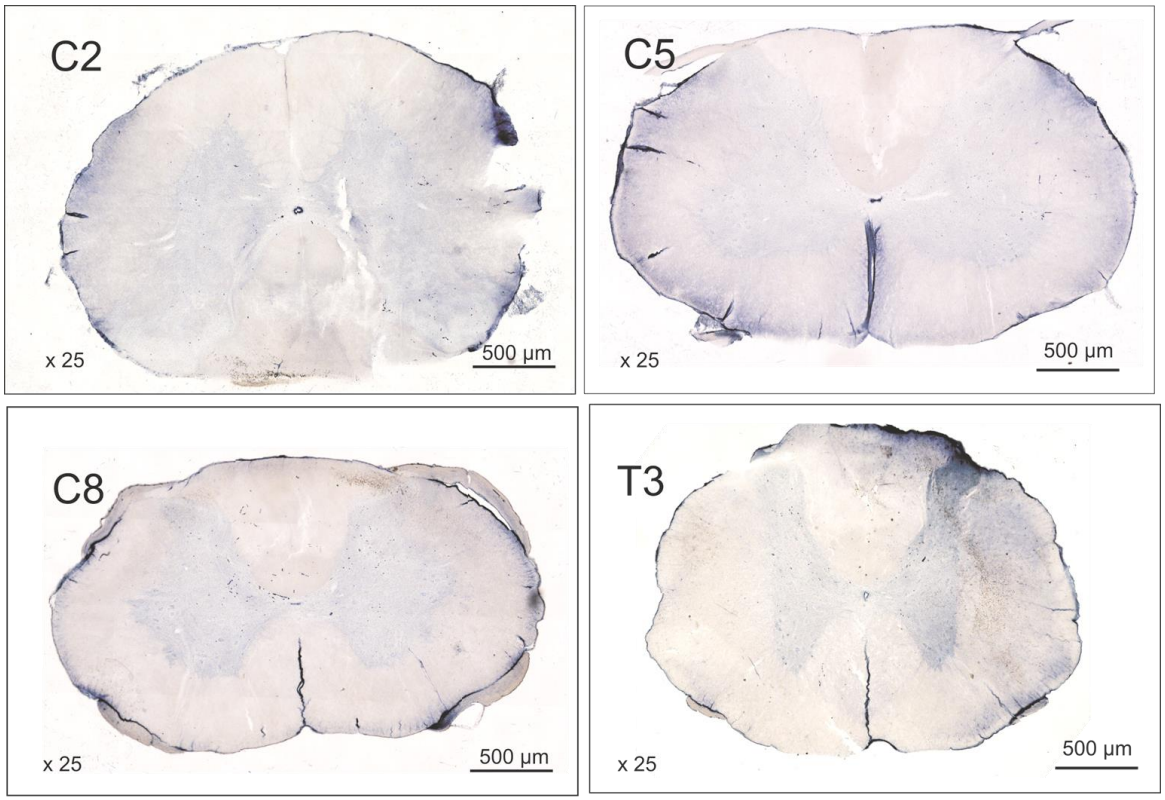


**Figure 5.4-2 HRP tracer in control animal after 5 minutes perfusion**

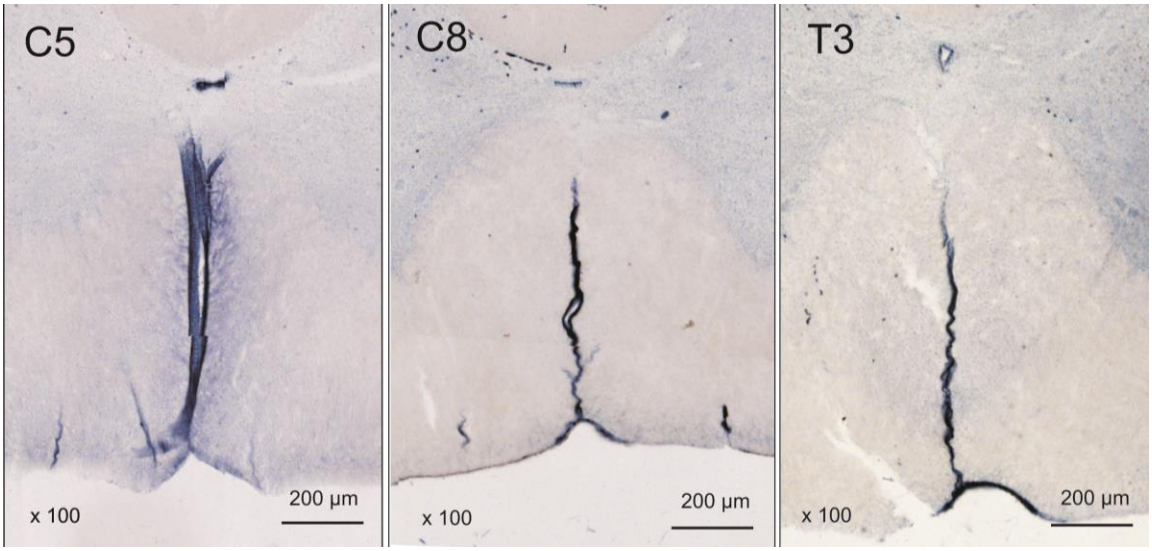


**Figure 5.4-3 Gradual decrease in HRP staining in the ventral median fissure and central canal from rostral-caudal direction in a control animal.**

In the arachnoiditis animals, there was a slower distribution of HRP tracer as compared with the control animals. More prominent staining was observed following 20 minute perfusion at the 1, 3, 6 and 12 week timepoints. Staining reached the lumbar levels in 35% of animals. The density of reaction product also decreased from rostral to caudal levels to the region of arachnoiditis. However, the degree of penetration along the ventral median fissure and perivascular spaces of the anterior spinal artery was increased at the levels of C6, C7, C8 and/or T1, when compared with the adjacent rostral levels. There was a marked decrease in staining of HRP reaction product caudal to the region of arachnoiditis (Figure 5.4-4).

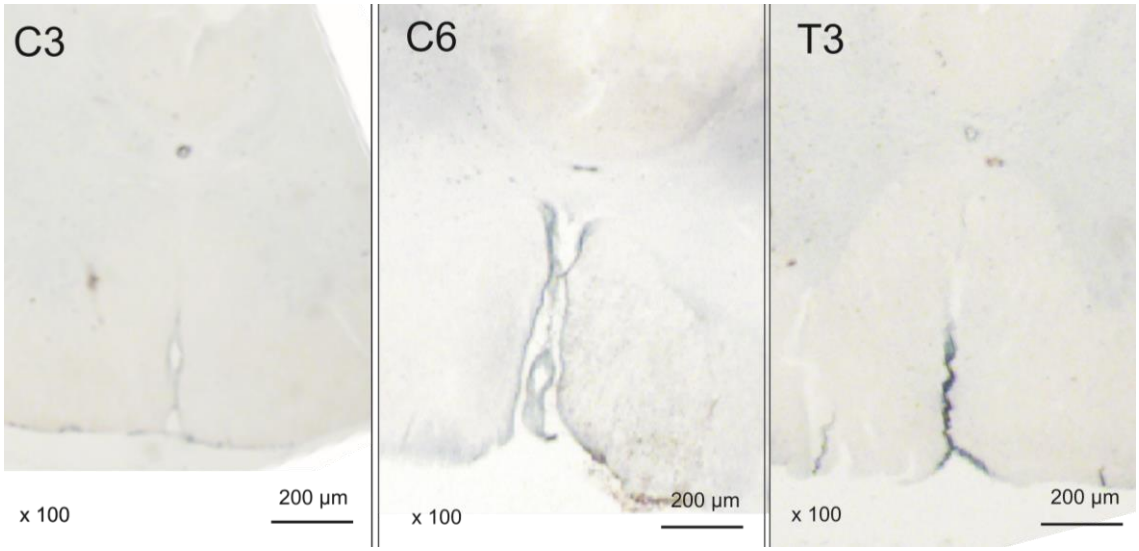


**Figure 5.4-4 Increased HRP staining in region of arachnoiditis.**

**More prominent HRP staining is noted in ventral median fissure and central canal at C6, than C3 or T3.**

Immunohistochemical localisation was performed in ten animals. Very faint positive labelling was observed in the ventral median fissure, central canal and peripheral perivascular spaces. The distribution of fluoresecent labeling correlated with the pattern observed with the corresponding TMB section in eight animals. The remaining two animals did not have display any TMB staining. However, autofluorescence was noted in the grey matter of the majority of the transverse sections, which could not be eliminated despite changing secondary antibody preparations and concentrations. Further immunohistochemistry was not performed on subsequent sections.

### 5.4.2 Semi-quantitative analyses

Across all timepoints, a marked decrease in staining caudal to the region of arachnoiditis was again noted, with only 10% of animals having grade 3 staining of the ventral median fissure below the level of arachnoiditis at T1. In contrast, 80% of control animals had grade 3 staining below the corresponding region. At the 20 minute perfusion interval, reaction product staining travelled deeper into the spinal cord at more caudal spinal

levels. In the arachnoiditis group, increasing perfusion time further increased the percentage of animals with greatest staining in the region of the arachnoiditis to 80%. This is graphically represented in Figure 5.4-5

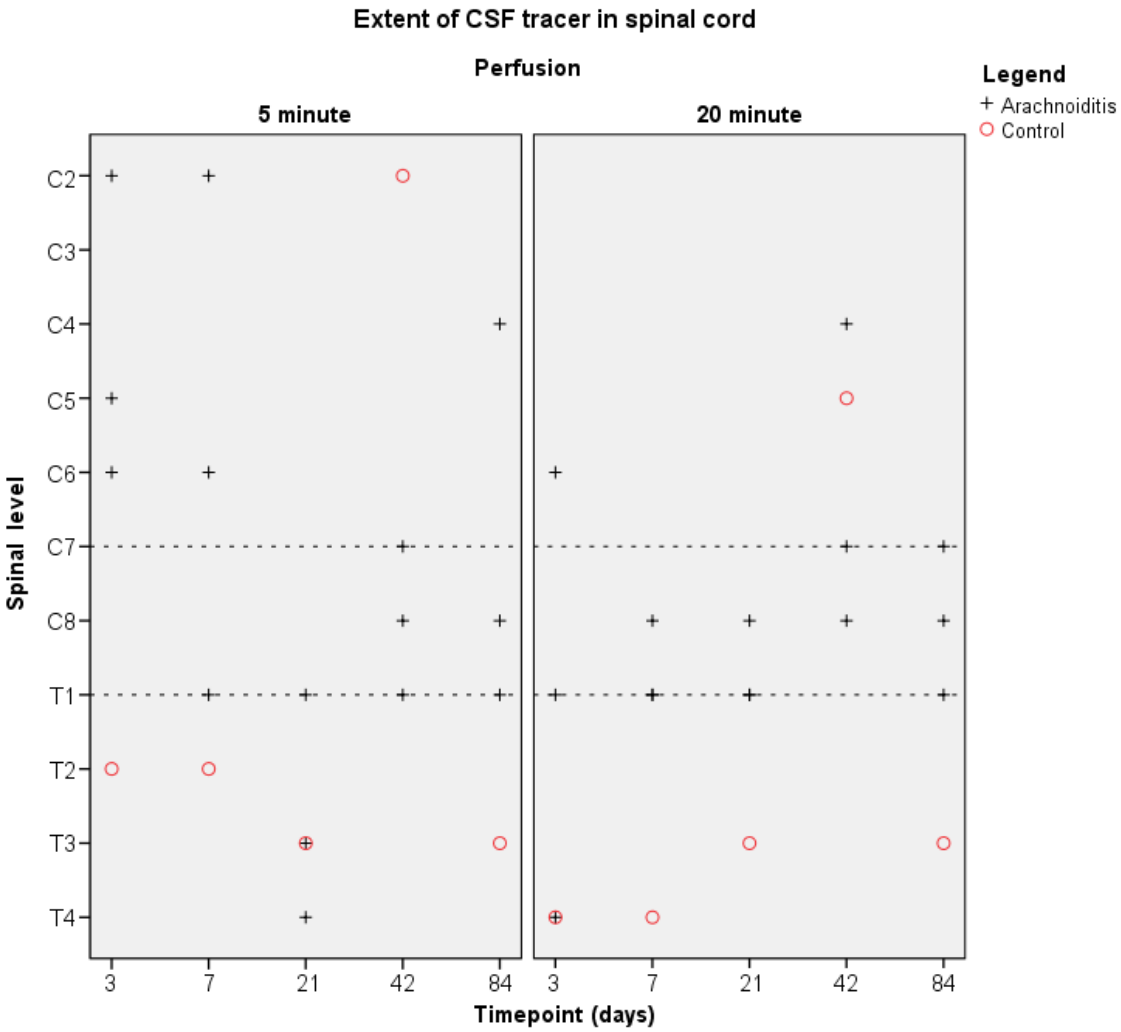


**Figure 5.4-5 Most caudal level at which reaction product staining was greatest. Dotted reference lines outline the regions of arachnoid adhesions in the arachnoiditis animals from C7 - T1**

A similar result was demonstrated in the central canal relative optical density. In the control group, ROD ratios were gradually decreasing in a caudal direction or constant between spinal cord levels in 70% of animals. In the arachnoiditis group, the central canal ROD ratios were increased at the level of C8, followed by a decrease at the T3 level. In Figure 5.4-6, this was most evident at the 1 (Panel A), 3 (Panel B), and 6 week (Panel C)

timepoints at 20 minute perfusion. At the 5 minute perfusion interval, there was less variation in ROD ratios, but higher at C8 at the 12 week timepoint (Panel D). In general, lower values for the central canal ROD ratios at the C8 level were detected when compared to the 20 minute perfusion interval at each timepoint.

An analysis of covariance revealed the main effect of spinal level (C2, C5, C8 and T3) was not statistically significant $F(3,1.873)$, $p = 0.139$. The main effect of group (arachnoiditis and control) was statistically significant $F(1,17.42)$, $p < 0.001$. Analysis of the interaction between group (arachnoiditis and control) with spinal level (C2, C5, C8 and T3) revealed central canal ROD ratios at the level of C8 in the experimental group were marginally higher than the control group. However, this interaction was not statistically significant, $F(3,1.456)$, $p=0.231$. The effect of time point was statistically significant, $F(4,13.882)$, $p < 0.001$, but not significant with respect to the effect of perfusion timing, $F(1,0.665)$, $p = 0.417$.

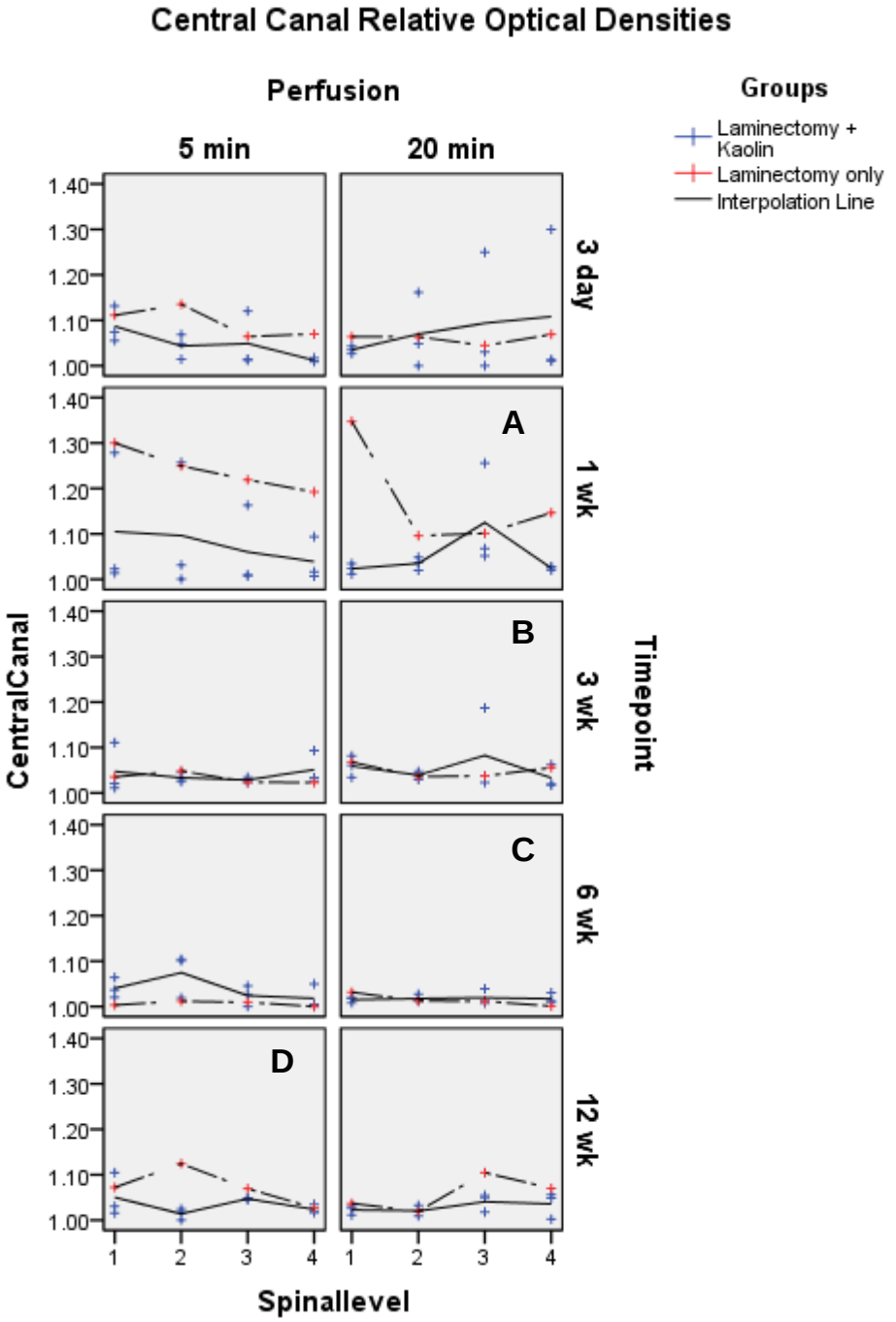


**Figure 5.4-6 Central Canal ROD ratios of each animal.**

**Spinal levels 1, 2, 3 and 4 refer to C2, C5, C8 and T3 levels respectively.**

## 5.5 Discussion

Post-traumatic syringomyelia is a recognised sequelae of spinal cord injuries, but its underlying pathophysiology is poorly understood. Current theories for the pathophysiology of post-traumatic syringomyelia do not adequately explain the complexity of the condition. Most of the existing theories for syringomyelia have focussed on Chiari-associated syrinxes, with only a limited number of theories on the post-traumatic type [147, 158, 161, 163, 164]. Histologically, Chiari-associated syrinxes tend to involve the central canal of the spinal cord, while post-traumatic syrinxes appear extra-canalicular [23, 97]. It is likely that different mechanisms of syrinx formation and expansion are present in both types of syringomyelia.

Arachnoiditis is an important aetiological association with post-traumatic syringomyelia [190, 193]. Although arachnoiditis can occur as a consequence of meningitis, spinal surgery, or myelograms, it most commonly occurs after spinal cord trauma, in which an initial hemorrhage might result in scarring in the subarachnoid space [84, 183, 481]. In fact, the association between arachnoiditis, spinal cord injury and syringomyelia was first recognised by Hallopeau in 1871 and Joffroy in 1887 [109]. Arachnoiditis encompasses scarring and thickening predominantly of the arachnoid mater within the subarachnoid space, although all three layers of the meninges may be involved [79]. Further evidence for the role of arachnoiditis in post-traumatic syringomyelia is demonstrated in animal studies of extracanalicular syrinx models. Despite the different methods used for syrinx induction, such as direct trauma or excitotoxic injury, the addition of subarachnoid kaolin to induce arachnoiditis consistently produced larger syrinx cavities in animal models [191, 321, 326].

It has been generally assumed that the source of syrinx fluid is cerebrospinal fluid, although an origin from extracellular fluid cannot be excluded [176]. Previous tracer studies on animal models have demonstrated the pattern of CSF flow into the spinal cord under normal physiological conditions, and into the syrinx cavity in a canalicular syrinx model [167-169]. In an extracanalicular model of syringomyelia, Brodbelt et al. reported movement of the CSF tracer, horseradish peroxidase (HRP), into the syrinx cavity and central canal along the perivascular spaces [2]. Interestingly, the degree of staining was more prominent at the level of the syrinx (C8 level) than more rostral adjacent levels (eg. C5 level), which suggests preferential CSF flow into the syrinx.

Using computational modelling, the effect of arachnoiditis on CSF flow within the spinal subarachnoid space has been studied. Carpenter et al. described an analytical model where pressure waves and "elastic jumps" from spinal subarachnoid space obstructions caused increases in pressure, driving fluid into the spinal cord [172]. Similarly, Bilston et al. used a symmetrical cylindrical two-dimensional model to show increased SAS pressures and CSF flow into the spinal cord [477]. It is suggested that spinal arachnoiditis may cause disturbances in CSF flow that will potentiate arterial pulsation driven perivascular flow and contribute to syrinx formation [183]. Recently, Bilston et al. reported that phase differences in timing of arterial and CSF pulsations might contribute to increased perivascular flow [171]. However, the precise mechanism by which CSF flow is potentiated into the spinal cord by arachnoiditis has still not yet been completely elucidated.

The current study aimed to confirm the findings from the computational studies and determine whether focal arachnoiditis alone would result in increased perivascular CSF flow into the spinal cord. In the current study, the general pattern of CSF tracer flow was

consistent with the findings from previous by Stoodley et al. and Brodbelt et al. [2, 167, 169]. The distribution of HRP reaction product staining was predominantly along the perivascular spaces around branches of the anterior spinal artery in the ventral median fissure. Lesser amounts of the tracers were observed in the perivascular spaces of the peripheral pial vessels and interstitial spaces in the grey and white matter. Staining of the central canal was noted mostly in the upper cervical sections and around the level of arachnoiditis. These findings would suggest preferential flow of CSF into the spinal cord via the perivascular spaces in the ventral median fissure, rather than transpial diffusion into the white matter.

Across all time points and perfusion intervals, a marked decrease in tracer staining was observed at levels below the region of arachnoiditis. In contrast, a gradual decrease in staining was present in the control animals below the corresponding spinal level. Only 10% of arachnoiditis animals displayed grade 3 staining caudal to T1, compared with 80% in the control animals.

At the level of arachnoiditis, there was increased perivascular flow with greater amounts of HRP reaction product at C8 than C5, as measured by the central canal ROD. This was evident with the 20 minute perfusion interval at the 1, 3 and 6 week time points (Figure 5.4-6). In summary, the findings suggest that arachnoiditis causes disturbances of CSF flow at the level of subarachnoid obstruction such that perivascular flow into the spinal cord is increased and fluid flow caudal to this region is slowed or markedly decreased.

In this study, a novel semi-quantitative method was developed for measurement of the intensity of HRP reaction product. Previous CSF tracer studies have only been qualitative and descriptive in nature. Due to the variability in the values for the intensity between animals, normalisation was required. The relative optical density of the reaction product

within each section was firstly normalised to the ROD of the medulla of the same animal, which was then normalised to the average ROD of the medulla of the whole cohort. The region of interest was arbitrarily determined to be a 30 pixel diameter around the central canal, which was approximately the distance between the central canal and the extent of the ventral median fissure.

Several limitations were evident arising from the present study. The use of subarachnoid kaolin to induce arachnoiditis was a well-established technique that has been used in other models of extra-canalicular syringomyelia [191, 193, 321, 326]. It involved a slow injection of kaolin suspension into the dorsal subarachnoid space to produce localised arachnoiditis. However, the extent and degree of obstruction of the spinal subarachnoid space could not be precisely controlled using current surgical techniques. Histologically, there was a tendency for the dorsal subarachnoid space to be more affected than the ventral space, which might not reflect the consequences of human spinal cord injury. The significant decrease in tracer signal caudal to the region of arachnoiditis might only represent the more severe spectrum of subarachnoid obstruction.

Secondly, CSF physiology in the subarachnoid space might have been disturbed by the introduction of CSF tracers into the cisterna magna. The use of a fine gauge needle, small volume and slow rate of injection and prevention of CSF leakage were measures to minimise any artefactual effect from the tracer injection, which could not be avoided [63]. Injection of CSF tracer is technically difficult because of the narrow space between the atlanto-occipital membrane and the underlying medulla. Two animals were excluded during the initial stages of the study, because the tracer injection was either: too deep, resulting in direct injection into the brainstem, or too shallow, with inadvertent CSF leakage.

The ideal CSF tracer remains to be developed. In this study, the use of HRP was associated with technical difficulties resulting in 18 animals being excluded from the study. HRP has been used in previous studies for CSF flow, and has numerous suitable properties [2, 63, 167, 359, 482, 483]. It has a molecular weight of 44,000 Da, which is ideal for assessments of bulk flow. It is fixed to tissues by perfusion with paraformaldehyde, and can be easily detected by a chromogenic reaction, such as TMB. Despite these advantages, HRP had variable enzymatic activity between individual batches that accounted for the differences in intensities of the reaction product. In some of the excluded animals, there was no reaction product detected at any spinal level. Attempts at rectifying this problem included: storage of unopened HRP vials in the -80 $^{0}$C freezer, and fresh preparation of HRP for each injection. Some specimens were processed with anti-HRP antibody to overcome concerns regarding the detection of HRP by using a chromogen. Immunohistochemical staining of HRP with anti-HRP antibodies correlated with the distribution of HRP on TMB staining in eight out of ten animals. However, the degree of autofluorescence on the majority of sections made it difficult to discern positive labeling of HRP.

In addition, HRP can only be visualised on histological sections from post-mortem specimens. In this study, comparisons of CSF flow were made on the assumption that variations between animals were negligible. The ideal scenario would be to inject a tracer that: (i) caused minimal disturbance to the CSF physiology, (ii) could be detectable by imaging in-vivo, and (iii) could be repeated in the same animal at various timepoints during the development of arachnoiditis. Such a technique would reduce the use of animals and overcome any variations between individual animals.

Another limitation of the study was the number of animals available for analysis. Greater statistical power could be obtained if the number of animals was increased, especially with the number of control animals at each timepoint. Although two perfusion intervals were used, no discernible differences were found between the 5 and 20 minute intervals. Reducing covariates by examining fewer timepoints and balancing numbers in the control and arachnoiditis groups might also help in accounting for anatomical and physiological variability.

Despite these limitations, the consistent finding in this study was that perivascular flow into the spinal cord was increased by spinal arachnoiditis. This finding is similar to observations made by Koyanagi et al., based on magnetic resonance imaging. Diffuse intramedullary hyperintensity on T2 weighted images at the level of arachnoid adhesions were reported, which might represent increased interstitial fluid into the spinal cord at the level of arachnoiditis, and lead to a "pre-syrinx" state [59, 183].

The implications for clinical practice are that treatment should focus on addressing the disturbances of CSF flow caused by arachnoiditis. This may involve untethering spinal cord, expansile duroplasty or a subarachnoid-subarachnoid shunt [183]. The putative mechanism of action for these treatments is unknown, but may be explained by reducing the effect of arachnoiditis. Future therapy developments may involve pharmacological treatments or novel surgical techniques that would reduce the extent of arachnoiditis following spinal cord injury to minimise the subsequent formation of syringomyelia.

## *5.6 Conclusion*

Using horseradish peroxidase, this study demonstrated that CSF flow into the spinal cord occurred predominantly along the ventral median fissure and was increased at the region

of arachnoiditis via perivascular spaces. Caudal to the region of arachnoiditis, there was a marked decrease in CSF flow. There were no discernable differences in CSF flow patterns over the timepoints from 3 days to 12 weeks. However, the variability in HRP reactivity in this study illustrated the need for a more consistent CSF tracer for future flow studies in investigations of syringomyelia.

## *5.7 Contributions to the study*

The operations, animal care, tissue processing and preparation of the manuscript and figures were performed by Dr Johnny Wong. Ms Angela Hwang was involved in animal care, tissue processing, data analysis, preparation of the statistical graphs and microscopic image acquisition.

# Chapter 6 Cerebrospinal fluid flow in spinal arachnoiditis using Alexa-Fluor 647 ovalbumin (AFO)

## *6.1 Abstract*

**Background**: The association between post-traumatic syringomyelia and spinal arachnoiditis is well-known. However, the precise mechanism by which arachnoiditis promotes syrinx formation and expansion has not been clearly understood. Observations based on MRI and computational modelling have suggested that obstructions to CSF flow at regions of arachnoiditis would lead to increased fluid flow into the spinal cord. In animal models, tracer studies using horseradish peroxidase (HRP) have similarly indicated increased perivascular flow into the spinal cord at regions of arachnoiditis. However, despite the usefulness of HRP in previous studies, concerns regarding the consistency of HRP reactivity have questioned its suitability and prompted the need for an alternative CSF tracer. Recently, in-vivo macroscopic fluorescent imaging system has been developed, which is capable of capturing fluorescent, radioactive and x-ray images in animals under general anaesthetic.

**Objective**: The objective of the study was to investigate the effect of spinal arachnoiditis on CSF flow in an animal model by using a fluorescent tracer, Alexa-Fluor 647 Ovalbumin (AFO), and to develop a method of evaluating CSF flow with a macroscopic fluorescent imaging system.

**Methods**: For this study, fourteen Sprague-Dawley rats were used. CSF flow was compared between experimental animals that had received spinal arachnoiditis induced

by a subarachnoid kaolin injection with control animals that had laminectomy only. In the first four animals, an intrathecal catheter was inserted at the atlanto-occipital membrane during the initial operation for subsequent CSF access. At the required timepoint, 10 μL of AFO was injected via the intrathecal catheter and in-vivo imaging under general anaesthetic was attempted. However, technical problems with detection of the fluorescent tracer were encountered. In the remaining ten animals, AFO was injected into the cisterna magna with a microsyringe at 3 days, 1, 3 and 6 weeks after the initial operation. Following perfusion at 20 minutes, the spinal cord was harvested and localisation of the tracers with macroscopic fluorescent imaging and fluorescent microscopy was performed post-mortem. Qualitative analyses were performed to assess the extent of tracer flow into the spinal cord.

**Results**: In-vivo imaging was unsuccessful in the four animals which had insertion of an intrathecal catheter. This was due to leakage of CSF tracer and the poor penetration of AFO through overlying bone and muscle. With the remaining ten animals, post-mortem imaging of harvested spinal cord tissue was successful in all animals. Microscopic images revealed AFO staining predominantly in the perivascular spaces of the branches of the anterior spinal artery in the ventral median fissure of all animals. On microscopy and macroscopic fluorescent imaging, there was a gradual decrease in tracer staining towards the caudal levels in the control animals. In contrast, there was an abrupt decrease caudal to the level of arachnoiditis in experimental animals. An increased amount of tracer was observed at the region of arachnoiditis, when compared with more rostral levels in the arachnoiditis animals, particularly at 6 weeks.

**Conclusion**: This study confirmed that perivascular CSF flow into the spinal cord was potentiated by spinal arachnoiditis using the Alexa-Fluor 647 conjugated ovalbumin.

AFO did not have adequate tissue penetration for *in-vivo* imaging under general anaesthetic. However, a novel post-mortem technique for macroscopic fluorescent tracer detection and analyses has been developed that may be useful for future flow studies.

**Keywords / Running title:** Running title: Cerebrospinal fluid flow in spinal arachnoiditis; Keywords: Cerebrospinal fluid, arachnoiditis, ovalbumin, syringomyelia

## 6.2 Introduction

Spinal arachnoiditis is a recognised aetiological factor in the development of post-traumatic syringomyelia [190, 193]. Arachnoiditis most commonly results from spinal cord trauma, in which an initial hemorrhage might result in scarring in the subarachnoid space, but can also occur after meningitis, spinal surgery, or myelograms [84, 183, 481]. It is postulated that spinal arachnoiditis causes disturbances to CSF flow in the spinal subarachnoid space, and contributes to increased fluid flow into the spinal cord, thus leading to a possible "pre-syrinx" state [59, 183]. Using computational modelling, it has been demonstrated that increased perivascular flow of CSF from the subarachnoid space into the spinal cord could be achieved in regions of arachnoiditis [170, 171, 477]. The exact mechanism for this has not yet been elucidated.

Previous animal studies have demonstrated increased perivascular CSF flow from the spinal subarachnoid space at regions of arachnoidtis and syringomyelia using horseradish peroxidase as a tracer [204]. However, concerns regarding the reliability of the chromogen reactivity of HRP have been mentioned in the previous chapter. Moreover, the advent of in-vivo macroscopic fluorescent imaging systems has raised the possibility of conducting repeated CSF flow studies over various time points in the same animal. The objective of the study was to investigate the effects of spinal arachnoiditis on CSF flow into the spinal cord using a fluorescent CSF tracer and to develop a novel technique of assessing CSF flow with an in-vivo macroscopic fluorescent imaging system.

## 6.3 Materials and methods

Following ethical approvals from the Macquarie University Animal Ethics Committee, 14 male Sprague-Dawley rats weighing 323 ± 95 g were used for the study. Similar to the

design used in previous tracer flow studies using HRP, the animals were divided into an experimental group, which received a laminectomy and induction of arachnoiditis, and a control group, which received a laminectomy only. One animal died from anaesthetic related complications and was excluded from the remainder of the study.

Of the 13 animals allocated to this study, in-vivo imaging of CSF flow was attempted in the first three animals, but problems with detection of the fluorescent tracer were experienced. These animals were excluded from further analyses. The subsequent ten animals were studied at 3 days, 1, 3 and 6 weeks, with the group allocations as shown in Table 6.3-1. All animals had an injection of AFO via a microsyringe, followed by perfusion at 20 minutes. Post-mortem multi-spectral and microscopic fluorescent imaging was performed. The experimental steps, including animal surgeries, image acquisition and tissue processing, have been summarised in Figure 6.3-1.

**Table 6.3-1 Allocation of animals with AFO tracer**

| **Procedure** | **Experimental groups** | **Time points** | | | | |
|---|---|---|---|---|---|---|
| | | 3 days | 1 week | 3 weeks | 6 weeks | 12 weeks |
| Laminectomy + intrathecal catheter | Control (No Kaolin) | 1 | - | - | - | 1 |
| | Arachnoiditis (SAS Kaolin) | - | - | - | - | 1 |
| Laminectomy + no catheter | Control (No Kaolin) | 1 | 1 | 1 | 2 | - |
| | Arachnoiditis (SAS Kaolin) | 1 | 1 | 1 | 2 | - |

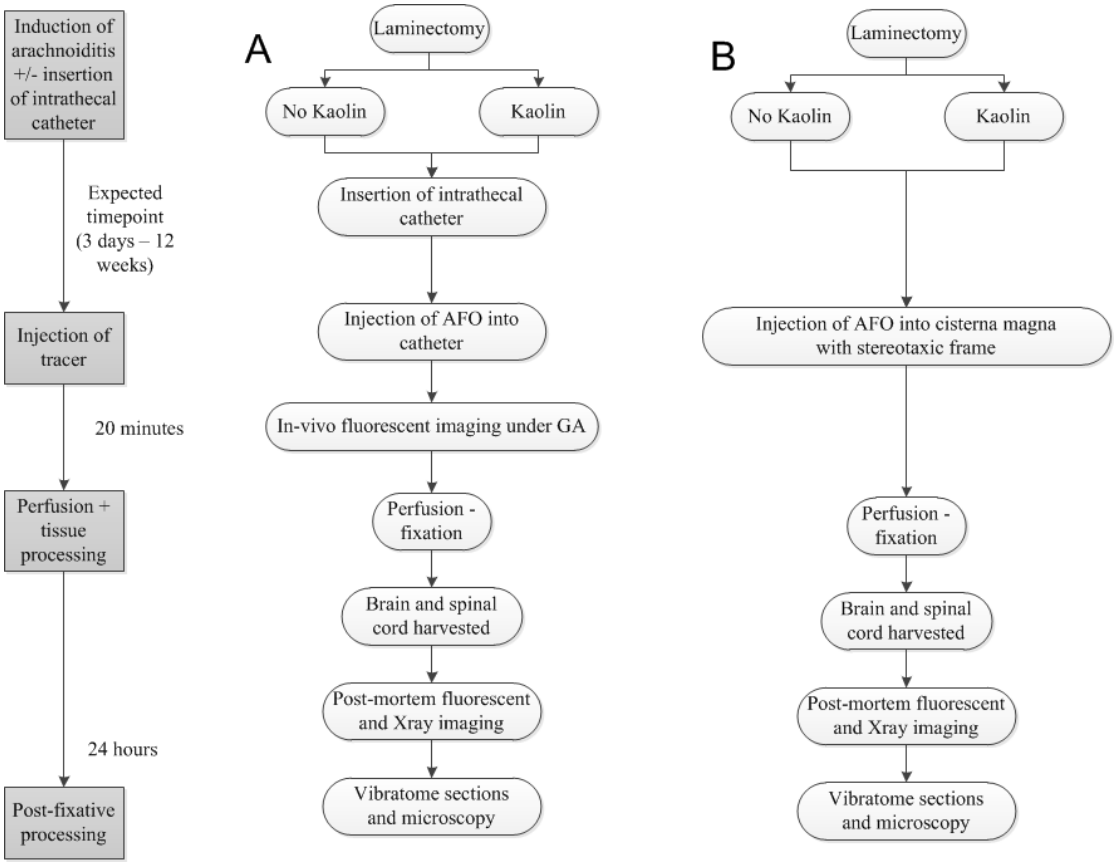


**Figure 6.3-1 Flowchart of processes used with AFO tracer**

**(A) Insertion of intrathecal catheter and in-vivo imaging after AFO injection into catheter; (B) Cisternal AFO injection and post-mortem processing**

## 6.3.1 Operative procedure

All surgical procedures were performed with strict aseptic technique under general anaesthesia. Isoflurane at 5% in 2 L oxygen was used for induction of anaesthetic and was subsequently reduced to 2.5% for maintenance of anaesthesia via a nose cone. The rats were positioned prone and the skin was shaved and prepared with povidone-iodine. A dorsal midline incision was made and a C7 – T1 laminectomy was performed with bony rongeurs in all animals under microscopic magnification.

In the arachnoiditis group, 5 µL of 250 mg/mL kaolin (Sigma-Aldrich) in 0.9% saline solution was measured out with a micropipette and slowly injected into the dorsal

subarachnoid space at the C8 level via 0.5mL 30G insulin syringe (Ultra-Fine II, Beckton Dickinson and Co, NE, US).

For the first three animals, an intrathecal catheter was inserted at the atlanto-occipital membrane via a separate incision at the craniocervical junction under the same anaesthetic. Following sharp incision into the cisterna magna, a custom made polyethylene catheter (Inner diameter = 0.60 mm Outer diameter = 0.96 mm) with a sealed distal end was inserted. The catheter was then secured with strong adhesive glue. The remaining ten animals did not have an intrathecal catheter inserted.

At the completion of the operation, a layered closure was performed with resorbable sutures to fascia and skin. The animals were allowed to recover with analgesia and antibiotic coverage as required and access to food ad libitum. They were monitored daily for 2 weeks post-operatively and then weekly until the experimental endpoint. Neurological deficits, excessive weight loss and signs of distress were recorded.

### 6.3.2 *In-vivo* imaging: Alexa-Fluor 647 Ovalbumin injection, macroscopic fluorescent imaging and perfusion-fixation

For in-vivo imaging in the first three animals, anaesthesia with isoflurane was administered via a nose cone at the required time point for the CSF tracer injection. The animals were positioned prone and the previous occipital incision was reopened under the operating microscope. The intrathecal catheter was exposed and the proximal end was accessed. Using a hand-held 10 µL microsyringe with a beveled needle (SGE International Pty Ltd, VIC, Australia), 10 µL injection of Alexa-Fluor 647 Ovalbumin (O34784, Invitrogen Corporation, NY, US) was slowly administered via the intrathecal catheter. AFO was prepared as a 10% solution mixed with phosphate buffered saline at

pH 7.4 and 0.01% sodium azide. Prior to in-vivo imaging, a custom-made cap was placed over the proximal end of the catheter to prevent leakage and the skin incision was extended to the lumbar region for exposure of the spinous processes to optimise detection of the fluorescent tracer within the spinal canal.

The animal was then positioned supine inside the macroscopic fluorescent imaging machine (In-Vivo MS FX Pro, Carestream Health, NY, US) while general anaesthesia was maintained via a nose cone. Serial fluorescent images were captured at 2 minute intervals with a 60 second exposure time (threshold for excitation) for 20 minutes. A localisation radiograph was performed prior to perfusion-fixation.

Perfusion-fixation was performed via an intracardiac injection of Heparin 5000IU, followed by an influx of fixative into the left ventricle. The right atrium was incised to permit efflux of blood and fixative. Each animal was rapidly perfused with 200 mL of 4% paraformaldehyde (Lancaster Synthesis Ltd, UK) in 0.1 M phosphate buffered saline (pH 7.4).

### 6.3.3 Post-mortem imaging: Alexa-Fluor 647 Ovalbumin injection, perfusion-fixation and macroscopic fluorescent imaging

For post-mortem imaging, the animals were reanaesthetised with isoflurance and were positioned prone and the atlanto-occipital membrane was exposed via a midline incision using the same technique as described in the CSF flow study using HRP. The neck was flexed to ensure that the atlanto-occipital membrane was taut. Using a stereotactic micromanipulator frame, a 10 μL microsyringe with a sharpened, bevelled needle (SGE International Pty Ltd, VIC, Australia) was introduced into the cisterna magna and withdrawn slightly to tent up the atlanto-occipital membrane. A 10 μL injection of AFO

was administered at a rate of 2 μL / min over 5 minutes. CSF leakage and light contamination in the AFO component was minimized. At 20 minutes post tracer injection, the needle was removed and the animal was positioned supine for perfusion-fixation as described previously.

After fixation, the brain and spinal cord were dissected out with the dura intact. X-ray and fluorescent imaging were promptly performed with a macroscopic fluorescent imaging machine (In-Vivo MS FX Pro, Carestream Health, NY, US). Prior to imaging, the region of arachnoiditis was identified macroscopically and marked by placement of hypodermic needles adjacent to the region. The intensity of the Alexa-Fluor 647 signal, as an indicator of the concentration of the ovalbumin CSF tracer, was detected by the fluorescent camera, set at excitation wavelength of 630 nm and emission wavelength of 700 nm. Fluorescent images were captured with exposure times of 5, 10, 15, 20 and 30 seconds. Without moving the specimen, radiographs were taken to localise the previously marked region of arachnoiditis.

### 6.3.4 Tissue processing

A solution of 4% paraformaldehyde was used to post-fix the specimens overnight. The dura and arachnoid adhesions were dissected off the spinal cord to aid sectioning. The extent of arachnoiditis was assessed macroscopically and recorded. Transverse sections of 50 μm thickness were produced with a vibratome from the cerebellum, medulla, C2 to T4 and L1 levels. The sections were floated in a bath containing 0.1M Tris buffer (pH 7.6) and were mounted on pre-coated glass slides (SuperFrost Plus, Menzel-Gläser, Braunschweig, Germany). Fluorescent mounting medium (DAKO, S3023, Carpinteria, CA, US) was applied and the slides were coverslipped.

### 6.3.5 Microscopic image acquisition

The sections were imaged using fluorescent microscopy with a Zeiss Axio Imager Z2 microscopes (Carl Zeiss Microimaging GmbH, Germany) respectively. Images were acquired serially from C2 – T4 for qualitative image analysis using the Axiovision program (Release 4.8.1, Carl Zeiss Microimaging GmbH, Germany) at x200 magnification with exposure time of 1500 ms for AlexaFluor 647, reflecting the Ovalbumin tracer.

Two independent observers, blinded to the group allocations, qualitatively assessed the AFO staining at each spinal level. Comparisons were made between the experimental groups (arachnoiditis or control), spinal levels (C2, C5, C8 or T3), and timepoints (3 days, 1, 3, or 6 weeks).

## *6.4 Results*

All animals in the study recovered from the initial operation without neurological deficits. In the animals that received an intrathecal catheter, a small subcutaneous CSF collection was noted for the first 2 weeks, which gradually resolved with no adverse effects. In the experimental animals, dense arachnoid adhesions were evident macroscopically at all timepoints except 3 days. In the control animals, arachnoid adhesions were not present. In all animals, there was no morphological evidence of spinal cord trauma or syrinx cavities.

### 6.4.1 In-vivo macroscopic fluorescent imaging

High fluorescent signal intensity was detected within the soft tissues of the occipital wound, which gradually increased over the 20 minute period. Despite attempts at

preventing CSF leakage, the soft tissue contamination with AFO indicated leakage of CSF tracer around the catheter.

### 6.4.2 Post-mortem macroscopic fluorescent imaging

Limited signal from the spinal cord was detected when the overlying laminae and muscle were intact, especially at the lower cervical and thoracic levels. The degree of AFO tracer penetrance was assessed with the removal of successive layers. (Figure 6.4-1)

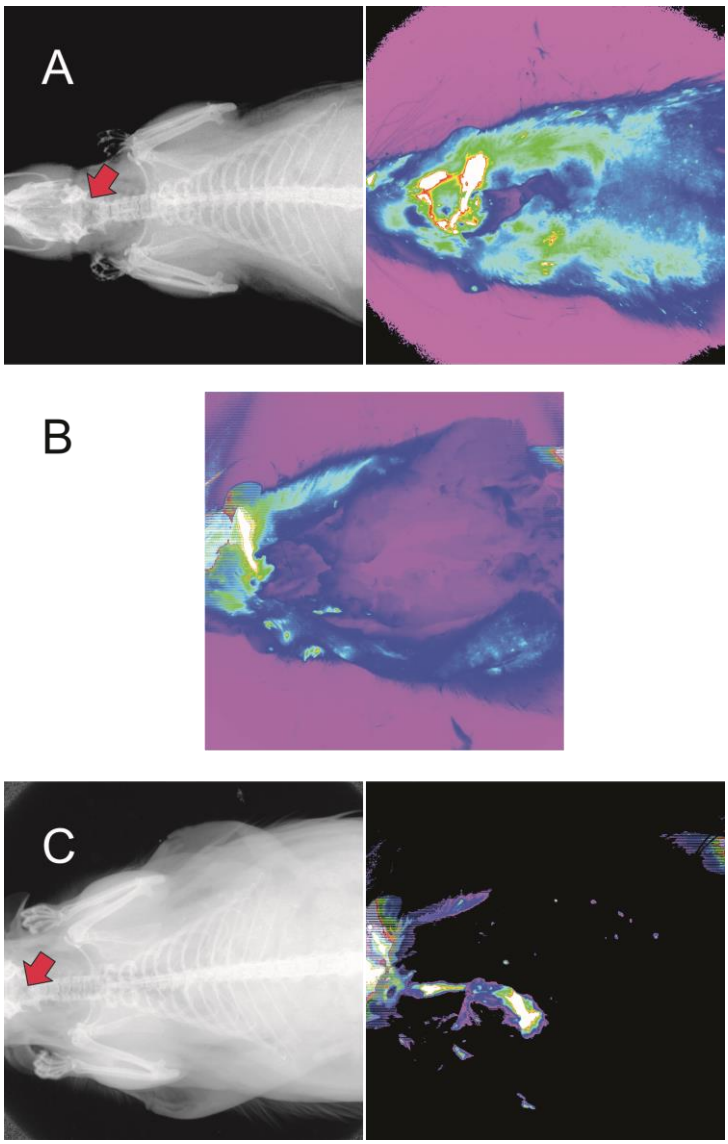


**Figure 6.4-1 Limited AFO penetrance through overlying tissues.**

**Post-mortem macroscopic fluorescent imaging was performed in the same animal, with: A) skin intact; B) skin removed, muscle intact; C) post-laminectomies. Red arrow indicates site of tracer injection.**

After the brain and spinal cord had been harvested, images captured by multispectral imaging demonstrated maximal fluorescence around the site of injection. This involved the brain and the C2 and C3 segments. The optimal exposure time was 10 seconds. In the control group, there was a gradual decrease in intensity from the cervical spinal cord to the mid-thoracic spinal cord at all time points (Figure 6.4-2). However, in the arachnoiditis group, there was an abrupt reduction in intensity immediately caudal to the region of arachnoiditis at all time points. In addition, at the 6 week time point, there was a focal area of increased intensity at the region of arachnoiditis between C7 and T1 levels when compared with areas immediately cranial to these levels (Figure 6.4-2). This appearance was not present either at the earlier time points in the arachnoiditis or control groups.

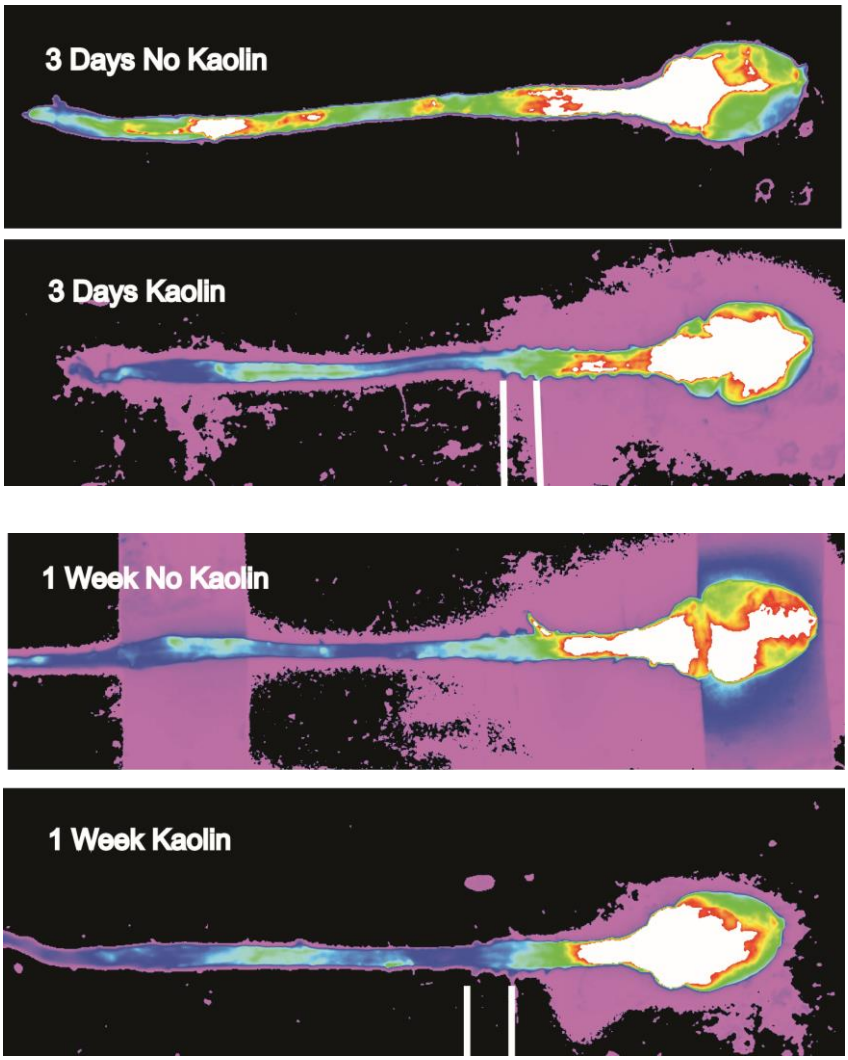

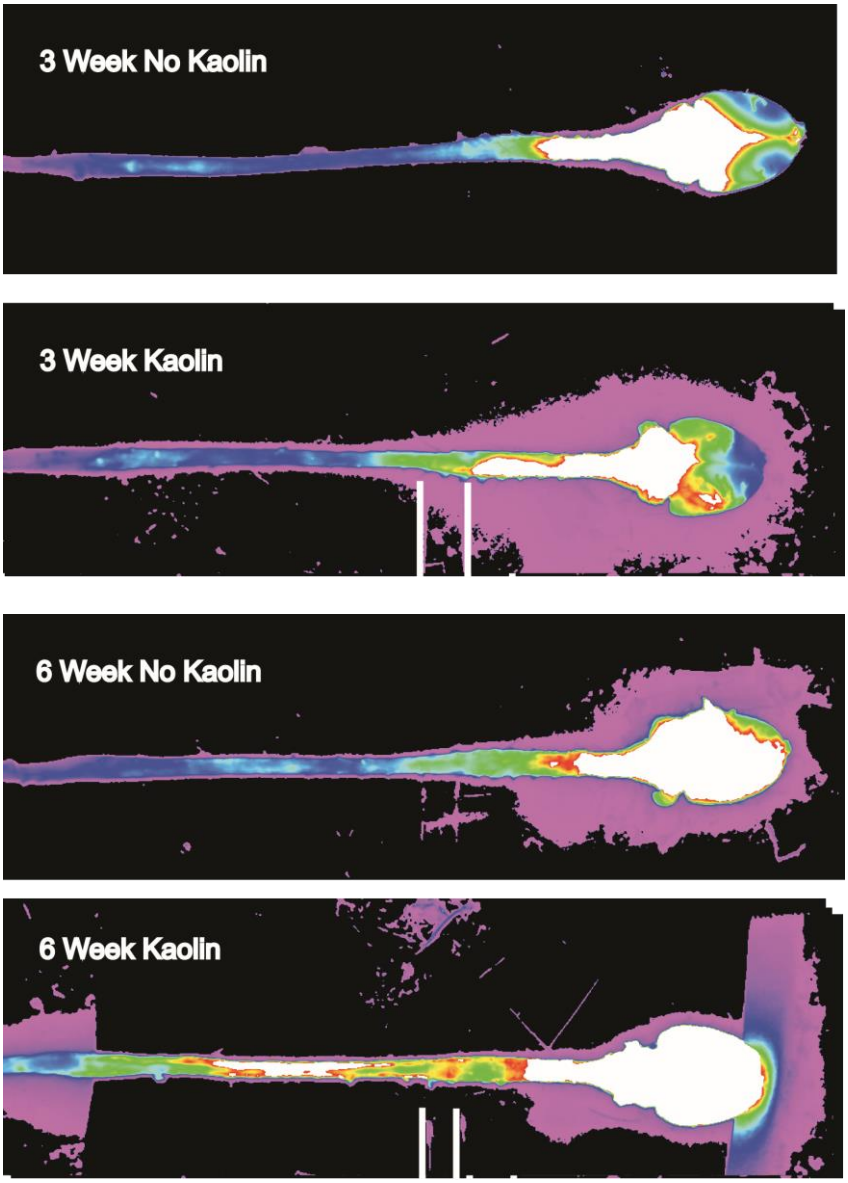


**Figure 6.4-2 Post-mortem macroscopic fluorescent imaging (3 days – 6 weeks)**
**White vertical lines indicate the region of arachnoiditis as observed macroscopically.**

### 6.4.3 Microscopic fluorescent imaging

On microscopic fluorescent staining, AFO tracer was detected in the perivascular spaces and ventral median fissure in a similar distribution to HRP staining. A more intense signal was detected within the central canal between C4 and C8 in the arachnoiditis animals, when compared with the corresponding controls.

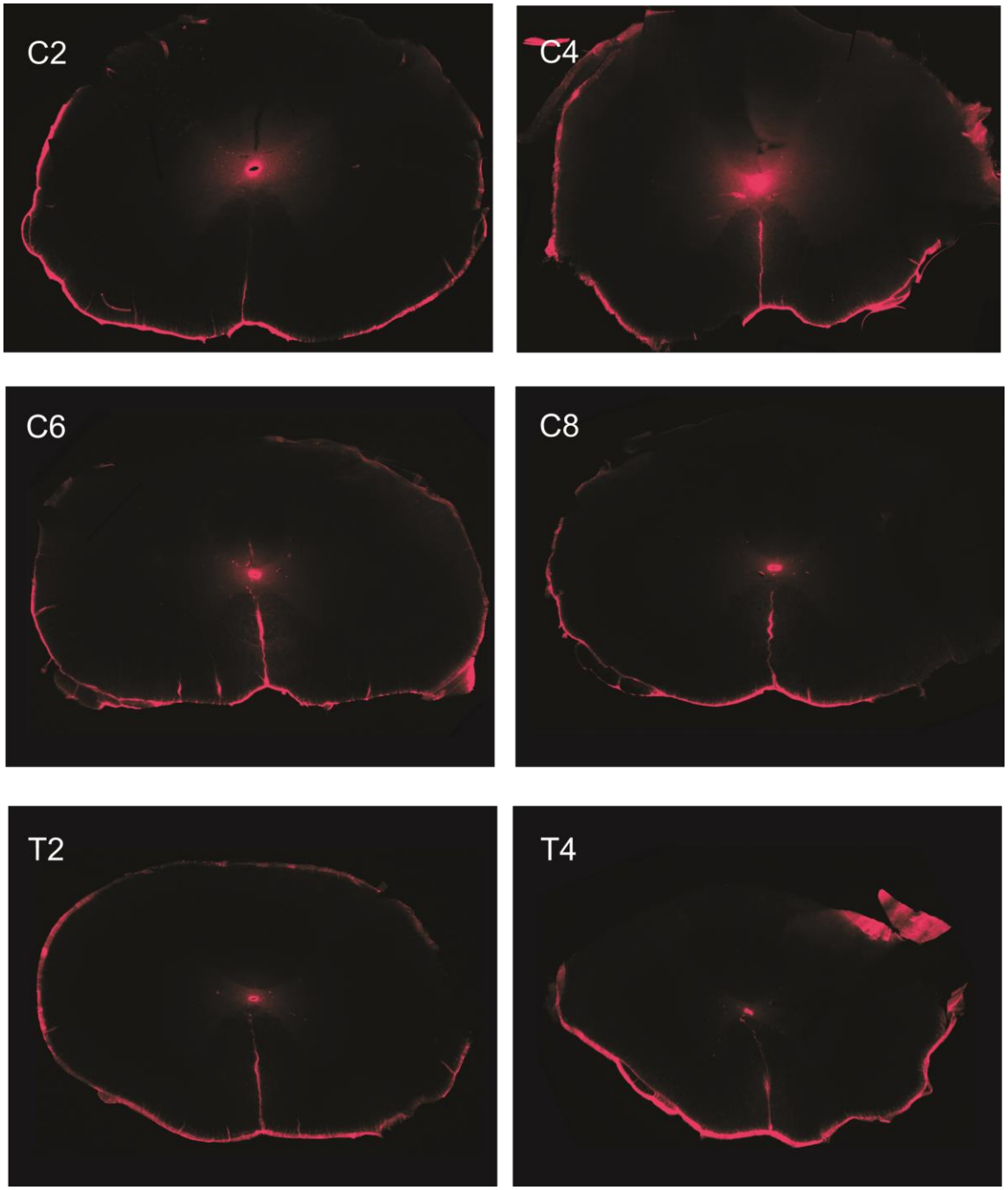


**Figure 6.4-3 Fluorescent microscopic sections from animal with arachnoiditis**

**AFO tracer was detected in perivascular spaces along ventral median fissure and central canal. Fluorescent signal was most prominently detected at the C4 and C6 levels.**

## *6.5 Discussion*

Syringomyelia is generally thought to be a condition caused by alterations in CSF dynamics. In post-traumatic syringomyelia, this may be caused by spinal arachnoiditis.

Based on observations made from MRI, it has been suggested that obstruction in the spinal subarachnoid space from arachnoiditis may result in diffuse intramedullary hyperintensity on T2 weighted images, which might represent increased interstitial fluid into the spinal cord [59, 183]. However, this has not been validated by experimental data. Computational models have also been reported the effects of arachnoiditis on CSF flow within the spinal subarachnoid space. Recently, Bilston et al. reported that phase differences in timing between arterial and CSF pulsations may contribute to increased perivascular flow [171]. Whether this phenomenon actually occurs in-vivo has not been established, but this is a postulated mechanism for spinal arachnoiditis to potentiate CSF flow into the spinal cord.

Previous in-vivo CSF tracer studies demonstrated that CSF flowed into the spinal cord via perivascular spaces under normal physiological conditions, and into the syrinx cavities in animal models of syringomyelia [167-169, 204]. In particular, Brodbelt et al. reported more prominent movement of HRP into the syrinx cavity and central canal than more rostral adjacent levels, suggesting preferential CSF flow into the syrinx [204].

HRP has been used in many studies as a tracer for neuronal studies, as well as CSF flow. It contains numerous suitable properties [63, 167, 204, 359, 482]. It has a molecular weight of 44,000 Da, which is ideal for assessments of bulk flow. It is fixed to tissues by perfusion with paraformaldehyde, and can be easily detected by a chromogenic reaction, such as TMB or DAB. Despite these advantages, recent experience in our laboratory group has been less favourable with inconsistent enzymatic activity between batches of HRP. In the previous study on CSF flow in spinal arachnoiditis, technical failures with HRP processing resulted in a significant number of animals being excluded from the study, such that in some animals, no reaction product was detected at all.

Many other tracers that have been used for assessing CSF flow in previous experimental studies. These include: Evans' blue, Blue dextran 2000, India ink, Prussian blue, fluorescin-labelled serum proteins and radioactive iodine [484-490]. Evan's blue has a molecular weight of 789 Da, which may represent the process of diffusion rather than bulk flow [485-487]. Blue dextran and India Ink are larger particles, which have less propensity for diffusion, but their movements are too slow to assess CSF bulk flow [486, 490]. Other tracers are toxic and make them unsuitable for repeated in-vivo experiments [490].

In this study, Alexa-Fluor 647 Ovalbumin was used. AFO has not been described previously in the literature as a CSF tracer, but has been mainly used in immunological studies [491, 492]. It has several characteristics that make it suitable as a CSF tracer: (1) Its molecular weight is similar to HRP (45,000 Da), which allows for assessment of bulk flow; (2) It is non-toxic for in-vivo experiments [491, 492]; (3) It is conjugated to a fluorescent particle, which can be visualised using a macroscopic fluorescent imaging machine and fluorescent microscopy. This allows for easier quantification of the amount of tracer within each section. The use of a near infrared conjugate (Alexa-Fluor 647) was to facilitate the detection of fluorescent signal because of better penetration through soft tissues.

The results of this CSF flow study with AFO suggest that arachnoiditis causes disturbances of CSF flow at the level of subarachnoid obstruction such that perivascular flow into the spinal cord is increased and fluid flow caudal to this region is markedly decreased. In both the macroscopic and microscopic fluorescent images, a marked decrease in tracer staining was observed at levels below the region of arachnoiditis with the experimental animals across all time points. In contrast, a gradual decrease in staining

was present in the control animals below the corresponding spinal level. This was demonstrated with the macroscopic and microscopic fluorescent images. At 6 weeks, there was increased signal at the level of arachnoiditis than the adjacent rostral levels. These findings were consistent with those from the previous study with HRP as the CSF tracer.

To the best of the authors' knowledge, this was the first study that has used macroscopic fluorescent imaging for assessing CSF flow. Initial attempts were made to perform in-vivo imaging under general anesthetic in the first four animals. However, several technical challenges were encountered, which could not be resolved. First, there were difficulties with the injection of the CSF tracer into the cisterna magna without tracer leakage. The macroscopic fluorescent imaging system could not used in conjunction with a stereotaxic frame and a needle could be not kept in-situ during imaging, hence an intrathecal catheter was designed and inserted at the initial operation. It was anticipated that a sufficient seal from post-operative soft tissue scarring would have developed around the intrathecal catheter to prevent leakage of CSF tracer at the required timepoint. However, CSF leaked predominantly into the soft tissues, and a very small amount of tracer descended down the spinal subarachnoid space. Secondly, there were problems with the penetration of the fluorescent tracer through the bone and muscle dorsal to the spinal cord. A limiting factor was the small volume of tracer that could be used, so that any artefactual disturbances to the CSF physiology would be minimised. Despite increasing the concentration of AFO, the tracer could only be visualised after laminectomies were performed along the entire spine.

There are several obvious benefits to an in-vivo imaging system over imaging of post-mortem specimens. First, it has the ability to capture serial images of the CSF tracer over

short time intervals, thus providing “snapshots” of CSF flow. Secondly, the possibility of repeated tracer studies after recovery from anaesthesia over selected timepoints permits comparison of CSF flow in the same animal as arachnoiditis and syringomyelia develop. For future in-vivo imaging studies, other tracers of similar molecular size may be useful, such as radioactively labeled proteins: I-125 labelled human serum albumin or C-14 labelled inulin [493, 494].

Another limitation of the study was the number of animals available for analysis, including the absence of a 12-week cohort. This would have been ideal to complement the HRP study.

Despite these limitations, the consistent finding between the current study using AFO and the previous study using HRP was that perivascular flow into the spinal cord was increased by spinal arachnoiditis. In addition, this study was a pilot study and proof of principle that macroscopic fluorescent imaging could be utilised in assessing CSF flow.

## *6.6 Conclusion*

Using Alexa-Fluor ovalbumin as a CSF tracer, this study has demonstrated that CSF flow into the spinal cord occurs predominantly along the ventral median fissure and is increased at the region of arachnoiditis via perivascular spaces, similar to previous studies. Caudal to the region of arachnoiditis, there was a marked decrease in CSF flow. This was the first study to use macroscopic fluorescent imaging for CSF flow, and may be a useful method for future studies in syringomyelia. Although the ideal CSF tracer remains to be discovered, the techniques used in this study could be adapted for in-vivo imaging of CSF flow.

## *6.7 Contributions to the study*

The operations, animal care, tissue processing and preparation of the manuscript and figures were performed by Dr Johnny Wong. Ms Angela Hwang was involved in animal care, tissue processing, data analysis, and image acquisition.

# Chapter 7 *In-vivo* telemetry of cerebrospinal fluid pulsations in spinal arachnoiditis

## *7.1 Abstract*

**Background**: Syringomyelia occurs commonly in association with Chiari malformations and spinal cord injuries. However, the pathophysiology of syringomyelia is still uncertain. Alterations to CSF flow and pulsations have generally been considered as important contributing factors to syrinx formation. Recent computational modeling and MRI studies have suggested that timing mismatches between arterial pulsations and CSF pulsations caused by disturbances to CSF flow, such as arachnoiditis, may be important in increasing perivascular CSF flow into the spinal cord.

**Objective:** The objective of this study was to determine whether CSF pulsation delay occurred as a result of arachnoiditis with in-vivo telemetry monitoring of CSF pressures in a sheep model.

**Methods**: Eight merino wethers were used for this study, in which six animals had a laminectomy and arachnoiditis induction with a subarachnoid kaolin injection, and two animals had a laminectomy only. In all animals, telemetry pressure transducers were implanted into the subarachnoid space cranial and caudal to the region of arachnoiditis, with implanted ECG leads. In-vivo CSF pulsation data was acquired weekly for 6 weeks. At the conclusion of the experiment, CSF flow studies were performed with a CSF tracer (horseradish peroxidase, HRP) injected into the subarachnoid space cranial to the region of arachnoiditis. The amplitude of CSF pressures, and the timing between QRS complexes on the ECG and systolic pulsations in the CSF were measured and analysed.

**Results**: Telemetry data was successfully obtained in six sheep for 4 – 5 week duration. There appeared to be a pulsation delay present in the arachnoiditis animals, which commenced beyond 2 weeks post-induction of arachnoiditis. Pulsation delay was not present in the control animals. The CSF flow study was only successful in one animal, due to technical difficulties with the HRP. The maximum amount of HRP reaction product was observed in the central canal and perivascular spaces at the region of arachnoiditis.

**Conclusion**: This was the first study to perform in-vivo telemetry monitoring of CSF pressures from the subarachnoid space from an ambulatory animal. In a sheep model of arachnoiditis, CSF pulsation delays were present across regions of arachnoiditis, but further studies are required to validate the results from the current study.

**Keywords / Running title:** Running title: Telemetry of CSF pulsations in spinal arachnoiditis; Keywords: Animal model. Arachnoiditis. Cerebrospinal Fluid. Post-traumatic Myelopathy. Syringomyelia

## 7.2 Introduction

Syringomyelia is a fluid-filled cavity within the spinal cord, which occurs in association with a number of conditions, including Chiari malformations, spinal cord trauma, spinal cord tumours and arachnoiditis from subarachnoid haemorrhage or meningitis [23]. Despite the numerous theories proposed regarding the pathophysiology of this condition, there has not been any satisfactory explanation for the formation and expansion of syrinx cavities [160]. Much attention has been placed on the Chiari-related syringomyelia and how alterations in CSF pressures from the cerebellar tonsils would promote CSF flow into the spinal cord, although most of the existing theories on this phenomenon lack experimental evidence. Analogous to the Chiari-related syrinxes, disturbances of CSF pulsations in the spinal subarachnoid space from arachnoiditis have been implicated as an important contributing factor to the pathogenesis of post-traumatic syringomyelia [63, 171, 204, 477].

The effect of arachnoiditis to CSF flow in the spinal subarachnoid space has previously been studied in animal and computational models. Using a rodent post-traumatic syringomyelia model, Brodbelt et al. demonstrated increased perivascular CSF flow at the level of a syrinx and arachnoiditis [204]. In earlier chapters of this thesis (Chapter 5 and 6), similar results were presented in a rodent model of arachnoiditis alone. Bilston et al. showed on a computational model that CSF flow from the spinal subrachnoid space into the spinal cord could be increased by phase differences between CSF and arterial pulsations [171]. It has been postulated that this phase difference occurred as a consequence of arachnoiditis. However, it has not yet been verified whether CSF pulsation delay actually occurs in-vivo. In fact, the nature of CSF pulsations in the spinal subarachnoid space is not well understood. The objective of the current study was to

monitor the CSF pulsations in the spinal subarachnoid space via a closed in-vivo telemetry system as spinal arachnoiditis developed and to determine whether CSF pulsation delay actually occurred.

## *7.3 Materials and methods*

Ethics approval was obtained from the IMVS Animal Ethics Committee, Adelaide, and eight merino wethers weighing 37.5 – 58.5 kg were used for this study. There were six animals allocated to the experimental group, which received a laminectomy and induction of arachnoiditis, and two animals to the control group, which had a laminectomy only. In all animals, pressure monitors were inserted for weekly telemetry recordings for 6 weeks. In the first two animals, the data recordings were suboptimal and could not be analysed. Thus, these animals were excluded from further analysis in this study.

### 7.3.1 Induction of arachnoiditis and insertion of telemetry pressure monitors

The use of kaolin in the subarachnoid space to induce arachnoiditis is a well-recognised technique. This has been used previously in a large model of extra-canalicular syringomyelia. All procedures were performed in a sterile field under general anaesthetic. Anaesthesia was induced with 1 g thiopenthal intravenously and maintained with 2.5 – 3% isoflurane via an endotracheal tube and mechanical ventilation. The sheep were positioned prone and the T2 – T4 spinous processes and laminae were exposed via a midline subperiosteal approach. Laminectomies at T2 and T3 were performed. Subcutaneous pockets were developed to accommodate the telemetry transmitter units (TR73P and TR73PB, Telemetry Research, Auckland, New Zealand), and secured on the thoracolumbar fascia with sutures. The dura was opened via two right paramedian

incisions, each measuring approximately 5 mm in length. Using a blunt hook to elevate the dura, pressure catheters were inserted into the subarachnoid space at a distance of 20 mm cranial and caudal to the durotomies. For ECG recordings, the biopotential leads from the TR73PB telemetry unit were tunnelled subcutaneously to bilateral incisions along intercostal spaces and buried within the intercostals muscles, as illustrated in Figure 7.3-1.

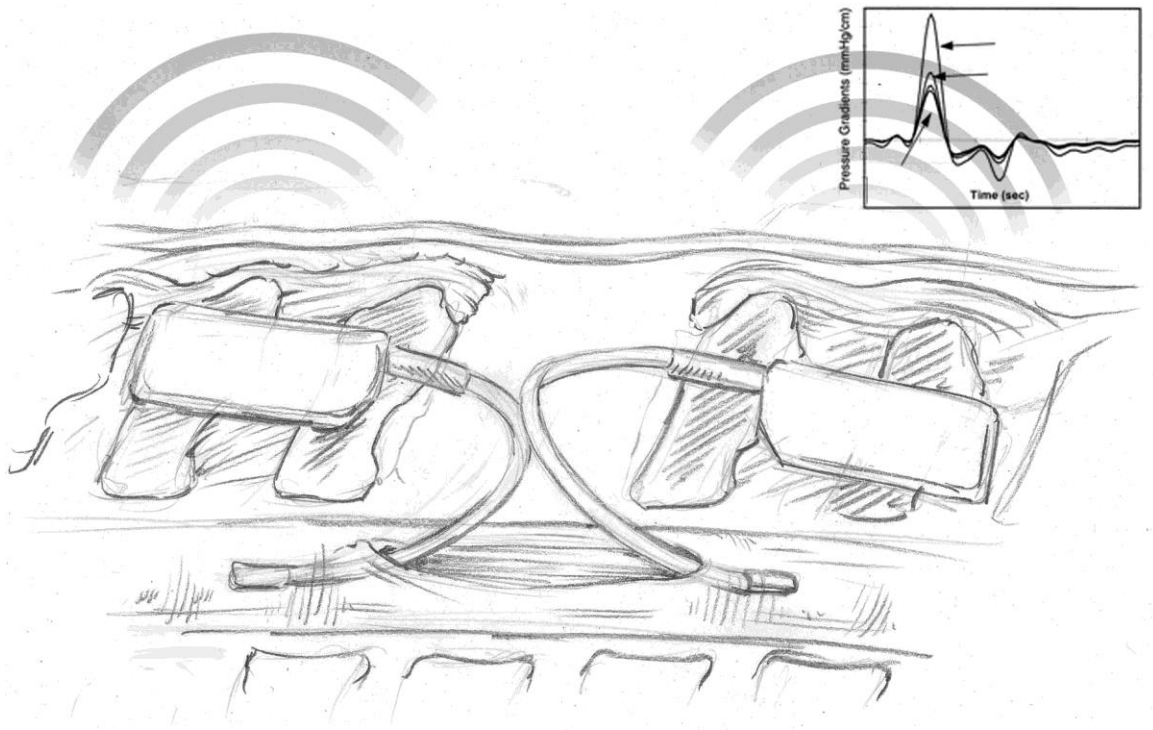


**Figure 7.3-1 Schematic illustration of the arrangement of cranial and caudal CSF pressure transducers implanted into the spinal subarachnoid space.**

In the control animals, kaolin was not injected into the subarachnoid space. In the arachnoiditis animals, 0.5 mL of 250 mg/mL kaolin solution was mixed with the thrombin component of a two-component fibrin sealant (Tisseel Duo 500, Baxter Healthcare Pty Ltd, NSW, Australia) and drawn up into the double-barrelled applicator. The kaolin and fibrin mixture was slowly injected into the subarachnoid space on both sides of the dural incisions to a total of 0.2 mL per sheep. The wound was closed in layers with Vicryl sutures. The sheep were allowed to recover with analgesic and antibiotic

coverage, and free access to food. They were monitored for neurologic deficits, excessive weight loss and signs of distress.

### 7.3.2 Telemetry recordings of CSF pulsations

Recordings of the CSF pressures and ECG via the telemetry system were made for 10 minutes every week for 6 weeks. The telemetry system consisted of: integrated gel-filled catheters that transduced pressures and transmitted data via a radiofrequency signal (Model TR73P and TR73PB). On the TR73BP monitor, additional biopotential leads permitted transmission of ECG signals. The signals were received by the TR871 units (Telemetry Research). The output signals were captured via a data acquisition system (Powerlab 8/35, AD instruments, CO, US) and recorded on the LabChart program (AD Instruments, CO, US).

During the recordings, the animals' posture and activities were annotated on the traces, for subsequent reference.

### 7.3.3 Injection of fluid tracer and perfusion/fixation

After 6 weeks, the animals were re-anaesthetised and positioned supine. The common carotid artery and jugular veins were dissected out in preparation for perfusion/fixation, as previously described by Santoreneos et al. [452]. The sheep were then repositioned prone and a new incision cranial to the laminectomy wound was made. Laminectomies of C7 and T1 were performed and 250 μL 4% Horseradish Peroxidase (Invitrogen CA, US) was injected into the subarachnoid space cranial to arachnoiditis over 5 minutes, using a hand-held 1 mL syringe with a 25G hypodermic needle.

At the completion of the experiment, the animals were repositioned for intravascular aldehyde perfusion 10 minutes after the HRP injection [452]. Heparin 5000 IU was

injected intravenously and the common carotid arteries were cannulated to allow influx of fixative. The fixative was directed proximally in the left common carotid and distally in the right common carotid. The internal jugular veins were divided on each side. Each animal was perfused with 10 L of 4% paraformaldehyde (Lancaster Synthesis Ltd, UK) in 0.1 M phosphate buffered saline (pH 7.4).

### 7.3.4 Tissue processing and retrieval of telemetry monitors

After perfusion, the pressure catheters and ECG leads were carefully dissected out, ensuring that the telemeters were intact. The thoracic spinal cord was dissected out of the spinal canal and post-fixed in 4% paraformaldehyde solution overnight. The dura and arachnoid were removed prior to sectioning. Transverse sections from T2 to T4 spinal cord levels of 50 μm thickness were produced with a vibratome and floated on a bath containing Tris Buffer (pH = 7.6). The sections were mounted on 3-amino propyl-triethoxy-silane (APT) coated glass slides and allowed to air dry for at least 4 hours.

Histological localisation of HRP was carried out using tetramethylbenzidine (TMB) as the chromogen. The sections were soaked in distilled water for 15 seconds, and then incubated in 0.01 M sodium acetate buffer (pH 3.3) containing 0.005% 3,3',4,4' TMB (Lancaster Synthesis Ltd, UK) and 0.1% sodium nitroferricyanide (III) dehydrate (Lancaster Synthesis Ltd, UK). The sections were incubated for a further 20 min following the addition of 30 μL of hydrogen peroxide to a final concentration of 0.01%. After washing in sodium acetate buffer (pH 3.3), the reaction product was stabilized in 5% ammonium molybdate (IV) tetrahydrate (Sigma-Aldrich, MO US) in 0.01 M sodium acetate buffer. Finally, the slides were washed in sodium acetate buffer for 30 seconds, dehydrated in graded ethanol, xylene and then coverslipped with DPX mounting medium (Scharlau Chemie SA, Spain).

### 7.3.5 Statistical analyses

The pulsation data was analysed in the following manner. Two 10 second intervals were selected from each data recording in which the CSF pulsation waves and ECG traces were all present with minimal affect from movement artefacts. A low-pass filter of maximum threshold at 40Hz for ECG and 10 Hz for CSF pressure was used. In regards to CSF pressures, the maximum and minimum amplitude of each CSF pressure trace were recorded. To determine the timing of the ECG and CSF pressure pulsations, the R-wave in the QRS-complex of the ECG was used as an indicator of cardiac systole, while the first peak in the cranial CSF pulsation after the QRS complex was interpreted as the systolic CSF pulsation. The corresponding caudal CSF pulsation wave was used, and the time intervals between the QRS and the cranial CSF transducer (labelled "QP interval"), and between cranial and caudal CSF transducers (labelled "PP interval") were calculated.

## *7.4 Results*

In the eight sheep used for this study, none of the animals developed permanent neurological deficits. One arachnoiditis animal developed transient neurological deficit with anorexia and weight loss for 1 week, but recovered with oral antibiotics. The telemetry transmitters did not cause any obvious distress in the animals and none of the animals developed any signs of infection.

### 7.4.1 Telemetry pulsation data

Data from the first two sheep were recorded at a frequency of 100 Hz, but the ECG trace was not available and the cardiac cycle could therefore not be assessed. From the following six sheep, CSF pulsation and ECG data were obtained at a frequency of 200 Hz for a minimum of 3 weeks in each sheep. Due to the limited battery life of the implanted

transmitters, recordings beyond the 5$^{th}$ week in the majority of the sheep demonstrated flat traces in either one or both transmitters despite applying the external charging device. These results could not be analysed and were excluded from further analysis.

## CSF pulsation waveforms

The cranial and caudal CSF pulsation waveforms were influenced by the respiratory rhythm, arterial pulse and movement artefacts, as demonstrated in Figure 7.4-1. However, several observations were noted from the recordings: (1) a large degree of variability was observed in each of the CSF pulsation waveforms; (2) All three traces were very sensitive to changes in posture or head position, which caused large movement artefacts across the three recordings; (3) The peaks in both cranial and caudal CSF pulsation waves correlated with the T-wave of the ECG trace and might correspond to the systolic arterial pulse; (4) The shape of cranial and caudal CSF pulsation waveforms was not identical, even when the animals were at rest; (5) At later periods after implantation of the transmitters, the amplitude of the CSF pulsations and the ECG QRS complexes decreased as the battery power in the transmitters diminished.

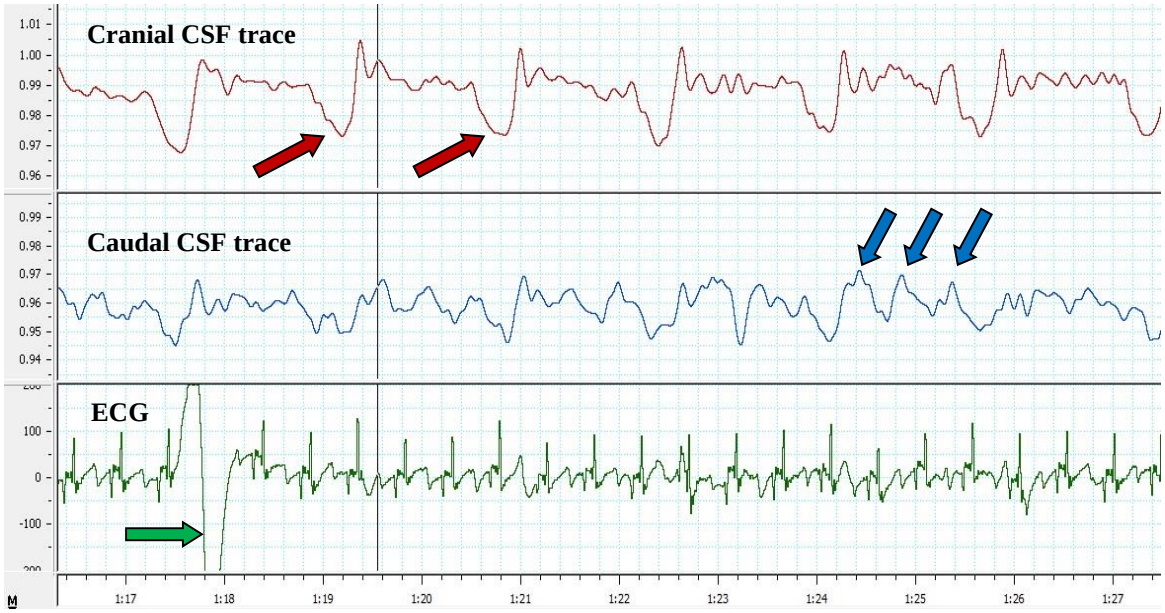


**Figure 7.4-1 CSF and ECG telemetry traces at implantation**

**The cranial and caudal CSF traces are shown in red and blue respectively. The ECG trace is indicated in green. Influences from respiration (red arrows), arterial pulsations (blue arrows) and movement artefacts (green arrow) are represented.**

## Attempted methods for analysis

Multiple digital filter settings were attempted, including high pass, low pass, notch filter and band pass, to reduce the artefactual noise in each pressure and ECG trace. The best result was noted with low-pass at maximum of 10 Hz with the CSF pulsation waves, and 40 Hz with ECG.

For calculation of pulsation timing across regions of arachoniditis between the cranial and caudal transmitters, the peaks of each CSF pulsation wave were used. However, due to the variability in the frequency and amplitude of the peaks in each CSF pulsation wave, mathematical transformations, such as Fourier transform, could not generate a consistent waveform for analysis.

## CSF pulsation amplititude

The CSF pressure transducers were pre-calibrated to measure pressure from -100 – 100 mmHg. The results of the CSF pulsation amplitudes in the arachnoiditis and control animals are summarised in Table 7.4-1 and Table 7.4-2.

**Table 7.4-1 Minimum-maximum amplitudes (in mmHg) of cranial and caudal CSF pulsation waves in arachnoiditis animals**

| Timepoint | Sheep 1 | | Sheep 2 | | Sheep 3 | | Sheep 4 | |
|---|---|---|---|---|---|---|---|---|
| | Min (mmHg) | Max (mmHg) | Min (mmHg) | Max (mmHg) | Min (mmHg) | Max (mmHg) | Min (mmHg) | Max (mmHg) |
| **Week 0** | | | | | | | | |
| Cranial | -3.3 | 3 | -7.2 | -3.3 | 8.5 | 10 | 7.9 | 10.8 |
| Caudal | -6.3 | -2.6 | -3.3 | -1.3 | 5.3 | 7.7 | 7.7 | 9.5 |
| **Week 1** | | | | | | | | |
| Cranial | -21 | -13 | 0.6 | 1.8 | 13.1 | 14.6 | -6.1 | -5.0 |
| Caudal | -7.8 | -5.4 | -3.9 | -2.6 | -1.1 | 3.1 | -8.0 | -6.6 |
| **Week 2** | | | | | | | | |
| Cranial | 22.2 | 32.8 | 2.6 | 5.6 | 10.2 | 11.8 | 17.0 | 18.1 |
| Caudal | 11.4 | 17.2 | 2.3 | 4.9 | 12.5 | 14.5 | 4.1 | 6.1 |
| **Week 3** | | | | | | | | |
| Cranial | -13.1 | -6.6 | -2.7 | 0.8 | -20.9 | -7.4 | 25.5 | 30.1 |
| Caudal | 20.8 | 23.8 | 3.8 | 6.6 | -7.3 | 1.9 | 2.7 | 5 |
| **Week 4** | | | | | | | | |
| Cranial | * | * | 34.3 | 40.9 | -14.8 | 1.3 | -9.6 | -7.8 |
| Caudal | * | * | 12.7 | 14.3 | -13.0 | -2.4 | -7.8 | -6 |
| **Week 5** | | | | | | | | |
| Cranial | * | * | 53.5 | 59.5 | * | * | * | * |
| Caudal | * | * | * | * | * | * | * | * |
| **Week 6** | | | | | | | | |
| Cranial | * | * | * | * | * | * | * | * |
| Caudal | * | * | * | * | * | * | * | * |

* indicates missing data due to flat battery or technical failure

**Table 7.4-2 Minimum-maximum amplitudes (in mmHg) of cranial and caudal CSF pulsation waves in control animals**

| Timepoint | Sheep 1 | | Sheep 2 | |
|---|---|---|---|---|
| | Min (mmHg) | Max (mmHg) | Min (mmHg) | Max (mmHg) |
| **Week 0** | | | | |
| Cranial | -9.7 | -8.6 | -0.6 | 2.3 |
| Caudal | 10.5 | 12.1 | 1.9 | 3.7 |
| **Week 1** | | | | |
| Cranial | 14.1 | 16 | 2.5 | 4.7 |
| Caudal | -4.2 | -1.5 | 30.5 | 33 |
| **Week 2** | | | | |
| Cranial | 17.2 | 19.3 | 0.8 | 3.1 |
| Caudal | 10 | 11.8 | 29.9 | 34.5 |
| **Week 3** | | | | |
| Cranial | 33.1 | 35.8 | * | * |
| Caudal | 68.1 | 71.5 | * | * |
| **Week 4** | | | | |
| Cranial | 22.1 | 23.6 | 6.9 | 12.5 |
| Caudal | 12.1 | 13.6 | 37.0 | 40.8 |
| **Week 5** | | | | |
| Cranial | 9.8 | 13.9 | * | * |
| Caudal | 5.2 | 9.2 | * | * |
| **Week 6** | | | | |
| Cranial | -11.7 | -8.5 | * | * |
| Caudal | -8.1 | -6.6 | * | * |

* indicates missing data from flat battery or technical failure

The minimum – maximum amplitude range for each transducer trace was within 10 mmHg. However, the absolute subarachnoid CSF pressure values varied widely, ranging from 0.6 to 59.5 mmHg. This variability may be due to changes to head and body posture during the recordings. Comparing the cranial pressure measurements to the corresponding caudal measurements, the caudal pressure was more likely to be slightly higher than the cranial pressure, but this pattern was not consistently observed over the

6 week recording period. In addition, there was no observable difference between the progressions of CSF pressures in the arachnoiditis, when compared with the control animals.

## ECG and CSF pulsation timing

The results of the ECG and CSF pulsation timing are summarised in Table 7.4-3 and Table 7.4-4.

**Table 7.4-3 ECG – Cranial CSF pulsation delay over 6 weeks**

| Time-point | Arachnoiditis | | | Control | | |
|---|---|---|---|---|---|---|
| | No. of recordings | Mean delay | Range | No. of recordings | Mean delay | Range |
| Week 0 | 4 | 0.21 | 0.19 – 0.24 | 2 | 0.15 | 0.15 – 0.16 |
| Week 1 | 4 | 0.24 | 0.15 – 0.38 | 2 | 0.16 | 0.16 – 0.17 |
| Week 2 | 4 | 0.27 | 0.23 – 0.37 | 2 | 0.18 | 0.16 – 0.20 |
| Week 3 | 4 | 0.25 | 0.19 – 0.34 | 1 | 0.19 | 0.19 |
| Week 4 | 3 | 0.21 | 0.18 – 0.24 | 2 | 0.22 | 0.21 – 0.246 |
| Week 5 | 1 | 0.23 | 0.23 | 1 | 0.21 | 0.21 |
| Week 6 | 0 | | | 1 | 0.15 | 0.15 |

**Table 7.4-4 Cranial – Caudal CSF pulsation delay over 6 weeks**

| Time-point | Arachnoiditis | | | Control | | |
|---|---|---|---|---|---|---|
| | No. of recordings | Mean delay | Range | No. of recordings | Mean delay | Range |
| Week 0 | 4 | 0.014 | 0.004 – 0.021 | 2 | 0.035 | 0.03 – 0.041 |
| Week 1 | 4 | 0.038 | 0.007 – 0.100 | 2 | 0.037 | 0.036 – 0.04 |
| Week 2 | 4 | 0.16 | 0.014 – 0.320 | 2 | 0.024 | 0.01 – 0.039 |
| Week 3 | 4 | 0.15 | -0.03 – 0.31 | 1 | 0.002 | 0.002 |
| Week 4 | 3 | 0.190 | 0.16 – 0.23 | 2 | 0.015 | 0.011 – 0.02 |
| Week 5 | 1 | 0.22 | 0.22 | 1 | 0.022 | 0.022 |
| Week 6 | 0 | | | 1 | 0.031 | 0.031 |

In the arachnoiditis animals, the mean delay between the QRS complex and the cranial CSF pulse was 0.211 s (range 0.193 – 0.237 s) at the time of implantation. This did not vary significantly as the arachnoiditis matured, as seen in Figure 7.4-2. However, the mean delay between the cranial and caudal CSF pulses gradually increased from week 2 in all animals. The mean time interval between the two transmitters increased from 0.014 s (range: 0.004 – 0.021 s) at implantation to 0.220 s (range: 0.206 – 0.233 s) at 5 weeks, as demonstrated in Figure 7.4-3.

In the control animals, the delay between the QRS complex and the cranial CSF transducer was similar to the arachnoiditis animals, with a mean delay of 0.152 s (range 0.146 – 0.158 s). There was no change to this delay interval at the later time points. The delay between the cranial and caudal transducers at implantation was similar to the arachnoiditis cohort, with an average of 0.033 s (range 0.030 – 0.041) However, the time interval between the two CSF pulses did not increase in the control animals, with a delay of 0.022 s at the 5 week timepoint, as seen in Figure 7.4-3.

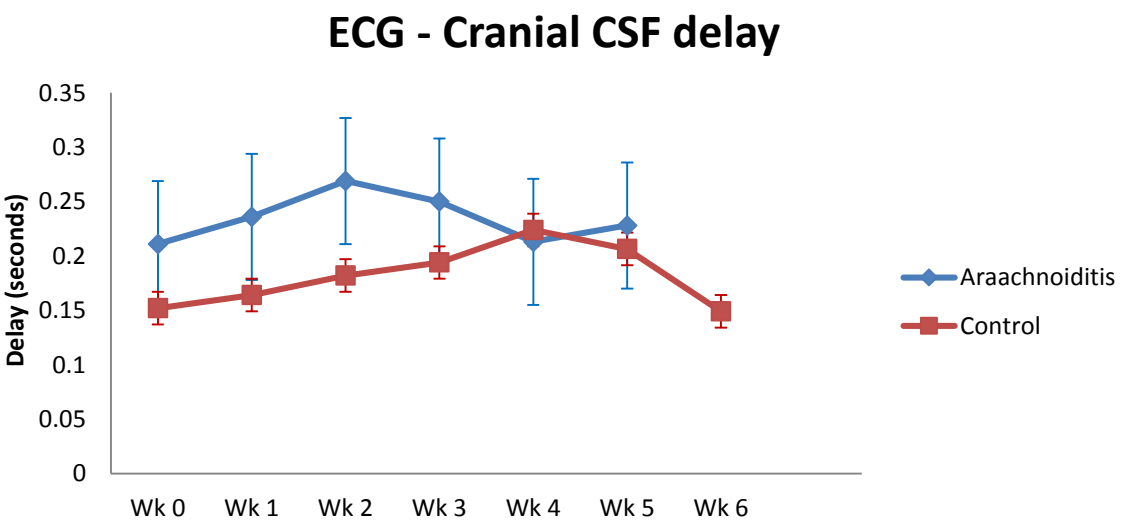


**Figure 7.4-2** **Mean ECG – cranial CSFpulsation delay in arachnoiditis and control animals**

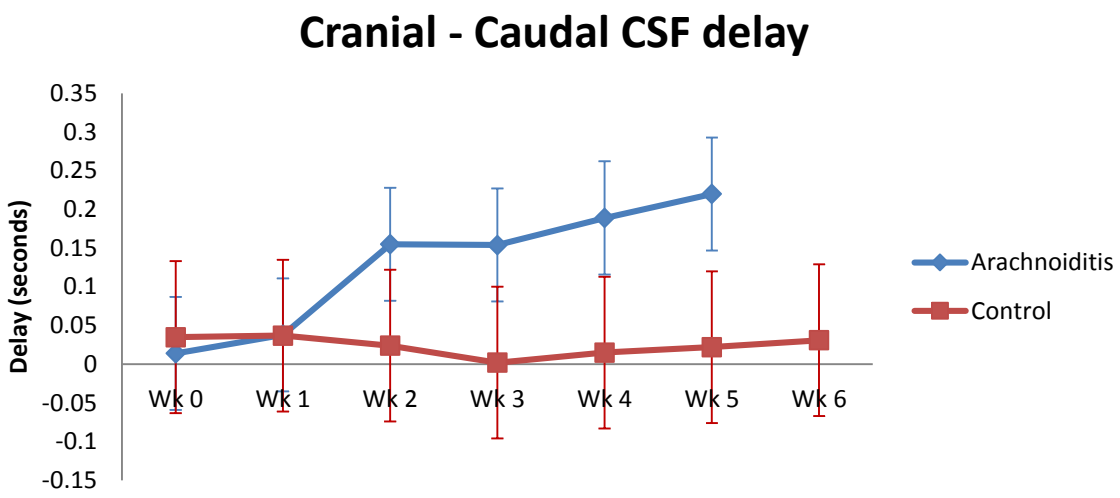


**Figure 7.4-3** **Mean Cranial – caudal CSF pulation delay in arachnoiditis and control animals**

### 7.4.2 CSF flow studies with HRP

CSF flow studies with HRP were performed in five sheep. The spinal cords were sectioned and processed with TMB staining. In two sheep, the amount of HRP injected was insufficient to be detected by TMB staining. In two sheep, technical problems were experienced with inconsistent TMB localisation due to variable HRP enzymatic activity despite increasing the volume of HRP injected from 10 µL to 250 µL.

HRP could be localised in only 1 sheep. HRP reaction product was identified in the peripheral perivascular spaces, and most prominently along the ventral median fissure and into the central canal. The pattern of distribution was consistent with previous studies by Stoodley et al. and Brodbelt et al, which studied CSF flow with HRP. There was increased HRP reaction product in the central canal at the region of arachnoiditis, when compared with the site of injection and caudal to the region of arachoniditis.

## 7.5 Discussion

The pathophysiology of syringomyelia is still poorly understood. It has generally been assumed that syrinx fluid is derived from CSF, although the veracity of this assumption has been debated recently [176]. Early hydrodynamic theories identified the cerebellar tonsils as the cause of obstruction to CSF flow, thus diverting fluid into the fourth ventricle and subsequently into the spinal cord via the central canal [147, 159]. However, it has subsequently been shown that communication between the fourth ventricle and the central canal of the spinal cord is rarely patent in human autopsy specimens [97]. Subsequent theories have postulated that the cerebellar tonsils might act as pistons in promoting CSF flow into the spinal cord via perivascular spaces, but such an explanation would not account for other causes of syringomyelia, for example, arachnoiditis at the foramen magnum or in the spinal subarachnoid space [163, 164, 495]. The problem with all existing theories lies with the observation that fluid within a syrinx cavity is under pressure, and the mechanism by which fluid moves into a syrinx cavity against a pressure gradient remains a mystery.

Although a complete understanding has not been obtained, it is generally agreed that syrinx formation and enlargement are related to CSF flow and pulsations. Bilston et al. proposed that CSF-arterial pulsation phase differences may account for increased perivascular flow into the spinal cord [171]. This may be caused by alterations to CSF flow by the cerebellar tonsils at the foramen magnum in Chiari malformation.

In fact, much is still unknown about CSF flow in the subarachnoid space and the nature of the pressure pulsation properties of the CSF waveform. CSF velocities and pulse profiles based on MRI studies have been investigated on syringomyelia patients with Chiari malformation. It has been demonstrated that patients with Chiari malformation type 1

have altered CSF pulse profiles in relation to the cardiac pulse when compared with normal volunteers, with improvement following posterior fossa decompression surgery [496, 497]. A recent study by Clarke et al. compared the features of CSF velocity-time profiles relative to the cardiac pulse on human MRI studies in Chiari patients with and without syringomyelia. It was found that patients with Chiari malformation without syringomyelia had a significantly earlier onset of caudal flow and peak velocity than normal subjects and Chiari patients with syringomyelia [498, 499]. The findings suggest that the offset in timing between the CSF pulsation and arterial pulsation may be important in the initiation of syrinx formation.

In a similar manner, arachnoiditis may cause disturbances of CSF flow in the spinal subarachnoid space. Previous experimental studies have demonstrated increased perivascular flow due to arachnoiditis in animal and computational studies [63, 171, 204, 478]. The actual mechanism of how this occurs has not been thoroughly investigated or understood. It has been postulated phase differences in the CSF pulsation and arterial pulsation profiles might result in increases in CSF perivascular flow. However, it has not been shown on an in-vivo animal model whether CSF pulsations are delayed by regions of arachnoiditis.

The current study was performed for several reasons. First, the nature of spinal subarachnoid CSF pulsations is not well understood and has not been adequately investigated in animal or human models. Secondly, telemetry technology has become available, which has been used in animal models for monitoring of physiological functions, such as blood pressure, respiratory rate, ECG, EMG and more recently intracranial pressure [500-502]. Thirdly, an ovine model of post-traumatic syringomyelia

has recently been developed, which can be used for investigating the CSF pulsation waveforms in an ambulent, unrestrained animal [63].

The sheep is the most suitable model for the current study. First, the size of the sheep spinal cord and subarachnoid space are comparable to human anatomy, being sufficiently large to permit the insertion of a subarachnoid catheter without significant tethering or mass effect on the spinal cord. Secondly, sheep are relatively docile animals, which are more likely to remain stationary for telemetry monitoring when performed over 10 minute periods. Although the monitoring did not cause significant distress to the animals, slight changes in head posture produced movement artefacts in the pulsation data. For future studies, using telemetry pressure monitoring in a smaller animal model may be a possibility, and permit longer duration of data acquisition. However, the use of a smaller quadruped model would still not be able to replicate the erect posture in humans and its effect on CSF pulsations.

To the best of the author's knowledge, this was the first study to provide in-vivo telemetry monitoring of CSF pressures in the spinal subarachnoid space. Previous studies of CSF pressure monitoring have either been performed on anaesthetised animals or in human patients with intracranial monitoring. Such pressure measurements might be influenced by anaesthetics and do not truly reflect the CSF pressures in an unrestrained animal. Real-time telemetry has been widely used on small and large animals for arterial and respiratory monitoring, and more recently, intracranial CSF pressures have been measured in a live rodent model using blood pressure monitors [501].

CSF pulsations within the spinal subarachnoid space are complex. Intracranial CSF pulsations have been investigated previously, and the ICP waveforms are known to consist of several harmonic components, namely, respiration, arterial and venous

pulsations, and slow waves [377, 379]. It is possible that other factors may also influence subarachnoid CSF pulsations, which have not been identified yet. Physical factors, such as the effect of posture, body movements, normal spinal subarachnoid space volume and compliance, may affect the CSF waveform, as well as pathological conditions, such as arachnoiditis, and spinal cord compression [380, 381].

In the current study, much variability in CSF pulsation waveforms was discovered. Influences from the arterial pulsation and respiration were noted, particularly in the CSF traces at the time of implantation (see Figure 7.4-1). However, in some traces, the arterial influences on the CSF traces were damped, possibly due to the pressure monitor being walled off from the CSF of the subarachnoid space. In addition, both the cranial and caudal CSF systolic peaks seemed to correlate with the T-wave on the ECG trace at the time of implantation. The waveforms also corresponded to respiratory rate. However, as arachnoiditis developed in the animal models over the ensuing week, there was a gradual increase in the delay between the peaks of the cranial and caudal pulsation waves. The cranial pulse more consistently corresponded with the ECG pulse. In the control animals, a pulsation delay between the cranial and caudal pulses could not be detected.

The amplitude of the pulsation wave demonstrated a large amount of variability, which may be due to the effects of posture and head position. No consistent patterns were found across the time periods from implantation to week 6 in both the arachnoiditis and control animals.

There were many limitations to the present study. First, the pressure monitors had gel-filled catheters that were fragile and pre-calibrated. These have been designed to capture larger amplitudes for arterial pressure pulses, rather than CSF pulsations. CSF pressure

changes were much reduced when compared with arterial pulses, and thus, the resolution of CSF pulsations was at the limits of the capability of the pressure monitors.

Other technical challenges included the battery life of the telemeters. Prior to implantation, the batteries for the telemeters were completely charged, but towards the end of the 6 week monitoring period, the quality of telemetry transmission and thus the pressure trace diminished due to the battery level within the telemeter. In fact, none of the recordings lasted the full 6 week period. Despite the capacity for recharging the batteries in-vivo, the telemeters did not perform consistently after recharging in-vivo.

The selection of the peaks and troughs of the CSF pulsation waveforms could not be easily identified. High and low pass filters were used to reduce the signal noise. Fourier transformation and other mathematical methods were applied to the data to discern the peak within each pulse, but due to inconsistency and complexity of the waveforms, regular patterns could not be identified. Another method that could display waveforms with clearer peaks and troughs is cardiac gaiting of the CSF pulsation waveform and averaging of the resultant waveforms. Although this method could be attempted, the ECG trace was not consistent or clear enough in many animals for cardiac gaiting to be applied.

Henry-Feugeas et al. used cine-MRI to analyse the components of spinal CSF pulsation and suggested that propagation of the CSF pulsations may be in different directions depending on the influences from the intracranial or local vascular pulsations, and this itself depended on the dorsal, ventral or lateral location within the subarachnoid space [373]. In the current study, the catheters were placed in the dorsal subarachnoid space, but based on the findings from Henry-Feugeas et al, the results may vary according to the location of the catheters when placed within the subarachnoid space.

Finally, there were inadequate numbers of animals in both the arachnoiditis and control groups used to make definitive conclusions about the pulsation data. More animals in both the arachnoiditis and control groups are required to confirm the presence of pulsation delay observed due to arachnoiditis. It would be of interest also to investigate if the same results would be observed in the post-traumatic syringomyelia model.

The current study is the first report of an in-vivo telemetry system used to record CSF pulsation pressures within the spinal subarachnoid space. In this sheep model of arachnoiditis, there is a suggestion that CSF pulsation delay occurs due to arachnoiditis, and this may contribute to the CSF-arterial pulsation phase difference observed on human MRI studies and in computational modeling. Further studies are required to validate the findings from the current study.

## 7.6 Conclusions

In this study, in-vivo telemetry of CSF pressures within the spinal subarachnoid space was performed on a sheep model of arachnoiditis. The results would suggest that CSF pulsation delays occur as a result of arachoniditis, and may contribute to increased perivascular CSF flow into the spinal cord.

## 7.7 Contributions to the study

This was a collaborative project between IMVS and Macquarie University from 2010 to 2012. The sheep operations were performed by Prof. Nigel Jones, Prof. Marcus Stoodley and Dr Johnny Wong. Animal care was performed by the laboratory staff at IMVS. Dr Stephen Helps, Dr Adam Wells, Dr Claire Jones and Mr Ryan Quarrington assisted in the telemetry recordings of the CSF subarachnoid pressures. Tissue processing of CSF tracers was performed by Dr Wong and Ms Angela Hwang. Data analysis was performed by Dr

Johnny Wong, Dr Shaokoon Cheng, Dr Mark Butlin and Prof. Lynne Bilston. The manuscript was prepared by Dr Johnny Wong.

# Chapter 8 Fluid outflow in large animal model of post-traumatic syringomyelia

This chapter has been published in *Neurosurgery*: Wong, J., Hemley, S., Jones, N., Cheng, S., Bilston, L., Stoodley, M., *Fluid Outflow in a Large Animal Model of Post-traumatic Syringomyelia.* Neurosurgery, 2012. **71**(2): p. 474-80.

## *8.1 Abstract*

**Background**: Post-traumatic syringomyelia affects approximately 28% of spinal cord injury patients and current treatments are often ineffective. The pathogenesis of this condition remains poorly understood. Previous reports have focused on pathways and mechanisms of fluid inflow, however disturbances of fluid outflow mechanisms and pathways may be important in syrinx formation and enlargement.

**Objective**: The objective of the study was to determine the route of fluid outflow from a syrinx in an animal model of post-traumatic syringomyelia.

**Methods**: A model of post-traumatic syringomyelia using excitotoxic amino acid and kaolin-induced arachnoiditis was created in 12 merino wethers. Six weeks after syrinx induction, the cavities were localised and a CSF tracer, (horseradish peroxidase, HRP), was injected into the syrinx under ultrasonic guidance. After 10 minutes, the animals were sacrificed and the spinal cords harvested for microscopy.

**Results**: An extra-canalicular syrinx developed in six of the 12 sheep. HRP was successfully injected into five out of the six syrinx cavities. HRP reaction product was observed in gray and white matter adjacent to the syrinx in a diffuse pattern. There were

moderate amounts of HRP around the central canal and perivascular spaces, and minimal amounts in the dorsal subarachnoid space.

**Conclusion**: In this model of post-traumatic syringomyelia, fluid outflow occurred in a diffuse manner into the surrounding extracellular space and towards the central canal and perivascular spaces. Fluid outflow may be an important consideration in the pathogenesis of syringomyelia and the development of new therapies.

**Keywords / Running title:** Running title: Fluid outflow in syringomyelia;

Keywords: Animal model. Cerebrospinal Fluid. Post-traumatic Myelopathy. Syringomyelia

## 8.2 Introduction

Post-traumatic syringomyelia is diagnosed in up to 28% of patients following a spinal cord injury [2, 29, 30, 34, 204]. The natural history of the disease is variable, with approximately 1 – 9% of spinal cord injury patients becoming symptomatic. In 32 – 40% of patients with post-traumatic syringomyelia, the clinical course will remain stable. In 33 – 43% of cases, the syrinx will slowly progress and, in 21 – 27% of cases, rapid deterioration occurs [2, 31, 40-42]. The symptoms of syringomyelia may present from 3 months to 34 years following the initial spinal cord injury [31, 201]. Treatment for this condition still presents a significant challenge with failure rates as high as 50% in many surgical series [34, 37, 38, 115, 126, 190, 480, 503]. More effective therapy for post-traumatic syringomyelia is unlikely until there is a better understanding of the underlying mechanisms of syrinx formation and enlargement.

The pathogenesis of syringomyelia is not completely understood. Most theories have focused on syringomyelia occurring in association with Chiari malformations, in which the syrinx cavity is located within the central canal [100, 147, 159, 161, 163, 164, 174, 248]. Post-traumatic syringomyelia generally occurs in the spinal cord parenchyma outside the central canal and presumably has a different aetiology [23, 176].

At a fundamental level, syrinx size must be a function of fluid inflow, fluid outflow, and the surrounding tissue properties. Previous studies have demonstrated cerebrospinal fluid (CSF) flow into syrinx cavities via perivascular spaces in canalicular and extra-canalicular models of syringomyelia [169, 204]. Since there is fluid flow into a syrinx cavity during periods of clinical stability, there must be equilibrium between fluid influx and efflux [2]. In the situation with an expanding syrinx, the fluid influx must exceed the fluid efflux.

Little is currently known about the routes of fluid efflux from syrinxes. The objective of this study was to study fluid outflow pathways in a sheep model of extra-canalicular syringomyelia.

## *8.3 Materials and methods*

Following ethics approval from the Animal Ethics Committees at University of Adelaide and Institute of Medical and Veterinary Sciences, Adelaide, 12 merino wethers weighing 38 – 50 kg underwent syrinx induction surgery with the intention of studying fluid outflow at 6 weeks. Four animals developed significant early hindlimb paralysis after the syrinx induction and were humanely killed as per the animal ethics protocol. These animals were excluded from further analysis. Fluid tracer injection studies were performed at 6 weeks after syrinx induction in the remaining eight animals.

### 8.3.1 Syrinx induction

The use of a combination of excitotoxic amino acid injection into the spinal cord parenchyma and kaolin in the subarachnoid space to model extracanalicular syringomyelia has previously been described in detail in the rodent model [195, 204]. A similar technique was used in Merino sheep for this experiment. All procedures were performed in a sterile field under general anaesthetic. Anaesthesia was induced with 1 g thiopental intravenously and maintained with 2.5 – 3% isoflurane via an endotracheal tube and mechanical ventilation. The sheep were positioned prone and the T2 – T4 spinous processes and laminae were exposed via a midline subperiosteal approach. Laminectomies at T2 and T3 were performed. The dura was opened via two right paramedian incisions, each measuring approximately 5 mm in length. A 10 μL microsyringe (SGE International Pty Ltd, Ringwood, Victoria, Australia) with a beveled

needle (0.19 mm outer diameter) was used to deliver four 5 μL intraparenchymal injections of 24 mg/mL quisqualic acid and 1% Evans Blue solution along the right dorsal root entry zones at a depth of 3 mm from the pial surface. Each injection was performed over 30 seconds with the needle held in situ for another 30 seconds to minimise leakage.

To produce arachnoiditis, 0.5 mL of 250 mg/mL kaolin solution was mixed with the thrombin component of a two-component fibrin sealant (Tisseel Duo 500, Baxter Healthcare Pty Ltd, Old Toongabbie, New South Wales, Australia) and drawn up into the double-barrelled applicator. The kaolin and fibrin mixture was slowly injected into the subarachnoid space on both sides of the dural incisions to a total of 0.2 mL per sheep. The wound was closed in layers with Vicryl sutures. The sheep were allowed to recover with analgesic and antibiotic coverage, and free access to food. They were monitored for neurologic deficits, excessive weight loss and signs of distress.

### 8.3.2 Injection of fluid tracer into syrinx cavity and perfusion/fixation

After 6 weeks, the animals were re-anesthetised and positioned supine. The common carotid arteries and jugular veins were dissected out in preparation for perfusion/fixation, as previously described by Santoreneos et al. [452]. The sheep were then repositioned prone and the previous laminectomy wound was reopened. Epidural scarring over the previous injection site was carefully removed ensuring that the dura remained intact. A portable ultrasound machine (Sonosite Micro Maxx$^{TM}$, Sonosite Inc., Washington, USA) was used to visualise the dura, subarachnoid space, spinal cord and cystic cavities within the spinal cord (Figure 8.3-1). Under ultrasound guidance, 10 μL 3% Horseradish Peroxidase (Invitrogen, Carlshad, California, USA) was injected into the cystic cavity over 5 minutes, using a hand-held 10 μL microsyringe with a bevelled needle (SGE International Pty Ltd).

At the completion of the experiment, the animals were repositioned for rapid intravascular aldehyde perfusion 10 minutes after the HRP injection [452]. Heparin 5000 IU was injected intravenously and the common carotid arteries were cannulated to allow influx of fixative. The fixative was directed proximally in the left common carotid artery and distally in the right common carotid artery. The internal jugular veins were divided on each side. Each animal was perfused with 10 L of 4% paraformaldehyde (Lancaster Synthesis Ltd, Morecambe, United Kingdom) in 0.1 M phosphate buffered saline (pH 7.4).

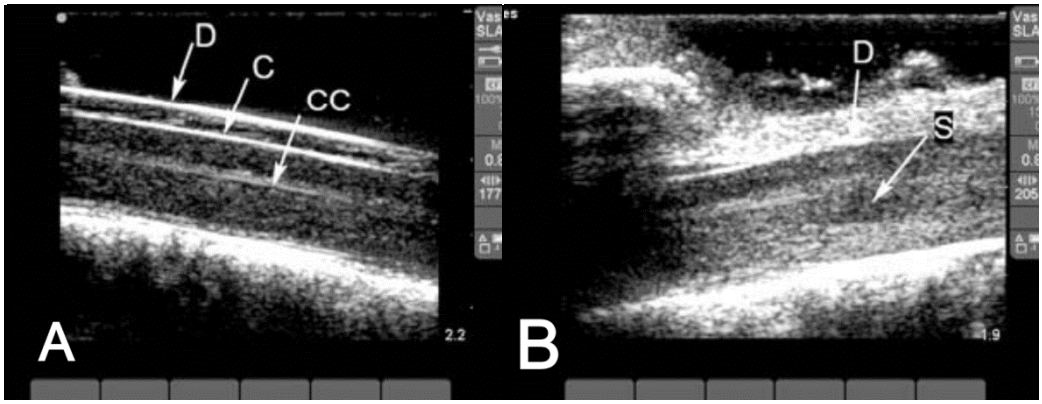


**Figure 8.3-1 Intraoperative longitudinal ultrasound images of the spinal cord.**
**(A) Normal sheep; (B) sheep with a post-traumatic syrinx. C, spinal cord; CC, central canal; D, dura; S, syrinx.**

### 8.3.3 Tissue processing

The thoracic spinal cord was dissected out of the spinal canal and post-fixed in 4% paraformaldehyde solution overnight. The dura and arachnoid were removed prior to sectioning. Transverse sections of 50 μm thickness from T2 to T4 spinal cord levels were produced with a vibratome and floated on a bath containing Tris Buffer (pH = 7.6). The sections were mounted on 3-amino propyl-triethoxy-silane (APT) coated glass slides and allowed to air dry for at least 4 hours.

Histological localisation of HRP was carried out using tetramethylbenzidine (TMB) as the chromogen. The sections were soaked in distilled water for 15 seconds, and then incubated in 0.01 M sodium acetate buffer (pH 3.3) containing 0.005% 3,3',4,4' TMB (Lancaster Synthesis Ltd) and 0.1% sodium nitroferricyanide (III) dehydrate (Lancaster Synthesis Ltd). The sections were incubated for a further 20 min following the addition of 30 μL of hydrogen peroxide to a final concentration of 0.01%. After washing in sodium acetate buffer (pH 3.3), the reaction product was stabilised in 5% ammonium molybdate (IV) tetrahydrate (Sigma-Aldrich, MO US) in 0.01 M sodium acetate buffer. Finally, the slides were washed in sodium acetate buffer for 30 seconds, dehydrated in graded ethanol, xylene and then coverslipped with DPX mounting medium (Scharlau Chemie SA, Barcelona, Spain).

### 8.3.4 Image acquisition

The sections were studied using light microscopy with a Zeiss Axio Imager Z1 microscope (Carl Zeiss Microimaging GmbH, Berlin, Germany). Photographs of the HRP reaction product were taken using the Axiovision program Release 4.8.1 (Carl Zeiss Microimaging GmbH) at x25 and x100 magnification.

## *8.4 Results*

A hypoechoic region within the spinal cord suggestive of an extra-canalicular syrinx cavity was detectable on intraoperative ultrasound in all animals. Histological examination revealed that a syrinx cavity was present in six of eight animals. In one of these, HRP was noted to have been injected into the cord parenchyma adjacent to the syrinx cavity, and this animal was excluded from further analysis. HRP was successfully injected into the syrinx cavity in the remaining five animals. The syrinx cavities varied

from 2 to 4 cm in length and from 1.5 to 3 cm in maximum diameter. The cavities were located mainly in the right dorsal horn.

At the level of the maximal diameter of the syrinx, dense HRP-TMB reaction product was observed in the gray and white matter immediately adjacent to the syrinx cavity, in the ependymal lining of the central canal and around blood vessels (Figure 8.4-1 A, C and D). The pattern of HRP distribution was different in the gray and white matter. In the gray matter, there was a diffuse spread of HRP towards the central canal. The appearance in the white matter was more variable. In three animals, HRP was visualised in a fibrillary pattern around white matter fibre bundles (Figure 8.4-1 B), however, in two animals, no specific pathways could be identified (Figure 8.4-1 E). There was less reaction product in the contralateral dorsal horn and peripheral regions of white matter towards the dorsal subarachnoid space (Figure 8.4-1 A). Minimal amounts of reaction product were observed at the cranial and caudal extents of the syrinx cavities.

In the animal in which HRP was not successfully injected into the syrinx cavities but into the spinal cord parenchyma, reaction product was observed diffusing through the spinal cord parenchyma away from the injection site towards the central canal (Figure 8.4-2 A & B). No specific pathways were identified.

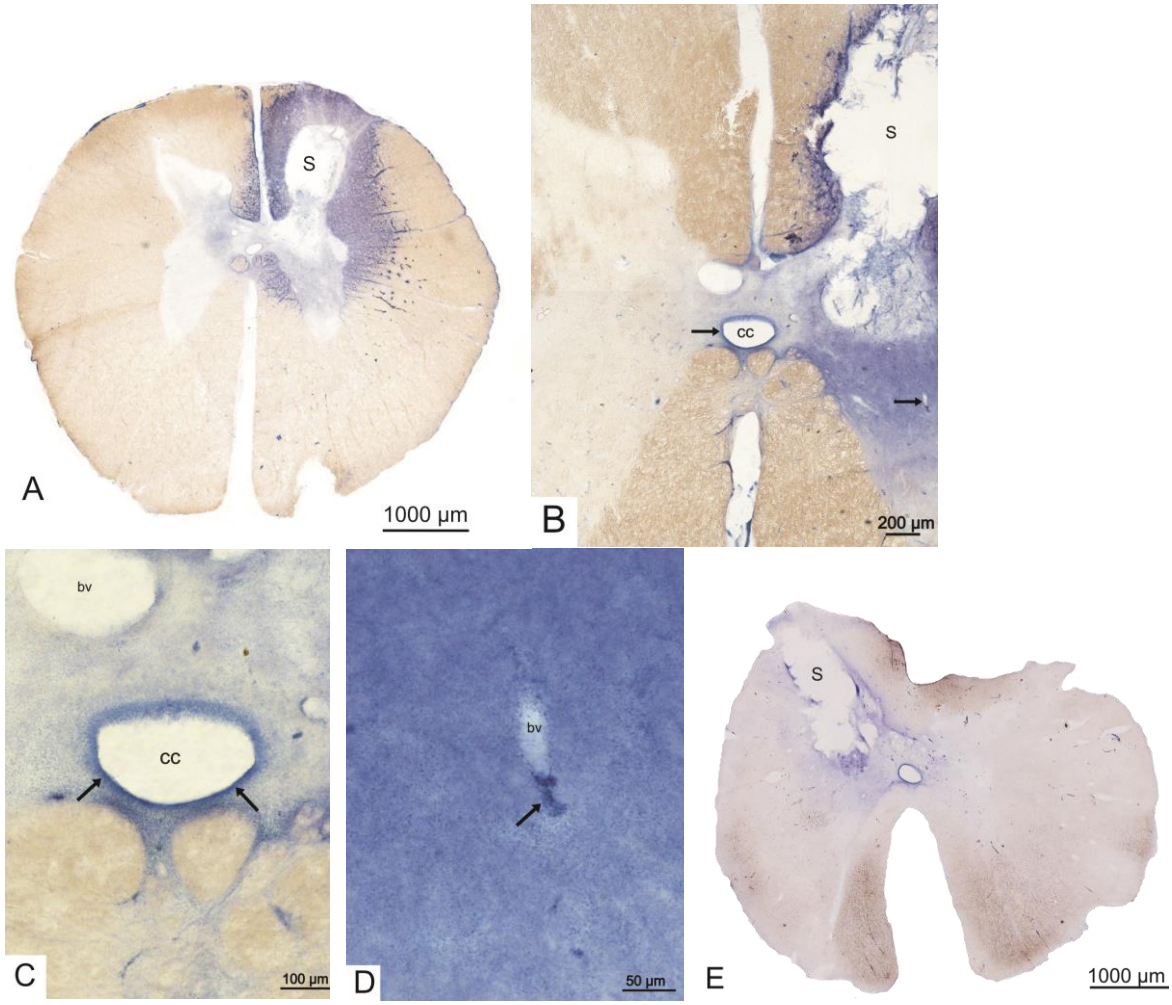


**Figure 8.4-1 Histological section of a sheep spinal cord with post-traumatic syrinx**

**(A) Syrinx (S) present in the grey matter at low magnification. (B) Low-magnification image in a syrinx animal demonstrating the fibrillary pattern around white matter fibre bundles. (C) High-magnification image of area in (B) indicated by arrows demonstrating the flow of HRP from the syrinx into the grey matter and around central canal (cc). (D) High-magnification image of area in (B) demonstrating an accumulation of HRP around blood vessels (bv). (E) Low-magnification image in a syrinx animal without the fibrillary pattern in the white matter.**

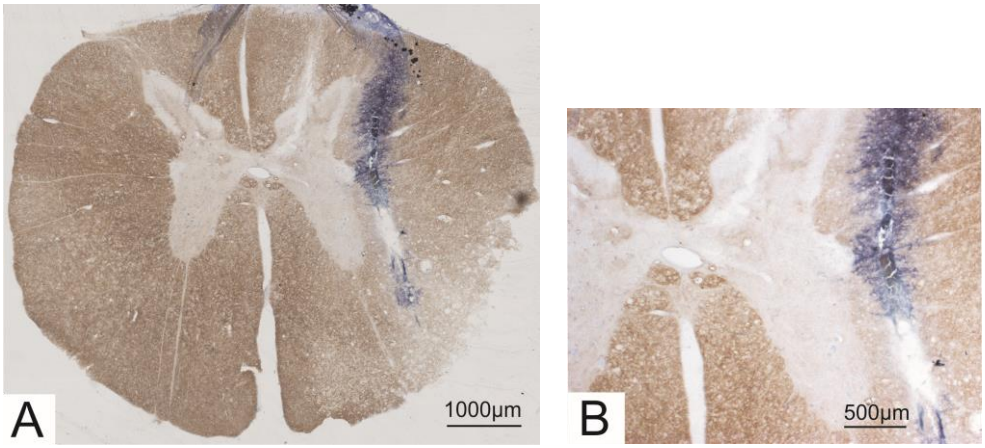


**Figure 8.4-2 Histological section of spinal cord with no syrinx.**

**(A) Histological section of a sheep spinal cord at low magnification in which a syrinx cavity did not develop. Horseradish peroxidase (HRP) was injected into the spinal cord parenchyma, and HRP reaction product can be seen in the surrounding white and grey matter and central canal. (B) High magnification in the grey matter and white matter adjacent to the injection site.**

## *8.5 Discussion*

Across the world, spinal cord injuries occur with an annual incidence of 15 – 40 cases per million with aetiologies including motor vehicle accidents, assault, recreational activities and work-related injuries [504]. Of these patients, a significant proportion will subsequently develop post-traumatic syringomyelia. The condition may be asymptomatic or result in neuropathic pain, weakness, numbness, or even death [43-46]. The natural history of syringomyelia is unpredictable, and is marked by periods of clinical stability and subsequent deterioration. Progressive enlargement of the syrinx cavity can occur many years after the initial spinal cord injury. Treatment of post-traumatic syringomyelia has often been difficult. The main treatment options, spinal cord untethering by arachnolysis and direct syrinx shunting, have both been associated with favorable short-term results, but high long-term failure rates [29]. The pathogenesis of syringomyelia still remains enigmatic. Improvements in treatment are unlikely to be achieved until there is a better understanding of the underlying mechanisms for syrinx initiation and expansion.

Much attention has been paid to syrinx fluid inflow, which has been presumed to originate largely from CSF in the subarachnoid space. Myelographic studies in humans have demonstrated that CSF flows into syrinx cavities [41, 43, 505]. In animal models of canalicular and extracanalicular syringomyelia using CSF tracers injected into the cisterna magna, fluid has been shown to flow from the subarachnoid space into the syrinx cavity and central canal via perivascular spaces [169, 204]. This flow was also shown to be dependent on arterial pulsations and is enhanced in the region of the syrinx despite evidence of the syrinx fluid being under high internal pressure [168, 204, 248, 328].

Explanations for the mechanism by which CSF enters the syrinx cavity from the subarachnoid space remain contentious. Earlier theories of the pathogenesis of syringomyelia have mainly involved hydrodynamic explanations for the occurrence of canalicular syringomyelia in association with abnormalities at the craniocervical junction [147, 159, 161, 163, 164, 174]. These do not adequately explain the pathogenesis of post-traumatic syringomyelia, where the craniocervical junction is usually normal and the syrinx cavities are extracanalicular. Williams [147] postulated that increased CSF pulsations from the subarachnoid space might be transmitted towards the syrinx cavity, which cause a "sloshing" phenomenon, leading to dissection of the spinal cord parenchyma and subsequent syrinx expansion. Bilston et al. [171] postulated that decoupling of CSF-arterial pulsations in the subarachnoid space as a result of arachnoiditis might enhance CSF flow through the perivascular spaces and then into syrinxes.

More recently, even the origin of syrinx fluid has been debated, with speculation that syrinx fluid may be derived at least in part from an accumulation of extracellular fluid generated from the spinal microcirculation [1, 138, 176]. Klekamp [1] proposed that

syrinx formation might be due to an accumulation of extracellular fluid in the spinal cord. This could potentially occur due to an inability to remove extracellular fluid because of a blockage of CSF pathways; or, extracellular fluid volume exceeding interstitial space capacity. This could occur as a result of blockage of perivascular spaces, cord tethering or changes in arterial and venous blood flow. Greitz [176] postulated that disturbances of the microcirculation might cause an imbalance between extracellular fluid filtration and absorption, leading to spinal cord edema and subsequent syrinx formation. Spinal cord edema and the syrinx cavity would then increase interstitial pressure, compress the venules and increase venous resistance, which would promote further transcapillary fluid filtration. This theory implies that there is a dynamic balance of extracellular fluid flow between the spinal cord vasculature, the interstitial spaces and, possibly, the syrinx cavity.

To date, there has been very little consideration of fluid flow out of syrinxes. Basic physics requires that syrinx enlargement occurs when fluid inflow exceeds outflow. Because the evidence from animal studies suggests that fluid inflow appears to be a continuous process, there must be equilibrium between fluid inflow and outflow during periods of syrinx stability. Brodbelt et al [204] suggested that fluid flow out of a syrinx may occur via a transparenchymal route. To the best of our knowledge, there have been no previous experimental studies of fluid outflow.

Although computational modelling is used to study many aspects of syrinx pathophysiology, it was not feasible to use such techniques for this study. To confirm the presence and direction of fluid outflow, direct manipulation of the syrinx is required and this is possible only in a large animal model. Therefore, to study syrinx fluid outflow, a large animal model was developed.

The excitotoxic amino acid and arachnoiditis model of post-traumatic syringomyelia has been well-described previously in rodents [195, 311, 321]. This model mimics the excitotoxic component of spinal cord injury and produces an extracanalicular syrinx in 82% of animals [321]. This is consistent with the Milhorat [23] classification of syringomyelia, which was based on histopathological findings, including the observation that post-traumatic syringomyelia was characterised by extracanalicular cavities. Other animal models, including the weight-drop and arachnoiditis model of post-traumatic syringomyelia in rats and rabbits have produced lower rates of syrinx formation and high rates of paraplegia [191, 321, 326]. Although the rodent excitotoxic acid and arachnoiditis model has been used previously to investigate fluid flow in the spinal cord parenchyma via perivascular spaces, that model was too small for precise tracer injections into the syrinx [204]. The sheep spinal cord is comparable in size to the human spinal cord, and is large enough to permit localisation of the syrinx cavity via ultrasonography, and injection of fluid tracers under direct guidance.

To the best of our knowledge, this is the first published report of an ovine model of post-traumatic syringomyelia. The syrinx formation rate was 50% in the present study (75% of surviving animals), and histological sections resembled those of the human post-traumatic syringomyelia [97]. The cavities were separate from the central canal and had irregular edges lined by gliotic tissue or cellular debris. The tissue surrounding the main cavity had enlarged perivascular spaces and smaller cystic cavities. The procedure described was technically difficult and the 4 cases associated with significant early hind-limb weakness occurred during our initial experience with this technique. It is hoped that the ovine model will be useful for other investigations into post-traumatic syringomyelia, particularly those involving pressure measurement and surgical interventions.

In this study, the CSF tracer HRP was injected into the syrinx cavity with a microsyringe to determine the presence and route of fluid outflow. HRP has a number of properties that make it suitable for investigations of syrinx fluid flow, and it has been used in previous studies of CSF flow in animal models of syringomyelia [167, 169, 328]. Its molecular weight (44,000 Da) is ideal for assessing bulk flow of CSF, rather than simple diffusion, and it can be rapidly anchored in-situ by perfusion-fixation. HRP can also be sensitively labelled with TMB. The introduction of a CSF tracer might disturb fluid flow by increasing the pressure within the syrinx or by the needle track providing an additional outflow pathway. A small-gauge needle and the low volume and slow rate of injection have been used to minimise the effect of any artefactual disturbances to fluid flow. However, it should be noted that the total fluid injected in the cavity was up to one-third of the total syrinx volume over a 5-minute injection period; thus, the outflow route may have been abnormally altered by an increase in internal syrinx pressure.

The pattern of HRP distribution in this extracanalicular syrinx model suggests the tracer is carried by bulk fluid flow into the adjacent gray and white matter. There was no consistent pattern of preferential flow via specific pathways or in particular directions, although there was more staining in the gray matter than in adjacent white matter regions (Figure 8.4-1 A). This might reflect higher diffusivity of water in the radial direction in gray matter compared to white matter, as has been observed in diffusion tensor imaging in vivo.[506] There was a concentration of HRP reaction product around the central canal and perivascular spaces. This suggests that there is bidirectional flow from the syrinx to the perivascular spaces, which are known to be a key fluid inflow pathway. Furthermore, it suggests that obstruction in the extracellular space or further downstream in the outflow pathway may lead to an accumulation of fluid (and edema), as suggested by Klekamp et al.[1] Glial scar formation and mechanical loading, which may obstruct or compress the

extracellular space could also reduce outflow by increasing resistance to fluid transport through the extracellular spaces. Also, fluid accumulation within the extracellular space may subsequently coalesce, which could explain the development of multi-loculated syrinxes over time.

This study has demonstrated that a high volume of HRP reaction product accumulated in the surrounding spinal parenchyma within the short period of time between the microinjection and perfusion-fixation. These findings confirm what has been observed from intraoperative ultrasonography and recent cine- and cardiac-gated balanced fast-field echo sequences on 3-T MRI: that spinal cord pulsation and CSF and syrinx fluid movements are highly dynamic processes [56]. In addition, syrinx cavities have been observed to collapse within minutes during arachnolysis and spinal cord untethering procedures. In such instances, the alteration in the balance between fluid inflow and outflow has resulted in a dramatic and often rapid reduction in the size of syrinx cavities.

The present study, in agreement with previous studies on fluid flow, suggests that syrinx fluid inflow and outflow occur as bulk flow, rather than simple diffusion. The rapid interaction between fluid influx and efflux suggests that specific fluid channels may be involved. Recently, there have been increasing interests in the role of aquaporins and intracellular fluid movement throughout the body, and it may be that these water channel membrane proteins are involved in fluid movement into and out of syrinx cavities [386, 404, 419, 424].

Much is still unknown about the nature of syrinx fluid outflow. The rate of fluid inflow vs outflow, the mechanism by which outflow occurs and where the extracellular fluid travels from the surrounding parenchyma have not yet been elucidated. Factors influencing outflow might include venous and cord tissure pressures, levels of aquaporin expression,

and blood-spinal cord barrier integrity. Although in this study there was a suggestion of increased flow towards the central canal, perivascular spaces and subarachnoid space in the present study, it remains to be determined whether the majority of fluid can move across the glia limitans interna and into the central canal.

## *8.6 Conclusions*

Although most studies have focused on fluid inflow, this is the first study to confirm the presence of fluid outflow pathways in syringomyelia. This study has demonstrated that fluid outflow occurs in a diffuse manner into the extracellular space surrounding the syrinx cavity and then preferentially towards the central canal and the perivascular spaces. It is also the first description of an excitotoxic acid and arachnoiditis model of post-traumatic syringomyelia in sheep, which may be a useful model for future investigations that require a large-animal model.

## *8.7 Contributions to the study*

This was a collaborative project between the University of Adelaide, IMVS, University of NSW and Macquarie University from 2006 to 2010. The senior authors, Prof. Nigel Jones and Prof. Marcus Stoodley performed the majority of the sheep operations for syrinx induction and injection of CSF tracers. The last two sheep used in the project were operated on by Prof. Stoodley and Dr Johnny Wong. Tissue processing, data analysis and preparation of figures were performed by Drs Johnny Wong and Sarah Hemley. The manuscript was prepared by Dr Johnny Wong, and edited by the other authors on the paper.

# Chapter 9 Aquaporin-4 and Aquaporin-1 expression in spinal cord injury and post-traumatic syringomyelia

## *9.1 Abstract*

**Background**: The pathophysiology of spinal cord injury and post-traumatic syringomyelia is inadequately understood. They are both associated with spinal cord oedema, which may be mediated by specialised water channels, known as aquaporins. Aquaporin-4 (AQP4) and aquaporin-1 (AQP1) have been investigated in spinal cord injury. Previous studies investigating the expression of AQP4 in animal models of spinal cord injury have produced conflicting results. However, in an excitotoxic model of post-traumatic syringomyelia, AQP4 expression was up regulated.

**Objective**: The objective of the study was to investigate the expression of AQP4 and AQP1 in a rodent contusional model of spinal cord injury and an impact model of post-traumatic syringomyelia.

**Methods**: Fifty-three Sprague-Dawley rats were used in this study. The animals were allocated to three groups: Spinal cord injury (SCI), post-traumatic syringomyelia (PTS) and control, which received a laminectomy only. A contusional spinal cord injury with a computerised impactor was induced at C8 in 24 animals in the SCI group. In the PTS group, additional subarachnoid kaolin was injected in 24 animals. After perfusion-fixation and tissue processing, AQP4 expression was localised using immunohistochemistry using a dual labelling technique with GFAP. The results were analysed using qualitative and quantitative methods. A triple labelling technique with AQP4, AQP1 and GFAP was

attempted but was abandoned due to technical difficulties. AQP1 expression was therefore not assessed.

**Results**: There were no notable differences observed between the SCI and PTS groups at all time points. On qualitative assessment, there was a decrease in AQP4, but an increase in GFAP expression at 1 week around the site of spinal cord injury. However, there was a gradual increase in AQP4 expression from 3 weeks to 6 weeks, which was maintained at 12 weeks. On quantitative assessment, control groups generally had higher AQP4/GFAP ratio. Both the SCI and PTS groups showed similar results, with a gradual increase in AQP4/GFAP expression from week 3 – 6, but a decrease at the 12 week timepoint.

**Conclusion**: Although reactive astrocytic migration occurs during the acute stages of spinal cord injury, AQP4 expression is initially decreased. At later stages of spinal cord injury and post-traumatic syringomyelia development, AQP4 expression is increased and remains elevated up to 12 weeks post initial trauma.

**Keywords / Running title:** Running title: Aquaporin-4 expression in a rodent model of spinal cord injury and post-traumatic syringomyelia; Keywords: Aquaporins, impactor, spinal cord injury models, post-traumatic myelopathy, syringomyelia

## 9.2 Introduction

Approximately 15 – 40 patients per million people world-wide are affected by traumatic spinal cord injury per year.[504, 507, 508] Commonly, it is caused by motor vehicle accidents, recreational activities, assaults and work-related injuries [63, 504]. It is a devastating condition that causes a significant burden of disease to society across the world. Previously regarded as a rare complication of spinal cord injury, post-traumatic syringomyelia is diagnosed in 21 – 28% of patients following a spinal cord injury [2, 321]. In both conditions, treatments have been generally ineffective. In spinal cord injury, the rationale for treatment has mainly been supportive that aim to limit secondary insult to the spinal cord, prevent associated complications from immobility and rehabilitation. In post-traumatic syringomyelia, operative interventions have been the main modality of treatment. However, most surgical series have reported high rates of recurrence [37, 38, 190, 480]. A better understanding of the pathophysiology in both conditions is required for the development of novel treatments.

Spinal cord oedema is a common association with spinal cord injury and syrinx formation, but the mechanism for spinal cord oedema is at present incompletely understood [419, 424]. Recently, there has been much interest in aquaporins, which are protein channels specialized for water transport, and have been implicated to play a contributory role in many conditions, including spinal cord oedema [388, 391, 410, 419, 420, 424]. Aquaporin-4 (AQP4) and aquaporin-1 (AQP1) have been investigated in the setting of spinal cord injury in murine and rodent models [420, 424]. Similarly, AQP4 has been investigated recently in syringomyelia [232, 426, 427]. However, there have been conflicting results regarding the expression of AQP4 after spinal cord injury in different animal studies. The objective of this study was to investigate the expression of AQP4 and

AQP1 in a contusional spinal cord injury model and an impact model of post-traumatic syringomyelia, and to determine whether there was an association between AQP4, AQP1 and these conditions.

## *9.3 Materials and methods*

Ethical approval was obtained from the Macquarie University Animal Ethics Committee prior to the commencement of this project. In total, 53 male Sprague-Dawley rats weighing 464 ± 64 g were used. The animals were divided into 3 groups: spinal cord injury, post-traumatic syringomyelia and control, and were studied at 1- , 3- , 6- and 12-weeks following the initial operation. At each time point, 6 animals were allocated to the spinal cord injury group, 6 animals were allocated to the post-traumatic syrinx group and 1 animal was in the control group (Table 9.3-1). One animal died in the immediate post-operative period from anaesthetic complications and was excluded from the rest of the study.

**Table 9.3-1 Allocation of animals in the AQP expression study.**

| **Experimental group** | **Procedure** | **Time points** | | | |
|---|---|---|---|---|---|
| | | 1 week | 3 weeks | 6 weeks | 12 weeks |
| Control | Laminectomy only | 1 | 1 | 1 | 1 |
| Spinal cord injury | Laminectomy + Impact | 6 | 6 | 6 | 6 |
| Post-traumatic syringomyelia | Laminectomy + Impact + Kaolin | 6 | 6 | 6 | 6 |

### 9.3.1 Operative procedure

Under general anaesthetic, all procedures were performed with strict aseptic technique. Isoflurane at 4% was used for induction of anaesthetic and was subsequently reduced to 2 – 2.5% for maintenance of anaesthesia via a nose cone. The rats were positioned prone on the operating stage, and the operation site was prepared with povidone-iodine after skin shaving. Under magnification with the operating microscope, the C6 – T2 spinous processes, laminae and lateral masses were exposed via a midline incision. A C7 – T1 laminectomy was performed with bony rongeurs in all animals. The control group of animals had a laminectomy only, and a spinal cord impact was not performed.

In the spinal cord injury and post-traumatic syringomyelia groups, the Infinite-Horizon spinal cord impactor (Precision Systems and Instrumentation, LLC, US) was used to induce a mild contusional spinal cord injury after the completion of the laminectomy. Stabilizing clamps were attached to the lateral masses of C6 and transverse processes of T2. The operating stage was then positioned such that the impactor tip was aligned over the midline of the spinal cord at the C8 level. A programmed force of 75 kDyn with a dwell time of less than 0.1 sec was delivered using the computer software provided (IH Spinal Cord Impactor v.5.0.4, Precision Systems and Instrumentation, LLC, US).

In the post-traumatic syringomyelia group, additional arachnoiditis was induced following the spinal cord impact. This was performed by measuring out 10 μL of 250 mg/mL kaolin (Sigma-Aldrich) in 0.9% saline solution with a micropipette and slowly injecting the solution into the subarachnoid space via 0.5mL 30G insulin syringe (Ultra-Fine II, Beckton Dickinson and Co, NE, US).

At the completion of the operation, a layered closure was performed with resorbable sutures to fascia and skin. The animals were allowed to recover with analgesia and antibiotic coverage as required and access to food ad libitum. They were monitored for neurologic deficits, excessive weight loss and signs of distress.

### 9.3.2 Perfusion-fixation and tissue processing

At the completion of the experiment, the animals were anaesthetised with 4% isoflurane. Heparin 5000 IU was injected via an intracardiac injection and the left ventricle was cannulated to allow influx of fixative. The right atrium was incised to permit efflux of blood and fixative. Each animal was perfused with 400 mL of 4% paraformaldehyde (Lancaster Synthesis Ltd, UK) in 0.1 M phosphate buffered saline (pH 7.4).

The brain and spinal cord were dissected out and post-fixed in 4% paraformaldehyde solution overnight. The spinal cord was divided into individual specimens according to the spinal cord level from C2 to T4. The specimens were processed in paraffin over a 4-hour cycle in an automated tissue processor (Leica ASP200S, Leica) and then embedded in paraffin wax blocks. Transverse sections of 5 μm thickness were produced with a microtome and were mounted on glass slides. The slides were allowed to air dry for at least 4 hours prior to antigen retrieval processing and immunofluorescent staining.

### 9.3.3 Immunohistochemical staining

#### Triple-labelling with AQP4, AQP1 and GFAP

An initial optimisation study was performed to co-localise AQP4, AQP1 and GFAP with a triple labelling technique. Sections from animals in each group at the 6 week time point (SCI, PTS and control) were used. Deparaffinisation and rehydration with xylene and

gradient ethanol washes were performed prior to antigen retrieval with 0.1M citrate buffer (pH 6.0) at $95^0$C for 20 minutes. The slides were blocked with 10% normal donkey serum and incubated first with primary anti-Aquaporin 4 (1:50 dilution, SC-20812, Rabbit Polyclonal IgG, 0.2mg/ml, Santa Cruz, CA, US) overnight and then with secondary donkey anti-rabbit Alex Fluor 594 (1:400 dilution, A21207, Invitrogen Life Technologies, NY, US). Anti-AQP1 (1:10, SC-34009, goat polyclonal, Santa Cruz, CA, US) and anti-GFAP (1:800, MAB360, Mouse IgG1 mAb, 1mg/ml, Chemicon Millipore, CA, US) were applied for 2 hours, and secondary antibodies were subsequently applied with Donkey anti-goat Dylight 488(1:400, ab96875, Abcam, MA, US) and Donkey anti-mouse Dylight 649 (1:400, 715-495-140, Jackson Immunoresearch Laboratories, PA, US). The sections were finally incubated in DAPI (1 μg/mL) for 1 minute, coverslipped with fluorescent mounting medium (DAKO, S3023, Carpinteria, CA, US).

## Dual-labelling with AQP4 and GFAP

After deparaffinisation and rehydration with xylene and gradient ethanol washes, antigen retrieval was performed with 0.1M citrate buffer (pH 6.0) at $95^0$C for 20 minutes. The sections were cooled to room temperature and were blocked with 10% normal donkey serum. Primary antibodies were applied with anti-Aquaporin 4 (1:50 dilution, SC-20812, Rabbit Polyclonal IgG, 0.2mg/ml, Santa Cruz, CA, US) and anti-GFAP (1:800, MAB360, Mouse IgG1 mAb, 1mg/ml, Chemicon Millipore, CA, US) and incubated in a humidifier at $37^0$C for 2 hours. This was followed by incubation with secondary antibodies, Donkey anti-rabbit IgG-Alexa Fluor 594 (1:400, A21207, Invitrogen Life Technologies, NY, US) and Donkey anti-mouse IgG-Dylight 649 (1:400, 715-495-140, Jackson Immunoresearch Laboratories, PA, US) for 1 hour. The sections were finally incubated in DAPI (1 μg/mL)

for 1 minute, coverslipped with fluorescent mounting medium (DAKO, S3023, Carpinteria, CA, US) and allowed to cure for 24 hours at room temperature.

### 9.3.4 Image acquisition and processing

The sections were studied using fluorescent microscopy with a Zeiss Axio Imager Z2 microscope (Carl Zeiss Microimaging GmbH, Germany). Photographs of the immunohistochemistry sections were taken using the Axiovision program (Release 4.8.1, Carl Zeiss Microimaging GmbH, Germany) at × 200 magnification. For triple labelling, fluorescent images with exposure times of 300 ms for AlexaFluor 594 and 1500 ms for both Dylight 488 and 649.

For dual labelling, fluorescent images were obtained with exposure times of 300 ms for AlexaFluor 594, reflecting AQP4 expression and 1500 ms for DyLight 649, reflecting GFAP expression. The sections were analysed using both qualitative and quantitative methods. Qualitative comparisons were made between the regions immediately around the cavity with regions of the spinal cord unaffected by the spinal cord impact. Comparisons were made between spinal levels of the same animal, the time points and the experimental group. Signal integrated density was quantified using the Image-J software, the steps of which are demonstrated in Figure 9.3-1. Measurements of the integrated density of the perimeter around the cavity were obtained by first outlining a 400 pixel margin by using the “selection brush” function to obtain an overall average (Figure 9.3-1 A). In addition, separate circular areas of 400 pixel diameter in size representing normal grey and white matter were compared with the adjacent areas of the cavity perimeter within the same section. The representative regions were the dorsal and ventral horns, dorsal columns and ventral tracts. In sections without a cavity, only measurements of the integrated density of the representative normal grey and water

matter were made (Figure 9.3-1 B). Secondly, the threshold settings were applied at minimum of 20 and maximum of 254 for both GFAP and AQP4 (Figure 9.3-1 C). The integrated density of AQP4 and GFAP were determined by using the "Analyze – Set measurements" and "Analyze – Measure" functions (Figure 9.3-1 D). Finally, the integrated signal intensity of AQP4 was compared to the GFAP expression by converting the intensity as an AQP4:GFAP signal intensity ratio.

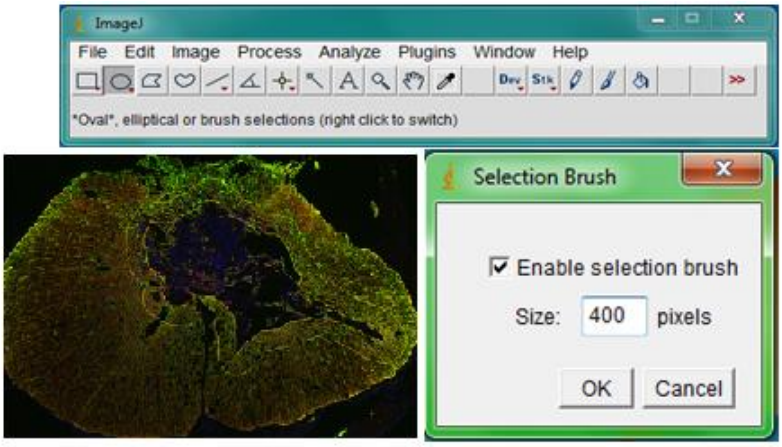


Figure 9.3-1 A

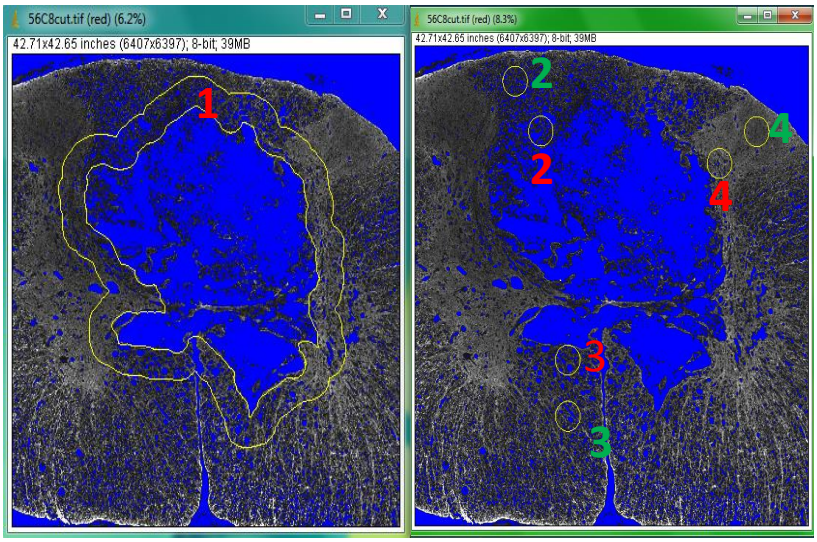


Figure 9.3-1 B

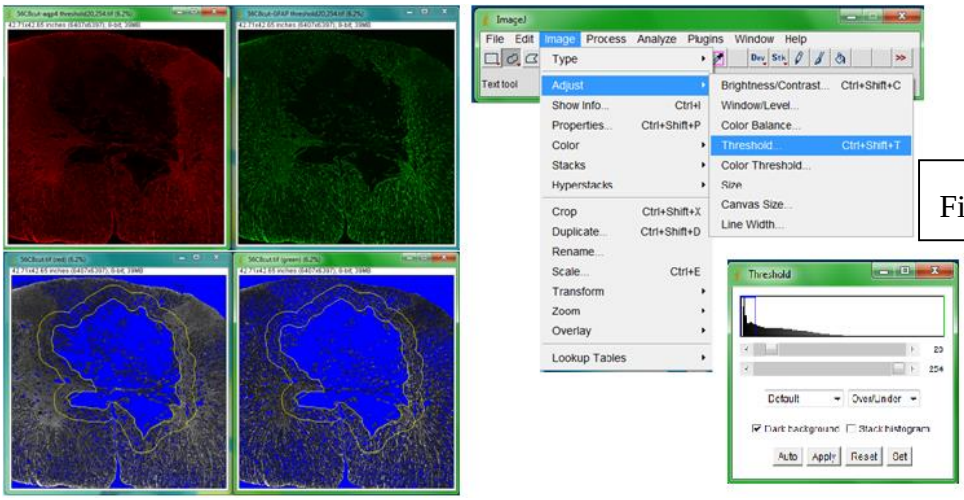


Figure 9.3-1 C

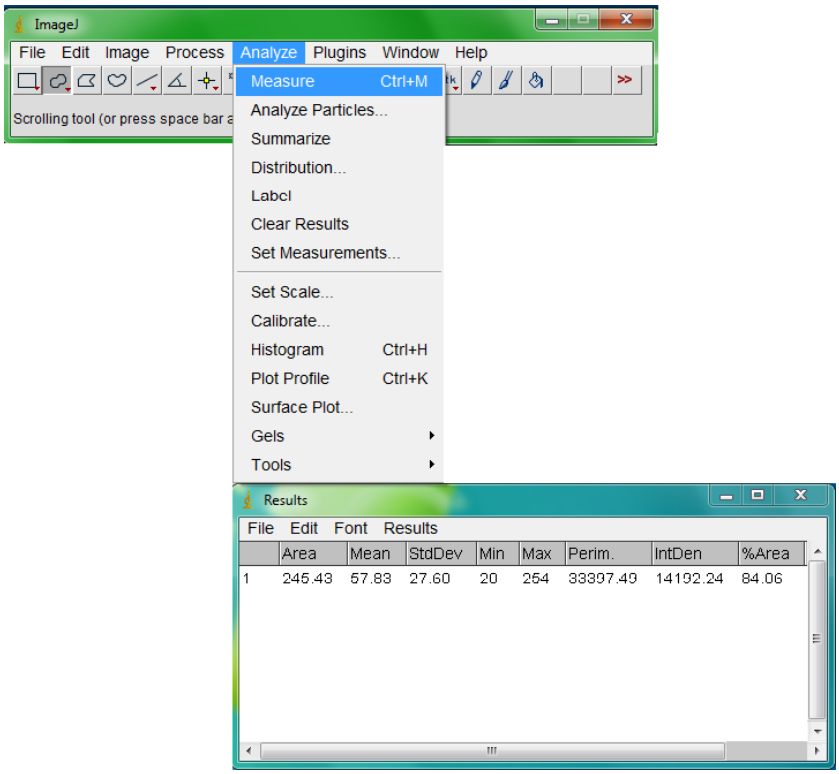


Figure 9.3-1 D

**Figure 9.3-1 Steps to quantitative analysis using Image-J software**

**(A) Outlining the perimeter of the syrinx cavity with 400 pixel margin; (B) Representative samples of the syrinx cavity and surrounding parenchyma; (C) Setting thresholds for AQP4 and GFAP expression; (D) Using the analyse-measure function to measure signal intensity.**

## 9.3.5 Statistical analysis

Data was expressed as the mean ± SE for the mean intensity. The statistical difference between the three groups at each time points was determined by a univariate analysis of

variance (ANOVA). A value of $p<0.05$ was considered statistically significant. Software used included Microsoft Excel 2007 (Microsoft Corp, Redmond, WA) and IBM SPSS v.19 (IBM Corp, Armonk, NY)

## *9.4 Results*

In the animals allocated to the spinal cord injury and post-traumatic syringomyelia groups, cavities developed within the spinal cord sections in 92% of animals. Cavities were absent in two animals in the 12 week PTS group, and one animal in the 12 week SCI and 3 week PTS groups. These four animals were excluded from the qualitative and quantitative analyses of AQP4 and GFAP expression.

### 9.4.1 Triple labelling with AQP4, AQP1 and GFAP

Triple labelling was attempted and performed in one animal from each of the spinal cord injury, post-traumatic syringomyelia and control groups at the 6 week time point (Figure 9.4-1). After initial antibody optimisation, expression of AQP4, AQP1 and GFAP with triple labelling was detectable in only 1 specimen. However, in the majority of the specimens, minimal AQP1 expression was observed when AQP4 and AQP1 antibodies were combined with triple labelling. When stained separately from AQP4, AQP1 expression was detectable in the distribution of the cell bodies of the neurons in the grey matter. Trials with different primary anti-AQP1 antibodies were performed with similarly poor results, thus suggesting an interaction between the anti-AQP1 and anti-AQP4 antibodies.

Triple labelling was therefore abandoned and a separate dual labelling study with AQP4 and GFAP was performed. A dual-labelled AQP1 and GFAP study will be performed in the future.

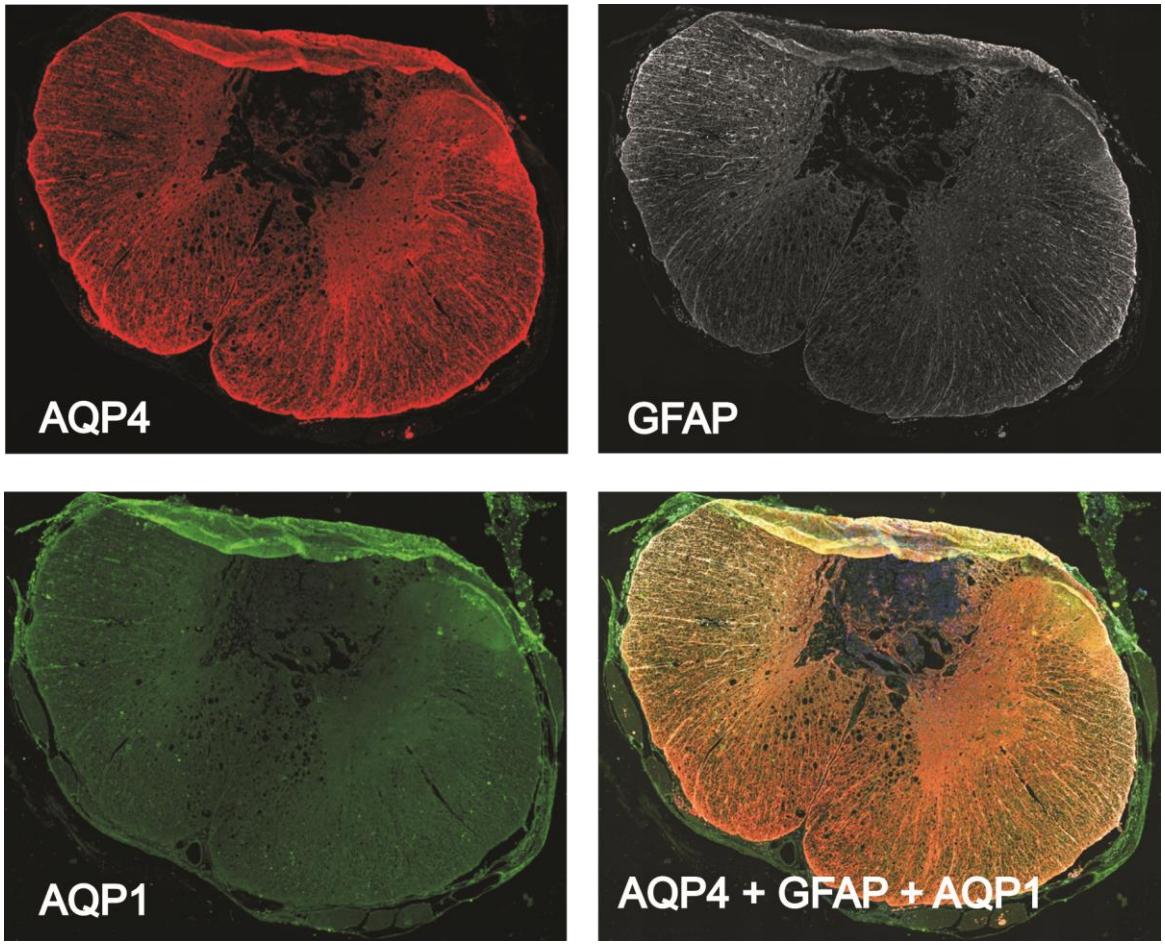


**Figure 9.4-1 Immunohistochemical staining for (i) AQP4, (ii) GFAP, (iii) AQP1, and (iv) triple labelling with AQP4, GFAP and AQP1.**

### 9.4.2 Dual labelling with AQP4 and GFAP

## Qualitative assessment

In the control group, expression of AQP4 and GFAP was present in a typical distribution of a normal spinal cord section, namely, along the glia limitans externa, central canal, in the astrocytic processes of grey and white matter. No notable differences were observed in the expression of GFAP and AQP4 between the SCI and PTS groups at all time points.

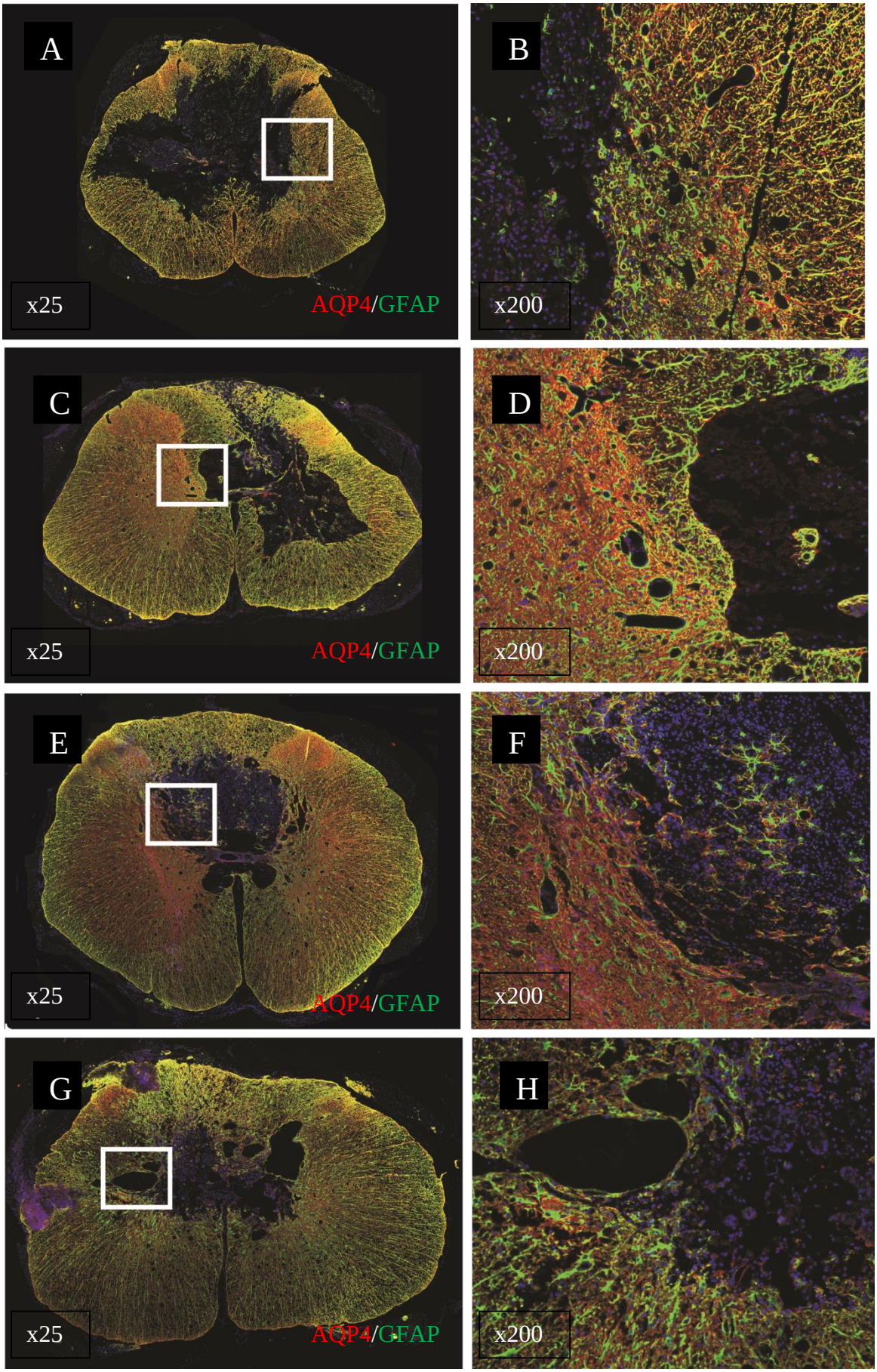
A
x25
AQP4/GFAP
B
x200
C
x25
AQP4/GFAP
D
x200
E
x25
AQP4/GFAP
F
x200
G
x25
AQP4/GFAP
H
x200

**Figure 9.4-2 AQP4 (in red) and GFAP (in green) expressions at C8 level in PTS model from 1 – 12 weeks .**

**(On previous page) Low and high magnification images with relative decrease in AQP4 expression seen at 1 week (A, B) in the region around the syrinx cavity; Increased expression of AQP4 at 3 weeks (C, D) and 6 weeks (E, F); Decreased expression seen at 12 weeks (G, H).**

At the 1-week time point, there was an increased expression of GFAP in the region surrounding the site of the cavity at the C8 level, with decreased expression of AQP4 when compared with the normal white and grey matter (Figure 9.4-2 A, B).

At the 3- and 6- week time points, less intense expression of GFAP with slightly greater AQP4 expression was observed in the perimeter of the cavity, although the GFAP expression was still elevated when compared with normal grey and white matter (Figure 9.4-2 C – F). At 12 weeks, there appeared to be an overall decrease in AQP4 staining in both the SCI and PTS groups (Figure 9.4-2 G, H). Co-localisation between the GFAP and AQP4 staining was variable with no consistent pattern observed between individual animals even within the same time point. There might be a slight trend of increasing co-localisation observed at the later time points of 6 and 12 weeks.

## Quantitative assessment

The integrated signal densities were stratified according to the time point, experimental group (control, SCI or PTS models) and the presence of a syrinx cavity, due to effect modification. Using one-way ANOVA, the combined effects of experimental group, time point and syrinx cavity were statistically significant $F(19, 10.474)$, $p < 0.001$. The mean integrated signal densities have been graphed in Figure 9.4-3. This indicates that the control groups generally have higher AQP4/GFAP ratio. Both the SCI and PTS groups showed similar results. With regards to time point, there appeared to be gradual increase in AQP4/GFAP expression from week 3 – 6, but this decreases at the 12 week timepoint. For this analysis, the separate effects of sampling location were not accounted for.

Furthermore the PTS groups appear to have lower AQP4/GFAP thatn the SCI group. No consistent patterns were observed with regards to the sampling location within the spinal cord or in the perimeter surrounding the syrinx cavity.

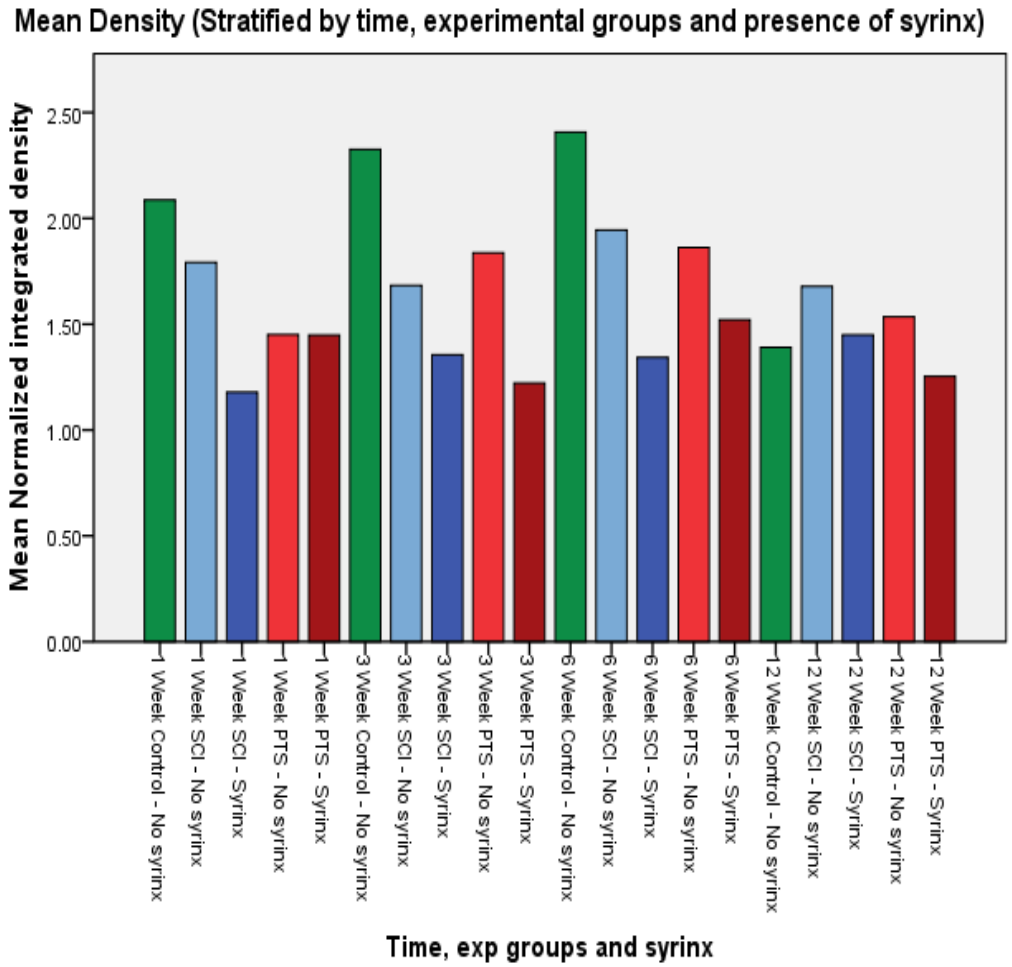


**Figure 9.4-3 Mean integrated signal intensity for groups stratified according to time point, experimental group and presence of a syrinx.**

**Green indicates control group; Light and dark blue indicate SCI groups without and with a syrinx cavity respecctively; Light and dark red indicate PTS groups without and with a syrinx cavity respectively.**

## 9.5 Discussion

Aquaporins are a family of proteins that contain a central core with minimal resistance to water permeability, allowing bi-directional water movement across lipid cell membranes [386]. Since the serendipitous discovery of AQP1 by Agre et al. in 1991, thirteen types of aquaporins have been identified in human tissue, and there has been increasing interest in the role of aquaporins in many conditions affecting water homeostasis [389, 390, 395, 509, 510]. In the central nervous system, the predominant aquaporin is AQP4, although lower levels of AQP1 and AQP9 expression have also been localised within the CNS. AQP4 protein is most abundant in astroglial cells at interfaces between brain and fluid [386]. Specifically, AQP4 is expressed in the astrocytic end feet surrounding capillaries, glia limitans and ependymal lining of the ventricles and central canal [402]. In addition, AQP4 has been shown to be important in cell migration in reactive astrocytes [408]. AQP1 has been localized in the apical membrane of the choroid plexus epithelium in the brain, and, in the spinal cord, the ependymal lining of the central canal neurons and grey matter astrocytes in the dorsal horn [400, 511].

The function of AQP4 and AQP1 in the central nervous system has been investigated in the setting of cerebral oedema following trauma or ischaemia, hydrocephalus, and spinal cord injuries [395, 404, 410, 415, 420, 424]. Based on animal studies, it is evident that AQP4 has different functions in various types of oedema. In AQP4 knockout mice models of cytotoxic cerebral oedema, AQP4 deletion was associated with a significantly longer survival [415]. However, this beneficial effect was not evident in models of vasogenic oedema [391, 413]. In fact, worsened neurological outcome was observed in AQP4-deficient mice with vasogenic cerebral oedema. Similarly, in a contusional spinal cord injury model, AQP-deficient mice had larger cysts and worse neurological outcomes

than wildtypes [421]. In rodent spinal cord injury, AQP4 expression was reduced at the initial stages of injury, followed by a sustained increase in expression with chronic spinal cord injury [419]. It has been postulated that decreased AQP4 expression in acute spinal cord injury might be associated with vasogenic oedema and, at the later stages of spinal cord injury, increased AQP4 expression might contribute to cytotoxic oedema [419]. In relation to syringomyelia, the expression of AQP4 was recently investigated by Aghayev et al. and Hemley et al. using different rodent models of syringomyelia with contrasting results [232, 426, 427].

AQP1 in the central nervous system has been less extensively investigated. Studies of AQP1 knockout mice have demonstrated a decrease in water transport across the choroid plexus epithelium and its deletion may be beneficial in brain trauma [400]. In addition, Nesic et al. reported sustained increased expression of AQP1 in a rodent contusion model of spinal injury, which acted independently of AQP4.

The roles of AQP4 and AQP1 within the spinal cord in both spinal cord injury and post-traumatic syringomyelia have not been established. In particular, existing studies have reported conflicting results regarding the expression of AQP4 in both spinal cord injury and syringomyelia. The present study was conducted to compare the temporal changes in AQP4 and AQP1 expression in a contusional model of spinal cord injury and an impact model of post-traumatic syringomyelia with existing models of spinal cord injury and syringomyelia [423].

On the qualitative analyses, the results of the current study are consistent with those reported by Nesic et al. following a contusional spinal cord injury [424]. AQP4 expression was initially decreased in comparison with GFAP, which was evident at the 1 week time point. However, beyond 3 weeks, there was less intense GFAP expression with

increasing AQP4 expression observed in the margin of the cystic cavity from spinal cord injury. In the post-traumatic syringomyelia group, the results were consistent with those described by Hemley et al., in which AQP4 expression became more robust after 3 weeks [426]. Using an excitotoxic extracanalicular model, Hemley et al. showed that AQP4 expression was most abundant at 12 weeks, which was somewhat dissimilar to the results of the present study. In the present study, AQP4 expression increased at weeks 3 and 6, but began to decline at week 12. Aghayev et al. used a model of communicating syringomyelia, which involved a subarachnoid injection of kaolin at the cisterna magna. AQP4 expression was initially down-regulated during syrinx induction, but no differences were observed when compared with controls. A similar finding was observed in a separate study performed in our laboratory group, in which a non-communicating canalicular model of syringomyelia was used. Expression of GFAP and AQP4 was not significantly different around the central canal between the syrinx and control animals [427].

A new quantitative method for calculating AQP4 expression was devised in this study. Previous studies assessed AQP4 expression either qualitatively by comparing the expression in different regions within a spinal cord section or quantitatively by Western blotting to evaluate the total AQP expression of each individual spinal cord section. Therefore, western blotting results were measurements of the average protein expression within each spinal cord section and quantitative comparisons between regions within each individual section could not be made. In this study, the expression of AQP4 and GFAP in tissues adjacent to the cystic cavity was measured by selecting a pre-determined region with a perimeter of 400 pixels from the cavity edge and measuring the integrated density. Due to variations between individual spinal cord levels and animals, normalisation of the AQP4 expression was performed and expressed as a ratio to GFAP expression. To

compare with the corresponding regions of normal grey and white matter, representative regions of 400 pixel diameter were selected.

The quantitative analyses demonstrated that no significant differences were observed between the spinal cord injury only and the post-traumatic syrinx groups. There was a decreased AQP4 expression at 1 week, but slightly increased expression at weeks 3 and 6. Within the same time and experimental groups, sections with a syrinx cavity appeared to have lower expression of AQP4 relative to GFAP than the surrounding regions without a cavity. However, the control group had higher intensity of AQP4, which was maintained throughout all the timepoints.

To the best of the authors' knowledge, the present study was the first study to describe a technique of triple-labelling of AQP4, AQP1 and GFAP. Unfortunately, there were interactions between the anti-AQP4 and anti-AQP1 antibodies, such that the concentration of anti-AQP1 antibody required for detecting AQP1 expression made it unfeasible to continue with the triple labelling technique. Separate dual labelling studies were therefore planned and the results of dual labelled AQP4 and GFAP were presented in this study. However, due to time constraints, dual labelling with AQP1 and GFAP has not been conducted and will be done as a future project in our laboratory group.

There were several limitations to the present study. The inclusion of one control animal at each time point as representative of uninjured spinal cord was inadequate to make a meaningful quantitative assessment of AQP4 expression. A larger number of animals for the control group would improve the power of statistical analyses.

The time period investigated in the current study was between 1 to 12 weeks, which was appropriate for studying the development of post-traumatic syringomyelia. A previous study using an excitotoxic model of post-traumatic syringomyelia by Hemley et al.

demonstrated increased AQP4 expression from 3 weeks after syrinx induction [426]. However, this time period only represented the transition from acute to chronic spinal injury. To analyse changes in aquaporin expression in the acute stages of spinal cord injury, earlier time points are required.

Comparisons between the peri-cavity area with representative regions of normal grey matter and white matter were expressed as a ratio in this study. The selection of dorsal horn and dorsal columns as representative areas of normal grey and white matter respectively was associated with sampling bias. Due to the constraints of the Image-J software, measurements of AQP4 expression from the entire spinal cord section were not possible.

Another limitation of the study was the method of assessing AQP4 and GFAP expression by using integrated density. Immunodensity measurements are notorious for inaccuracies due to variations during tissue processing and image acquisition. Changes to exposure times and threshold values can significantly alter the results of immunodensity. Future experiments could use immunoblotting techniques for quantification of AQP4 and GFAP expression.

This study has confirmed the associations between AQP4 expression, contusional spinal cord injury and post-traumatic syringomyelia. Aquaporins are bidirectional water channels, which permit water movement both into and out of cell membranes. Therefore, increased expression of AQP4 could represent increased fluid flow into the site of spinal cord injury and syringomyelia, and thus contribute to increased spinal cord oedema. Alternatively, the increased expression could function potentially as a compensatory response to remove excess water from the spinal cord parenchyma. The use of AQP4 knockout mice in a post-traumatic syringomyelia model may be a possible method of

addressing this dilemma, although a murine model of syringomyelia is not available at present. Another method is to use pharmacological agents to modulate AQP4 function in animal models and to evaluate the neurological function or the cavity size on histological sections.

## 9.6 Conclusion

In the current study, AQP4 expression was increased over time in a contusional spinal cord injury model and an impactor model of post-traumatic syringomyelia. No obvious differences were observed between the spinal cord injury and the post-traumatic syringomyelia groups. A triple labelling technique with AQP4, AQP1 and GFAP expression was attempted, but this requires further refinement. Further studies will investigate the exact function of AQP4 and the expression of AQP1 in animal models of spinal cord injury and post-traumatic syringomyelia.

## 9.7 Contributions to the study

The operations, animal care, tissue processing, data analysis and preparation of the manuscript and figures were performed by Dr Johnny Wong. Ms Xin Song was involved in the tasks of tissue processing, image acquisition and measurements of aquaporin expression.

# Chapter 10 The effect of Aquaporin-4 modulation in a rodent model of post-traumatic syringomyelia

## *10.1 Abstract*

**Background**: The pathophysiology of post-traumatic syringomyelia remains enigmatic, and improved treatments are unlikely to be developed until a better understanding is obtained. Existing theories have focussed on fluid flow into syrinx cavities, in which aquaporins may have a contributory role. Aquaporin-4 (AQP4) is a dedicated water channel in the central nervous system that has been shown to be expressed more abundantly in post-traumatic syringomyelia. However, it has not been established whether AQP4 acts to promote fluid inflow, or as a compensatory mechanism to remove water from a syrinx cavity.

**Objective:** The aim of this study was to investigate the effect of aquaporin-4 modulation on pre-existing post-traumatic syrinxes.

**Methods:** Thirty-two male Sprague Dawley rats underwent syrinx induction surgery using the excitotoxic extracanalicular syringomyelia model. In two animals, peri-operative complications occurred and were excluded. At 6 weeks following the initial surgery, ten animals in each AQP4 modulation treatment group (control, agonist, and antagonist) were given daily intraperitoneal injections of the treatment agent for 5 days. The animals were then perfused-fixed and the specimens were processed for histological analyses and immunohistochemistry.

**Results:** All animals developed a syrinx cavity typical of post-traumatic syringomyelia. In the agonist group, there was more vacuolation in the spinal cord parenchyma when compared with other treatment groups. The size and area of the cavities were smaller in the agonist group than the antagonist group. The average percentage area of the epicenter of the syrinx cavities was smallest in the agonist group (4.6%), followed by control (5.0%) and antagonist group (5.6%), $p = 0.21$. On immunohistochemistry, AQP4 expression was present at the glia limitans, normal grey and white matter. Along the margins of the syrinx cavity, there was less expression of AQP4 in the agonist group when compared with the control group. AQP4 was most abundantly expressed along the margin in the antagonist group.

**Conclusions:** This study suggested a direct association between AQP4 and post-traumatic syringomyelia. There was a trend towards larger syrinx cavities and increased AQP4 expression in the margins of the syrinx cavity with AQP4 inhibition. AQP4 in post-traumatic syringomyelia may function as a compensatory response to remove excess fluid from the syrinx cavity into the spinal cord parenchyma.

## *10.2 Introduction*

Post-traumatic syringomyelia remains a difficult and challenging condition to treat. Despite being increasingly recognised through improved magnetic resonance imaging, the efficacy rates from treatment for this condition remain unsatisfactory [2]. Recurrence rates following surgical intervention in the long-term are about 50% [37, 38, 78, 126, 190, 480]. More effective therapy is unlikely to be developed until a more complete understanding of the factors contributing to syrinx formation and enlargement is obtained.

The pathophysiology of post-traumatic syringomyelia remains perplexing. It is likely that a dynamic balance exists between fluid flow into and out of a syrinx cavity [63]. At a fundamental level, during periods of clinical stability, fluid inflow must balance fluid outflow, and during syrinx expansion, fluid inflow exceeds outflow [63]. Most existing theories have concentrated on how perturbations of CSF flow in the subarachnoid space would result in increased fluid flow into the spinal cord, and subsequently, into the syrinx cavity. However, a major obstacle that cannot be explained is how fluid would enter the syrinx cavity despite observations that the intracavity fluid pressure within a syrinx is so high [193]. Alternative sources of fluid have been suggested, including aquaporins.

Aquaporins are a family of bidirectional transmembrane proteins that are dedicated to water transport [386]. Recent studies have shown that AQP4 expression is increased in post-traumatic syringomyelia, but it has not been established whether AQP4 acts to promote fluid inflow, or as a compensatory mechanism to remove excess water from the syrinx cavity [426]. The objective of this study was to investigate whether modulation of AQP4 function would result in a change in the size of the syrinx cavities, and thus determine its role in fluid movement in post-traumatic syringomyelia.

## *10.3 Materials and methods*

After ethical approval was granted from the Macquarie University Animal Ethics Committee, 32 male Sprague-Dawley rats weighing 370 – 616 g (Average: 416 g) were used. One animal died unexpectedly from unknown cause at 3 weeks after the initial operation and another animal was euthanased on the third post-operative day due to tail necrosis from caudal artery thrombosis. Both animals were excluded from the remainder of the study.

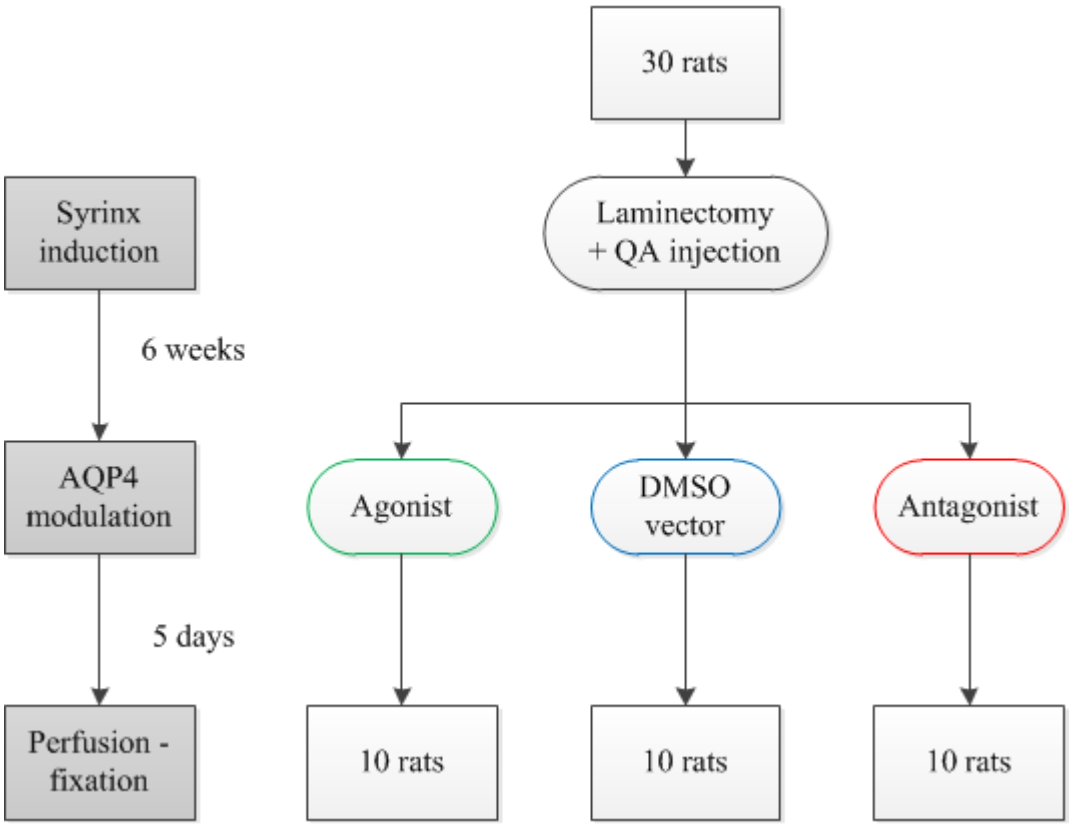


**Figure 10.3-1 Flowchart of animals for AQP4 modulation**

The study consisted of three aquaporin modulation treatment groups (Control, agonist and antagonist), with 10 animals allocated to each treatment group, as shown in Figure 10.3-1. All the animals underwent syrinx induction using the excitotoxic post-traumatic model, as previously described by Yang et al. [195]. At 6 weeks post-syrinx induction, the allocated

treatment agent was administered daily for 5 days. The animals were then euthanased by perfusion-fixation. The outcome measures were neurological function, overall syrinx formation rate, the AP and lateral dimensions of the cavity, area of cavity and number of levels involved.

### 10.3.1 Post-traumatic syrinx induction

All procedures were performed in a sterile field under general anaesthetic. Anaesthesia was induced with 4% isoflurane and subsequently maintained with 2 – 2.5% isofluorane via a nose cone. The rats were positioned prone and the skin was shaved and prepared with povidone-iodine. Under magnification with the operating microscope, C7 – T1 laminectomy was performed with bony rongeurs through a midline incision. An initial puncture of the meninges was performed with a 0.5mL 30G insulin syringe (Ultra-Fine II, Beckton Dickinson and Co, NE ,US). A 10-μL syringe (SGE International Pty Ltd, VIC, Australia), attached to a glass needle tip (outer diameter 50 μm), was used to deliver four 0.5 μL intraparenchymal 24 mg/mL of quisqualic acid and 1% Evans Blue solution. Each injection was administered with the needle held in a stereotaxic micromanipulator (Stoelting, Illionois, USA) between C7 and T1 levels at approximately 0.5 mm right of midline, being careful to avoid pial blood vessels over the spinal cord. To induce arachnoiditis, a 5 μL injection of 250 mg/mL kaolin (Sigma-Aldrich) in 0.9% saline solution was measured out with a micropipette and slowly administered into the subarachnoid space via 0.5mL 30G insulin syringe (Ultra-Fine II, Beckton Dickinson and Co, NE ,US) following the quisqualic acid injection. A layered closure was performed with resorbable sutures to fascia and skin. The animals were allowed to recover with analgesia and antibiotic coverage as required and access to food ad libitum. They were monitored for neurologic deficits, excessive weight loss and signs of distress.

### 10.3.2 Administration of AQP4 Modulation agents

At 6 weeks following the syrinx induction, the animals were given 5 daily doses of the allocated treatment agent. Under a short inhalational anaesthetic with 4% isoflurane, the animals were positioned supine for an intraperitoneal injection of either: control (DMSO vector), agonist (600µM AqF026 in DMSO vector) or antagonist (600µM AqB050 in DMSO vector). The DMSO vector was prepared at a dilution of 1:100 DMSO (Sigma-Aldrich) in 0.9% Sodium Chloride. The agonist and antagonist agents were produced by Prof Andrea Yool at the University of Adelaide. The daily dose of the respective agents was calculated according to the weight of the animals at 0.25 mL / 100 g. At the conclusion of each injection, the animals were allowed to recover from anesthetic and were monitored for weight loss and signs of distress.

### 10.3.3 Perfusion and fixation

After the administration of five doses of aquaporin modulation agents, the animals were anesthetized with 4% isoflurane. Heparin 5000 IU was injected via an intracardiac injection and the left ventricle was cannulated to allow influx of fixative. The right atrium was incised to permit efflux of blood and fixative. Each animal was perfused with 400 mL of 4% paraformaldehyde (Lancaster Synthesis Ltd, UK) in 0.1 M phosphate buffered saline (pH 7.4).

### 10.3.4 Tissue processing, histology and immunohistochemistry

The brain and spinal cord were dissected out and post-fixed in 4% paraformaldehyde solution overnight. The spinal cord was divided into individual specimens according to the spinal cord level from C2 to T4. The specimens were processed in paraffin over a 4-

hour cycle in an automated tissue processor (Leica ASP200S, Leica) and then embedded in paraffin wax blocks. Transverse sections of 5 μm thickness were produced with a microtome and were mounted on glass slides. The slides were allowed to air dry for at least 4 hours prior to staining.

Haemotoxylin and Eosin (H&E) staining was carried out using the Lillie-Mayer protocol. After gradient ethanol baths and xylene washes, the slides were coverslipped with DPX mounting medium (Scharlau Chemie SA, Spain) and allowed to dry in a 37 $^0$C oven for 3 days.

For immunohistochemistry, deparaffinisation and rehydration with xylene and gradient ethanol washes was performed prior to antigen retrieval with 0.1M citrate buffer (pH 6.0) at 95$^0$C for 20 minutes. The sections were cooled to room temperature and were blocked with 10% normal donkey serum. Primary antibodies were applied with anti-Aquaporin 4 (1:50 dilution, SC-20812, Rabbit Polyclonal IgG, 0.2mg/ml, Santa Cruz, CA, US) and anti-GFAP (1:800, MAB360, Mouse IgG1 mAb, 1mg/ml, Chemicon Millipore, CA, US) and incubated in a humidifier at 37$^0$C for 2 hours. This was followed by incubation with secondary antibodies, Donkey anti-rabbit IgG-Alexa Flour 594 (1:400, A21207, Invitrogen Life Technologies, NY, US) and Donkey anti-mouse IgG-Dylight 649 (1:400, 715-495-140, Jackson Immunoresearch Laboratories, PA, US) for 1 hour. The sections were finally incubated in DAPI (1 μg/mL) for 1 minute, coverslipped with fluorescent mounting medium (DAKO, S3023, Carpinteria, CA, US) and allowed to cure for 24 hours at room temperature.

### 10.3.5 Image acquisition and processing

The sections were studied using light microscopy with a Zeiss Axio Imager Z2 microscope (Carl Zeiss Microimaging GmbH, Germany). Photographs of the H&E sections were taken using the Axiovision program (Release 4.8.1, Carl Zeiss Microimaging GmbH, Germany) at x50 magnification. The dimensions and areas of the cavity size were calculated using the "measure - length" and "measure – outline" functions respectively on the Axiovision program (Release 4.8.1, Carl Zeiss Microimaging GmbH, Germany), as illustrated in Figure 10.3-2.

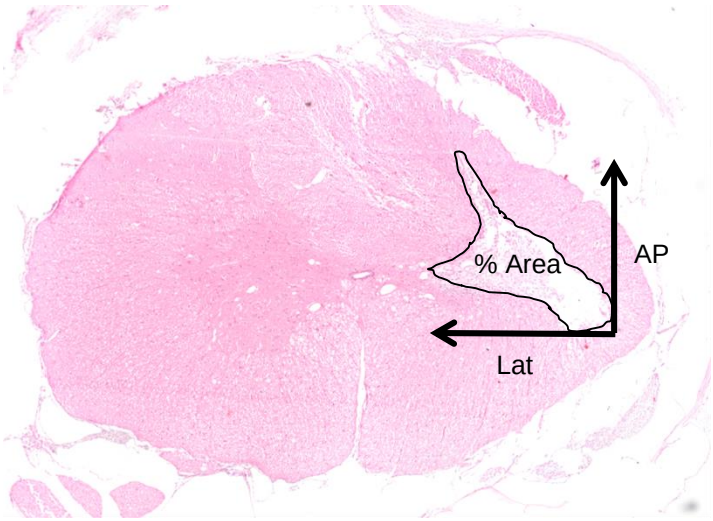


**Figure 10.3-2 Measurements for cavity dimensions and areas**

Photographs of the immunohistochemistry sections were taken at x200 magnification with exposure times of 300 ms for AlexaFluor 594, reflecting AQP4 expression and 1500 ms for DyLight 649, reflecting GFAP expression. The sections were analysed qualitatively for the overall distribution of AQP4 and GFAP expression within the section.

### 10.3.6 Statistical analysis

The outcome measures were the cavity dimensions, area of the cavity and percentage area of the cavity size relative to the area of the spinal cord per spinal section. For each animal, the number of levels and an average of the two spinal levels with the highest percentage areas were determined. Data was expressed as the Mean + SE for the above variables. A value of $p<0.05$ was considered statistically significant. Software used included Microsoft Excel 2007 (Microsoft Corp, Redmond, WA) and IBM SPSS v.19 (IBM Corp, Armonk, NY)

## *10.4 Results*

### 10.4.1 Neurological function

Of the 30 animals that underwent syrinx induction, mild forelimb weakness developed in two control animals from the initial operation. Both animals recovered to normal function over 2 weeks, but in one animal, this was associated with overgrooming of the forelimb. Mild hindlimb weakness was present in one animal from the antagonist group in the immediate post-operative period, and improved to normal gait within 3 weeks. No animals developed worsening neurological function over the study period.

### 10.4.2 Histological appearances on H&E

Syrinx cavities developed in all animals in the present study. No distinctive differences in the histological appearances were discerned between the agonist, antagonist and control groups. On histological sections, the cavities involved the dorsal horn, and were associated with necrosis and inflammatory infiltrate, as previously described by Brodbelt et al. [321]. The cavities were largest at the C8 level, although they also involved C7 and

T1 levels to a lesser extent. There was evidence of surrounding vacuolations in the spinal cord parenchyma around the cavity, which was more prominent in the agonist group when compared with the antagonist group, as illustrated in Figure 10.4-1.

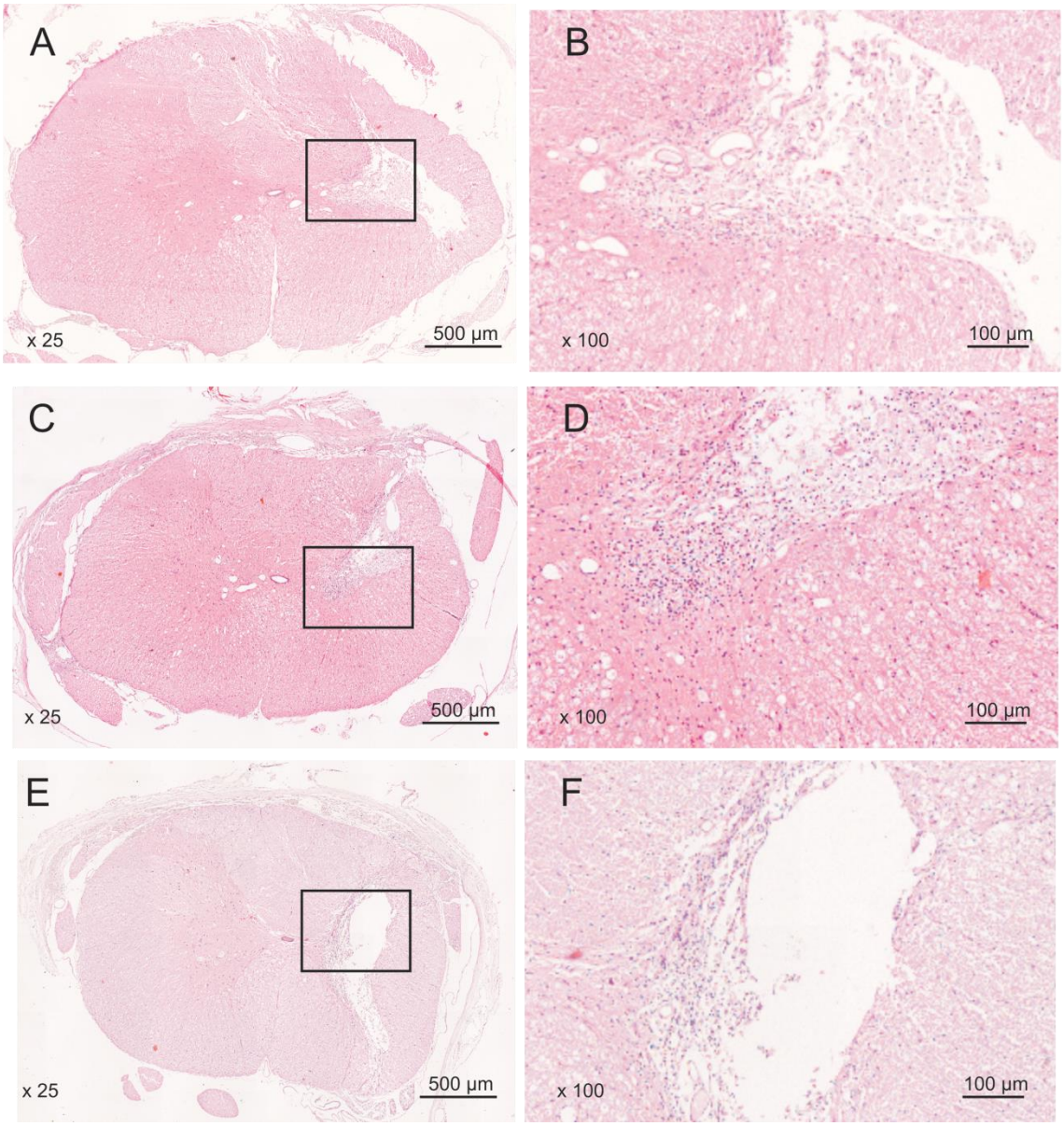


**Figure 10.4-1 Histological images at C8 level for AQP modulation groups.**

**(A, B) Control group at low- and high-power magnification respectively; (C,D) Agonist group at low- and high-power magnification. Increased vaculoation is seen in the perimeter of the syrinx cavity; (E, F) Antagonist group at low- and high-power magnification respectively. A larger cavity with less surrounding vacuolation is noted.**

### 10.4.3 Cavity measurements

The average number of spinal levels, measurements of the cavity dimensions, area of cavity and percentage area of the cavity to spinal cord at C7, C8 and T1 are shown in Table 10.4-1 and Table 10.4-2. There were some variations between individual animals in the spinal level at which the epicenter of the syrinx cavity occurred. To account for this, the average of two spinal levels with the highest percentage areas was used to estimate the percentage area at the epicenter of the cavity, as shown in Table 10.4-1.

**Table 10.4-1 AQP modulation results: No. of levels and area**

| AQP4 modulation group | No. of animals | Overall cavity rate (%) | Mean No. of levels | Mean C7 % area of cord | Mean C8 % area of cord | Mean T1 % area of cord | Max 2 levels % area of cord |
|---|---|---|---|---|---|---|---|
| Control | 10 | 100 | 3.2 | 4.3 | 5.2 | 2.0 | 5.0 |
| Agonist | 10 | 100 | 2.7 | 2.9 | 4.5 | 1.9 | 4.6 |
| Antagonist | 10 | 100 | 3.0 | 3.4 | 6.1 | 2.8 | 5.6 |

**Table 10.4-2 AQP modulation results: Dimensions.**

| AQP4 modulation group | No. of animals | Mean C7 AP (μm) | Mean C7 Lat (μm) | Mean C8 AP (μm) | Mean C8 Lat (μm) | Mean T1 AP (μm) | Mean T1 Lat (μm) |
|---|---|---|---|---|---|---|---|
| Control | 10 | 890 | 550 | 740 | 700 | 370 | 310 |
| Agonist | 10 | 650 | 440 | 850 | 700 | 150 | 250 |
| Antagonist | 10 | 750 | 500 | 1030 | 680 | 400 | 360 |

Across all outcomes, the agonist group of animals had a lower average number of spinal levels involved, smaller cavity dimensions, area and percentage area than the antagonist group, as demonstrated in Figure 10.4-2 A - C. In the percentage area at the epicenter, as calculated from the average of the two spinal levels with the maximum percentage areas, the agonist group had the lowest area (4.6%), followed by the control group (5.0%) and antagonist group (5.6%). This is graphically represented in Figure 10.4-2 D. When

comparing the maximum areas between the agonist and antagonist groups using Student *t*-test, the C8 % area and maximum 2 level % area were not statistically significant ($p$= 0.25 and 0.21 respectively).

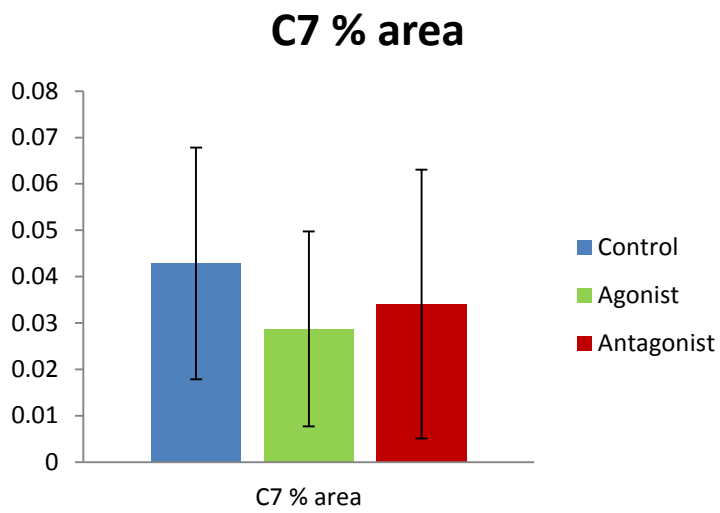


Fig 10.4-2 A

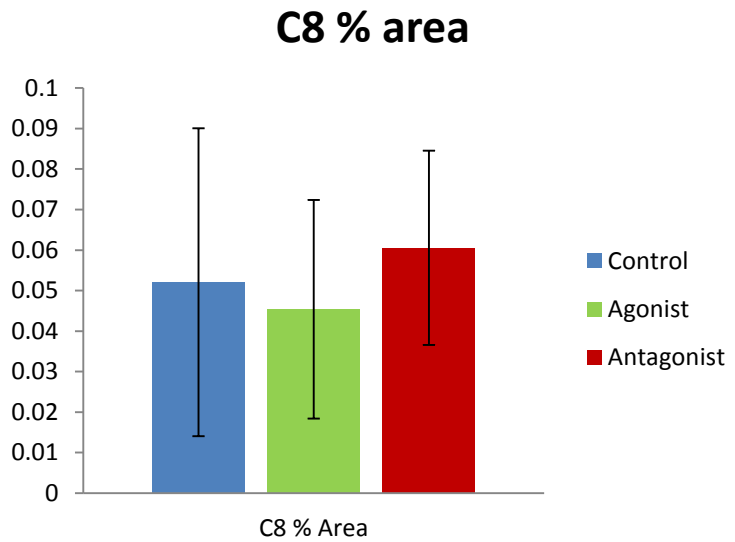


Fig 10.4-2 B

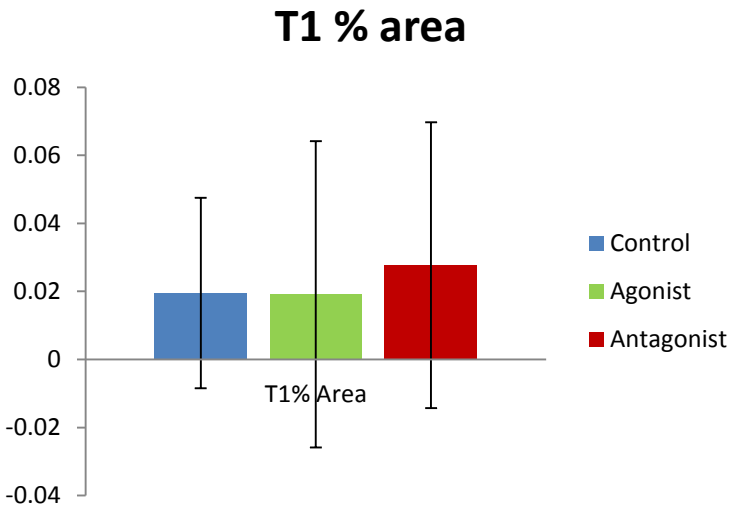


Fig 10.4-2 C

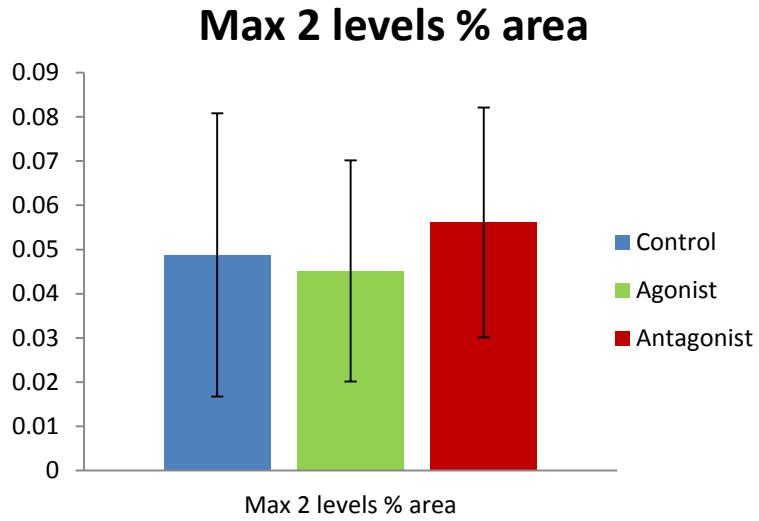


Fig 10.4-2 D

**Figure 10.4-2 Percentage area of syrinx cavity to spinal cord at: (A) C7 level; (B) C8 level; (C) T1 level; (D) Average of maximum 2 levels**

## 10.4.4 AQP4/GFAP immunohistochemistry

Immunofluorescent imaging revealed AQP4 expression in a typical distribution as previously described by Hemley et al. [426]. On sections without a syrinx cavity, AQP4 was expressed in a normal pattern, which was present predominantly in the astrocytic processes along the glia limitans externa and grey matter, with less expression within the white matter (Figure 10.4-3). On the sections with a syrinx cavity, there was slightly

increased expression of AQP4 along the margins of the syrinx cavity in all treatment groups. However, there was comparatively greater GFAP expression than AQP4 in the same regions in all groups, with a limited amount of colocalisation (Figure 10.4-3).

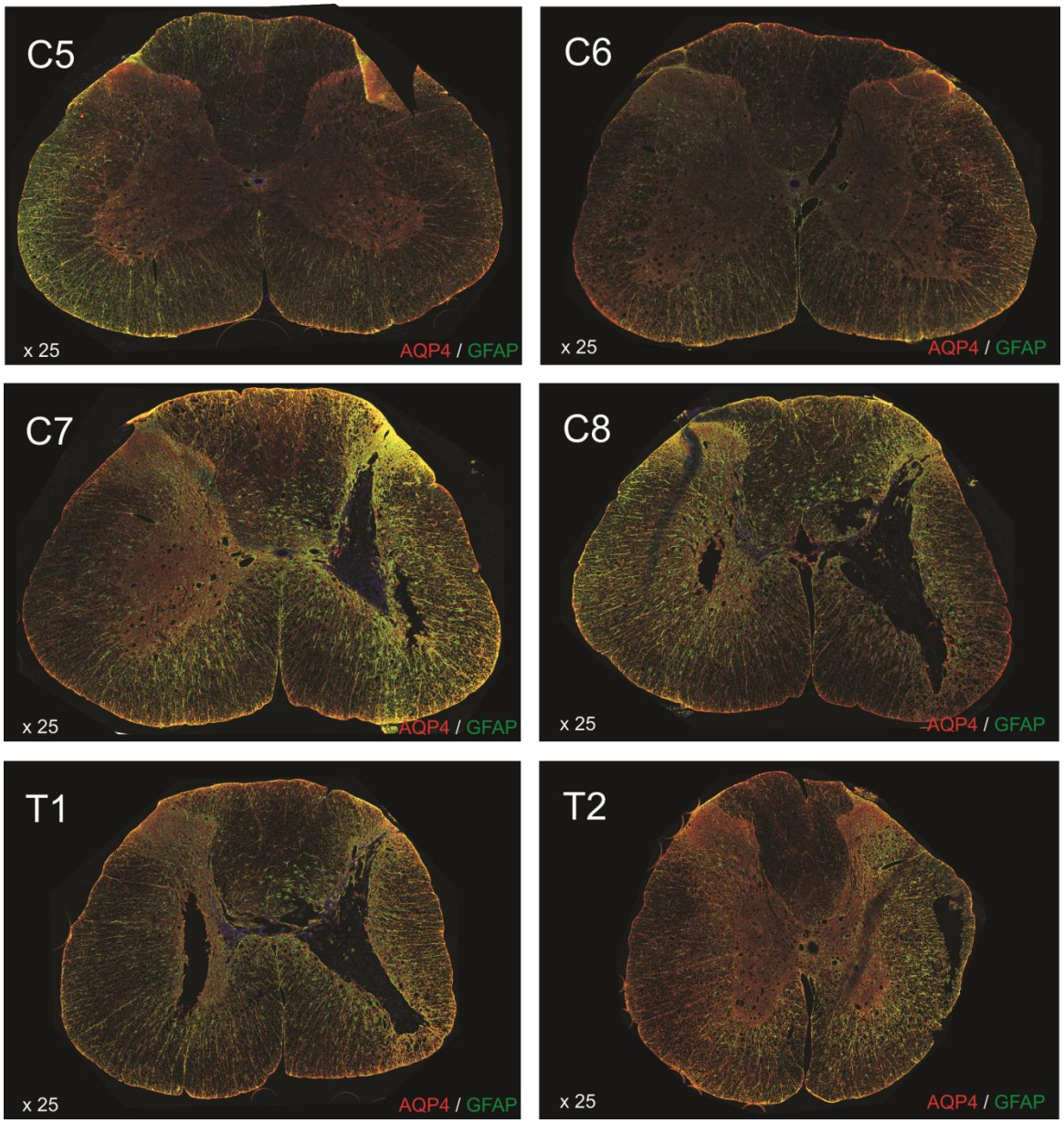


**Figure 10.4-3 AQP4 / GFAP expression in control animal from C5 to T2 levels.**

**In sections without a syrinx cavity (C5, C6 and T2), AQP4 was expressed at the glia limitans and grey matter. Increased GFAP expression was observed at the perimeter ofthe syrinx cavity, with slight increase in AQP4 expression (between C7 and T1 levels).**

When comparing the AQP4 expression in the margins of the syrinx cavity across the treatment groups, the least amount of expression was observed in the agonist group,

followed by the control group. The greatest amount of expression was identified in the antagonist group, with greater degree of colocalisation with GFAP (Figure 10.4-4).

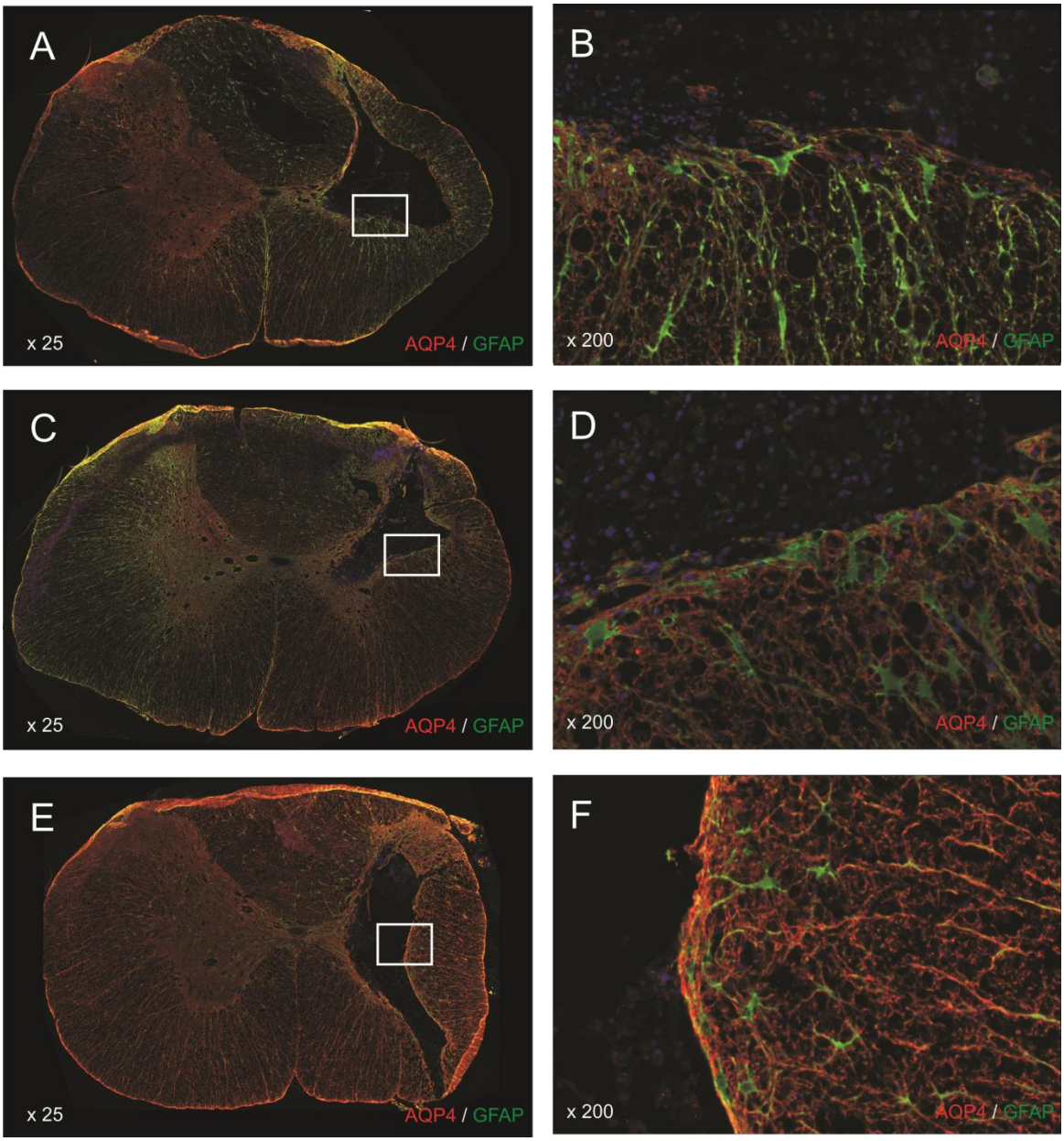


**Figure 10.4-4 AQP4 / GFAP expression at C8 level across AQP modulation groups.**

**(A, B) Control group at low- and high-power magnification respectively; (C, D) Agonist group at low- and high-power magnification respectively, demonstrating reduced AQP4 and GFAP expression; (E, F) Antagonist group at low- and high-power magnification respectively. Increased AQP4 expression is observed.**

## *10.5 Discussion*

Spinal cord injury affects approximately 2.5 million people worldwide, with about 130,000 new injuries occurring each year [512]. In about a quarter of these patients, syringomyelia will eventually develop from several months to many years after the initial injury. At present, there is still an inadequate understanding of how syringomyelia forms following spinal cord injury. It has been recently recognised that disturbances of CSF flow within the subarachnoid space due to arachnoiditis caused by the initial trauma are likely to contribute to increased inflow into the spinal cord and syrinx cavity.[171, 204] However, there may be additional sources of fluid inflow, such as disruptions of the blood-spinal cord barrier and, more recently, aquaporins have been implicated [213, 427].

Of the thirteen aquaporins that have been identified in the human body, AQP4 is the predominant aquaporin within the central nervous system. It is most abundantly expressed by astroglial cells at the blood-brain barrier, glia limitans and ependyma.[513] It has been reported that the rodent spinal cord contains the highest AQP4 expression than other organs [514].

The precise role of AQP4 in the central nervous system has not been completely elucidated. Besides being involved in cell migration of reactive microglia and neural signal transduction, AQP4 has a major role in water influx and efflux within astrocytes, and thus, clearance of water from the central nervous system [388, 407, 408]. AQP4 has been investigated in a number of brain conditions, including cerebral oedema from trauma, ischaemia and hydrocephalus, and spinal cord pathologies, such as spinal cord trauma and ischaemia, multiple sclerosis, neuromyelitis optica and amyotrophic lateral sclerosis [387, 388, 391, 404, 424].

In studies of AQP4 expression in spinal cord injuries, AQP4 expression was found to be decreased during the acute stages of spinal cord trauma in a rodent model, and was subsequently increased at the chronic stages of cord injury. Elevated expression of AQP4 in the later stages of spinal cord injury was thought to reflect astrocytic swelling from cytotoxic oedema [419]. Furthermore, deletion of AQP4 in AQP-null mice showed decreased astrocytic swelling and improved neurological outcomes, when compared with wildtype mice [420, 515]. Thus, AQP4 deficiency was thought to be neuroprotective, presumably due to decreased cytotoxic oedema.

In a recent study on post-traumatic syringomyelia by Hemley et al., AQP4 expression was shown to be increased beyond 3 weeks from syrinx induction, with the greatest expression at 12 weeks [426]. The function of AQP4 in this setting has not been elucidated. It is possible that AQP4 may contribute to increased influx of fluid into the syrinx cavity, thus contributing to syrinx enlargement. Alternatively, the increased expression of AQP4 in the later stages of post-traumatic syrinx development might be a compensatory response to remove excess fluid from the syrinx cavity.

A number of methods have been used to modulate the function of AQP4. These include the use of phorbol esters, vasopressin antagonisits, edaravone, hypoxia, melatonin, hyperosmotic agents, diuretics such as amiloride and bumetanide [387, 410, 436, 439-445]. Many of these methods have been limited by their toxicity, low efficacy or lack of specificity [436]. In particular, phorbol esters have been demonstrated to decrease cerebral oedema from trauma and ischaemia in rodent models by AQP4 downregulation [439-441]. However, long-term use has been associated with toxicity, such as haemorrhagic and intersitital pneumonitis and fibrosis, decreased granulocyte count and carcinogenesis [439, 441]. Recently, Yool et al. developed an aquaporin agent, which

specifically targets the central pore within the aquaporin protein through which the water molecules travel. Based on the diuretic, bumetanide, AqB013 has been shown to be active on the AQP1 and AQP4 proteins in in-vitro cultures of oocytes [436]. Further refinements of the formulation for AqB013 have yielded another AQP4 antagonist, AqB050, and an AQP4 agonist, AqF026. These agents have been trialled on in-vitro oocyte cultures, and mice models of hydrocephalus (Personal communication, Yool et al.).

The results from the present study demonstrated that there was an overall trend with the smallest syrinx cavities being in the AQP4 agonist group, followed by the vector control group, and the largest cavities in the AQP4 antagonist group. This was consistently observed across most of the measurements performed, particularly in the percentage area of the cavity to spinal cord area, and the percentage area of the cavity epicenter. The current study would suggest that augmenting AQP4 function may result in a reduction in the size of existing syrinx cavities. In contrast, inhibition of AQP4 tends to produce larger syrinx cavities. Since AQP4 is a bi-directional water channel, AQP4 might act to remove excess fluid, rather than contributing to fluid inflow into a syrinx.

A previous study from our laboratory group identified the presence of fluid outflow pathways in a sheep excitotoxic extracanalicular syrinx model [63]. It demonstrated that fluid outflow occurred in a diffuse manner into the interstitial spaces, and subsequently, towards the central canal and, to a lesser extent, the subarachnoid space. Perhaps, AQP4 is a potential mechanism by which fluid outflow occurs into the surrounding interstitial spaces. On the histological sections, there were more vacuolations in the agonist group in the surrounding spinal cord parenchyma adjacent to the syrinx cavity, which may suggest the influence of AQP4 function. If indeed the function of AQP4 is to remove excess fluid from established syrinx cavities, then the increase in AQP4 expression at later timepoints

after syrinx induction may be a reaction to increased fluid inflow as the syrinx cavity enlarges.

On immunohistochemistry, the distribution of AQP4 and GFAP expression was consistent with the findings from previous studies [232, 402]. AQP4 was expressed predominantly along the glia limitans externa, grey matter and in the regions adjacent to the syrinx cavity. However, there was a proportionally greater increase in GFAP expression than AQP4, which was also observed by Hemley et al. [426]. Based on qualitative assessments, AQP4 expression was interestingly greatest in the antagonist group, and the least expression was observed in the agonist group. This observation has not yet been verified by quantitative analysis, but could potentially be explained as a response to AQP modulation agents. When antagonist treatment is given, AQP4 expression might increase as a compensatory feedback response to AQP4 inhibition. According to Ghabriel et al., vasogenic cerebral oedema occurred following downregulation of AQP4 in the setting of a traumatic brain injury, but improved with restoration of AQP4 [516]. The speed of this restoration was consistent with post-translational modification, rather than enhanced protein synthesis [401, 516].

There were several limitations to this study. The current study was essentially a pilot study that demonstrated a proof of concept. Only one timepoint (6 weeks following syrinx induction) was selected for investigation because a syrinx cavity was consistently established at 6 weeks based on previous studies [321]. In addition, it was demonstrated in the study by Hemley et al. that AQP4 expression was increased after 3 weeks [426]. For future studies, it might be worthwhile to investigate if changes in syrinx size would be consistently observed at various timepoints and with different durations of modulation treatment. Also, it has been assumed in this study that the AQP4 modulation agents were

adequately absorbed through intraperitoneal injections to reach therapeutic levels in the serum. The precise pharmokinetics and pharmodynamics of the modulation agents, particularly at the level of the spinal cord, have not been thoroughly investigated yet.

The excitotoxic extracanalicular model of post-traumatic syringomyelia was selected in this study for several reasons. The excitotoxic model was an established model and was previously used in the study of AQP4 expression by Hemley et al. [426]. The results of this study would only be applicable if the excitotoxic model was representative of the human condition. Recently, our laboratory group developed a direct impact model of post-traumatic syringomyelia by using a computerised motorised spinal cord impactor and arachnoiditis (See Chapter 4). In addition, AQP4 expression in an impactor model of post-traumatic syringomyelia was performed and showed similar findings with gradual increase in AQP4 expression over time. Future study of AQP4 modulation in the setting of a contusional model of spinal cord injury and an impactor model of post-traumatic syringomyelia would be of interest to verify if the results from this study were consistently observed.

The current study provides further evidence that there is a dynamic balance between fluid inflow and outflow. The fact that AQP4 modulation agents could affect the size of syrinx cavities confirms the role that aquaporins have in syrinx pathophysiology. Although the findings from this study are still preliminary, the fact that AQP4 modulation could influence the equilibrium between fluid inflow and outflow opens up exciting possibilities for potential pharmacological development. Perhaps, pharmaceutical modulation of aquaporins may be a therapeutic option for patients of, not only spinal cord injury patients, but also, post-traumatic syringomyelia in the future.

## *10.6 Conclusion*

In a rodent model of post-traumatic syringomyelia, the application of AQP4 agonists resulted in the trend towards smaller syrinx cavities and a decrease in the expression of AQP4 around the syrinx cavity, while AQP4 antagonists seemed to produce larger syrinxes and increased AQP4 expression. It is postulated that AQP4 functions as a compensatory mechanism to promote fluid outflow in post-traumatic syringomyelia, and alterations to AQP4 expression are feedback responses to the modulation treatment.

## *10.7 Contributions to the study*

The operations, animal care, tissue processing, data analysis and preparation of the manuscript and figures were performed by Dr Johnny Wong. Ms Angela Hwang was involved in animal care, tissue processing and image acquisition. Ms Xin Song was involved in immunohistochemistry and image acquisition.

# Chapter 11 General discussion

## *11.1 Pathophysiology of post-traumatic syringomyelia*

Syringomyelia remains a debilitating condition for patients because of its progressive symptoms, an enigmatic condition for researchers to understand in regards to the pathophysiology, and a frustrating condition for physicians in terms of its poor long-term efficacy from treatment. This is particularly so with post-traumatic syringomyelia, as compared with Chiari-related syrinxes.

The plethora of theories and the spectrum of different treatment options available are indications of the limited understanding of the disease process currently. Fundamental facts about the condition, such as the source and composition of syrinx fluid, have not yet been answered. The approach adopted in investigating post-traumatic syringomyelia in this thesis has been based on the necessary steps to the development of novel treatments:

First, more fundamental information regarding the nature of syrinx fluid needs to be obtained. Secondly, reproducible and reliable models are required to replicate the condition, so that theories regarding the pathophysiological processes involved may be validated. Lastly, modulation of these processes needs to be developed. It is hoped that this will lead to implications for new treatments, resulting in syrinx resolution and symptomatic improvement (Figure 11.1-1).

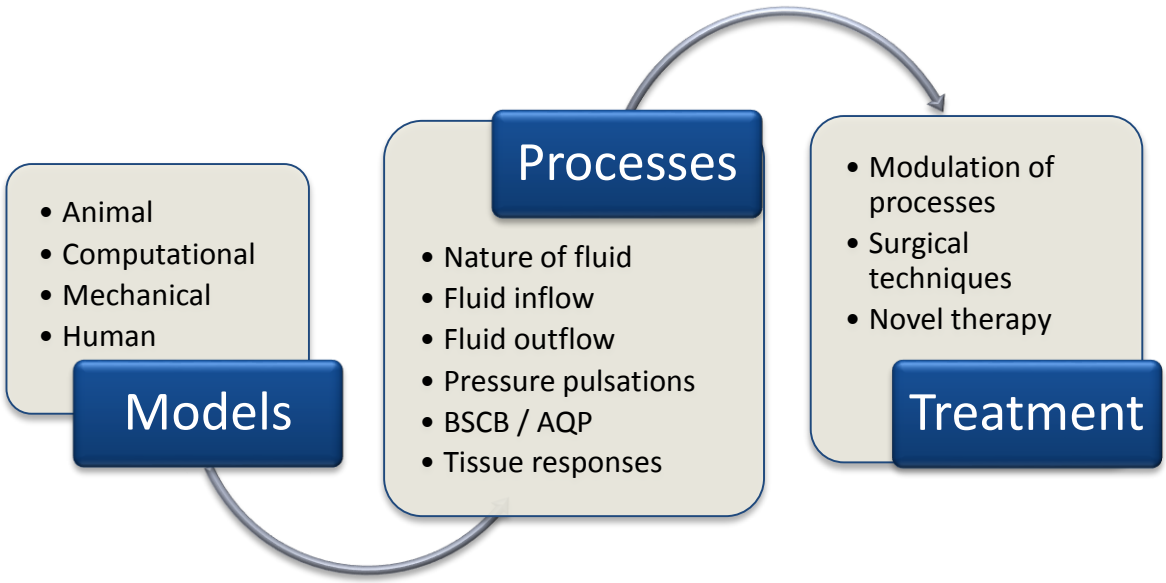


**Figure 11.1-1 Conceptual approach to syringomyelia research**

### 11.1.1 Nature of syrinx fluid

Syrinx fluid has been assumed to be originated from CSF. However, this has been debated recently, with some authors suggesting an alternative source of extracellular fluid. Biochemical analysis of syringomyelia fluid was performed to determine the composition of syrinx fluid. This was the first study that directly compared the biochemistry of syrinx fluid with CSF from the adjacent subarachnoid space. The results indicated limited differences in the electrolyte levels between syrinx fluid and CSF. Based on the results of this study, there was no evidence to discount the contribution of CSF to syrinx fluid. However, an extracellular fluid source could not be excluded, and this is unlikely to be resolved through further clinical studies.

### 11.1.2 Models of syringomyelia

The excitotoxic model of post-traumatic syringomyelia in rodents has been well described [195, 311, 321]. This was used in the AQP4 modulation study because of previous work

done in our research group, confirming the up-regulation of AQP4 in post-traumatic syringomyelia using this model. Spinal cord cavitations developed in all animals in this study, which compared favourably with the 80 – 90% syrinx induction rate in previous studies [321].

A large animal was required for ultrasound guided injections of tracers into the syrinx cavity to assess fluid outflow. This was the first study to describe a sheep excitotoxic extra-canalicular syringomyelia model, which had histological resemblance to human syrinxes. Syrinx cavities developed in 75% of animals and severe neurological deficits were noted in 33% of animals during the initial stages of learning the technique [63]. Although the syrinx induction rates in sheep were lower than in rats, this model will be a useful large model of syringomyelia for further studies in the future, including CSF telemetry.

The rationale for developing a direct impact model of post-traumatic syringomyelia has been outlined in this thesis. The Infinite-Horizon spinal cord impactor is a reliable method of delivering a pre-determined force to the spinal cord, with correlation to the extent of neurological deficits and the size of cavities histologically. A cavity developed in 92% of animals, which resembled human syrinxes histologically. However, the animals at the 12-week time-point were associated with a lower incidence of cavities and more variability in the force delivered. Subsequent studies performed in our research group using this technique have demonstrated enlarging syrinxes over time, with the largest cavities at the 12 week timepoint. The impactor model of syringomyelia is likely to be a useful model of syringomyelia. Furthermore, the cavities were consistently larger in animals with additional arachnoiditis from kaolin injections, which confirm the importance of

arachnoiditis to syrinx pathophysiology, similar to previous studies by Cho et al. and Seki et al. [191, 326].

However, spinal cord injury comprises a number of processes, including contusion, compression, ischaemia, and secondary excitotoxic insults. A contusional model will not reflect all these aspects. Compression models, such as aneurysm clips, calibrated forceps and thecal-sac constriction, may be alternative models that provide supplementary results, as observed in the AQP4 studies [419, 421, 422].

### 11.1.3 Pathophysiological processes

Numerous hydrodynamic theories have been proposed outlining the mechanism for CSF flow into syrinxes. Not many theories have considered the effect of fluid outflow. The natural history of syringomyelia is characterised by periods of stability and progression. During times of stability, fluid inflow must equal fluid outflow.

In terms of fluid inflow, there has been convincing evidence that CSF enters syrinx cavities via perivascular spaces [169, 204]. Bilston et al. postulated that CSF-arterial pulsation due to arachnoiditis may contribute to increased perivascular flow [171]. Subsequent computational models have confirmed the plausibility of CSF-arterial pulsation delays, but further *in-vivo* validation was necessary [205, 384]. The contribution of arachnoiditis to perivascular flow and validation of CSF-arterial pulsation delays in-vivo were examined in this thesis.

Using two different CSF tracers, CSF flow was demonstrated to be increased in the region of arachnoiditis along perivascular spaces. Technical challenges were encountered during this study, which related to the detection of HRP. HRP detection was impaired due to its variable enzymatic activity and a new tracer, Alexa-Fluor 647 Ovalbumin, was

used. These results concurred with the HRP studies. AFO also permitted the use of macroscopic fluorescent imaging technology to visualise the flow of tracer on a macroscopic scale. To the author's knowledge, this was the first study to use this technology to evaluate CSF flow. The benefit of AFO was that fluorescent microscopic images could also be obtained and its intensity might be more easily quantifiable.

Pressure manometry of CSF within the subarachnoid space had previously been performed in anaesthetised animals by Williams [239]. The effect of anaesthesia on arterial and respiratory variations could not be excluded. Telemetry monitoring of arterial pressures in non-anaesthetised animals had been performed previously in small and large animals. However, CSF pressures in the spinal subarachnoid space have never been monitored in unrestrained animals before, and the pulsation study in sheep was the first of its kind to use this telemetry equipment for CSF pressures. In this study, it was demonstrated that CSF pulsations across regions of arachnoiditis were increasingly delayed over the course of 6 weeks. Interestingly, the increase in pulsation delay concurred with a recent computational study by Cheng et al., who demonstrated that a shift in timing of the CSF cycle was dependent on the degree of subarachnoid space obstruction [517]. In particular, dorsal subarachnoid obstruction appeared to cause more significant delays. The implications from these findings are relevant to the rationale behind different surgical treatments. Expansile duraplasty or placement of a subarachnoid-subarachnoid shunt across regions of arachnoiditis may be effective not necessarily by providing an alternative route for CSF flow, but they may function by reducing the CSF-arterial pulsation delay. Thus, it may not be as important to ensure that the spinal cord is completely untethered by adhesiolysis, which may be associated with undue manipulation of the spinal cord. Perhaps, dorsal adhesiolysis alone may be sufficient to restore the normal timing between CSF and arterial pulsations.

The fluid outflow study has demonstrated that outflow occurs in a diffuse pattern away from the syrinx cavity towards the central canal and subarachnoid space, without any distinctive pathways. Previous studies by Milhorat et al. indicated a “sink action” towards the central canal, which was confirmed by CSF tracer studies by Stoodley et al. [167, 246]. The predominant fluid outflow towards the central canal may reflect the normal pattern of fluid drainage from the spinal cord parenchyma. As an alternative explanation, Klekamp suggested that extracellular fluid might drain towards the subarachnoid space, and syrinxes developed due to an obstruction to extracellular fluid outflow [1]. In summary, the pattern of interstitial fluid flow from the spinal cord parenchyma is still speculative. However, the presence of a fluid outflow in this study indicates that improving outflow mechanisms may be just as important in treating syringomyelia. Expansile duraplasty or syrinx-subarachnoid shunts may improve fluid outflow into the subarachnoid space.

Molecular changes with AQP expression in the setting of spinal cord injury and post-traumatic syringomyelia were investigated. Previous studies in our group demonstrated an increase in AQP4 expression in an excitotoxic extra-canalicular model of syringomyleia. The AQP4 and AQP1 expression studies were performed to validate the findings on the impactor model. Unfortunately, technical problems were encountered with AQP1 immunofluorescent staining, and this section of the study was not completed. Overall, the expression of AQP4 was increased in both the spinal cord injury and post-traumatic syrinx groups at the 3- and 6-week timepoints, but was decreased by 12 weeks. This may suggest that AQP may be important in the subacute period of spinal cord injury.

### 11.1.4 Modulation of processes and treatment implications

Evaluating the effect of AQP4 modulation on syringomyelia was an important study to determine whether there was a causal association between AQP4 function and syringomyelia. In this study, two AQP4 modulation agents, an agonist and an antagonist, were administered to animals with existing syrinxes. Previous experiments with these agents at the Univeristy of Adelaide had been performed as in-vitro studies on oocytes, and in-vivo studies in mouse models of hydrocephalus. This was the first study to use such agents in the setting of post-traumatic syringomyelia and spinal cord injury. The results demonstrated that the syrinx cavities were largest in the antagonist group, and smallest in the agonist group. This may suggest that AQP4 expression was increased in post-traumatic syringomyelia to promote fluid outflow. This concurs with findings from Nesic et al., who postulated that AQP4 was important at the later stages of spinal cord injury with vasogenic oedema [419]. Obviously, these findings are preliminary and further validation is required. However, it holds some hope for the development of a potential therapeutic agent in the future.

## *11.2 Future investigations*

The studies presented in this thesis have raised multiple questions, which need further examination.

With the syrinx fluid biochemistry study, only five patients were recruited for this study, and more patients will give greater statistical power to determine the significance of the small differences in the electrolytes of CSF and syrinx fluid. The biochemical profile consisted of a basic panel only, and additional tests could be performed. These may include cytology, electrophoresis, specific proteins, such as immunoglobulins and

proteoglycans. More specific tests may provide further insight into other processes of syrinx formation. In addition, information on the extracellular space and fluid can be obtained via animal studies. Iontophoresis is a technique that has been used to calculate the extracellular space volume in glioma specimens [518]. This could be applied onto our rodent syrinx and arachnoiditis models, in which the extracellular space volume could be calculated withinin the spinal cord. Patch-clamping techniques may be necessary to sample fluid from cells around syrinx cavities.

The impactor study used multiple animals at different timepoints. Individual variations could not be eliminated, and comparisons were made on the assumption that such variations had limited influence. Ideally, cavities could be monitored in the same individual animal at multiple time points with non-invasive imaging prior to sacrifice of the animal. Recently, a 9-Tesla MRI has become available for use in our research group and further validation of the impactor model could be performed.

Several methological problems were encountered with the CSF flow studies in this thesis. The problems with HRP detection and AFO penetration had already been mentioned. The ideal study would be to examine CSF flow in the same anaesthetised animal at multiple timepoints. An attempt was made to perform the in-vivo tracer studies under general anaesthetic, but multiple technical problems were encountered that could not be resolved within the scope of this thesis. To overcome the problem of leakage after tracer injection, a custom-made intrathecal catheter and cap were designed. However, persistent leakage of tracer around the catheter occurred. Moreover, the fluorescent tracer did not have adequate penetration through the bony laminae and soft tissues to be detected with the multi-spectral camera. Radioactive tracers, such as 125-iodine, or 14-carbon, are known

to have greater penetrance, but may be limited by the biosafety and ethical considerations for recovery experiments. Further refinement of such techniques is therefore required.

The CSF-arterial pulsation study has not been applied in the extracanalicular sheep model. This would validate the results and theories by Bilston et al. and Martin et al. [171, 384]. Some limitations of the current study will need to be addressed in future studies. The pressure catheters are pre-calibrated and gel-filled, thus making them very fragile and difficult to explant after each round of experiments. In addition, servicing of the equipment required returning the catheters to the manufacturers for refurbishment, adding to the overall costs of the project. The pressure traces had many artefacts, which were not easily corrected by filtering or mathematical transformations. A more sophisticated method of analysis may need to be developed.

Triple labelling of AQP4, AQP1 and GFAP was attempted for the AQP expression study, but could not be completed due to difficulties with the AQP1 labelling. Further work will follow to complete this study. Other studies may involve the Kir-4 channel that is associated with AQP4 expression. Perhaps, the Kir-4 may channel may generate the ionic gradient to promote water movement. Colocalisation of the Kir-4 channel may provide another target for modulation and potential therapeutic development.

Finally, the aquaporin modulation study shows early promise, but will need further validation in other models. More importantly, it will be worthwhile to assess whether administering the agents at the time of the initial spinal cord injury or syrinx induction would reduce the incidence of subsequent syrinx formation.

# Chapter 12 Conclusions

A unifying hypothesis that encompasses and explains the mechanisms involved for all types of syringomyelia seems unlikely. Syringomyelia may be the manifestation of different associated conditions, and different mechanisms may be involved in each type of syringomyelia. Better understanding of the pathogenesis of syringomyelia requires the collaboration between the various techniques, such as clinical and radiological observations, computational modeling and testing of hypotheses and validation on animal studies.

In this thesis, each stage of post-traumatic syringomyelia formation was considered. Experimental studies were performed to develop a direct impact model of syringomyelia, to confirm the effect of arachnoiditis on perivascular CSF flow and on CSF-arterial pulsation delays, and to evaluate the fluid outflow pathways. Molecular changes, such as the expression of AQP4, were investigated in animal models of syringomyelia. Perhaps, the most exciting finding was the role of AQP4 modulation on post-traumatic syringomyelia. Promotion of AQP4 function resulted in a reduction in the size of syrinxes, while inhibition caused syrinx enlargement. Modulation of aquaporins may provide a potential method for pharmaceutical therapy for syrinomyelia in the future.

# Chapter 13 Appendices

## *13.1 Publications*

1. **Wong, J.**, Hemley, S., Jones, N., Cheng, S., Bilston, L., Stoodley, M., *Fluid Outflow in a Large Animal Model of Post-traumatic Syringomyelia.* Neurosurgery, 2012. **71**(2): p. 474-80.
2. Cheng, S., Stoodley, M.A., **Wong, J**., Hemley, S., Fletcher, D.F., Bilston, L.E., *The presence of arachnoiditis affects the characteristics of CSF flow in the spinal subarachnoid space: a modelling study.* Journal of Biomechanics, 2012. **45**(7): p. 1186-91.
3. **Wong, J.**, Gragnaniello, C., Nader, R., Stoodley, M.A., *Syringo-subarachnoid and syringopleural shunts*, in *Neurosurgery Tricks of the Trade*, R. Nader, S. Berta, and M. Levy, Editors. 2013, Thieme New York. p. 644 – 647.
4. Stoodley, M.A., Bilston, L.E., Brodbelt, A.R., Hemley, S.J., **Wong, J.H.**, *The Filling Mechanism*, in *Syringomyelia: A Disorder of CSF Circulation*, G. Flint and C. Rusbridge, Editors. 2014, Springer: Heidelberg. p. 87 – 102.

## *13.2 Manuscripts in preparation or submitted for publication*

1. **Wong, J.H.**, Song, X., Bilston, L.E., Stoodley, M.A., *Direct trauma model of post-traumatic syringomyelia with computer-controlled motorized spinal cord impactor.* Journal of Neurotrauma (manuscript in preparation)
2. **Wong, J.H.**, Liu, S., Koustais, S., Stoodley, M.A., *Syringomyelia and foramen magnum arachnoiditis. Review of literature and implications for treatment.* Journal of Clinical Neuroscience (manuscript in preparation)

3. **Wong, J.H.**, Hemley, S.J., Bilston, L.E., Brodbelt, A.R., Stoodley, M.A., *Biochemical analysis of syringomyelia fluid*. Journal of Clinical Neuroscience (manuscript in preparation)
4. Hu, H.Z, **Wong, J.**, Song, S., Taylor, R., Thompson, P., Stoodley, M. *Glial responses in a rat model of post-traumatic syringomyelia*. Nature Spinal Cord (manuscript in preparation)

## 13.3 Presentations at scientific meetings

1. **Wong, J.**, Hwang, A., Song, X., Yool, A., Bilston, L., Stoodley, M. *The effect of aquaporin-4 modulation on post-traumatic syringomyelia in a rodent model.* Neurosurgical Society of Australasia Annual Scientific Meeting, October 2012, Gold Coast, Queensland (Awarded the Peter Leech Memorial Prize for best research paper by a neurosurgical trainee)
2. **Wong, J.**, Hwang, A., Stoodley, M. *Cerebrospinal fluid flow in spinal arachnoiditis and post-traumatic syringomyelia.* Neurosurgical Society of Australasia Annual Scientific Meeting, October 2012, Gold Coast, Queensland
3. **Wong, J.**, Song, X., Stoodley, M. *A reproducible impact model of post-traumatic syringomyelia.* Neurosurgical Society of Australasia Annual Scientific Meeting, September 2011, Denaru Island, Fiji
4. **Wong, J.**, Song, X., Hwang, A., Stoodley, M. *A reproducible impact model and evolving concepts of fluid flow in post-traumatic syringomyelia.* Adelaide Centre for Spinal Research Spinal Symposium IX, August 2011, Glenelg, South Australia.

5. **Wong, J.,** Stoodley, M. *Developing a reproducible impact model for post-traumatic syringomyelia.* International Symposium for Syringomyelia. December 2010, Berlin, Germany.
6. **Wong, J.,** Stoodley, M. *Developing a reproducible impact model for post-traumatic syringomyelia.* Surgical Research Society of Australasia, 47th Annual Scientific Meeting. November 2010, Adelaide, South Australia.
7. **Wong, J.H.Y**., Hemley, S.J., Jones, N.R., Stoodley, M.A. *Fluid outflow pathways in post-traumatic syringomyelia.* Neurosurgical Society of Australasia Annual Scientific Meeting, September 2010, Sunshine Coast, Queensland.
8. **Wong, J.,** Stoodley, M. *Developing a direct trauma model for post-truamatic syringomyelia: Preliminary findings.* Adelaide Centre for Spinal Research Spinal Symposium VIII, August 2010, Adelaide, South Australia.

## 13.4 Prizes and scholarships

1. Peter Leech Memorial Prize 2012 – Awarded to the best research paper by a neurosurgical trainee at the Neurosurgical Society of Australasia Annual Scientific Meeting
2. Royal Australasian College of Surgeons - *Sir Roy McCaughey Surgical Research Fellowship* 2011
3. Neurosurgical Society of Australasia – *Research Scholarship* 2011
4. Royal Australasian College of Surgeons – *Eric Bishop Scholarship* 2010
5. Macquarie University – *Post-graduate Research Fund Scholarship* 2010
6. Neurosurgical Society of Australasia – *Synthes Spinal Research Scholarship* 2009

Pages 318-320 of this thesis have been removed as they may contain sensitive/confidential content

## *13.6 Operative monitoring and post-operative monitoring sheets*

**Operative Monitoring Sheet**

| AQP Modulation | Rat No. | | Survival: | Laml + Q4 Inject + Kaolin | | ARA no. 2010/26 | | |
|---|---|---|---|---|---|---|---|---|
| Date | Body weight: | | | maintenance: Isoflurane | | Chief Investigator | | Prof H. Stoodley |
| Surgeon | spp/sex: rat/male | | Antibiotic: no | mask/intub: nose cone | | Contact | | J Wong |
| Asslst | strain: SD | | Induction: Isoflurane | analgesic: 0.2-0.25 mL temgesic | | Tel. | | 9.8E+07 |
| Time | On table | 5 | 10 | 15 | 30 | 45 | 60 | 1:15 | 1:30 | 1:45 | 2:00 |
| actual | | | | | | | | | | | |
| O2 L/min | | | | | | | | | | | |
| anaesthetic | | | | | | | | | | | |
| pedal W. reflex | | | | | | | | | | | |
| respiration | | | | | | | | | | | |
| core body temp | | | | | | | | | | | |
| periphery colour | | | | | | | | | | | |
| notes | | | | | | | | | | | |
| Post op | Time 0 | 5 | 10 | 15 | 30 | 45 | 60 | | | | |
| actual | | | | | | | | | | | |
| respiration | | | | | | | | | | | |
| ambulation | | | | | | | | | | | |
| core body temp | | | | | | | | | | | |
| ml temgesic | | | | | | | | | | | |
| ml saline | | | | | | | | | | | |
| notes | | | | | | | | | | | |
| Operative notes and comments | | | | | | | | | | | |

## Post-Operative/Acute Treatment Animal Monitoring Sheet: OBSERVATION RECORDS

| | | | |
|---|---|---|---|
| Chief Investigator: | Dr Marcus Stoodley (ASAM) | | |
| ARA no: | 2009/49 | | EMERGENCY CONTACT: Johnny Wong |
| Animal ID: | Rat No. 18 | 06B3DACF | Mobile: 0414506521 |
| Date of procedure: | 11/02/2011 | | |
| Procedure undertaken: | Laminectomy + Kaolin | | Initial Weight: 388.8g |

1) DETAILS OF ANY ABNORMAL FINDINGS MUST BE RECORDED ON THE INCIDENT RECORD; Refer to ASAM SOP for score criteria.
2) Animals found to be exhibiting significant abnormalities must be euthanased immediately and reported to the Animal Welfare Officer

| | Days Post-Op | 1 | 2 | 3 | 4 | 5 | 6 | 7 | 8 | 9 | 10 | 11 | 12 | 13 | 14 |
|---|---|---|---|---|---|---|---|---|---|---|---|---|---|---|---|
| | Date & Time: | | | | | | | | | | | | | | |
| | Observer's Initials (print): | | | | | | | | | | | | | | |
| | Body Weight: | . | . | . | . | . | . | . | . | . | . | . | . | . | . |
| Subjective score | (Score /10) | | | | | | | | | | | | | | |
| Distant Examination | (Score /16) | . | . | . | . | . | . | . | . | . | . | . | . | . | . |
| | Coat appearance ( /3) | . | . | . | . | . | . | . | . | . | . | . | . | . | . |
| | Behaviour ( /3) | . | . | . | . | . | . | . | . | . | . | . | . | . | . |
| | Breathing ( /3) | | | | | | | | | | | | | | |
| | Gait ( /3) | | | | | | | | | | | | | | |
| | Posture ( /3) | | | | | | | | | | | | | | |
| Close Examination | (Score /8) | . | . | . | . | . | . | . | . | . | . | . | . | . | . |
| | Body weight ( /3) | | | | | | | | | | | | | | |
| | Wound site ( /3) | | | | | | | | | | | | | | |
| | Wound palpation ( /3) | | | | | | | | | | | | | | |
| TOTAL | (SCORE /34) | . | . | . | . | . | . | . | . | . | . | . | . | . | . |

## *13.7 Paraffin embedding and staining protocols*

### 13.7.1 Paraffin Embedding Schedule (Leica ASP200S)

**Table 13.7-1 Paraffin embedding schedule for Leica ASP200S**

| Substance | Concentration | Time | Temperature |
|---|---|---|---|
| Formalin | | 30 minutes | |
| Ethanol | 70% | 10 minutes | |
| Ethanol | 90% | 10 minutes | |
| Ethanol | 100% | 10 minutes | |
| Ethanol | 100% | 10 minutes | |
| Ethanol | 100% | 20 minutes | |
| Ethanol | 100% | 20 minutes | |
| Xylene | | 10 minutes | |
| Xylene | | 10 minutes | |
| Xylene | | 20 minutes | |
| Paraffin Wax | | 20 minutes | $65^0$C |
| Paraffin Wax | | 20 minutes | $65^0$C |
| Paraffin Wax | | 30 minutes | $65^0$C |

### 13.7.2 Haematoxylin and eosin staining (Lillie-Mayer method)

**Table 13.7-2 Haematoxylin and eosin staining (Lillie-Mayer) method**

| Substance | Time |
|---|---|
| Xylene | 2 minutes |
| Xylene | 2 minutes |
| Ethanol 100% | 1 minute |
| Ethanol 90% | 1 minute |
| Distilled $H_2O$ | 1 minute |
| Haematoxylin | 5 minutes |
| Running $H_2O$ | Rinse for 1 minute |
| Differentiator (2% Acid alcohol) | 1 quick dip |
| Distilled $H_2O$ | 15 seconds |
| Blueing solution (supersaturated $Li_2CO_3$) | 10 – 15 seconds |
| Running $H_2O$ | Rinse for 5 minutes |
| Eosin Working Solution | 2 minutes |
| Ethanol 90% | 15 seconds |
| Ethanol 100% | 15 seconds |
| Ethanol 100% | 15 seconds |
| Xylene | 2 minutes |
| Xylene | 2 minutes |
| Mounting agent (Depex) + coverslipping | |

### 13.7.3 TMB staining for HRP

**Table 13.7-3 TMB staining method for HRP**

| Substance | Time |
|---|---|
| Distilled $H_2O$ | 15 seconds |
| Sodium nitroferricyanide (III) di hydrate & TMB | Combine and incubate for 20 minutes, stirring with low heat |
| Hydrogen Peroxide (30 μL) | Add, and incubate for 20 minutes |
| Sodium Acetate Buffer | 15 seconds |
| Sodium Acetate Buffer | 15 seconds |
| Ammonium Molybdate | 15 minutes |
| Sodium Acetate Buffer | 30 seconds |
| Ethanol 95% | 30 seconds |
| Ethanol 100% | 30 seconds |
| Ethanol 100% | 30 seconds |
| Xylene | 2 minutes |
| Xylene | 2 minutes |
| Mounting agent (Depex) + coverslipping | |

# Chapter 14 References


1. Klekamp, J., *The pathophysiology of syringomyelia - historical overview and current concept.* Acta Neurochirurgica, 2002. **144**(7): p. 649-64.

2. Brodbelt, A.R. and M.A. Stoodley, *Post-traumatic syringomyelia: a review.* Journal of Clinical Neuroscience, 2003. **10**(4): p. 401-8.

3. Pearce, J.M.S., *Syringes and syringomyelia.* European Neurology, 2005. **54**(4): p. 243.

4. Hakan, T., *Neurosurgery and a small section from the Greek myth: the God Pan and Syrinx.* Childs Nervous System, 2009. **25**(12): p. 1527-9.

5. Gutmann, L., *Personal history: the pipes of pan.[see comment]*. Neurology, 2005. **64**(8): p. 1483-4.

6. Estienne, C., *La Dissection des Parties du corps humain divisee en trois livres*1546, Paris: Simon de Collines.

7. Brunner, J.C., *De Hydrocephalo, sive Hydrops capitis*, in *Sepelchretum, Book 1*, T. Bonneti, Editor 1700, Cramer and Perachin: Geneva. p. 396.

8. Madsen, P.W., 3rd, R.P. Yezierski, and V.R. Holets, *Syringomyelia: clinical observations and experimental studies.* Journal of Neurotrauma, 1994. **11**(3): p. 241-54.

9. Abbe, R. and W.B. Cooley, *Syringomyelia. Operation: exploration of cord, withdrawal of fluid, exhibition of patient.* J Nerv Ment Dis, 1892. **19**: p. 512-520.

10. Schijman, E. and E. Schijman, *History, anatomic forms, and pathogenesis of Chiari I malformations.* Childs Nervous System, 2004. **20**(5): p. 323-8.

11. Bejjani, G.K., *Definition of the adult Chiari malformation: a brief historical overview.* Neurosurgical Focus, 2001. **11**(1): p. 1-8.

12. Cleland, J., *Contribution to the study of spina bifida, encephalocoele, and anencephalus.* J Anat Physiol, 1883. **17**: p. 257-292.

13. Chiari, H., *Yber Veranderungen des Kleinhirns infolge von Hydrocephalie des Grosshirns.* Dtsch Med Wochenschr, 1891. **17**: p. 1172-1175.

14. Chiari, H., *Uber Veranderungen des Kleinhirns, des Pons und der Medulla oblongata infolge von kongenitaler Hydrocephalie des Grosshirns.* Denkschr Akad Wiss Wien, 1896. **63**: p. 71-116.

15. Bastian, H.C., *On a case of concussion-lesion, with extensive secondary degenerations of the spinal cord, followed by general muscular atrophy.* Med Chir Trans (Series II), 1867: p. 499-542.

16. Silver, J.R., *History of post-traumatic syringomyelia: post traumatic syringomyelia prior to 1920.* Spinal Cord, 2001. **39**(3): p. 176-83.

17. Ollivier-d'Anger, C.P., *De la moelle epiniere et ses maladies*. 2nd ed1827, Paris: Chez Crevot.

18. Klekamp, J. and M. Samii, *Syringomyelia: diagnosis and treatment*2002, Heidelberg: Springer-Verlag Berlin.

19. Poser, C.M., *The relationship between syringomyelia and neoplasms.* , ed. C.C. Thomas1956, Springfield.

20. Ballantine, H.T.J., R.G. Ojemann, and J.H. Drew, *Syringohydromyelia*, in *Progress in Neurological Surgery*, H. Krayenbuhl, M. P.E., and W.H. Sweet, Editors. 1971, Karger: Basel. p. 227 - 245.

21. Barnett, H.J., A.T. Jousse, and M.J. Ball, *Pathology and pathogenesis of progressive cystic myelopathy as a late sequel to spinal cord injury*, in *Syringomyelia*, H.J. Barnett, J.B. Foster, and P. Hudgson, Editors. 1973, W.B. Saunders: London. p. 179 - 219.

22. Di Lorenzo, N. and F. Cacciola, *Adult syringomielia. Classification, pathogenesis and therapeutic approaches.* Journal of Neurosurgical Sciences, 2005. **49**(3): p. 65-72.

23. Milhorat, T.H., *Classification of syringomyelia.* Neurosurgical Focus, 2000. **8**(3): p. E1.

24. Reddy, K.K.V., M.R. Del Bigio, and G.R. Sutherland, *Ultrastructure of the human posttraumatic syrinx.* Journal of Neurosurgery, 1989. **71**(2): p. 239-243.

25. Oakley, J.C., G.A. Ojemann, and E.C. Alvord, Jr., *Posttraumatic syringomyelia. Case report.* Journal of Neurosurgery, 1981. **55**(2): p. 276-81.

26. Sherman, J.L., A.J. Barkovich, and C.M. Citrin, *The MR appearance of syringomyelia: new observations.* AJR. American journal of roentgenology, 1987. **148**(2): p. 381-91.

27. Batzdorf, U., *Primary spinal syringomyelia. Invited submission from the joint section meeting on disorders of the spine and peripheral nerves, March 2005.* Journal of neurosurgery. Spine, 2005. **3**(6): p. 429-35.

28. Brickell, K.L., et al., *Ethnic differences in syringomyelia in New Zealand.* Journal of Neurology, Neurosurgery & Psychiatry, 2006. **77**(8): p. 989-91.

29. Bonfield, C.M., et al., *Surgical management of post-traumatic syringomyelia.* Spine, 2010. **35**(21 Suppl): p. S245-58.

30. Carroll, A.M., et al., *Post-traumatic syringomyelia: a review of the cases presenting in a regional spinal injuries unit in the north east of England over a 5-year period.* Spine, 2005. **30**(10): p. 1206-10.

31. Rossier, A.B., et al., *Posttraumatic cervical syringomyelia. Incidence, clinical presentation, electrophysiological studies, syrinx protein and results of conservative and operative treatment.* Brain, 1985. **108**(Pt 2): p. 439-61.

32. Umbach, I. and A. Heilporn, *Review article: post-spinal cord injury syringomyelia.* Paraplegia, 1991. **29**(4): p. 219-21.

33. Edgar, R. and P. Quail, *Progressive post-traumatic cystic and non-cystic myelopathy.* British Journal of Neurosurgery, 1994. **8**(1): p. 7-22.

34. Batzdorf, U., *Primary spinal syringomyelia: a personal perspective.* Neurosurgical Focus, 2000. **8**(3): p. E7.

35. Squier, M.V. and R.P. Lehr, *Post-traumatic syringomyelia.* Journal of Neurology, Neurosurgery & Psychiatry, 1994. **57**(9): p. 1095-8.

36. Sett, P. and H.A. Crockard, *The value of magnetic resonance imaging (MRI) in the follow-up management of spinal injury.[Erratum appears in Paraplegia 1992 Feb;30(2):151], [Erratum appears in Paraplegia 1992 Jan;30(1):76].* Paraplegia, 1991. **29**(6): p. 396-410.

37. Lee, T.T., et al., *Surgical treatment of post-traumatic myelopathy associated with syringomyelia.* Spine, 2001. **26**(24 Suppl): p. S119-27.

38. Lee, T.T., et al., *Outcome after surgical treatment of progressive posttraumatic cystic myelopathy.* Journal of Neurosurgery, 2000. **92**(2 Suppl): p. 149-54.

39. Birbamer, G., et al., *Spontaneous collapse of posttraumatic syringomyelia: serial magnetic resonance imaging.* European Neurology, 1993. **33**(5): p. 378-81.

40. Mariani, C., et al., *The natural history and results of surgery in 50 cases of syringomyelia.* Journal of Neurology, 1991. **238**(8): p. 433-8.

41. Schlesinger, E.B., et al., *Hydromyelia: clinical presentation and comparison of modalities of treatment.* Neurosurgery, 1981. **9**(4): p. 356-65.

42. el Masry, W.S. and A. Biyani, *Incidence, management, and outcome of post-traumatic syringomyelia. In memory of Mr Bernard Williams.* Journal of Neurology, Neurosurgery & Psychiatry, 1996. **60**(2): p. 141-6.

43. Biyani, A. and W.S. el Masry, *Post-traumatic syringomyelia: a review of the literature.* Paraplegia, 1994. **32**(11): p. 723-31.

44. Honan, W.P. and B. Williams, *Sensory loss in syringomyelia: not necessarily dissociated.* Journal of the Royal Society of Medicine, 1993. **86**(9): p. 519-20.

45. Nakamura, M., et al., *Clinical significance and prognosis of idiopathic syringomyelia.* Journal of Spinal Disorders & Techniques, 2009. **22**(5): p. 372-5.

46. Todor, D.R., H.T. Mu, and T.H. Milhorat, *Pain and syringomyelia: a review.* Neurosurgical Focus, 2000. **8**(3): p. E11.

47. Ono, A., et al., *Surgical outcomes of foramen magnum decompression for syringomyelia associated with Chiari I malformation: relation between the location of the syrinx and body pain.* Journal of Orthopaedic Science, 2010. **15**(3): p. 299-304.

48. Nakamura, M., et al., *Retrospective study of surgery-related outcomes in patients with syringomyelia associated with Chiari I malformation: clinical significance of changes in the size and localization of syrinx on pain relief.* Journal of Neurosurgery: Spine, 2004. **100**(3): p. 241-244.

49. Attal, N., et al., *Effects of surgery on the sensory deficits of syringomyelia and predictors of outcome: a long term prospective study.* Journal of Neurology, Neurosurgery & Psychiatry, 2004. **75**(7): p. 1025-1030.

50. Berry, R.G., R.A. Chambers, and F.D. Lublin, *Syringoencephalomyelia (Syringocephalus).* Journal of Neuropathology & Experimental Neurology, 1981. **40**(6): p. 633-644.

51. Nogues, M.A., *Syringomyelia and syringobulbia.* Handbook of Clinical Neurology, 1987. **6**(50): p. 443 - 464.

52. Hida, K., et al., *Pediatric syringomyelia with chiari malformation: its clinical characteristics and surgical outcomes.* Surgical Neurology, 1999. **51**(4): p. 383-90; discussion 390-1.

53. Isu, T., et al., *Scoliosis associated with syringomyelia presenting in children.* Child's nervous system : ChNS : official journal of the International Society for Pediatric Neurosurgery, 1992. **8**(2): p. 97-100.

54. Kan, S., et al., *Delayed CT metrizamide enhancement of syringomyelia secondary to tumor.* AJNR. American journal of neuroradiology, 1983. **4**(1): p. 73-8.

55. Mehalic, T.F., R.T. Pezzuti, and B.I. Applebaum, *Magnetic Resonance Imaging and Cervical Spondylotic Myelopathy.* Neurosurgery, 1990. **26**(2): p. 217-227.

56. Gottschalk, A., et al., *Dynamic visualization of arachnoid adhesions in a patient with idiopathic syringomyelia using high-resolution cine magnetic resonance imaging at 3T.* Journal of magnetic resonance imaging : JMRI, 2010. **32**(1): p. 218-22.

57. Akiyama, Y., et al., *Interstitial spinal-cord oedema in syringomyelia associated with Chiari type 1 malformations.* Journal of neurology, neurosurgery, and psychiatry, 2008. **79**(10): p. 1153-8.

58. Levy, E.I., et al., *Spinal cord swelling preceding syrinx development. Case report.[Erratum appears in J Neurosurg 2000 Apr;92(2 Suppl):249].* Journal of Neurosurgery, 2000. **92**(1 Suppl): p. 93-7.

59. Fischbein, N.J., et al., *The "presyrinx" state: a reversible myelopathic condition that may precede syringomyelia.* Ajnr: American Journal of Neuroradiology, 1999. **20**(1): p. 7-20.

60. Donauer, E. and K. Rascher, *Syringomyelia: a brief review of ontogenetic, experimental and clinical aspects.* Neurosurgical review, 1993. **16**(1): p. 7-13.

61. Panigrahi, M., et al., *CSF flow study in Chiari I malformation.* Child's nervous system : ChNS : official journal of the International Society for Pediatric Neurosurgery, 2004. **20**(5): p. 336-40.

62. Lichtor, T., P. Egofske, and N. Alperin, *Noncommunicating cysts and cerebrospinal fluid flow dynamics in a patient with a Chiari I malformation and syringomyelia--part II.* Spine, 2005. **30**(12): p. 1466-72.

63. Wong, J., et al., *Fluid outflow in a large-animal model of posttraumatic syringomyelia.* Neurosurgery, 2012. **71**(2): p. 474-80.

64. Koc, K., et al., *Chiari 1 malformation with syringomyelia: correlation of phase-contrast cine MR imaging and outcome.* Turkish Neurosurgery, 2007. **17**(3): p. 183-92.

65. Dohrmann, G.J. and J.M. Rubin, *Intraoperative ultrasound imaging of the spinal cord: Syringomyelia, cysts, and tumors — A preliminary report.* Surgical Neurology, 1982. **18**(6): p. 395-399.

66. Moriwaka, F., et al., *[Epidemiology of syringomyelia in Japan--the nationwide survey]*. Rinsho shinkeigaku = Clinical neurology, 1995. **35**(12): p. 1395-7.

67. Milhorat, T.H., et al., *Chiari I malformation redefined: clinical and radiographic findings for 364 symptomatic patients.[see comment]*. Neurosurgery, 1999. **44**(5): p. 1005-17.

68. Fernandez, A.A., et al., *Malformations of the craniocervical junction (Chiari type I and syringomyelia: classification, diagnosis and treatment).* BMC musculoskeletal disorders, 2009. **10 Suppl 1**: p. S1.

69. Aboulezz, A.O., et al., *Position of cerebellar tonsils in the normal population and in patients with Chiari malformation: a quantitative approach with MR imaging.* Journal of computer assisted tomography, 1985. **9**(6): p. 1033-6.

70. Brodbelt, A.R., M.A. Stoodley, and N.R. Jones, *Non-traumatic syringomyelia*, in *The Cervical Spine*, C.R. Clark, Editor 2005, Lippincott Williams & Wilkins: Philadelphia. p. 746 - 767.

71. Masur, H. and C. Oberwittler, *Syringomyelia in Chiari malformation: relation to extent of cerebellar tissue herniation.* Neurosurgery, 1993. **33**(5): p. 948-9.

72. Stovner, L.J. and P. Rinck, *Syringomyelia in Chiari malformation: relation to extent of cerebellar tissue herniation.* Neurosurgery, 1992. **31**(5): p. 913-7; discussion 917.

73. Narayan, P., et al., *Clinical significance of cervicomedullary deformity in Chiari II malformation.* Pediatric neurosurgery, 2001. **35**(3): p. 140-4.

74. Iskandar, B.J., et al., *The resolution of syringohydromyelia without hindbrain herniation after posterior fossa decompression.* Journal of Neurosurgery, 1998. **89**(2): p. 212-6.

75. Iskandar, B.J., et al., *The resolution of syringohydromyelia without hindbrain herniation after posterior fossa decompression.* Neurosurgical Focus, 2000. **8**(3): p. 1-5.

76. Tubbs, R.S., et al., *Analysis of the posterior fossa in children with the Chiari 0 malformation.* Neurosurgery, 2001. **48**(5): p. 1050-4; discussion 1054-5.

77. Klekamp, J., et al., *Syringomyelia in association with tumours of the posterior fossa. Pathophysiological considerations, based on observations on three related cases.* Acta Neurochirurgica, 1995. **137**(1-2): p. 38-43.

78. Klekamp, J., et al., *Syringomyelia associated with foramen magnum arachnoiditis.* Journal of Neurosurgery, 2002. **97**(3 Suppl): p. 317-22.

79. Barnett, H.J. and A.T. Jousse, *Syringomyelia as a late sequel to traumatic paraplegia and quadriplegia - clinical features.*, in *Syringomyelia*, H.J. Barnett, J.B. Foster, and P. Hudgson, Editors. 1973, W.B. Saunders: London. p. 129-153.

80. Barnett, H.J., *Syringomyelia associated with spinal arachnoiditis*, in *Syringomyelia*, H.J. Barnett, J.B. Foster, and R.J. Hudgins, Editors. 1973, WB Saunders: London. p. 220 - 244.

81. Koyanagi, I., et al., *Clinical features and pathomechanisms of syringomyelia associated with spinal arachnoiditis.* Surgical Neurology, 2005. **63**(4): p. 350-5; discussion 355-6.

82. Reis, A.J., *New surgical approach for late complications from spinal cord injury.* BMC surgery, 2006. **6**: p. 12.

83. Brammah, T.B. and M.I. Jayson, *Syringomyelia as a complication of spinal arachnoiditis.* Spine, 1994. **19**(22): p. 2603-5.

84. Caplan, L.R., A.B. Norohna, and L.L. Amico, *Syringomyelia and arachnoiditis.* Journal of neurology, neurosurgery, and psychiatry, 1990. **53**(2): p. 106-13.

85. Mallucci, C.L., et al., *Idiopathic syringomyelia and the importance of occult arachnoid webs, pouches and cysts.* British Journal of Neurosurgery, 1997. **11**(4): p. 306-9.

86. Parker, F., N. Aghakhani, and M. Tadie, *[Non-traumatic arachnoiditis and syringomyelia. A series of 32 cases]*. Neuro-Chirurgie, 1999. **45 Suppl 1**: p. 67-83.

87. Samii, M. and J. Klekamp, *Surgical results of 100 intramedullary tumors in relation to accompanying syringomyelia.* Neurosurgery, 1994. **35**(5): p. 865-73; discussion 873.

88. Fox, J.L., et al., *Syrinx of the conus medullaris and filum terminale in association with multiple hemangioblastomas.* Surgical Neurology, 1985. **24**(3): p. 265-71.

89. Nagahiro, S., et al., *Syringomyelia and syringobulbia associated with an ependymoma of the cauda equina involving the conus medullaris: case report.* Neurosurgery, 1986. **18**(3): p. 357-60.

90. Erkan, K., F. Unal, and T. Kiris, *Terminal syringomyelia in association with the tethered cord syndrome.* Neurosurgery, 1999. **45**(6): p. 1351-9; discussion 1359-60.

91. Erkan, K., et al., *Treatment of terminal syringomyelia in association with tethered cord syndrome: clinical outcomes with and without syrinx drainage.* Neurosurgical Focus, 2000. **8**(3): p. E9.

92. Iskandar, B.J., et al., *Terminal syringohydromyelia and occult spinal dysraphism.* Journal of Neurosurgery, 1994. **81**(4): p. 513-9.

93. Koyanagi, I., et al., *Surgical treatment of syringomyelia associated with spinal dysraphism.* Child's nervous system : ChNS : official journal of the International Society for Pediatric Neurosurgery, 1997. **13**(4): p. 194-200.

94. Butteriss, D.J. and D. Birchall, *A case of syringomyelia associated with cervical spondylosis.* The British journal of radiology, 2006. **79**(946): p. e123-5.

95. Kimura, R., et al., *Syringomyelia caused by cervical spondylosis.* Acta Neurochirurgica, 2004. **146**(2): p. 175-8.

96. Kaar, G.F., J.M. N'Dow, and S.H. Bashir, *Cervical spondylotic myelopathy with syringomyelia.* British Journal of Neurosurgery, 1996. **10**(4): p. 413-5.

97. Milhorat, T.H., et al., *Pathological basis of spinal cord cavitation in syringomyelia: analysis of 105 autopsy cases.* Journal of Neurosurgery, 1995. **82**(5): p. 802-12.

98. Hirata, Y., Y. Matsukado, and M. Kaku, *Syringomyelia associated with a foramen magnum meningioma.* Surgical Neurology, 1985. **23**(3): p. 291-4.

99. Quencer, R.M., T. el Gammal, and G. Cohen, *Syringomyelia associated with intradural extramedullary masses of the spinal canal.* AJNR. American journal of neuroradiology, 1986. **7**(1): p. 143-8.

100. Milhorat, T.H., et al., *Anatomical basis of syringomyelia occurring with hindbrain lesions.* Neurosurgery, 1993. **32**(5): p. 748-54; discussion 754.

101. Kastrup, A., T. Nägele, and H. Topka, *Spontaneous resolution of idiopathic syringomyelia.* Neurology, 2001. **57**(8): p. 1519-1521.

102. Kyoshima, K., et al., *Spontaneous resolution of syringomyelia: report of two cases and review of the literature.* Neurosurgery, 2003. **53**(3): p. 762-8; discussion 768-9.

103. Ataizi, S., et al., *Spontaneously resorbed idiopathic syringomyelia: a case report.* Turkish Neurosurgery, 2007. **17**(4): p. 247-50.

104. Brodbelt, A.R. and M.A. Stoodley, *Syringomyelia and the arachnoid web.* Acta Neurochirurgica, 2003. **145**(8): p. 707-11; discussion 711.

105. Kyoshima, K., et al., *Syringomyelia without hindbrain herniation: tight cisterna magna. Report of four cases and a review of the literature.* Journal of Neurosurgery, 2002. **96**(2 Suppl): p. 239-49.

106. Kaden, B., et al., *Disappearance of syringomyelia following resection of extramedullary lesion. A contribution to the aetiological enigma of syringomyelia.* Acta Neurochirurgica, 1993. **123**(3-4): p. 211-3.

107. Holly, L.T., et al., *Treatment of posttraumatic syringomyelia with extradural decompressive surgery.* Neurosurgical Focus, 2000. **8**(3): p. E8.

108. Wiedemayer, H., et al., *Operative treatment and prognosis of syringomyelia.* Neurosurgical review, 1994. **17**(1): p. 37-41.

109. Shannon, N., et al., *Clinical features, investigation and treatment of post-traumatic syringomyelia.* Journal of neurology, neurosurgery, and psychiatry, 1981. **44**(1): p. 35-42.

110. Vernon, J.D., J.R. Silver, and L. Symon, *Post-traumatic syringomyelia: the results of surgery.* Paraplegia, 1983. **21**(1): p. 37-46.

111. Lyons, B.M., et al., *The diagnosis and management of post traumatic syringomyelia.* Paraplegia, 1987. **25**(4): p. 340-50.

112. Rocque, B.G., et al., *Treatment practices for Chiari malformation Type I with syringomyelia: results of a survey of the American Society of Pediatric Neurosurgeons.* Journal of Neurosurgery: Pediatrics, 2011. **8**(5): p. 430-437.

113. Kotil, K., et al., *Delamination technique together with longitudinal incisions for treatment of Chiari I/syringomyelia complex: a prospective clinical study.* Cerebrospinal Fluid Research, 2009. **6**: p. 7.

114. Attenello, F.J., et al., *Suboccipital decompression for Chiari I malformation: outcome comparison of duraplasty with expanded polytetrafluoroethylene dural substitute versus pericranial autograft.* Childs Nervous System, 2009. **25**(2): p. 183-90.

115. Aghakhani, N., et al., *Surgical treatment of posttraumatic syringomyelia.* Neurosurgery, 2010. **66**(6): p. 1120-7; discussion 1127.

116. Aghakhani, N., et al., *Long-term follow-up of Chiari-related syringomyelia in adults: analysis of 157 surgically treated cases.* Neurosurgery, 2009. **64**(2): p. 308-15; discussion 315.

117. Levy, W.J., L. Mason, and J.F. Hahn, *Chiari malformation presenting in adults: a surgical experience in 127 cases.* Neurosurgery, 1983. **12**(4): p. 377-90.

118. Milhorat, T.H., W.D. Johnson, and J.I. Miller, *Syrinx shunt to posterior fossa cisterns (syringocisternostomy) for bypassing obstructions of upper cervical theca.* Journal of Neurosurgery, 1992. **77**(6): p. 871-4.

119. Williams, B., *Simultaneous cerebral and spinal fluid pressure recordings. 2. Cerebrospinal dissociation with lesions at the foramen magnum.* Acta Neurochirurgica, 1981. **59**(1-2): p. 123-42.

120. Guyotat, J., et al., *Syringomyelia associated with type I Chiari malformation. A 21-year retrospective study on 75 cases treated by foramen magnum decompression with a special emphasis on the value of tonsils resection.* Acta Neurochirurgica, 1998. **140**(8): p. 745-54.

121. Park, J.K., et al., *Presentation and management of Chiari I malformation in children.* Pediatric neurosurgery, 1997. **26**(4): p. 190-6.

122. Wong, J., et al., *Syringo-subarachnoid and syringopleural shunts*, in *Neurosurgery Tricks of the Trade*, R. Nader, S. Berta, and M. Levy, Editors. 2014, Thieme New York. p. 644-7.

123. Peerless, S.J. and Q.J. Durward, *Management of syringomyelia: a pathophysiological approach.* Clinical neurosurgery, 1983. **30**: p. 531-76.

124. Hida, K., et al., *Surgical indication and results of foramen magnum decompression versus syringosubarachnoid shunting for syringomyelia associated with Chiari I malformation.* Neurosurgery, 1995. **37**(4): p. 673-8; discussion 678-9.

125. Sgouros, S. and B. Williams, *A critical appraisal of drainage in syringomyelia.* Journal of Neurosurgery, 1995. **82**(1): p. 1-10.

126. Batzdorf, U., J. Klekamp, and J.P. Johnson, *A critical appraisal of syrinx cavity shunting procedures.* Journal of Neurosurgery, 1998. **89**(3): p. 382-8.

127. Tator, C.H. and C. Briceno, *Treatment of syringomyelia with a syringosubarachnoid shunt.* The Canadian journal of neurological sciences. Le journal canadien des sciences neurologiques, 1988. **15**(1): p. 48-57.

128. Iwasaki, I.K., K. Hida, H. Abe, Y., *Syringo-subarachnoid shunt for syringomyelia using partial hemilaminectomy.* British Journal of Neurosurgery, 1999. **13**(1): p. 41-45.

129. Iwasaki, Y., et al., *Syringo-subarachnoid shunt for syringomyelia using partial hemilaminectomy.* British Journal of Neurosurgery, 1999. **13**(1): p. 41-5.

130. Iwasaki, Y., et al., *Reevaluation of syringosubarachnoid shunt for syringomyelia with Chiari malformation.* Neurosurgery, 2000. **46**(2): p. 407-12; discussion 412-3.

131. Gezen, F., et al., *Application of syringosubarachnoid shunt through key-hole laminectomy. Technical note.* Neurosurgical Focus, 2000. **8**(3): p. E10.

132. Falci, S., et al., *Obliteration of a posttraumatic spinal cord cyst with solid human embryonic spinal cord grafts: first clinical attempt.* Journal of Neurotrauma, 1997. **14**(11): p. 875-84.

133. Lam, S., U. Batzdorf, and M. Bergsneider, *Thecal shunt placement for treatment of obstructive primary syringomyelia.* Journal of neurosurgery. Spine, 2008. **9**(6): p. 581-8.

134. Chang, H.S., et al., *Subarachnoid pressure-dependent change in syrinx size in a patient with syringomyelia associated with adhesive arachnoiditis. Case report.* Journal of Neurosurgery Spine, 2005. **2**(2): p. 209-14.

135. Kawaguchi, T., et al., *Syringomyelia with obstructive hydrocephalus at the foramens of Luschka and Magendie successfully treated by endoscopic third ventriculostomy.* Surgical Neurology, 2009. **71**(3): p. 349-52.

136. Wetjen, N.M., J.D. Heiss, and E.H. Oldfield, *Time course of syringomyelia resolution following decompression of Chiari malformation Type I.* Journal of neurosurgery. Pediatrics, 2008. **1**(2): p. 118-23.

137. Newton, E.J., *Syringomyelia as a manifestation of defective fourth ventricular drainage.* Annals of the Royal College of Surgeons of England, 1969. **44**(4): p. 194-213.

138. Levine, D.N., *The pathogenesis of syringomyelia associated with lesions at the foramen magnum: a critical review of existing theories and proposal of a new hypothesis.* Journal of the Neurological Sciences, 2004. **220**(1-2): p. 3-21.

139. Mavinkurve, G.G., et al., *Familial Chiari type I malformation with syringomyelia in two siblings: case report and review of the literature.* Child's nervous system : ChNS : official journal of the International Society for Pediatric Neurosurgery, 2005. **21**(11): p. 955-9.

140. Zakeri, A., F.E. Glasauer, and J.G. Egnatchik, *Familial syringomyelia: case report and review of the literature.* Surgical Neurology, 1995. **44**(1): p. 48-53.

141. Bentley, S.J., M.J. Campbell, and P. Kaufmann, *Familial syringomyelia.* Journal of neurology, neurosurgery, and psychiatry, 1975. **38**(4): p. 346-9.

142. Caraceni, T. and P. Giovannini, *Familial syringomyelia: a report of four cases.* Archiv fur Psychiatrie und Nervenkrankheiten, 1977. **224**(4): p. 331-40.

143. Speer, M.C., et al., *A genetic hypothesis for Chiari I malformation with or without syringomyelia.* Neurosurgical Focus, 2000. **8**(3): p. E12.

144. Koc, K., et al., *Familial syringomyelia in two siblings: case report.* Turkish Neurosurgery, 2007. **17**(4): p. 251-4.

145. Hida, K., et al., *Birth injury as a causative factor of syringomyelia with Chiari type I deformity.* Journal of neurology, neurosurgery, and psychiatry, 1994. **57**(3): p. 373-4.

146. Newman, P.K., T.R. Terenty, and J.B. Foster, *Some observations on the pathogenesis of syringomyelia.* Journal of Neurology, Neurosurgery & Psychiatry, 1981. **44**(11): p. 964-969.

147. Williams, B., *On the pathogenesis of syringomyelia: a review.* Journal of the Royal Society of Medicine, 1980. **73**(11): p. 798-806.

148. Williams, B., *Difficult labour as a cause of communicating syringomyelia.* Lancet, 1977. **2**(8028): p. 51-3.

149. Milhorat, T.H. and R.M. Kotzen, *Stenosis of the central canal of the spinal cord following inoculation of suckling hamsters with reovirus type I.* Journal of Neurosurgery, 1994. **81**(1): p. 103-6.

150. Milhorat, T.H., R.M. Kotzen, and A.P. Anzil, *Stenosis of central canal of spinal cord in man: incidence and pathological findings in 232 autopsy cases.* Journal of Neurosurgery, 1994. **80**(4): p. 716-22.

151. Tabor, E.N. and U. Batzdorf, *Thoracic spinal Pantopaque cyst and associated syrinx resulting in progressive spastic paraparesis: case report.* Neurosurgery, 1996. **39**(5): p. 1040-2.

152. Appleby, A., et al., *Syringomyelia due to chronic arachnoiditis at the foramen magnum.* Journal of the Neurological Sciences, 1969. **8**(3): p. 451-64.

153. Blagodatsky, M.D., et al., *Surgical treatment of "hindbrain related" syringomyelia: new data for pathogenesis.* Acta Neurochirurgica, 1993. **124**(2-4): p. 82-5.

154. Blaylock, R.L., *Hydrosyringomyelia of the conus medullaris associated with a thoracic meningioma: case report.* Journal of Neurosurgery, 1981. **54**(6): p. 833-5.

155. Durward, Q.J., et al., *Selective spinal cordectomy: clinicopathological correlation.* Journal of Neurosurgery, 1982. **56**(3): p. 359-67.

156. Gull, W., *Case of progressive atrophy of the muscles of the hands: enlargement of the ventricle of the cord in the cervical region, with atrophy of the gray matter (hydromyelus).* Guys Hospital Report (3rd series), 1862. **8**: p. 244 - 250.

157. Lichtenstein, B.W., *Distant neuroanatomic complications of spina bifida (spinal dysraphism). Hydrocephalus, Arnold-Chiari malformation, stenosis of aquaeduct of Sylvius, etc.; pathogenesis and pathology.* Arch Neurol Psychiatry, 1942. **47**: p. 195 - 214.

158. Gardner, W.J. and J. Angel, *The mechanism of syringomyelia and its surgical correction.* Clinical Neurosurgery, 1958. **6**: p. 131-40.

159. Gardner, W.J. and J. Angel, *The cause of syringomyelia and its surgical treatment.* Cleveland Clinic Quarterly, 1958. **25**(1): p. 4-8.

160. Stoodley, M.A., et al., *The Filling Mechanism,* in *Syringomyelia: A Disorder of CSF Circulation*, G. Flint and C. Rusbridge, Editors. 2014, Springer: Heidelberg. p. 87-102.

161. Ball, M.J. and A.D. Dayan, *Pathogenesis of syringomyelia.* Lancet, 1972. **2**(7781): p. 799-801.

162. Aboulker, J., *[Syringomyelia and intra-rachidian fluids. X. Rachidian fluid stasis]*. Neuro-Chirurgie, 1979. **25 Suppl 1**: p. 98-107.

163. Heiss, J.D., et al., *Elucidating the pathophysiology of syringomyelia.* Journal of Neurosurgery, 1999. **91**(4): p. 553-62.

164. Oldfield, E.H., et al., *Pathophysiology of syringomyelia associated with Chiari I malformation of the cerebellar tonsils. Implications for diagnosis and treatment.* Journal of Neurosurgery, 1994. **80**(1): p. 3-15.

165. Davis, C.H. and L. Symon, *Mechanisms and treatment in post-traumatic syringomyelia.* British Journal of Neurosurgery, 1989. **3**(6): p. 669-74.

166. Ellertsson, A.B. and T. Greitz, *The distending force in the production of communicating syringomyelia.* Lancet, 1970. **1**(7658): p. 1234.

167. Stoodley, M.A., N.R. Jones, and C.J. Brown, *Evidence for rapid fluid flow from the subarachnoid space into the spinal cord central canal in the rat.* Brain Research, 1996. **707**(2): p. 155-64.

168. Stoodley, M.A., et al., *Arterial pulsation-dependent perivascular cerebrospinal fluid flow into the central canal in the sheep spinal cord.* Journal of Neurosurgery, 1997. **86**(4): p. 686-93.

169. Stoodley, M.A., B. Gutschmidt, and N.R. Jones, *Cerebrospinal fluid flow in an animal model of noncommunicating syringomyelia.* Neurosurgery, 1999. **44**(5): p. 1065-75; discussion 1075-6.

170. Bilston, L.E., et al., *Arterial pulsation-driven cerebrospinal fluid flow in the perivascular space: a computational model.* Computer Methods in Biomechanics & Biomedical Engineering, 2003. **6**(4): p. 235-41.

171. Bilston, L.E., M.A. Stoodley, and D.F. Fletcher, *The influence of the relative timing of arterial and subarachnoid space pulse waves on spinal perivascular cerebrospinal fluid flow as a possible factor in syrinx development.* Journal of Neurosurgery, 2010. **112**(4): p. 808-813.

172. Carpenter, P.W., K. Berkouk, and A.D. Lucey, *Pressure wave propagation in fluid-filled co-axial elastic tubes. Part 2: Mechanisms for the pathogenesis of syringomyelia.* Journal of Biomechanical Engineering, 2003. **125**(6): p. 857-63.

173. Elliott, N.S., D.A. Lockerby, and A.R. Brodbelt, *The pathogenesis of syringomyelia: a re-evaluation of the elastic-jump hypothesis.* Journal of Biomechanical Engineering, 2009. **131**(4): p. 044503.

174. Koyanagi, I. and K. Houkin, *Pathogenesis of syringomyelia associated with Chiari type 1 malformation: review of evidences and proposal of a new hypothesis.* Neurosurgical Review, 2010. **33**(3): p. 271-84; discussion 284-5.

175. Josephson, A., et al., *A spinal thecal sac constriction model supports the theory that induced pressure gradients in the cord cause edema and cyst formation.* Neurosurgery, 2001. **48**(3): p. 636-45; discussion 645-6.

176. Greitz, D., *Unraveling the riddle of syringomyelia.* Neurosurgical Review, 2006. **29**(4): p. 251-63; discussion 264.

177. Rusbridge, C., D. Greitz, and B.J. Iskandar, *Syringomyelia: current concepts in pathogenesis, diagnosis, and treatment.* Journal of veterinary internal medicine / American College of Veterinary Internal Medicine, 2006. **20**(3): p. 469-79.

178. Ravaglia, S., et al., *Pathogenetic role of myelitis for syringomyelia.* Clinical neurology and neurosurgery, 2007. **109**(6): p. 541-6.

179. Lohle, P.N., et al., *The pathogenesis of syringomyelia in spinal cord ependymoma.* Clinical neurology and neurosurgery, 1994. **96**(4): p. 323-6.

180. Barnett, H.J., *Syringomyelia and tumours of the nervous system*, in *Syringomyelia*, H.J. Barnett, J.B. Foster, and P. Hudgson, Editors. 1973, Saunders: London. p. 245 - 301.

181. Lonser, R.R., J.A. Butman, and E.H. Oldfield, *Pathogenesis of tumor-associated syringomyelia demonstrated by peritumoral contrast material leakage. Case illustration.* Journal of neurosurgery. Spine, 2006. **4**(5): p. 426.

182. Lonser, R.R., et al., *Edema is a precursor to central nervous system peritumoral cyst formation.* Annals of Neurology, 2005. **58**(3): p. 392-9.

183. Koyanagi, I., et al., *Clinical features and pathomechanisms of syringomyelia associated with spinal arachnoiditis.* Surgical Neurology, 2005. **63**(4): p. 350-355.

184. Joffroy, A. and C. Achard, *De la myelite cavitaire (observations; reflexions; pathogenic des cavites).* Arch Physiol Norm Pathol, 1887. **10**: p. 435 - 472.

185. Tauber, E.S. and O.R. Langworthy, *A study of syringomyelia and the formation of cavities in the spinal cord.* Journal of nervous and mental disease, 1935. **81**: p. 245 - 264.

186. Netsky, M.G., *Syringomyelia; a clinicopathologic study.* A.M.A. archives of neurology and psychiatry, 1953. **70**(6): p. 741-77.

187. Milhorat, T.H., et al., *Intraoperative improvement of somatosensory evoked potentials and local spinal cord blood flow in patients with syringomyelia.* Journal of Neurosurgical Anesthesiology, 1996. **8**(3): p. 208-15.

188. Young, W.F., R. Tuma, and T. O'Grady, *Intraoperative measurement of spinal cord blood flow in syringomyelia.* Clinical neurology and neurosurgery, 2000. **102**(3): p. 119-23.

189. Feigin, I., J. Ogata, and G. Budzilovich, *Syringomyelia: the role of edema in its pathogenesis.* Journal of neuropathology and experimental neurology, 1971. **30**(2): p. 216-32.

190. Klekamp, J., et al., *Treatment of syringomyelia associated with arachnoid scarring caused by arachnoiditis or trauma.* Journal of Neurosurgery, 1997. **86**(2): p. 233-40.

191. Cho, K.H., et al., *Experimental model of posttraumatic syringomyelia: the role of adhesive arachnoiditis in syrinx formation.* Journal of Neurosurgery, 1994. **80**(1): p. 133-9.

192. Hoffman, G.S., et al., *Spinal arachnoiditis. What is the clinical spectrum? II. Arachnoiditis induced by Pantopaque/autologous blood in dogs, a possible model for human disease.* Spine, 1983. **8**(5): p. 541-51.

193. Klekamp, J., et al., *Disturbances of cerebrospinal fluid flow attributable to arachnoid scarring cause interstitial edema of the cat spinal cord.* Neurosurgery, 2001. **48**(1): p. 174-85; discussion 185-6.

194. McLaurin, R., et al., *Myelomalacia and multiple cavitations of spinal cord secondary to adhesive arachnoiditis; an experimental study.* A.M.A. archives of pathology, 1954. **57**(2): p. 138-46.

195. Yang, L., et al., *Excitotoxic model of post-traumatic syringomyelia in the rat.* Spine, 2001. **26**(17): p. 1842-9.

196. Tatara, N., *[Experimental syringomyelia in rabbits and rats after localized spinal arachnoiditis]*. No to shinkei = Brain and nerve, 1992. **44**(12): p. 1115-25.

197. Austin, J.W., M. Afshar, and M.G. Fehlings, *The relationship between localized subarachnoid inflammation and parenchymal pathophysiology after spinal cord injury.* J Neurotrauma, 2012. **29**(10): p. 1838-49.

198. Williams, B. and J. Bentley, *Experimental communicating syringomyelia in dogs after cisternal kaolin injection. Part 1. Morphology.* Journal of the Neurological Sciences, 1980. **48**(1): p. 93-107.

199. Nurick, S., J.A. Russell, and M.D. Deck, *Cystic degeneration of the spinal cord following spinal cord injury.* Brain : a journal of neurology, 1970. **93**(1): p. 211-22.

200. Abe, T., et al., *[Surgical treatment of syringomyelia]*. Rinsho Shinkeigaku - Clinical Neurology, 1995. **35**(12): p. 1406-8.

201. Schurch, B., W. Wichmann, and A.B. Rossier, *Post-traumatic syringomyelia (cystic myelopathy): a prospective study of 449 patients with spinal cord injury.* Journal of Neurology, Neurosurgery & Psychiatry, 1996. **60**(1): p. 61-67.

202. Wagner, F.C., Jr., J.C. VanGilder, and G.J. Dohrmann, *Pathological changes from acute to chronic in experimental spinal cord trauma.* Journal of Neurosurgery, 1978. **48**(1): p. 92-8.

203. Bertram, C.D., *Evaluation by fluid/structure-interaction spinal-cord simulation of the effects of subarachnoid-space stenosis on an adjacent syrinx.* Journal of Biomechanical Engineering, 2010. **132**(6): p. 061009.

204. Brodbelt, A.R., et al., *Fluid flow in an animal model of post-traumatic syringomyelia.* European Spine Journal, 2003. **12**(3): p. 300-6.

205. Elliott, N.S.J., D.A. Lockerby, and A.R. Brodbelt, *A lumped-parameter model of the cerebrospinal system for investigating arterial-driven flow in posttraumatic syringomyelia.* Medical Engineering & Physics, 2011. **33**(7): p. 874-882.

206. Chang, H.S. and H. Nakagawa, *Theoretical analysis of the pathophysiology of syringomyelia associated with adhesive arachnoiditis.* Journal of neurology, neurosurgery, and psychiatry, 2004. **75**(5): p. 754-7.

207. Bertram, C.D., A.R. Brodbelt, and M.A. Stoodley, *The origins of syringomyelia: numerical models of fluid/structure interactions in the spinal cord.* Journal of Biomechanical Engineering, 2005. **127**(7): p. 1099-109.

208. Bertram, C.D., L.E. Bilston, and M.A. Stoodley, *Tensile radial stress in the spinal cord related to arachnoiditis or tethering: a numerical model.* Medical & Biological Engineering & Computing, 2008. **46**(7): p. 701-7.

209. Demediuk, P., M. Lemke, and A.I. Faden, *Spinal cord edema and changes in tissue content of Na+, K+, and Mg2+ after impact trauma in rats.* Advances in neurology, 1990. **52**: p. 225-32.

210. Lemke, M. and A.I. Faden, *Edema development and ion changes in rat spinal cord after impact trauma: injury dose-response studies.* Journal of Neurotrauma, 1990. **7**(1): p. 41-54.

211. Mautes, A.E., et al., *Vascular events after spinal cord injury: contribution to secondary pathogenesis.* Physical therapy, 2000. **80**(7): p. 673-87.

212. Sharma, H.S. and Y. Olsson, *Edema formation and cellular alterations following spinal cord injury in the rat and their modification with p-chlorophenylalanine.* Acta neuropathologica, 1990. **79**(6): p. 604-10.

213. Hemley, S.J., et al., *Role of the blood-spinal cord barrier in posttraumatic syringomyelia.* Journal of neurosurgery. Spine, 2009. **11**(6): p. 696-704.

214. McGrath, J.T., *Spinal dysraphism in the dog. With comments on syringomyelia.* Pathologia veterinaria, 1965. **2**: p. Suppl:1-36.

215. Kuwamura, K., D.G. McLone, and A.J. Raimondi, *The central (spinal) canal in congenital murine hydrocephalus: morphological and physiological aspects.* Child's brain, 1978. **4**(4): p. 216-34.

216. Knowler, S.P., A.K. McFadyen, and C. Rusbridge, *Effectiveness of breeding guidelines for reducing the prevalence of syringomyelia.* The Veterinary record, 2011. **169**(26): p. 681.

217. Stalin, C.E., et al., *Radiographic morphology of the cranial portion of the cervical vertebral column in Cavalier King Charles Spaniels and its relationship to syringomyelia.* American journal of veterinary research, 2008. **69**(1): p. 89-93.

218. Rusbridge, C., et al., *Syringomyelia in cavalier King Charles spaniels: the relationship between syrinx dimensions and pain.* The Journal of small animal practice, 2007. **48**(8): p. 432-6.

219. Driver, C.J., et al., *Relationship of brain parenchyma within the caudal cranial fossa and ventricle size to syringomyelia in cavalier King Charles spaniels.* The Journal of small animal practice, 2010. **51**(7): p. 382-6.

220. Shaw, T.A., et al., *Increase in cerebellar volume in Cavalier King Charles Spaniels with Chiari-like malformation and its role in the development of syringomyelia.* PloS one, 2012. **7**(4): p. e33660.

221. Loderstedt, S., et al., *Distribution of syringomyelia along the entire spinal cord in clinically affected Cavalier King Charles Spaniels.* Veterinary journal, 2011. **190**(3): p. 359-63.

222. Rusbridge, C., *Chiari-like malformation with syringomyelia in the Cavalier King Charles spaniel: long-term outcome after surgical management.* Veterinary surgery : VS, 2007. **36**(5): p. 396-405.

223. Hu, H.Z., et al., *Histopathological investigation of syringomyelia in the Cavalier King Charles spaniel.* Journal of comparative pathology, 2012. **146**(2-3): p. 192-201.

224. Rusbridge, C. and S.P. Knowler, *Hereditary aspects of occipital bone hypoplasia and syringomyelia (Chiari type I malformation) in cavalier King Charles spaniels.* The Veterinary record, 2003. **153**(4): p. 107-12.

225. Rusbridge, C., et al., *Inherited occipital hypoplasia/syringomyelia in the cavalier King Charles spaniel: experiences in setting up a worldwide DNA collection.* The Journal of heredity, 2005. **96**(7): p. 745-9.

226. Nakamura, S., M.B. Camins, and G.M. Hochwald, *Pressure-absorption responses to the infusion of fluid into the spinal cord central canal of kaolin-hydrocephalic cats.* Journal of Neurosurgery, 1983. **58**(2): p. 198-203.

227. Rascher, K. and E. Donauer, *Experimental models of syringomyelia--personal observations and a brief look at earlier reports.* Acta Neurochirurgica, 1993. **123**(3-4): p. 166-9.

228. Schurr, P.H., R.L. McLaurin, and F.D. Ingraham, *Experimental studies on the circulation of the cerebrospinal fluid and methods of producing communicating hydrocephalus in the dog.* Journal of Neurosurgery, 1953. **10**(5): p. 515-25.

229. Hall, P.V., J. Muller, and R.L. Campbell, *Experimental hydrosyringomyelia, ischemic myelopathy, and syringomyelia.* Journal of Neurosurgery, 1975. **43**(4): p. 464-70.

230. Chakrabortty, S., et al., *Experimental syringomyelia: late ultrastructural changes of spinal cord tissue and magnetic resonance imaging evaluation.* Surgical Neurology, 1997. **48**(3): p. 246-54.

231. Chakrabortty, S., et al., *Experimental syringomyelia in the rabbit: an ultrastructural study of the spinal cord tissue.* Neurosurgery, 1994. **35**(6): p. 1112-20.

232. Aghayev, K., et al., *Expression of water channel aquaporin-4 during experimental syringomyelia.* Journal of Neurosurgery: Spine, 2011. **15**(4): p. 428-432.

233. Voelz, K., et al., *A ferritin tracer study of compensatory spinal CSF outflow pathways in kaolin-induced hydrocephalus.* Acta neuropathologica, 2007. **113**(5): p. 569-75.

234. Faulhauer, K. and E. Donauer, *Experimental hydrocephalus and hydrosyringomyelia in the cat. Radiological findings.* Acta Neurochirurgica, 1985. **74**(1-2): p. 72-80.

235. Hall, P.V., et al., *Radiosotope evaluation of experimental hydrosyringomyelia.* Journal of Neurosurgery, 1976. **45**(2): p. 181-7.

236. Hall, P.V., et al., *Clinical radiosotope investigations in hydrosyringomyelia and myelodysplasia.* Journal of Neurosurgery, 1976. **45**(2): p. 188-94.

237. Becker, D.P., J.A. Wilson, and G.W. Watson, *The spinal cord central canal: response to experimental hydrocephalus and canal occlusion.* Journal of Neurosurgery, 1972. **36**(4): p. 416-24.

238. Hall, P., et al., *Experimental syringomyelia: the relationship between intraventricular and intrasyrinx pressures.* Journal of Neurosurgery, 1980. **52**(6): p. 812-7.

239. Williams, B., *Experimental communicating syringomyelia in dogs after cisternal kaolin injection. Part 2. Pressure studies.* Journal of the Neurological Sciences, 1980. **48**(1): p. 109-22.

240. James, A.E., Jr., et al., *Evaluation of the central canal of the spinal cord in experimentally induced hydrocephalus.* Journal of Neurosurgery, 1978. **48**(6): p. 970-4.

241. West, R.J. and B. Williams, *Radiographic studies of the ventricles in syringomyelia.* Neuroradiology, 1980. **20**(1): p. 5-16.

242. Yamazaki, Y., et al., *Experimental model of chronic tonsillar herniation associated with early stage syringomyelia.* Acta neuropathologica, 1995. **90**(5): p. 425-31.

243. Yamazaki, Y., S. Tachibana, and K. Fujii, *Role of active cerebrospinal fluid transport in syrinx formation: An experimental study on a model of chronic*

*tonsillar herniation in rats*, in *Syringomyelia: Current concepts in pathogenesis and management*, N. Tamaki, U. Batzdorf, and T. Nagashima, Editors. 2001, Springer-Verlag: Tokyo. p. 56 - 61.

244. Williams, B. and R.O. Weller, *Syringomyelia produced by intramedullary fluid injection in dogs.* Journal of neurology, neurosurgery, and psychiatry, 1973. **36**(3): p. 467-77.

245. Milhorat, T.H., et al., *Histopathology of experimental hematomyelia.* Journal of Neurosurgery, 1991. **75**(6): p. 911-5.

246. Milhorat, T.H., et al., *Noncommunicating syringomyelia following occlusion of central canal in rats. Experimental model and histological findings.* Journal of Neurosurgery, 1993. **78**(2): p. 274-9.

247. Lee, G.Y., et al., *Origin of macrophages in a kaolin-induced model of rat syringomyelia: a study using radiation bone marrow chimeras.* Spine, 2005. **30**(2): p. 194-200.

248. Stoodley, M.A., et al., *Mechanisms underlying the formation and enlargement of noncommunicating syringomyelia: experimental studies.* Neurosurgical Focus, 2000. **8**(3): p. E2.

249. Tator, C.H. and M.G. Fehlings, *Review of the secondary injury theory of acute spinal cord trauma with emphasis on vascular mechanisms.* Journal of Neurosurgery, 1991. **75**(1): p. 15-26.

250. Tator, C.H., *Review of experimental spinal cord injury with emphasis on the local and systemic circulatory effects.* Neuro-Chirurgie, 1991. **37**(5): p. 291-302.

251. Onifer, S.M., et al., *Rat models of traumatic spinal cord injury to assess motor recovery.* Ilar Journal, 2007. **48**(4): p. 385-95.

252. Allen, A.R., *Surgery of experimental lesion of spinal cord equivalent to crush injury of fracture dislocation of spinal column. A preliminary report.* . JAMA : the journal of the American Medical Association, 1911. **57**: p. 878 - 880.

253. Allen, A.R., *Remarks of the histological changes in the spinal cord due to impact. An experimental study.* . Journal of nervous and mental disease, 1914. **41**: p. 141 - 147.

254. Collins, W.F., *A review and update of experiment and clinical studies of spinal cord injury.* Paraplegia, 1983. **21**(4): p. 204-19.

255. Gerber, A.M. and W.S. Corrie, *Effect of impounder contact area on experimental spinal cord injury.* Journal of Neurosurgery, 1979. **51**(4): p. 539-42.

256. Koozekanani, S.H., et al., *Possible mechanisms for observed pathophysiological variability in experimental spinal cord injury by the method of Allen.* Journal of Neurosurgery, 1976. **44**(4): p. 429-34.

257. Dohrmann, G.J. and M.M. Panjabi, *"Standardized" spinal cord trauma: biomechanical parameters and lesion volume.* Surgical Neurology, 1976. **6**(5): p. 263-7.

258. Dohrmann, G.L. and M.M. Panjabi, *Spinal cord deformation velocity, impulse, and energy related to lesion volume in "standardized" trauma.* Surgical forum, 1976. **27**(62): p. 466-8.

259. Young, W., *Spinal cord contusion models.* Progress in brain research, 2002. **137**: p. 231-55.

260. Goodkin, R. and J.B. Campbell, *Sequential pathologic changes in spinal cord injury: a preliminary report.* Surgical forum, 1969. **20**: p. 430-2.

261. Wrathall, J.R., R.K. Pettegrew, and F. Harvey, *Spinal cord contusion in the rat: Production of graded, reproducible, injury groups.* Experimental Neurology, 1985. **88**(1): p. 108-122.

262. Daniell, H.B., et al., *A method of quantitating injury inflicted in acute spinal cord studies.* Paraplegia, 1975. **13**(3): p. 137-42.

263. Panjabi, M.M. and J.R. Wrathall, *Biomechanical analysis of experimental spinal cord injury and functional loss.* Spine, 1988. **13**(12): p. 1365-70.

264. Khan, M. and R. Griebel, *Acute spinal cord injury in the rat: comparison of three experimental techniques.* The Canadian journal of neurological sciences. Le journal canadien des sciences neurologiques, 1983. **10**(3): p. 161-5.

265. Noble, L.J. and J.R. Wrathall, *Spinal cord contusion in the rat: morphometric analyses of alterations in the spinal cord.* Experimental neurology, 1985. **88**(1): p. 135-49.

266. Noble, L.J. and J.R. Wrathall, *An inexpensive apparatus for producing graded spinal cord contusive injury in the rat.* Experimental Neurology, 1987. **95**(2): p. 530-533.

267. Assenmacher, D.R. and T.B. Ducker, *Experimental traumatic paraplegia. The vascular and pathological changes seen in reversible and irreversible spinal-cord lesions.* The Journal of bone and joint surgery. American volume, 1971. **53**(4): p. 671-80.

268. Ducker, T.B., G.W. Kindt, and L.G. Kempf, *Pathological findings in acute experimental spinal cord trauma.* Journal of Neurosurgery, 1971. **35**(6): p. 700-8.

269. Ducker, T.B. and P.L. Perot, Jr., *Local tissue oxygen and blood flow in the acutely injured spinal cord.* Proceedings. Veterans Administration Spinal Cord Injury Conference, 1971. **18**: p. 29-32.

270. Ducker, T.B. and P.L. Perot, Jr., *Spinal cord oxygen and blood flow in trauma.* Surgical forum, 1971. **22**: p. 413-5.

271. Ducker, T.B. and P.L. Perot, Jr., *Spinal cord blood flow compartments.* Transactions of the American Neurological Association, 1971. **96**: p. 229-31.

272. Noble, L.J. and J.R. Wrathall, *Correlative analyses of lesion development and functional status after graded spinal cord contusive injuries in the rat.* Experimental neurology, 1989. **103**(1): p. 34-40.

273. Gruner, J.A., *A monitored contusion model of spinal cord injury in the rat.* Journal of Neurotrauma, 1992. **9**(2): p. 123-6; discussion 126-8.

274. Kwo, S., W. Young, and V. Decrescito, *Spinal cord sodium, potassium, calcium, and water concentration changes in rats after graded contusion injury.* Journal of Neurotrauma, 1989. **6**(1): p. 13-24.

275. Rabchevsky, A.G., et al., *Cyclosporin A treatment following spinal cord injury to the rat: behavioral effects and stereological assessment of tissue sparing.* Journal of Neurotrauma, 2001. **18**(5): p. 513-22.

276. Rabchevsky, A.G., et al., *Basic fibroblast growth factor (bFGF) enhances functional recovery following severe spinal cord injury to the rat.* Experimental neurology, 2000. **164**(2): p. 280-91.

277. Rabchevsky, A.G. and G.M. Smith, *Therapeutic interventions following mammalian spinal cord injury.* Archives of neurology, 2001. **58**(5): p. 721-6.

278. Anderson, T.E., *A controlled pneumatic technique for experimental spinal cord contusion.* Journal of neuroscience methods, 1982. **6**(4): p. 327-33.

279. Kearney, P.A., et al., *Interaction of contact velocity and cord compression in determining the severity of spinal cord injury.* Journal of Neurotrauma, 1988. **5**(3): p. 187-208.

280. Noyes, D.H., *Electromechanical impactor for producing experimental spinal cord injury in animals.* Medical & Biological Engineering & Computing, 1987. **25**(3): p. 335-40.

281. Noyes, D.H., *Correlation between parameters of spinal cord impact and resultant injury.* Experimental neurology, 1987. **95**(3): p. 535-47.

282. Somerson, S.K. and B.T. Stokes, *Functional analysis of an electromechanical spinal cord injury device.* Experimental neurology, 1987. **96**(1): p. 82-96.

283. Stokes, B.T. and S.K. Somerson, *Spinal cord extracellular microenvironment. Can the changes resulting from trauma be graded?* Neurochemical pathology, 1987. **7**(1): p. 47-55.

284. Scheff, S.W., et al., *Experimental modeling of spinal cord injury: characterization of a force-defined injury device.* Journal of Neurotrauma, 2003. **20**(2): p. 179-93.

285. Rabchevsky, A.G., et al., *Creatine diet supplement for spinal cord injury: influences on functional recovery and tissue sparing in rats.* Journal of Neurotrauma, 2003. **20**(7): p. 659-69.

286. Talac, R., et al., *Animal models of spinal cord injury for evaluation of tissue engineering treatment strategies.* Biomaterials, 2004. **25**(9): p. 1505-10.

287. Tarlov, I.M., H. Klinger, and S. Vitale, *Spinal cord compression studies. I. Experimental techniques to produce acute and gradual compression.* A.M.A. archives of neurology and psychiatry, 1953. **70**(6): p. 813-9.

288. Tarlov, I.M., *Spinal cord compression studies. III. Time limits for recovery after gradual compression in dogs.* A.M.A. archives of neurology and psychiatry, 1954. **71**(5): p. 588-97.

289. Tarlov, I.M. and H. Klinger, *Spinal cord compression studies. II. Time limits for recovery after acute compression in dogs.* A.M.A. archives of neurology and psychiatry, 1954. **71**(3): p. 271-90.

290. Rivlin, A.S. and C.H. Tator, *Regional spinal cord blood flow in rats after severe cord trauma.* Journal of Neurosurgery, 1978. **49**(6): p. 844-53.

291. Rivlin, A.S. and C.H. Tator, *Effect of duration of acute spinal cord compression in a new acute cord injury model in the rat.* Surgical Neurology, 1978. **10**(1): p. 38-43.

292. Gruner, J.A., A.K. Yee, and A.R. Blight, *Histological and functional evaluation of experimental spinal cord injury: evidence of a stepwise response to graded compression.* Brain research, 1996. **729**(1): p. 90-101.

293. Blight, A.R., *Morphometric analysis of blood vessels in chronic experimental spinal cord injury: hypervascularity and recovery of function.* Journal of the Neurological Sciences, 1991. **106**(2): p. 158-74.

294. Blight, A.R., *Morphometric analysis of a model of spinal cord injury in guinea pigs, with behavioral evidence of delayed secondary pathology.* Journal of the Neurological Sciences, 1991. **103**(2): p. 156-71.

295. Means, E.D., et al., *Effect of methylprednisolone in compression trauma to the feline spinal cord.* Journal of Neurosurgery, 1981. **55**(2): p. 200-8.

296. Noble, L.J. and J.A. Ellison, *Effect of transection on the blood-spinal cord barrier of the rat after isolation from descending sources.* Brain research, 1989. **487**(2): p. 299-310.

297. Bunge, M.B., *Transplantation of purified populations of Schwann cells into lesioned adult rat spinal cord.* Journal of Neurology, 1994. **242**(1 Suppl 1): p. S36-9.

298. Kao, C.C., L.W. Chang, and J.M. Bloodworth, *The mechanism of spinal cord cavitation following spinal cord transection. Part 3: Delayed grafting with and without spinal cord retransection.* Journal of Neurosurgery, 1977. **46**(6): p. 757-66.

299. Kao, C.C., L.W. Chang, and J.M. Bloodworth, Jr., *Axonal regeneration across transected mammalian spinal cords: an electron microscopic study of delayed microsurgical nerve grafting.* Experimental neurology, 1977. **54**(3): p. 591-615.

300. Kao, C.C., L.W. Chang, and J.M. Bloodworth, Jr., *The mechanism of spinal cord cavitation follwing spinal cord transection. Part 2. Electron microscopic observations.* Journal of Neurosurgery, 1977. **46**(6): p. 745-56.

301. Kao, C.C., L.W. Chang, and J.M. Bloodworth, Jr., *Electron microscopic observations of the mechanisms of terminal club formation in transected spinal cord axons.* Journal of neuropathology and experimental neurology, 1977. **36**(1): p. 140-56.

302. Xu, X.M., et al., *A combination of BDNF and NT-3 promotes supraspinal axonal regeneration into Schwann cell grafts in adult rat thoracic spinal cord.* Experimental neurology, 1995. **134**(2): p. 261-72.

303. Xu, X.M., et al., *Axonal regeneration into Schwann cell-seeded guidance channels grafted into transected adult rat spinal cord.* The Journal of comparative neurology, 1995. **351**(1): p. 145-60.

304. Liu, D., W. Thangnipon, and D.J. McAdoo, *Excitatory amino acids rise to toxic levels upon impact injury to the rat spinal cord.* Brain research, 1991. **547**(2): p. 344-8.

305. Panter, S.S., S.W. Yum, and A.I. Faden, *Alteration in extracellular amino acids after traumatic spinal cord injury.* Annals of Neurology, 1990. **27**(1): p. 96-99.

306. Simpson, R.K., Jr., C.S. Robertson, and J.C. Goodman, *Spinal cord ischemia-induced elevation of amino acids: extracellular measurement with microdialysis.* Neurochemical research, 1990. **15**(6): p. 635-9.

307. Faden, A.I. and R.P. Simon, *A potential role for excitotoxins in the pathophysiology of spinal cord injury.* Annals of Neurology, 1988. **23**(6): p. 623-6.

308. Faden, A.I., et al., *N-methyl-D-aspartate antagonist MK801 improves outcome following traumatic spinal cord injury in rats: behavioral, anatomic, and neurochemical studies.* Journal of Neurotrauma, 1988. **5**(1): p. 33-45.

309. Hao, J.X., et al., *Protective effect of the NMDA antagonist MK-801 on photochemically induced spinal lesions in the rat.* Experimental neurology, 1992. **118**(2): p. 143-52.

310. Yezierski, R.P., et al., *Excitotoxic spinal cord injury: behavioral and morphological characteristics of a central pain model.* Pain, 1998. **75**(1): p. 141-55.

311. Yezierski, R.P., et al., *Neuronal degeneration and spinal cavitation following intraspinal injections of quisqualic acid in the rat.* Journal of Neurotrauma, 1993. **10**(4): p. 445-56.

312. Pisharodi, M. and H.J. Nauta, *An animal model for neuron-specific spinal cord lesions by the microinjection of N-methylaspartate, kainic acid, and quisqualic acid.* Applied neurophysiology, 1985. **48**(1-6): p. 226-33.

313. Hadi, B., et al., *Lasting paraplegia caused by loss of lumbar spinal cord interneurons in rats: no direct correlation with motor neuron loss.* Journal of Neurosurgery, 2000. **93**(2 Suppl): p. 266-75.

314. Magnuson, D.S., et al., *Comparing deficits following excitotoxic and contusion injuries in the thoracic and lumbar spinal cord of the adult rat.* Experimental neurology, 1999. **156**(1): p. 191-204.

315. Fried, L.C., et al., *The animal experimental model ischemic injuries.* Proceedings. Veterans Administration Spinal Cord Injury Conference, 1973(19): p. 106.

316. Fried, L.C. and O. Aparicio, *Experimental ischemia of the spinal cord. Histologic studies after anterior spinal artery occlusion.* Neurology, 1973. **23**(3): p. 289-93.

317. Bunge, M.B., et al., *Characterization of photochemically induced spinal cord injury in the rat by light and electron microscopy.* Experimental neurology, 1994. **127**(1): p. 76-93.

318. Hao, J.X., et al., *Photochemically induced transient spinal ischemia induces behavioral hypersensitivity to mechanical and cold stimuli, but not to noxious-heat stimuli, in the rat.* Experimental neurology, 1992. **118**(2): p. 187-94.

319. Guizar-Sahagun, G., et al., *Development of post-traumatic cysts in the spinal cord of rats-subjected to severe spinal cord contusion.* Surgical Neurology, 1994. **41**(3): p. 241-9.

320. Freeman, L.W. and T.W. Wright, *Experimental observations of concussion and contusion of the spinal cord.* Ann Surg, 1953. **137**: p. 433-443.

321. Brodbelt, A.R., et al., *The role of excitotoxic injury in post-traumatic syringomyelia.* Journal of Neurotrauma, 2003. **20**(9): p. 883-93.

322. Cohen, W.A., et al., *Posttraumatic syrinx formation: experimental study.* AJNR. American journal of neuroradiology, 1985. **6**(5): p. 823-7.

323. Wagner, F.C., Jr. and W.B. Stewart, *Effect of trauma dose on spinal cord edema.* Journal of Neurosurgery, 1981. **54**(6): p. 802-6.

324. Wagner, F.C., Jr., J.C. Van Gilder, and G.J. Dohrmann, *The development of intramedullary cavitation following spinal cord injury: an experimental pathological study.* Paraplegia, 1977. **14**(4): p. 245-50.

325. Radojicic, M., et al., *Ascending central canal dilation and progressive ependymal disruption in a contusion model of rodent chronic spinal cord injury.* BMC Neurology, 2007. **7**: p. 30.

326. Seki, T. and M.G. Fehlings, *Mechanistic insights into posttraumatic syringomyelia based on a novel in vivo animal model. Laboratory investigation.* Journal of Neurosurgery Spine, 2008. **8**(4): p. 365-75.

327. Mizuno, J., et al., *Histological evaluation for the mechanism of syrinx formation in the rat experimental model with injury and secondary adhesive arachnoiditis*, in *Syringomyelia: current concept in pathogenesis and management*, N. Tamaki, U. Batzdorf, and T. Nagashima, Editors. 2001, Springer-Verlag: Tokyo. p. 49 - 55.

328. Brodbelt, A.R., et al., *Altered subarachnoid space compliance and fluid flow in an animal model of posttraumatic syringomyelia.* Spine, 2003. **28**(20): p. E413-9.

329. Tu, J., et al., *Differentiation of endogenous progenitors in an animal model of post-traumatic syringomyelia.* Spine, 2010. **35**(11): p. 1116-21.

330. Kiernan, J.A., *Spinal Cord*, in *Barr's The Human Nervous System: An anatomical viewpoint*, J.A. Kiernan, Editor 2005, Lippincott Williams & Wilkins: Philadelphia. p. 64 - 84.

331. Moore, K.L., A.F. Dalley, and A.M.R. Agur, *Clinically orientated anatomy*. 6th edition ed2010, Philadelphia: Wolters Kluwert / Lippincott Williams & Wilkins.

332. Larsen, W., *Human embryology*. 2nd edition ed1997, New York: Churchill Livingstone.

333. McMinn, R.M.H., *Spinal cord*, in *Last's Anatomy: regional and applied*, R.M.H. McMinn, Editor 1998, Churchill Livingstone: London. p. 619 - 627.

334. Young, B. and J. Heath, *Central nervous system*, in *Wheater's Functional Histology: a text and colour atlas*2000, Churchill Livingstone: London. p. 372 - 380.

335. Young, B. and J. Heath, *Nervous tissues*, in *Wheater's Functional Histology: a text and colour atlas*2000, Churchill Livingstone: London. p. 116 - 143.

336. Koshinaga, M. and S.R. Whittemore, *The temporal and spatial activation of microglia in fiber tracts undergoing anterograde and retrograde degeneration following spinal cord lesion.* Journal of Neurotrauma, 1995. **12**(2): p. 209-22.

337. Watanabe, T., et al., *Differential activation of microglia after experimental spinal cord injury.* Journal of Neurotrauma, 1999. **16**(3): p. 255-65.

338. Rexed, B., *The cytoarchitectonic organization of the spinal cord in the cat.* The Journal of comparative neurology, 1952. **96**(3): p. 414-95.

339. Anderson, C.R., et al., *The spinal cord: A Christopher and Dana Reeve foundation text and atlas.*2009, San Diego: Academic Press.

340. Rexed, B., *A cytoarchitectonic atlas of the spinal cord in the cat.* The Journal of comparative neurology, 1954. **100**(2): p. 297-379.

341. Molander, C., Q. Xu, and G. Grant, *The cytoarchitectonic organization of the spinal cord in the rat. I. The lower thoracic and lumbosacral cord.* The Journal of comparative neurology, 1984. **230**(1): p. 133-41.

342. Molander, C., et al., *Cytoarchitectonic organization of the spinal cord in the rat: II. The cervical and upper thoracic cord.* The Journal of comparative neurology, 1989. **289**(3): p. 375-85.

343. Hashizume, Y., K. Yasui, and M. Yoshida, *Age-related morphological change of the central canal of the human spinal cord and the mechanism of syrinx formation in syringomyelia and hydromyelia*, in *Syringomyelia: Current concepts in pathogenesis and management*, N. Tamaki, U. Batzdorf, and T. Nagashima, Editors. 2001, Springer-Verlag: Tokyo. p. 31 - 39.

344. Brodbelt, A. and M. Stoodley, *CSF pathways: a review.* British Journal of Neurosurgery, 2007. **21**(5): p. 510-20.

345. Del Bigio, M.R., *The ependyma: a protective barrier between brain and cerebrospinal fluid.* Glia, 1995. **14**(1): p. 1-13.

346. Rafols, J.A. and H.G. Goshgarian, *Spinal tanycytes in the adult rat: a correlative Golgi gold-toning study.* The Anatomical record, 1985. **211**(1): p. 75-86.

347. Weller, R.O., *Microscopic morphology and histology of the human meninges.* Morphologie : bulletin de l'Association des anatomistes, 2005. **89**(284): p. 22-34.

348. Nicholas, D.S. and R.O. Weller, *The fine anatomy of the human spinal meninges. A light and scanning electron microscopy study.* Journal of Neurosurgery, 1988. **69**(2): p. 276-82.

349. Reina, M.A., et al., *The origin of the spinal subdural space: ultrastructure findings.* Anesthesia and analgesia, 2002. **94**(4): p. 991-5, table of contents.

350. Parkinson, D., *Human spinal arachnoid septa, trabeculae, and "rogue strands".* The American journal of anatomy, 1991. **192**(4): p. 498-509.

351. Santillan, A., et al., *Vascular anatomy of the spinal cord.* Journal of NeuroInterventional Surgery, 2012. **4**(1): p. 67-74.

352. Lamin, S. and J.J. Bhattacharya, *Vascular Anatomy of the Spinal Cord and Cord Ischaemia.* Practical Neurology, 2003. **3**(2): p. 92-95.

353. Johnston, M., *The Importance of Lymphatics in Cerebrospinal Fluid Transport.* Lymphatic Research and Biology, 2003. **1**(1): p. 41-45.

354. Foldi, M., *The brain and the lymphatic system revisited.* Lymphology, 1999. **32**(2): p. 40-4.

355. Koh, L., A. Zakharov, and M. Johnston, *Integration of the subarachnoid space and lymphatics: is it time to embrace a new concept of cerebrospinal fluid absorption?* Cerebrospinal Fluid Research, 2005. **2**: p. 6.

356. Boulton, M., et al., *Lymphatic drainage of the CNS: effects of lymphatic diversion/ligation on CSF protein transport to plasma.* The American journal of physiology, 1997. **272**(5 Pt 2): p. R1613-9.

357. Boulton, M., et al., *Contribution of extracranial lymphatics and arachnoid villi to the clearance of a CSF tracer in the rat.* The American journal of physiology, 1999. **276**(3 Pt 2): p. R818-23.

358. Abbott, N.J., et al., *Structure and function of the blood–brain barrier.* Neurobiology of disease, 2010. **37**(1): p. 13-25.

359. Rennels, M.L., et al., *Evidence for a 'paravascular' fluid circulation in the mammalian central nervous system, provided by the rapid distribution of tracer protein throughout the brain from the subarachnoid space.* Brain research, 1985. **326**(1): p. 47-63.

360. Wagner, H.J., C. Pilgrim, and J. Brandl, *Penetration and removal of horseradish peroxidase injected into the cerebrospinal fluid: role of cerebral perivascular spaces, endothelium and microglia.* Acta neuropathologica, 1974. **27**(4): p. 299-315.

361. Hutchings, M. and R.O. Weller, *Anatomical relationships of the pia mater to cerebral blood vessels in man.* Journal of Neurosurgery, 1986. **65**(3): p. 316-25.

362. Palmer, A.M., *The role of the blood-CNS barrier in CNS disorders and their treatment.* Neurobiology of disease, 2010. **37**(1): p. 3-12.

363. Ichikawa, H. and K. Itoh, *Blood-arachnoid barrier disruption in experimental rat meningitis detected using gadolinium-enhancement ratio imaging.* Brain Res, 2011. **1390**: p. 142-9.

364. Kimelberg, H.K., *Water homeostasis in the brain: Basic concepts.* Neuroscience, 2004. **129**(4): p. 851-860.

365. Ganong, W.F., *Review of medical physiology*. 21st edition ed, ed. J. Foltin, et al.2003, New York: McGraw-Hill

366. Brown, P.D., et al., *Molecular mechanisms of cerebrospinal fluid production.* Neuroscience, 2004. **129**(4): p. 957-70.

367. Jones, H.C., *Cerebrospinal Fluid Research: A new platform for dissemination of research, opinions and reviews with a common theme.* Cerebrospinal Fluid Research, 2004. **1**(1): p. 1.

368. Milhorat, T.H., et al., *Choroid plexus papilloma. I. Proof of cerebrospinal fluid overproduction.* Child's brain, 1976. **2**(5): p. 273-89.

369. Hammock, M.K. and T.H. Milhorat, *The cerebrospinal fluid: current concepts of its formation.* Annals of clinical and laboratory science, 1976. **6**(1): p. 22-6.

370. Milhorat, T.H., et al., *Normal rate of cerebrospinal fluid formation five years after bilateral choroid plexectomy. Case report.* Journal of Neurosurgery, 1976. **44**(6): p. 735-9.

371. Czosnyka, M., et al., *Cerebrospinal fluid dynamics.* Physiological measurement, 2004. **25**(5): p. R51-76.

372. Greitz, D., T. Greitz, and T. Hindmarsh, *A new view on the CSF-circulation with the potential for pharmacological treatment of childhood hydrocephalus.* Acta paediatrica, 1997. **86**(2): p. 125-32.

373. Henry-Feugeas, M.C., et al., *Origin of subarachnoid cerebrospinal fluid pulsations: a phase-contrast MR analysis.* Magnetic resonance imaging, 2000. **18**(4): p. 387-95.

374. Davson, H. and M.B. Segal, *Physiology of the CSF adn blood brain barriers*1996, Boca Raton: CRC Press.

375. Mollanji, R., et al., *Comparison of cerebrospinal fluid transport in fetal and adult sheep.* American journal of physiology. Regulatory, integrative and comparative physiology, 2001. **281**(4): p. R1215-23.

376. Bozanovic-Sosic, R., R. Mollanji, and M.G. Johnston, *Spinal and cranial contributions to total cerebrospinal fluid transport.* American journal of physiology. Regulatory, integrative and comparative physiology, 2001. **281**(3): p. R909-16.

377. Czosnyka, M. and J.D. Pickard, *Monitoring and interpretation of intracranial pressure.* Journal of neurology, neurosurgery, and psychiatry, 2004. **75**(6): p. 813-21.

378. Greitz, D., et al., *Pulsatile brain movement and associated hydrodynamics studied by magnetic resonance phase imaging. The Monro-Kellie doctrine revisited.* Neuroradiology, 1992. **34**(5): p. 370-80.

379. Bhadelia, R.A., et al., *Cerebrospinal fluid pulsation amplitude and its quantitative relationship to cerebral blood flow pulsations: a phase-contrast MR flow imaging study.* Neuroradiology, 1997. **39**(4): p. 258-64.

380. Nakamura, K., K. Urayama, and Y. Hoshino, *Lumbar cerebrospinal fluid pulse wave rising from pulsations of both the spinal cord and the brain in humans.* Spinal cord, 1997. **35**(11): p. 735-9.

381. Nakamura, K., K. Urayama, and Y. Hoshino, *Site of origin of spinal cerebrospinal fluid pulse wave.* Journal of orthopaedic science : official journal of the Japanese Orthopaedic Association, 1998. **3**(1): p. 60-6.

382. Martin, B.A., et al., *Syringomyelia Hydrodynamics: An In Vitro Study Based on In Vivo Measurements.* Journal of Biomechanical Engineering, 2005. **127**(7): p. 1110-1120.

383. Martin, B.A., et al., *Spinal Subarachnoid Space Pressure Measurements in an In Vitro Spinal Stenosis Model: Implications on Syringomyelia Theories.* Journal of Biomechanical Engineering, 2010. **132**(11): p. 111007.

384. Martin, B.A., et al., *A coupled hydrodynamic model of the cardiovascular and cerebrospinal fluid system.* American Journal of Physiology - Heart & Circulatory Physiology, 2012. **302**(7): p. H1492-509.

385. Milhorat, T.H., et al., *Intramedullary pressure in syringomyelia: clinical and pathophysiological correlates of syrinx distension.* Neurosurgery, 1997. **41**(5): p. 1102-10.

386. Agre, P., et al., *Aquaporin water channels – from atomic structure to clinical medicine.* The Journal of Physiology, 2002. **542**(1): p. 3-16.

387. Yool, A.J., *Aquaporins: multiple roles in the central nervous system.* Neuroscientist, 2007. **13**(5): p. 470-85.

388. Tait, M.J., et al., *Water movements in the brain: role of aquaporins.* Trends Neurosci, 2008. **31**(1): p. 37-43.

389. Ishibashi, K., S. Hara, and S. Kondo, *Aquaporin water channels in mammals.* Clinical & Experimental Nephrology, 2009. **13**(2): p. 107-17.

390. Ishibashi, K., et al., *The evolutionary aspects of aquaporin family.* American Journal of Physiology - Regulatory, Integrative and Comparative Physiology, 2011. **300**(3): p. R566-R576.

391. Papadopoulos, M.C., et al., *Aquaporin-4 and brain edema.* Pediatric Nephrology, 2007. **22**(6): p. 778-84.

392. Badaut, J., S. Ashwal, and A. Obenaus, *Aquaporins in cerebrovascular disease: a target for treatment of brain edema?* Cerebrovascular Diseases, 2011. **31**(6): p. 521-31.

393. Zelenina, M., *Regulation of brain aquaporins.* Neurochemistry International, 2010. **57**(4): p. 468-488.

394. Gonen, T. and T. Walz, *The structure of aquaporins.* Quarterly Reviews of Biophysics, 2006. **39**(4): p. 361-96.

395. Verkman, A.S., *Aquaporins in clinical medicine.* Annual Review of Medicine, 2012. **63**: p. 303-16.

396. Gunnarson, E., M. Zelenina, and A. Aperia, *Regulation of brain aquaporins.* Neuroscience, 2004. **129**(4): p. 947-55.

397. Longatti, P.L., et al., *Choroid plexus and aquaporin-1: a novel explanation of cerebrospinal fluid production.* Pediatr Neurosurg, 2004. **40**(6): p. 277-83.

398. Oshio, K., et al., *Aquaporin-1 deletion reduces osmotic water permeability and cerebrospinal fluid production.* Acta Neurochirurgica - Supplement, 2003. **86**: p. 525-8.

399. Longatti, P., et al., *Aquaporin(s) expression in choroid plexus tumours.* Pediatr Neurosurg, 2006. **42**(4): p. 228-33.

400. Oshio, K., et al., *Expression of the aquaporin-1 water channel in human glial tumors.* Neurosurgery, 2005. **56**(2): p. 375-81; discussion 375-81.

401. Donkin, J.J. and R. Vink, *Mechanisms of cerebral edema in traumatic brain injury: therapeutic developments.* Current Opinion in Neurology, 2010. **23**(3): p. 293-9.

402. Nielsen, S., et al., *Specialized Membrane Domains for Water Transport in Glial Cells: High-Resolution Immunogold Cytochemistry of Aquaporin-4 in Rat Brain.* The Journal of Neuroscience, 1997. **17**(1): p. 171-180.

403. Jung, J.S., et al., *Molecular characterization of an aquaporin cDNA from brain: candidate osmoreceptor and regulator of water balance.* Proceedings of the National Academy of Sciences of the United States of America, 1994. **91**(26): p. 13052-6.

404. Bloch, O. and G.T. Manley, *The role of aquaporin-4 in cerebral water transport and edema.* Neurosurgical Focus, 2007. **22**(5): p. E3.

405. Owler, B., T. Pitham, and D. Wang, *Aquaporins: relevance to cerebrospinal fluid physiology and therapeutic potential in hydrocephalus.* Cerebrospinal Fluid Research, 2010. **7**(1): p. 15.

406. Binder, D.K., et al., *Increased seizure duration and slowed potassium kinetics in mice lacking aquaporin-4 water channels.* GLIA, 2006. **53**(6): p. 631-6.

407. Papadopoulos, M.C., S. Saadoun, and A.S. Verkman, *Aquaporins and cell migration.* Pflugers Arch, 2008. **456**(4): p. 693-700.

408. Saadoun, S., et al., *Involvement of aquaporin-4 in astroglial cell migration and glial scar formation.* Journal of Cell Science, 2005. **118**(Pt 24): p. 5691-8.

409. Taya, K., et al., *Effect of secondary insults upon aquaporin-4 water channels following experimental cortical contusion in rats.* Journal of Neurotrauma, 2010. **27**(1): p. 229-39.

410. Rao, K.V.R., et al., *Aquaporin-4 Expression in Cultured Astrocytes after Fluid Percussion Injury.* Journal of Neurotrauma, 2011. **28**(3): p. 371-381.

411. Tran, N.D., et al., *Aquaporin-1-mediated cerebral edema following traumatic brain injury: effects of acidosis and corticosteroid administration.* Journal of Neurosurgery, 2010. **112**(5): p. 1095-104.

412. Ding, J.Y., et al., *Hypoxia-inducible factor-1α signaling in aquaporin upregulation after traumatic brain injury.* Neuroscience Letters, 2009. **453**(1): p. 68-72.

413. Manley, G.T., et al., *New insights into water transport and edema in the central nervous system from phenotype analysis of aquaporin-4 null mice.* Neuroscience, 2004. **129**(4): p. 983-91.

414. Bloch, O., et al., *Accelerated progression of kaolin-induced hydrocephalus in aquaporin-4-deficient mice.* J Cereb Blood Flow Metab, 2006. **26**(12): p. 1527-1537.

415. Manley, G.T., et al., *Aquaporin-4 deletion in mice reduces brain edema after acute water intoxication and ischemic stroke.* Nature Medicine, 2000. **6**(2): p. 159-63.

416. Paul, L., et al., *Expression of aquaporin 1 and 4 in a congenital hydrocephalus rat model.* Neurosurgery, 2011. **68**(2): p. 462-73.

417. Bennett, J.L., et al., *Intrathecal pathogenic anti-aquaporin-4 antibodies in early neuromyelitis optica.* Annals of Neurology, 2009. **66**(5): p. 617-29.

418. Jarius, S. and B. Wildemann, *AQP4 antibodies in neuromyelitis optica: diagnostic and pathogenetic relevance.* Nat Rev Neurol, 2010. **6**(7): p. 383-392.

419. Nesic, O., et al., *Acute and chronic changes in aquaporin 4 expression after spinal cord injury.* Neuroscience, 2006. **143**(3): p. 779-92.

420. Saadoun, S., et al., *Greatly improved neurological outcome after spinal cord compression injury in AQP4-deficient mice.* Brain, 2008. **131**(Pt 4): p. 1087-98.

421. Kimura, A., et al., *Protective role of aquaporin-4 water channels after contusion spinal cord injury.* Annals of Neurology, 2010. **67**(6): p. 794-801.

422. Saadoun, S. and M.C. Papadopoulos, *Aquaporin-4 in brain and spinal cord oedema.* Neuroscience, 2010. **168**(4): p. 1036-46.

423. Nesic, O., et al., *Aquaporin 1 - a novel player in spinal cord injury.* J Neurochem, 2008. **105**(3): p. 628-40.

424. Nesic, O., et al., *Aquaporins in spinal cord injury: the janus face of aquaporin 4.* Neuroscience, 2010. **168**(4): p. 1019-1035.

425. Oshio, K., et al., *Expression of aquaporin water channels in mouse spinal cord.* Neuroscience, 2004. **127**(3): p. 685-93.

426. Hemley, S., et al., *Aquaporin-4 expression in post-traumatic syringomyelia.* Journal of Neurotrauma, 2013. **30**(16): p. 1457-67.

427. Hemley, S., et al., *Aquaporin-4 expression and blood-spinal cord permeability in canalicular syringomyelia.* Journal of Neurosurgery Spine, 2012. **17**(6): p. 602-12.

428. Binder, D.K., et al., *Increased seizure threshold in mice lacking aquaporin-4 water channels.* Neuroreport, 2004. **15**(2): p. 259-62.

429. Binder, D.K., et al., *Increased seizure duration in mice lacking aquaporin-4 water channels.* Acta Neurochirurgica - Supplement, 2006. **96**: p. 389-92.

430. Saadoun, S., et al., *Aquaporin-4 expression is increased in oedematous human brain tumours.* Journal of Neurology, Neurosurgery & Psychiatry, 2002. **72**(2): p. 262-265.

431. Yukutake, Y., et al., *Mercury chloride decreases the water permeability of aquaporin-4-reconstituted proteoliposomes.* Biology of the Cell, 2008. **100**(6): p. 355-363.

432. Wen, H., et al., *Ontogeny of water transport in rat brain: postnatal expression of the aquaporin-4 water channel.* European Journal of Neuroscience, 1999. **11**(3): p. 935-945.

433. Ron, N.P., et al., *Ontogeny and the effects of corticosteroid pretreatment on aquaporin water channels in the ovine cerebral cortex.* Reproduction, Fertility and Development, 2005. **17**(5): p. 535-542.

434. Vajda, Z., et al., *Increased Aquaporin-4 Immunoreactivity in Rat Brain in Response to Systemic Hyponatremia.* Biochemical and Biophysical Research Communications, 2000. **270**(2): p. 495-503.

435. Søgaard, R. and T. Zeuthen, *Test of blockers of AQP1 water permeability by a high-resolution method: no effects of tetraethylammonium ions or acetazolamide.* Pflügers Archiv European Journal of Physiology, 2008. **456**(2): p. 285-292.

436. Migliati, E., et al., *Inhibition of aquaporin-1 and aquaporin-4 water permeability by a derivative of the loop diuretic bumetanide acting at an internal pore-occluding binding site.* Molecular Pharmacology, 2009. **76**(1): p. 105-12.

437. Preston, G.M., et al., *The mercury-sensitive residue at cysteine 189 in the CHIP28 water channel.* Journal of Biological Chemistry, 1993. **268**(1): p. 17-20.

438. Yool, A.J., E.A. Brown, and G.A. Flynn, *Roles for novel pharmacological blockers of aquaporins in the treatment of brain oedema and cancer.* Clinical & Experimental Pharmacology & Physiology, 2010. **37**(4): p. 403-9.

439. Fazzina, G., et al., *The protein kinase C activator phorbol myristate acetate decreases brain edema by aquaporin 4 downregulation after middle cerebral artery occlusion in the rat.* J Neurotrauma, 2010. **27**(2): p. 453-61.

440. Kleindienst, A., et al., *Modulation of AQP4 expression by the protein kinase C activator, phorbol myristate acetate, decreases ischemia-induced brain edema.* Acta Neurochirurgica - Supplement, 2006. **96**: p. 393-7.

441. Karasu, A., et al., *The effects of protein kinase C activator phorbol dibutyrate on traumatic brain edema and aquaporin-4 expression.* Ulusal Travma ve Acil Cerrahi Dergisi = Turkish Journal of Trauma & Emergency Surgery: TJTES, 2010. **16**(5): p. 390-4.

442. Amorini, A.M., J.G. Dunbar, and A. Marmarou, *Modulation of aquaporin-4 water transport in a model of TBI.* Acta Neurochirurgica - Supplement, 2003. **86**: p. 261-3.

443. Taya, K., et al., *Modulation of AQP4 expression by the selective V1a receptor antagonist, SR49059, decreases trauma-induced brain edema.* Acta Neurochirurgica - Supplement, 2008. **102**: p. 425-9.

444. Okuno, K., et al., *The modulation of aquaporin-4 by using PKC-activator (phorbol myristate acetate) and V1a receptor antagonist (SR49059) following middle cerebral artery occlusion/reperfusion in the rat.* Acta Neurochirurgica - Supplement, 2008. **102**: p. 431-6.

445. Kikuchi, K., et al., *Edaravone attenuates cerebral ischemic injury by suppressing aquaporin-4.* Biochemical and Biophysical Research Communications, 2009. **390**(4): p. 1121-1125.

446. Tanimura, Y., Y. Hiroaki, and Y. Fujiyoshi, *Acetazolamide reversibly inhibits water conduction by aquaporin-4.* Journal of Structural Biology, 2009. **166**(1): p. 16-21.

447. Huber, V.J., et al., *Inhibition of aquaporin 4 by antiepileptic drugs.* Bioorg Med Chem, 2009. **17**(1): p. 418-24.

448. Huber, V.J., et al., *Identification of arylsulfonamides as Aquaporin 4 inhibitors.* Bioorganic & Medicinal Chemistry Letters, 2007. **17**(5): p. 1270-3.

449. Yang, B., H. Zhang, and A.S. Verkman, *Lack of aquaporin-4 water transport inhibition by antiepileptics and arylsulfonamides.* Bioorganic & Medicinal Chemistry, 2008. **16**(15): p. 7489-7493.

450. O'Donnell, M.E., et al., *Bumetanide inhibition of the blood-brain barrier Na-K-Cl cotransporter reduces edema formation in the rat middle cerebral artery occlusion model of stroke.* Journal of cerebral blood flow and metabolism : official journal of the International Society of Cerebral Blood Flow and Metabolism, 2004. **24**(9): p. 1046-56.

451. Basso, D.M., et al., *MASCIS evaluation of open field locomotor scores: effects of experience and teamwork on reliability. Multicenter Animal Spinal Cord Injury Study.* Journal of Neurotrauma, 1996. **13**(7): p. 343-59.

452. Santoreneos, S., et al., *A technique for in vivo vascular perfusion fixation of the sheep central nervous system.* Journal of Neuroscience Methods, 1998. **79**(2): p. 195-9.

453. Pearce, J.M. and J.M.S. Pearce, *Syringes and syringomyelia.* European Neurology, 2005. **54**(4): p. 243.

454. Itoh, Y., et al., *Spinal cord edema preceding syringomyelia associated with Chiari I malformation--case report.* Neurologia Medico-Chirurgica, 2002. **42**(9): p. 410-3.

455. Li, K.C. and M.C. Chui, *Conventional and CT metrizamide myelography in Arnold-Chiari I malformation and syringomyelia.* American Journal of Neuroradiology, 1987. **8**(1): p. 11-7.

456. Chapman, P.H. and D.M. Frim, *Symptomatic syringomyelia following surgery to treat retethering of lipomyelomeningoceles.* Journal of Neurosurgery, 1995. **82**(5): p. 752-755.

457. Fishman, R.A., J. Ransohoff, and E.F. Osserman, *Factors influencing the concentration gradient of protein in cerebrospinal fluid.* Journal of Clinical Investigation, 1958. **37**(10): p. 1419-24.

458. Gerber, J., et al., *Lumbar and ventricular CSF protein, leukocytes, and lactate in suspected bacterial CNS infections.* Neurology, 1998. **51**(6): p. 1710-4.

459. Weisner, B. and W. Bernhardt, *Protein fractions of lumbar, cisternal, and ventricular cerebrospinal fluid. Separate areas of reference.* Journal of the Neurological Sciences, 1978. **37**(3): p. 205-14.

460. Weller, R.O., *Pathology of cerebrospinal fluid and interstitial fluid of the CNS: significance for Alzheimer disease, prion disorders and multiple sclerosis.* Journal of neuropathology and experimental neurology, 1998. **57**(10): p. 885-94.

461. Abbott, N.J., *Evidence for bulk flow of brain interstitial fluid: significance for physiology and pathology.* Neurochemistry International, 2004. **45**(4): p. 545-552.

462. Cserr, H.F. and C.S. Patlak, *Secretion and bulk flow of interstitial fluid.* , in *Physiology and Pharmacology of the Blood-Brain Barrier.*, M.W.B. Bradbury, Editor 1992, Springer: Berlin. p. 245-261.

463. Freeman, L.W., *Ascending Spinal Paralysis.* Journal of Neurosurgery, 1959. **16**(1): p. 120-122.

464. Laha, R.K., H.G. Malik, and R.A. Langille, *Post-traumatic syringomyelia.* Surgical Neurology, 1975. **4**(6): p. 519-22.

465. Nurick, S., J.A. Russell, and M.D. Deck, *Cystic degeneration of the spinal cord following spinal cord injury.* Brain, 1970. **93**(1): p. 211-22.

466. Werner, A., et al., *[Apropos of 4 observations on late cervical syringomyelia following medullar injury]*. Schweizer Archiv fur Neurologie, Neurochirurgie und Psychiatrie, 1969. **104**(1): p. 77-86.

467. Castillo, M., et al., *Syringomyelia as a consequence of compressive extramedullary lesions: postoperative clinical and radiological manifestations.* American Journal of Roentgenology, 1988. **150**(2): p. 391-396.

468. Nagelhus, E.A., T.M. Mathiisen, and O.P. Ottersen, *Aquaporin-4 in the central nervous system: cellular and subcellular distribution and coexpression with KIR4.1.* Neuroscience, 2004. **129**(4): p. 905-13.

469. Olsen, M.L., et al., *Functional expression of Kir4.1 channels in spinal cord astrocytes.* GLIA. **53**(5): p. 516-28.

470. Newman, E.A., D.A. Frambach, and L.L. Odette, *Control of extracellular potassium levels by retinal glial cell K+ siphoning.* Science, 1984. **225**(4667): p. 1174-5.

471. Pannicke, T., et al., *A potassium channel-linked mechanism of glial cell swelling in the postischemic retina.* Molecular & Cellular Neurosciences, 2004. **26**(4): p. 493-502.

472. Bordey, A., et al., *Electrophysiological characteristics of reactive astrocytes in experimental cortical dysplasia.* Journal of Neurophysiology, 2006. **85**(4): p. 1719-31.

473. MacFarlane, S.N. and H. Sontheimer, *Electrophysiological changes that accompany reactive gliosis in vitro.* Journal of Neuroscience, 1997. **17**(19): p. 7316-29.

474. Kwon, B.K., et al., *Inflammatory and structural biomarkers in acute traumatic spinal cord injury.* Clin Chem Lab Med, 2011. **49**(3): p. 425-33.

475. Kwon, B.K., et al., *Cerebrospinal fluid inflammatory cytokines and biomarkers of injury severity in acute human spinal cord injury.* J Neurotrauma, 2010. **27**(4): p. 669-82.

476. Barnett, H.J., et al., *Post-traumatic syringomyelia.* Paraplegia, 1971. **9**(1): p. 33-7.

477. Bilston, L.E., D.F. Fletcher, and M.A. Stoodley, *Focal spinal arachnoiditis increases subarachnoid space pressure: a computational study.* Clinical Biomechanics, 2006. **21**(6): p. 579-84.

478. Cheng, S., et al., *The presence of arachnoiditis affects the characteristics of CSF flow in the spinal subarachnoid space: a modelling study.* Journal of Biomechanics, 2012. **45**(7): p. 1186-91.

479. Liu, X.Z., et al., *Neuronal and Glial Apoptosis after Traumatic Spinal Cord Injury.* The Journal of Neuroscience, 1997. **17**(14): p. 5395-5406.

480. Sgouros, S. and B. Williams, *Management and outcome of posttraumatic syringomyelia.* Journal of Neurosurgery, 1996. **85**(2): p. 197-205.

481. Schwartz, E.D., et al., *Posttraumatic syringomyelia: pathogenesis, imaging, and treatment.* American Journal of Roentgenology, 1999. **173**(2): p. 487-92.

482. Cifuentes, M., et al., *Distribution of intraventricularly injected horseradish peroxidase in cerebrospinal fluid compartments of the rat spinal cord.* Cell and Tissue Research, 1992. **270**(3): p. 485-494.

483. Cifuentes, M., et al., *Decreased cerebrospinal fluid flow through the central canal of the spinal cord of rats immunologically deprived of Reissner's fibre.* Experimental Brain Research, 1994. **98**(3): p. 431-440.

484. Rammling, M., et al., *Evidence for reduced lymphatic CSF absorption in the H-Tx rat hydrocephalus model.* Cerebrospinal Fluid Research, 2008. **5**(1): p. 15.

485. Milhorat, T.H., *The third circulation revisited.* Journal of Neurosurgery, 1975. **42**(6): p. 628-45.

486. Cserr, H.F. and L.H. Ostrach, *Bulk flow of interstitial fluid after intracranial injection of blue dextran 2000.* Experimental Neurology, 1974. **45**(1): p. 50-60.

487. Milhorat, T.H., R.W. Johnson, and W.D. Johnson, *Evidence of CSF flow in rostral direction through central canal of spinal cord in rats,* in *Hydrocephalus: pathogenesis and treatment.* , N. Matsumoto and N. Tamski, Editors. 1992, Springer-Verlag: Tokyo. p. 207-217.

488. Klatzo, I., et al., *Observations on the Passage of the Fluorescein Labeled Serum Proteins (Flsp) from the Cerebrospinal Fluid.* Journal of Neuropathology & Experimental Neurology, 1964. **23**: p. 18-35.

489. Brierley, J.B., *The penetration of particulate matter from the cerebrospinal fluid into the spinal ganglia, peripheral nerves, and perivascular spaces of the central nervous system.* Journal of Neurology, Neurosurgery & Psychiatry, 1950. **13**(3): p. 203-15.

490. Howarth, F. and E.R. Cooper, *The fate of certain foreign colloids and crystalloids after subarachnoid injection.* Acta Anatomica, 1955. **25**(2-4): p. 112-40.

491. Nakano, H., et al., *Pulmonary CD103+ dendritic cells prime Th2 responses to inhaled allergens.* Mucosal Immunol, 2012. **5**(1): p. 53-65.

492. Wikstrom, M.E., et al., *Influence of Mucosal Adjuvants on Antigen Passage and CD4+ T Cell Activation during the Primary Response to Airborne Allergen.* The Journal of Immunology, 2006. **177**(2): p. 913-924.

493. Boulton, M., et al., *Drainage of CSF through lymphatic pathways and arachnoid villi in sheep: measurement of 125I-albumin clearance.* Neuropathology & Applied Neurobiology, 1996. **22**(4): p. 325-33.

494. Proescholdt, M.G., et al., *Studies of cerebrospinal fluid flow and penetration into brain following lateral ventricle and cisterna magna injections of the tracer [14C]inulin in rat.* Neuroscience, 1999. **95**(2): p. 577-592.

495. Oldfield, E.H., *Cerebellar tonsils and syringomyelia.* Journal of Neurosurgery, 2002. **97**(5): p. 1009-10; discussion 1010.

496. Ellenbogen, R.G., et al., *Toward a rational treatment of Chiari I malformation and syringomyelia.* Neurosurgical Focus, 2000. **8**(3): p. E6.

497. McGirt, M.J., et al., *Relationship of Cine Phase-Contrastmri to Outcome After Decompressionfor Chiari I Malformation.* Neurosurgery, 2006. **59**(1): p. 140-146 10.1227/01.neu.0000243293.46319.35.

498. Pinna, G., et al., *Cerebrospinal fluid flow dynamics study in Chiari I malformation: implications for syrinx formation.* Neurosurgical Focus, 2000. **8**(3): p. E3.

499. Clarke, E.C., M.A. Stoodley, and L.E. Bilston, *Changes in temporal flow characteristics of CSF in Chiari I Malformation with and without syringomyelia: Implications for theory of syrinx development* 2012: Sydney.

500. Malpas, S., *A novel implantable blood pressure telemetry device; Comparison between data sciences and telemetry research systems.* Journal of Pharmacological and Toxicological Methods, 2009. **60**(2): p. 235.

501. Silasi, G., C.L. MacLellan, and F. Colbourne, *Use of Telemetry Blood Pressure Transmitters to Measure Intracranial Pressure (ICP) in Freely Moving Rats.* Current Neurovascular Research, 2009. **6**(1): p. 62-69.

502. Lim, K., et al., *Comparison of blood pressure and sympathetic activity of rabbits in their home cage and the laboratory environment.* Experimental Physiology, 2012. **97**(12): p. 1263-1271.

503. Cacciola, F., et al., *Syringopleural shunt as a rescue procedure in patients with syringomyelia refractory to restoration of cerebrospinal fluid flow.* Neurosurgery, 2009. **65**(3): p. 471-6; discussion 476.

504. Sekhon, L.H. and M.G. Fehlings, *Epidemiology, demographics, and pathophysiology of acute spinal cord injury.* Spine, 2001. **26**(24 Suppl): p. S2-12.

505. Ikata, T., K. Masaki, and S. Kashiwaguchi, *Clinical and experimental studies on permeability of tracers in normal spinal cord and syringomyelia.* Spine, 1988. **13**(7): p. 737-41.

506. Rossi, C., et al., *Water diffusion anisotropy in white and gray matter of the human spinal cord.* Journal of Magnetic Resonance Imaging, 2008. **27**(3): p. 476-482.

507. Lasfargues, J.E., et al., *A model for estimating spinal cord injury prevalence in the United States.* Paraplegia, 1995. **33**(2): p. 62-68.

508. Saito, F., et al., *Spinal Cord Injury Treatment With Intrathecal Autologous Bone Marrow Stromal Cell Transplantation: The First Clinical Trial Case Report.* The Journal of Trauma and Acute Care Surgery, 2008. **64**(1): p. 53-59 10.1097/TA.0b013e31815b847d.

509. Mulders, S.M., et al., *Water channel properties of major intrinsic protein of lens.* Journal of Biological Chemistry, 1995. **270**(15): p. 9010-16.

510. Verkman, A.S., *Aquaporins at a glance.* Journal of Cell Science, 2011. **124**(13): p. 2107-2112.

511. Shields, S.D., et al., *Anatomical and functional analysis of aquaporin 1, a water channel in primary afferent neurons.* Pain, 2007. **131**(1): p. 8-20.

512. Thuret, S., L.D.F. Moon, and F.H. Gage, *Therapeutic interventions after spinal cord injury.* Nature Reviews Neuroscience, 2006. **7**(8): p. 628-43.

513. Nielsen, S., et al., *Aquaporins in complex tissues. II. Subcellular distribution in respiratory and glandular tissues of rat.* American Journal of Physiology - Cell Physiology, 1997. **273**(5): p. C1549-C1561.

514. Shibuya, S., et al., *Aquaporin 4 mRNA Levels in Neuromuscular Tissues of Wild-type and Dystrophin-deficient Mice.* The Tohoku Journal of Experimental Medicine, 2008. **215**(4): p. 313-319.

515. Zador, Z., et al., *Role of aquaporin-4 in cerebral edema and stroke.* Handbook of Experimental Pharmacology, 2009(190): p. 159-70.

516. Ghabriel, M.N., A. Thomas, and R. Vink, *Magnesium restores altered aquaporin-4 immunoreactivity following traumatic brain injury to a pre-injury state.* Acta Neurochirurgica - Supplement, 2006. **96**: p. 402-6.

517. Cheng, S., et al., *The presence of arachnoiditis affects the characteristics of CSF flow in the spinal subarachnoid space: A modelling study.* Journal of Biomechanics, 2012(0).

518. Zamecnik, J., *The extracellular space and matrix of gliomas.* Acta neuropathologica, 2005. **110**(5): p. 435-42.